University *of the* Western Cape

Method development for selective recovery of Rare Earths Elements from Phosphogypsum waste

by

Jean-Luc Mukaba Muvumbu

MSc & BSc in Chemistry (University of the Western Cape)

A thesis submitted in fulfilment of the requirement for degree of
Doctor in Philosophy in Chemistry

In the

Faculty of Natural Sciences
Department of Chemistry

Supervisor: Prof. Leslie Petrik
Co-supervisor: Dr. Chuks Paul Eze

December 2021

http://etd.uwc.ac.za/

DECLARATION

I declare that "*Method development for selective recovery of Rare Earths Elements from Phosphogypsum waste*" is my own work, that it has not been submitted for any degree or examination in any other university and that all the sources I have used or quoted have been indicated and acknowledged by means of complete references.

UNIVERSITY *of the*
WESTERN CAPE

Jean-Luc Mukaba

i

KEYWORDS

Acid leaching

Adsorption
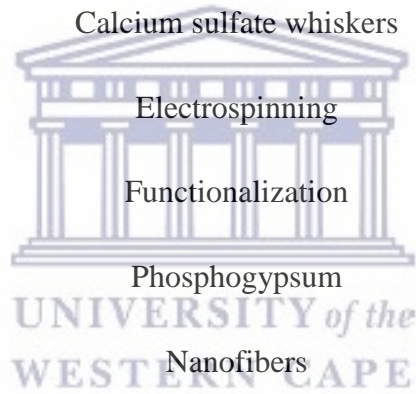
Blending

Calcium sulfate whiskers

Electrospinning

Functionalization

Phosphogypsum

Nanofibers

Rare earths elements

Recrystallization

ABSTRACT

The need for rare earth elements (REEs) in current technologies has motivated countries with high imports dependency to search for alternatives sources. Several studies have been carried out to investigate the feasibility for REE extraction and recovery through the recycling of low value waste streams. Amongst these waste streams, phosphogypsum (PG) which is a major by-product from phosphoric acid processing has drawn research attention as it contains up to an average of 0.4 wt % of REEs. To date, a number of approaches have been reported on REE extraction from PG leaches after a total or partial dissolution. Amongst all the approaches, adsorption was found as one of the most promising due to its high efficiency, availability and simplicity. A number of adsorbents have been investigated so far but only a few have specific functional groups for REE extraction from a complex mixture in solution. This study therefore focused first on evaluating a combined up concentration of REEs via the synthesis of calcium sulfate whiskers (CSWs) for possible valorisation and large scale utilization of PG waste, and secondly, on the fabrication of nanofibers containing REE selective ligands for extraction of REEs from resulting solutions.

The synthesis of CSWs was carried out in this study in an attempt to concentrate the REEs in PG filtrates after removal of CSWs. These experiments were carried out in HCl or HNO_3 solutions. The elemental composition was determined by ICP-OES/MS or NAA and the structural changes were determined through FTIR, XRD, SEM and TGA. The obtained results showed that the dissolution and recrystallization processes during the synthesis of CSWs were able to enrich the REEs up to 97 % in HCl or HNO_3 filtrate solutions. The FTIR, XRD and TGA analysis revealed that CSWs were successfully synthesized through the dissolution and recrystallization method. Microscopic SEM images and macroscopic images of CSWs respectively further confirmed the whisker like and fibrous structure.

For the fabrication of adsorbents, the characterizations of polystyrene (PS) support and modified PS nanofibers (blended with di-(2-ethylhexyl) phosphoric acid and

iii

surface modified with diglycolic acid ligands) were done using SEM, ATR-FTIR, and TGA. The SEM technique conducted on the unmodified PS nanofibers obtained at different concentrations of PS solution showed that a PS concentration of 14 wt% in a mixture of DMF:THF (3:1) solvent was the best condition for fabrication of PS nanofibers as it led to electrospun nanofiber mats free of beads with an average fibre diameter of 750 nm. PS polymer concentration of 14 wt% was further used for the modifications processes with di-(2-ethylhexyl) phosphoric acid or diglycolic acid ligands for direct blending or surface modification respectively at different concentrations of the ligands. The ATR-FTIR spectra of the modified fibres supported by the TGA and SEM results confirmed the presence or grafting of the main functional groups of the ligands onto the PS backbone.

The results from different batch adsorption studies have shown that the di-(2-ethylhexyl) phosphoric acid and diglycolic acid ligands were able to increase the adsorption capacity of PS support for REEs (Ce^{3+}, Nd^{3+}) and Ca^{2+} (as representative metal ions of PG leachate). The optimum adsorption capacities of PS nanofibers modified with di-(2-ethylhexyl) phosphoric acid (DH-PS20-nfs) and diglycolic acid (DG-PS2-nfs) ligands were respectively 107 g/mg and 89 g/mg at pH 4.0 and 5.0 at an initial concentration of 160 mg/L and contact time of 60 min. The difference in terms of the adsorption capacities at these conditions for DH-PS20 and DG-PS2 nanofiber mats, was attributed to the unique characteristic of each ligand grafted onto the PS support. The experimental data obtained from the adsorption studies fitted the Langmuir isotherms better than the Freundlich isotherms suggesting that the adsorption of Ce^{3+}, Nd^{3+} and Ca^{2+} took place as a monolayer process occurring on the homogeneous surface of the nanofiber adsorbents. The kinetic rate was best described with the pseudo second-order model. The results furthermore showed that the modified nanofibers were able to be regenerated using 1.0 M HNO_3 and to withstand up to three cycles. The selective adsorption of REEs (Ce^{3+}, Nd^{3+}) and Ca^{2+} from PG leachates indicated that REEs-Ca^{2+} separation could be achieved from PG filtrate. SEM-EDS mapping further confirmed the availability of Ce^{3+}, Nd^{3+} and Ca^{2+} on the surface of DH-PS20 and DG-PS2 nanofibers after adsorption.

iv

Publication

- **Mukaba, J.L**., Eze, C.P., Pereao, O. and Petrik, L.F., (2021). Rare Earths' Recovery from Phosphogypsum: An Overview on Direct and Indirect Leaching Techniques. *Minerals*, *11*(10), p 1051. https://doi.org/10.3390/min11101051

- Uche, C.C., **Mukaba, J.L.M**., Bode-Aluko, C.A., Pereao, O. and Petrik, L., 2020. Immobilization of Metal Selective Ligands upon Polymer Nanofibers: Successes and Challenges. *Multidisciplinary Digital Publishing Institute Proceedings*, *57*(1), p.67.

Drafted manuscripts

- **Mukaba, J.LM**., Eze, C.P. and Petrik, L.F. Leachability of rare earths elements via recrystallization of South African phosphogypsum waste. *Progress in Crystal Growth and Characterization of Materials.*

- **Mukaba, J.LM**., Eze, C.P. and Petrik, L.F. Adsorption studies of Ce^{3+}, Nd^{3+} and Ca^{2+} using DH-PS20 and DG-PS2 modified nanofibers. *Separation and Purification Technology*

Presentation

- **Mukaba, J.LM.** and Petrik. L.F. Method development for selective recovery of rare earths metals from phosphogypsum waste. *Mining and Nuclear Engineering Graduate Seminar. Missouri University of science and Technology. Missouri, Rolla/ United States of America, 16 April 2018.*

- **Mukaba, J.L.M**; Eze,Ch.P; Frontasyeva,M.V; Doucet, J.F and Leslie P.F. Method development for selective recovery of rare earths from phosphogypsum. *Minerals Research Showcase 2017 conference sponsored by the Southern African Institute of Mining and Metallurgy (SAIMM) of the Western Cape branch. Philippi Village, Cape Town, South Africa. 3 - 4 August 2017.*

DEDICATION

This work is dedicated to

Jessica Ilunga Mukaba (**wife**),

Elior Imani Mukaba (**son**)

Brigitte Kashala Kasongo (**mother**)

and

In loving memory of

Prospère Kyungu Mukaba alias Mundanda (**father**)

vii

My special thanks go to my family, to my mother Brigittes Kashala Kasongo, my sisters (Lydia Kazadi Kabemba and Belinda Kasongo) and my brothers (Prince Mukaba and Jean-louis Kashala), my uncle Antonios Kazadi Kay and his wife Christel Kakom and their children for the encouragements, prayers and supports. Many thanks to pastor Jean Munyungu and also to the patriarch of the Mwamba's family, Mr. Jean-Félix Kanonge Mwamba (father in-law) for their prayers and encouragements. Thanks to my friends Dr. Deogracias Kishabongo, Ir. Guy Ngombe and Ir. Serge Bwilu for encouragement and support throughout this journey.

Last but not least, my very special thanks go to my wife Mrs. Jessica Ilunga Mukaba, the love of my heart for all her prayers, support, patience, advice and encouragement throughout this journey. I will always appreciate it. Thank you sweet heart. Special thanks also to my son, Elior Imani Mukaba for his patience all the time that I was absent at home for research trip or laboratory work. I love you so much son, you are such a blessing for me.

TABLE OF CONTENTS

LIST OF FIGURES

xviii

LIST OF TABLES

UNIVERSITY *of the*

WESTERN CAPE

LIST OF EQUATIONS

UNIVERSITY of the
WESTERN CAPE

ABBREVIATIONS

ATR	Attenuated Total Reflectance
CIS	Commonwealth of Independence States
CSW	Calcium Sulfate Whisker
D2EHPA	Di-(2-ethylhexyl) phosphoric acid
DH	Dihydrate
DGA	Diglycolic acid
DMF	N,N-dimethylformamide
EDTA	Ethylene diamine tetra acetic acid
FTIR	Fourier Transform Infrared
HH	Hemihydrate
JINR	Joint Institute for Nuclear Research
LLE	Liquid-liquid extraction
NAA	Neutron Activation Analysis
PG	Phosphogypsum
PS	Polystyrene
REO	Rare Earth Oxide
REE	Rare Earth Element
SEM	Scanning Electron Microscopy
SLE	Solid-Liquid Extraction
SPE	Solid Phase Extraction
SKK	Steenkampskraal
SX	Solvent Extraction
TGA	Thermogravimetric analysis
THF	Tetrahydrofuran
XRF	X-ray Fluorescence
XRD	X-ray powder diffraction
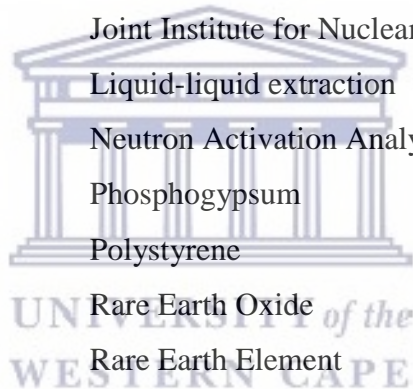
CHAPTER 1

1. INTRODUCTION

1.1 Introduction

The present chapter gives a general introduction and brief description of this study. The first section of this chapter provides background information on the current role of rare earth elements in advanced technologies as well as their supply, demand, production and scarcity. The background also highlights different sources of rare earths, with particular attention on phosphogypsum waste as a potential secondary source and the application of modified nanofibers for the recovery of these elements. The second section of this chapter outlines the research motivation, the aims, objectives, research questions, research approach and the hypothesis of the study based on the literature review which is presented in Chapter two. The scope and delimitation of the study and the structure in which the thesis is built are presented at the end of this chapter.

1.2 Background

Rare earth elements (REEs) refer to a group of metals that include yttrium, 14 elements of the lanthanide series and scandium. Promethium and its isotopes have short half-lives and are radioactive, and therefore it is generally excluded from the lanthanide series (Du & Graedel, 2011). The REEs have various common physical and chemical proprieties. These proprieties have made them useful in several growing applications and they are indispensable for current critical technologies (Cardoso et al., 2016; Sun et al., 2019). For instance, neodymium (Nd) is vital for high performance permanent magnets, while yttrium (Y) is considered as a promising raw material for super conductors. The use of Nd or Y in these intermediate products, viz. magnets or super conductors, provide a unique performance when incorporated in final products such as wind turbines, hybrid and

1

electric vehicles applications. Such input from REEs in current innovation has significantly influenced the demand of these metals worldwide (Dushyantha et al., 2020). China has been playing a dominant role in the mining and production of the REEs since 1990 and most of the countries where these metals are part of important innovation technologies completely depend on the importations from China (Massari & Ruberti, 2013; Zhou, 2017; Long et al., 2012; USGS, 2018). However, the growth in the manufacturing industries has caused China to become one of the major consumers of REEs. This trend has consequently reduced export quotas from China and increased the price of the REEs on the global market (Golev et al., 2014). The availability of REEs is therefore, described to be at risk because of the current state of affairs, where China controls over 90 % of the mining and production of REEs worldwide (Blisset et al., 2014, Tunsu et al., 2015). It is historically known in respect of the mining of important metals around the world that a much lower level of market concentration can harm manufacturing firms. For instance, the Democratic Republic of Congo (DRC), formerly the Republic of Zaire had control of about 48 % of cobalt supply in 1978 worldwide. Yet, political unrest in the DRC resulted in a disruption to global supply that was known as the "Cobalt Crisis" which affected many firms in the world (Alonso et al., 2012). The need of REEs in current technologies worldwide and the problematic restriction imposed by China have motivated countries with high imports dependency such as the European Unions (EU) to search for alternatives sources in attempt to balance and remediate the supply and market of REEs (Massari & Ruberti, 2013; Blisset et al., 2014). The use of REEs is expected to increase and will affect various innovative areas for the next decades (Seredin et al., 2013; Canovas et al., 2019).

To alleviate the shortage of REEs, search for new and mineable REE resources outside China or reopening of former REE mines were suggested (Massari & Ruberti, 2013; Tunsu et al., 2015). However, searching for new REE deposits or reopening formerly existing REE mines is economically costly (Tunsu et al., 2015; Jha et al., 2016). Several studies have been recently carried out to investigate the feasibility of REE extraction and recovery through the recycling of low value waste

2

streams such as bauxite residue, mine tailings, phosphogypsum, slag and waste waters (McLellan et al., 2013; Bandara et al., 2014; Binnemans et al., 2013a, 2013b; Tunsu et al., 2015; Innocenzi et al., 2014). Amongst these waste streams or secondary resources, phosphogypsum has drawn the attention of the current research as a potential source for REE beneficiation. Phosphogypsum (PG) is a major by-product that is generated during the processing of phosphoric acid from phosphate rock (Koopman & Witkamp, 2000; Merwe et al., 2004). Phosphate rocks generally contain between 0.01 and 0.1 wt % of REEs, although some rocks such as those produced at Kola Peninsula in Russia may reach up to 1.0 wt % (Binnemans et al., 2013; 2015). Of the total concentration of REEs originally present in phosphate ores, approximately 70–85 % end up in the PG waste generated during the phosphoric acid processing while the rest remain dissolved in the leaching solution containing phosphoric acid (Zielinski et al., 1993; El-Didamony et al., 2012). The REE content in PG can reach up to an average of 0.4 wt %. which is far higher than other REE secondary sources but lower compared to primary deposits such as monazite which can reach up to 15 wt % (Binnemans et al., 2013). However, both the huge amounts of PG (over 150 million tonnes) produced worldwide per year and the amount of REEs encapsulated (approximately 21 million tonnes), make it a valuable source if the price of metals extracted (i.e. REEs) is higher to compensate for the extraction costs (Yahorava et al, 2016; Wu et al., 2018). Nevertheless, the recovery of all REEs from PG without the destruction of the lattice is impossible. The earliest studies indicated that about 50 % of REEs presents in phosphogypsum can be recovered through acid leaching processes (Habashi, 1985). To date, a number of processes have been reported on REE recovery where a total or partial dissolution of PG has been applied (Yahorava et al, 2016). These approaches have been utilised mainly in attempts to increase the leaching efficiencies prior to REE recovery. Preston et al., (1996) described a method of REE recovery from South African calcium sulfate sludge (phosphogypsum) which consisted of mixing dilute nitric acid (1.0 M) and calcium nitrate ($Ca(NO_3)_2$) solutions. Their results showed that the addition of $Ca(NO_3)_2$ as carrier of Ca^{2+} ions enhanced the leaching yield of REEs from PG. In contrast, Lokshin and co-workers

3

did not observe an enhanced leaching efficiency of REEs upon the addition of calcium nitrate (Lokshin et al., 2002). A method proposed by Walawalkar et al., (2016) involves the addition of calcium sulfate anhydrite seeds to the leached solution resulting in the rejection of calcium sulfate from the leached solution, and reducing the concentration of calcium, and consequently high leaching efficiency of REEs. The dissolution and recrystallization of PG with attention to REE extraction and recovery have been also suggested (Zielinski et al., 1993; Koopman & Witkamp, 2000; Safiulina et al., 2015). However, the recrystallization depends essentially upon the type of PG (Abramov et al, 2013). For instance, in a hemihydrate form of PG ($CaSO_4 \cdot 0.5H_2O$), REEs do not isomorphously co-crystallise with the lattice but exist in a separate phase offering an opportunity for REE recovery during the conversion of $CaSO_4 \cdot 0.5H_2O$ to $CaSO_4 \cdot 2H_2O$ (calcium sulfate dihydrate) (Lokshin et al., 2002; Abramov et al, 2013; Kandil et al., 2017). For such a process, the hydration proceeds through the dissolution of $CaSO_4 \cdot 0.5H_2O$, bringing all REE ions into the solution, which in turn inhibit the crystallisation of the dehydrate (Zielinski et al., 1993). Yahorava et al, (2016) carried out a hydrothermal treatment of PG containing slurry in an autoclave prior to its recrystallization and REE recovery. The method was promising with regard to REE recovery but a number of parameters such as residence time in the autoclave, impact of seeding and solids content still required optimization and verification to apply this method at industrial level. A study conducted by Genkin et al., (2013) has reported an improvement on REE concentrate while recrystallizing PG hemihydrate ($CaSO_4 \cdot 0.5H_2O$) and anhydrite ($CaSO_4$) into $CaSO_4 \cdot 2H_2O$ in the presence of calcium nitrate under sub-acidic medium (pH >1).The dissolution was carried out with strong acid (pKa < 0). Their results showed that the increase in Ca^{2+} ions concentration favours the recovery of REEs but this increase made the formation of $CaSO_4 \cdot 2H_2O$ less favourable. Other approaches for enhancing the leaching efficiency of REEs from PG such as microwave treatment, or a pre-heating process are also discussed in the literature (Binnemans et al., 2013, 2015; Walawalkar et al., 2016).

Various methods of recovery and separation of REEs from PG leach solution such as liquid–liquid extraction, precipitation, electro-deposition, electrolytic concentration, membrane filtration, ion exchange and adsorption exist but are either ineffective and/ or very expensive, especially when dealing with lower concentrations of these elements (Pereao et al., 2018; Hidayah et al., 2017, 2018). Among these approaches, liquid-liquid extraction (LLE) is the most used technique due to its excellent selectivity and large loaded capacity for metal ions (Xie et al., 2014). The extraction and separation in LLE is generally driven by the preferential distribution of individual REE between two immiscible liquid phases that are in contact with each other (Abreu & Morais, 2014). Organophosphorus REE extractants such as di-(2-ethylhexyl) phosphoric acid (D2EHPA) have been widely reported for REE recovery and separation in LLE process (Basualto et al., 2013; Xie et al., 2014). Benzene, cyclohexane, tetrachloromethane, kerosene and xylene are the most common used diluents in LLE, and their efficiencies increase as follows benzene < xylene < tetrachloromethane < cyclohexane < kerosene (Innocenzi et al., 2018). Despite the remarkable advantages of LLE for REE recovery such as the suitability over a wide range of operation scales and relatively simple equipment, this method suffers from low separation efficiency as well as production of a huge amount of waste materials (Da Silva et al., 2019). For instance, it has been reported that the production of 1 ton of rare earth oxides (REOs) in China produces about 60 000 m^3 of waste gases, 200 m^3 wastewater and 1.4 tons of radioactive waste (Khodakarami & Alagha, 2020).

Thus, alternative approaches of REE recovery such as solid-liquid extraction (SLE) or solid phase extraction (SPE) has been recently suggested in the literature (Hidayah et al., 2017). The approach consists of immobilizing most known REE ligands such as D2EHPA on a solid support to avoid the utilisation of huge amount of solvent required in LLE (Zawierucha et al., 2016; Fimognari et al., 2018; Da Silva et al., 2019). Furthermore, this approach differs from the conventional LLE since there is no organic diluent such as kerosene that is required and thus, reducing the environmental impacts associated with solvent evaporation and losses by entrainment in the aqueous solution (Yadav et al., 2013, Da Silva et al., 2019).

5

However, compared to conventional LLE, SLE systems generally suffer from a relatively low contact area between the surface of the support modified with the ligands and the solution containing metal ions to be recovered (Da Silva et al., 2019). This low contact area is the main disadvantage encountered within the SPE process since it hinders the mass transport between the solution and the solid support, which makes the process less efficient. An approach to overcome this issue is to make use of high surface area supports such as polymeric nanofibers that offer enhanced interactions, high porosity and flexibility (Rathna et al., 2013; Liao et al., 2014; Luo et al., 2015; Pereao et al., 2019a).

Modified polymer nanofibers as carriers of ligands for REEs separation and recovery have been widely discussed in the recent literature and the electrospinning technique has been found to be a versatile means of production of these materials (Chipara et al., 2013; Pereao et al., 2019a). Organic ligands such as diglycolic anhydride (DGA) can also be immobilized on the surface of polymer nanofiber for REE adsorption and separation from aqueous solutions (Shinozaki et al., 2018). Synthetic polymers such as polystyrene are popular, and this low cost organic polymer has been used long before as a ligand support due its outstanding physical and reactive properties (Bessbousse et al., 2009). For instance, Pereao et al., (2020) recently modified polystyrene nanofibers with DGA ligand for adsorption of Ce and Nd from aqueous solution and showed that the adsorption capacity of the modified polystyrene increased.

This study therefore focuses above all on the dissolution and recrystallization of PG waste and subsequent extraction and recovery of REEs from PG leachate using modified polymer nanofibers. These nanofiber adsorbents will be developed and designed using polystyrene as support of D2EHPA and DGA ligands.

6

1.3 Research motivation

The use of REEs will continue to increase due to their unique physicochemical properties that make them indispensable for current modern industries where China remains in control of the global production and mining. Furthermore, and importantly, the restrictions imposed by China in terms of exports will also affect the modern industry due to a supply shortage. South Africa is a growing economy where technologies are prominent in various domains such as electronics, electric cars, energy production, etc. This is expected to grow for the next decades and will involve key metals in particular REEs. Steenkampskraal mine located in the Western Cape Province was previously used for the extraction of thorium, and REEs associated with this mine were considered as a gangue. This mine is highly radioactive and was shut down in 1963; many attempts to reopen it were unsuccessful. Phosphogypsum (PG) is a potential source of REEs available in South Africa that is generated either from phosphoric acid or fertilizer productions. PG is composed of fine-grained particles that require less physical treatment (grinding etc.) compared to primary resources of REEs such as bastnaesite, xenotime and monazite. It can therefore be directly treated through the hydrometallurgical approach in an attempt to concentrate REEs prior to their recovery and separation. Various approaches have been undertaken to access on the feasibility of REE recovery from the PG at a large scale but many are still uneconomical and at research scale. Currently South Africa does not have established plants with a protocol describing the recovery and separation of REEs from a locally generated pulp of PG. Designing a protocol for REE recovery and their subsequent separation from a pulp of PG could be a big step to overcome both the environmental issues related with huge amount of PG stockpiles and to balance the foreseen supply shortage of REEs.

1.4 Objectives and research questions

The present study aims to develop a method to up-concentrate and identify an approach of REE recovery from a pulp of phosphogypsum (PG) generated in South Africa. The crucial achievements of this study will be respectively accomplished through the objectives and responses to research questions below:

1.4.1 Objectives:

This study intends to:

- fully characterize the PG feedstock in attempts to quantify the REEs and understand the mineralogical forms in which they exist.
- identify an effective leaching technique of REEs from PG that is feasible for both small and large scale.
- prepare a polystyrene electrospun nanofiber as support for REE ligands by using the electrospinning approach.
- modify the   surface of polystyrene using D2EHPA and DGA ligands as potential adsorbents of REEs.
- investigate the batch adsorption of REEs from a leachate of PG pulp using modified D2EHPA and DGA electrospun nanofibers.
- determine the reusability cycles of modified electrospun nanofibers

1.4.2 Research questions

The aforementioned overall objectives of this study will be achieved by answering the following developed research questions:

- What are (is) the most prevailing REEs of the untreated PG under investigation?

- What will the most feasible and efficient approach be between the direct and indirect acid leaching (recrystallization) to concentrate the REEs from PG waste?
- Is it possible to recrystallize the phosphogypsum?
- Can D2EHPA or DGA ligand be doped or grafted on polystyrene support to produce DH-PS and DG-PS adsorbents?
- Can DH-PS and DG-PS nanofibers adsorb REEs (Ce^{3+}, Nd^{3+}) and Ca^{2+} better than unmodified polystyrene nanofibers (PS14-nfs)?
- Are DH-PS and DG-PS nanofiber mats reusable and how many times will it be possible to reuse each?

1.5 Hypothesis

REE recovery and separation using organic solvent extractants or ligands from aqueous solutions is possible. Therefore, solid extractant nanofibers (DH-PS and DG-PS) containing most known REE ligands/ extractant will be suitable for the recovery and separation of REEs from a real solution of PG.

1.6 Research approach

In attempts to achieve the objectives set in this study and answer the questions developed above, an extensive critical review on REE recovery from PG was carried out, and some aspects of various approaches were adopted giving rise to the experimental conditions. Based on the objectives assigned, this study was divided in three main phases. The first phase consisted of identifying the appropriate conditions to obtain high REE concentrate from PG pulp. In this regard, three inorganic acids namely HCl, H_2SO_4 and HNO_3 were used for both direct and indirect leaching (dissolution and recrystallization process) of PG and; the main parameters investigated were solid to liquid ratios, residence time, temperature, acid concentration and agitation. The optimization of these parameters was carried out following the experimental protocol, which entails to vary one parameter at a time

9

while keeping the others constant. The second phase focused on the preparation of polystyrene nanofibers support using electrospinning technique. The surface of the obtained polystyrene electrospun nanofibers was modified with D2EHPA or DGA ligand. This modification was carried out through blending or chemical method and the concentration of the ligand was the main parameter varied at this step. The third phase of this study dealt with the recovery of REEs from a leachate of PG pulp which was carried out in a batch adsorption process on modified polystyrene based D2EHPA or DGA nanofibers. Since the PG pulp obtained from the leaching is highly acidic, dilutions were carried out based on the initial (original) concentration of the pulp solution for each adsorption experiment. The effects of pH and contact time were mainly investigated at this step. The materials used or obtained in this study were mainly characterized using scanning electron microscopy (SEM), X-ray diffraction (XRD), Fourier transform infrared spectroscopy (FTIR), Inductively coupled plasma (ICP)- optic emission spectroscopy (OES) or mass spectroscopy (MS), X-ray fluorescence (XRF), Neutron activation analysis (NAA), Nitrogen adsorption-desorption for surface area analysis through BET and thermal gravimetric analysis (TGA) for a better understanding. For instance, the surface morphology and thermal changes of phosphogypsum and electrospun nanofiber composites were characterized by SEM and TGA respectively. The XRD and FTIR were used to determine the mineral composition and structural bonding respectively while the chemical composition of solid of phosphogypsum and all liquid samples (solutions) was carried through XRF and ICP-MS (or ICP-OES) respectively. For total elemental composition, the solid sample was digested in a hot HNO_3 (6 M) for about 30 min using a solid-liquid ratio of 1:20. All liquid samples generated were diluted to an appropriate volume and dilution factor prior to analysis.

1.7 Scope and delimitation of the study

The current study is a contribution to a broader research topic in South Africa regarding waste management and valorisation. This study focused particularly on phosphogypsum (PG) produced in South Africa and attempted to explore its

practical utilisation for REE reclamation. The extraction of REEs with polymer modified nanofibers through the solid phase extraction method has great advantages to overcome some limitations encountered in conventional techniques such as solvent extraction. Several organic polymers have been electrospun using electrospinning which is a versatile method for fabrication of nanofiber modification. In this study, polystyrene polymer was chosen as it is affordable, readily available and easy to electrospin. REE ligands, D2EHPA and DGA, were used for modification of electrospun nanofibers. These two ligands are relatively affordable and readily available as commercial extractant mostly used in solvent extraction. In this study, only bench experiments have been carried out. Suggestions and recommendations on REE recovery are given based on different characterizations performed and the sequence was mainly motivated by the need to acquire a particular information.

1.8 Thesis structure

Except for this general introductory chapter that presents an overview of information from which this research was developed, this thesis has six more chapters, which are listed below:

Chapter Two: This chapter presents a literature review on general physicochemical characteristics of REEs, their current supply, demand, production, market trend and scarcity. Different approaches of REE extraction and recovery from phosphogypsum waste which combined hydrometallurgical processes (direct or indirect leaching) and polymer nanofibers were also deeply reviewed. The principle of characterization techniques that were used in the experimental section of this study as elaborated in chapter three were also discussed.

Chapter Three: This chapter will give a detailed account of experimental procedures and characterization techniques that were used throughout this study in

order to achieve the objectives and answer the research questions that were developed in section 1.4.2. of chapter one.

Chapter Four: This chapter will set the stage for the onward chapters by giving a full characterization of the phosphogypsum feedstock as well as the polymer electrospun nanofibers and their derivatives. The characterizations of all materials were carried out as set in chapter three.

Chapter Five: This chapter will present and discuss the results from the direct and indirect acid leaching of the phosphogypsum for REE extraction. The two approaches were investigated in attempts to identify the best route suitable for REE extraction that can also be used at large scale. The last approach is promising since it leads to a new pure recrystallized gypsum referred as calcium whiskers that can be used for various application. The chapter sets also the stage for chapter six.

Chapter Six: This chapter will present and discuss the results from the batch adsorption of REEs from mimicked solutions and PG leachates using modified nanofiber adsorbents. The possibility for recyclability as well as stability of the adsorbents will also be discussed in this chapter.

Chapter Seven: This chapter will draw conclusions and give recommendations from different findings. The novelty of this research will be also highlighted as a contribution of the present work to the existing literature.

Research output

This section will present the manuscripts that will be published throughout this study as well as conferences proceeding/or research visits attended locally or abroad.

References

This section will give in an alphabetical order all the references including books, journals, web sites consulted throughout this study.

Appendices

This section lists detailed data and other related materials useful for the reader but which were not included in the body of this study.

CHAPTER 2

2. LITERATURE REVIEW

2.1 Introduction

This chapter presents a literature review on general physicochemical characteristics of REEs, their current supply, demand, production, market trend and scarcity. Different approaches of REE extraction and their recovery from phosphogypsum waste using hydrometallurgical processes (direct or indirect leaching) and modified polymer nanofibers are also reviewed in detail. The principle behind the characterization techniques are elaborated. This chapter ends with a short summary that contains the main research gaps that were identified and from which the study was developed.

2.2 Rare earths elements

Rare earths elements (REEs) are metals of the lanthanide series on the periodic table, commonly referred to as lanthanides, with atomic numbers ranging from 57 to 71. Scandium (Sc) and yttrium (Y) are associated with lanthanides as they display similar chemical properties (atomic radii, ionization energies and melting points) and usually occur naturally in the same bearing minerals. The REEs can further be classified in subgroups as light (LREEs) or heavy (HREEs) based upon their relative atomic weights (Massari & Ruberti, 2013; McLemore, 2015). The LREEs include: lanthanum (La), cerium (Ce), praseodymium (Pr), neodymium (Nd), promethium (Pm), samarium (Sm) and europium (Eu) while HREEs comprise gadolinium (Gd), terbium (Tb), dysprosium (Dy), holmium (Ho), erbium (Er), thulium (Tm), ytterbium (Yb) and lutetium (Lu). Sc is usually excluded from this classification due to its deviating properties while Y is classified among the HREEs due to its physical and chemical properties that are similar to this subgroup even though it is the lightest element among all the REEs (Massari & Ruberti, 2013,

14

Papangelakis & Moldoveanu, 2014). In addition to the above classification, the REEs can be classified into three groups based on their relative demand in industry, as follows: critical (Nd, Eu, Tb, Dy, Y and Er), uncritical (La, Pr, Sm and Gd) and excessive (Ce, Ho, Tm, Yb and Lu) metals (Seredin & Dai, 2012). Generally, this classification reflects the relative values of REEs on the market because, the uncritical and excessive REEs have a low cost compared to critical metals (Peramaki, 2014).

The chemical properties of most REEs is as a result of lanthanide contraction, which is the overall decrease in atomic and ionic radii with increased atomic numbers from La through Lu. This contraction is due to incomplete mutual shielding of the 4f-electrons (Seredin & Dai, 2012; Dushyantha et al., 2020). REEs are highly electropositive and occur mainly as ionic compounds due to their low ionisation potentials. As a consequence, the valence shells of REEs consist of deeply buried 4f orbitals in which the 4f electrons are not available for covalent bonding (Dushyantha et al., 2020). The oxidation state of III is common for all REEs whether in solution or solid compounds. However, some REEs can occur at oxidation states of II and IV due to their special stability of the f-shell which can be found empty, half-filled or fully filled. For this reason, Eu^{2+} and Yb^{2+} (f^0 and f^7) as well as Ce^{4+} and Tb^{4+} (f^7 and f^{14}) occurrence is possible (Bunzli, 2014; Peramaki, 2014; Eggert et al., 2016).

The cations at oxidation states II or IV compared to III clearly display different properties that allow processes such as mutual separation to take place through selective oxidation or reduction methods (Bunzli, 2014). This relatively small variation in terms of the oxidation states as well as the large ionic radii of REEs compared to the rest of elements on the periodic table allow them to form a variety of complexes in a wide selection of coordination numbers ranging between 6 and 12 (Gupta & Krishnamurthy,1992). Therefore, complexes such as those of citrates, cyclopentadienyls, acetyl acetoneoxalates and ethylenediaminetetraacetic (EDTA) are common. However, the large size of trivalent REEs compared to other cations

results in smaller electrostatic forces of attractions. Thus, only strong ligands thermodynamically form stable complexes that can be isolated (Gupta & Krishnamurthy, 1992). The stability of ligand complexes generally increases with decrease in radii of the REEs due to lanthanide contraction.

2.3 REE abundance

REEs are not in reality rare as their name indicates. The term "rare" solely refers to the lack of large deposits that are characteristic for other elements such as base metals (copper, silver and gold) as well as their low concentrations widely distributed in the earth s' crust. REEs follow the Oddo-Harkins rule, meaning that REEs with even atomic numbers are usually more abundant than their odd-numbered neighbours (Massari & Ruberti, 2013). Therefore, the concentrations of HREEs are commonly smaller than LREEs (Table 2.1). The average abundance of REEs in the earth's crust varies from 66 ppm in Ce, 40 ppm in Nd and 35 ppm in La to 0.5 ppm in Tm, disregarding the extremely rare Pm. Thus, Ce is the most abundant REE in the earth's crust followed by Nd and La (Uchida et al., 2006). The abundance of REEs and in particular for the element Ce is fairly similar to other common and much environmentally studied elements such as copper, zinc, nickel and lead (Golev et al., 2014). Furthermore, the scarcest REEs such as Lu and Tm, are actually more abundant in the earth's crust than cadmium (Cd) and selenium (Se). Table 2.1. gives the estimated abundance of REEs in the earth's crust while Figure 2.1. shows the abundance of different elements in the earth's crust.

Table 2.1: Estimated abundance (ppm) of LHREEs and HREEs in the earth's crust adapted from Long et al., (2012).

LREEs		HREEs	
Sc	5–22	Tb	0.7–3
La	5–39	Dy	3–8
Ce	20–70	Ho	0.7–2
Pr	4–9	Er	2–7
Nd	12–42	Tm	0.2–1
Sm	5–8	Yb	0.3–8
Pm*	-	Lu	0.4–2
Eu	0.2–2	Y	24–70
Gd	4–8		
Total	**55.2–200**	**Total**	**31.3–101**

*: does not occur naturally in the earth's crust
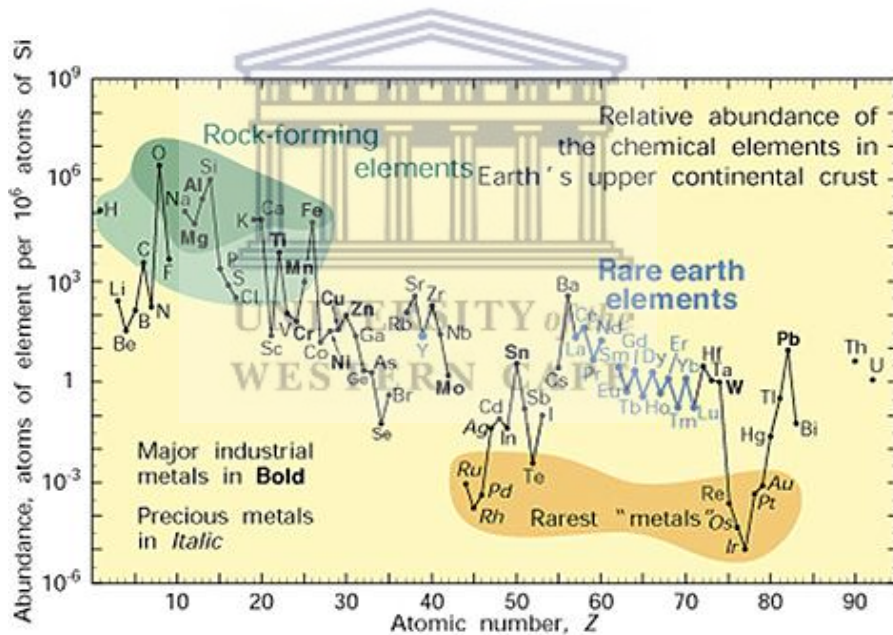
Figure 2.1: Relative abundance of different elements in the upper continental of the earth's crust as function of atomic number. Adapted from USGS, (2002).

2.4 Reserves and deposits of REEs

It is important here to highlight two terms namely "reserve" and "deposit". The former is usually defined as REE resources for industrial production while the latter refers just to REE resources. Thus, in terms of REE deposits, Brazil leads with about

17

32 % followed by China (22 %); Commonwealth of Independence States (CIS) or Former Soviet Union (12 %); Vietnam (9 %); Australia (8 %) and the United States (7 %) (Zhanheng, 2011). Despite that the REEs are distributed in many deposits, only a proportion of these can be considered economic to develop and mine (Zhanheng, 2011). In other word, only quite abundant deposits can be called REE reserves. Globally, there is about one hundred million tons of reserves of rare earths oxides (REOs) that are presently accessible and scattered across more than 30 countries (Jordens et al., 2013, Jha et al., 2016; Chen, 2011). China occupies the first position with more than 60 % (55 million tons); CIS is in the second position with about 17 % (19 million tons); United States, the third position with a quota of about 12 % (13 million tons) followed by India (3.1 million tons); Australia (1.6 million tons); Brazil (0.48 million tons); Malaysia (0.3 million tons) and other countries around the world with approximately 20 % (22 million tons) (Massari & Ruberti, 2013).

The mining and production of REEs have been dominated by China since 1990 (Golev et al., 2014). For instance, in 2010, of an estimated world production of 134, 000 tons, about 130, 000 tons (97 %) of REOs came from China (Tunsu et al., 2015; Jordens et al., 2013; Jha et al., 2016). However, with the flourishing growth in the manufacturing industries which ranked China among the major consumers of REEs, the yearly export quotas for countries outside of China were revised and reduced (Chen 2011, Chi et al., 2001, Jordens et al., 2013). The export quota declined from about 50 % in 2008 until its abolition in 2014 and remained the same from 2014 to 2017 until its modest increase in 2018 (Mancheri et al., 2019). The Chinese control over the amounts of REOs yearly has led to significant price fluctuations in particular for the elements such as Nd, Dy, Eu, Y and Tb that are mostly used in sustainable applications (Tunsu et al., 2015). This situation has prompted a search for new deposits of REOs as well as the reopening of other known deposits such as the Mountain Pass in the United States which was reopened back in 2012 (Tunsu et al., 2015). In Africa and particularly in South Africa Steenkampskraal and Zandkopsdrift deposits have been widely discussed as

potential REE deposits that could counterbalance the Chinese market and production (Jepson, 2012).

Steenkampskraal (SKK) and Zandkopsdrift are located in the provinces of the Western Cape and Northern Cape respectively (Jepson, 2012). SKK is a monazite based resource and was formerly operated by Anglo American South Africa between 1953 and 1963. The operational activity at this mine was mainly focused on the extraction of thorium (Th) that was back in time exported to the United Kingdom where it was used as nuclear fuel. During that time, the small amount of REEs associated with the mining of Th were considered as by-products although this was enough to make South Africa the earliest leader in terms of REEs production (Jepson, 2012). However, the use of uranium (U) as fuel in nuclear plants strongly reduced the demand of Th and consequently the SKK mine was shut down. Years later, as the market of REEs grew due to their extensive applications in many industries, there was a need to reopen this mine. Two attempts to reopen were made in 1997 and 2008 respectively. Unfortunately, both attempts failed due to depressed prices of REEs, which was the main concern in 1997 and 2008 (Jepson, 2012). Two years after, the Canadian company, Great Western Mineral Group Ltd (GWMG) made a substantial investment between 2011 and 2015 to bring the mine into production. Compared to other mining investments in which the GWMG was involved in, the SKK project seemed to offer interesting advantages as a formerly active mine. Mineral investigations by mineral resource estimation (MRE) of Canada at SKK confirmed that the Nd grade, on its own counted 2.58 % followed by 0.74 % for Pr, 0.14 % Dy and 0.03 % Tb. The combined grade of these four REEs is usually utilised to make magnets. Therefore, the combined grade of about 3.49 % present at SKK mine is higher than the total REEs grade of most of other REE deposits.

According to the MRE, the SKK deposit has an estimated lifetime of about 30 years and annual production of 2700 tons. Compared to other existing REE producers around the world such as Baotou (China), SKK is relatively small. However, the

market of REEs envisaged by the GWMG at SKK was considered interesting and noteworthy in the way that this project was a fully integrated complete supply chain outside of China. However, the GWMG project at SKK hit serious financial problems in early 2015, and the mine is currently owned by the Steenkampskraal Holdings Ltd. (SHL) since July 2015, operating as Steenkampskraal Thorium Limited (STL), a South African company with much emphasis on the extraction of Th rather than REEs (Blench, 2018).

Similar to SKK, Zandkopsdrift mine was also previously explored by Anglo American Corporation of South Africa until its acquisition in 2008 by Frontier Rare Earths, a mineral and development company focusing mainly on REEs. In December 2012, Frontier completed its definitive joint venture agreement with the Korea Resources Corporation (KORES) in relation to the development of Zandkopsdrift. The government of South Korea also designated REEs as strategic raw material for Korea's future economic growth and selected Zandkopsdrift as a prime source of their REEs supply. Under their agreement, KORES was expected to acquire an initial 10 % off-take of REEs production at the Zandkopsdrift with an open option to increase it up to 50 % depending on the definitive feasibility study of the Zandkopsdrift project (Jepson, 2012). KORES was wholly owned by the government of Korea and aimed to become the global top 20 mining company by 2020. Frontier aimed to be the early, significant and low cost producer of separated REEs from La to Dy plus Y at purities between 99 % and 99.999 %. The annual production target was set at about 20, 000 tons of separated REOs and was expected to start in 2018.

Compared to the SKK, Zandkopsdrift is a carbonatite-based deposit presenting greater technical difficulties in terms of extraction and separation that requires high costs. Despite these difficulties, this mine is a promising REE project development with its expected output of about 20, 000 tons a year as per 2015 estimations making it potentially one of the largest mines outside China. This deposit has a fairly high proportion of critical REEs such as Eu although its relatively low mineral grade is

a big issue compared to SKK. Furthermore, Th content is much lower at this deposit than at SKK mine (Jespon, 2012).

2.5 Minerals of REEs

REEs rarely form a continuous ore body but usually occur in a variety of accessory minerals such as carbonates, fluorides, phosphates and silicates; and in nature as part of the host mineral, and do not exist as native elemental metal. This is why their recovery is generally achieved through complex processing methods in order to break down the REE bearing mineral (Charalampides et al., 2015). Despite that, over 200 REE bearing minerals have been identified up to date, only three of them are economically exploitable and feasible for the extraction of REEs. These are bastanaesite, xenotime and monazite (Jordens et al., 2013, Charalampides et al., 2015). Bastnaesite is a carbonate-based mineral which is generally classified in three subgroups based on its chemical composition namely: bastnaesite (Ce), bastnaesite (La) and bastnaesite (Y) with respective formula of (Ce) CO_3F, (La) CO_3F and (Y) CO_3F. Bastnaesite minerals are mostly found in China (Bayan Obo mine) and in the United States (Mountain Pass mine). Similarly, to bastnaesite, monazite also has three subgroups depending upon the proportion of REE content namely monazite (Ce), monazite (La) and monazite (Nd). Unlike bastnaesite, monazite is a heavy mineral, which contains about 30 % and 1 % of thorium (Th) and uranium (U), respectively. The high proportion of these radioactive elements is a major concern and generally complicates the beneficiation process of REEs from this mineral. Xenotime is also one of the most commercially viable resource of REEs which is generally found as a phosphate based mineral phase containing mostly yttrium (Y) phosphate. This mineral contains about 60 % of REOs from which most of the elements are heavy REEs and are usually found associated with a minor proportion of monazite (Jordens et al., 2013).

2.6 Applications of REEs

REEs are not substitutable for some specific applications since each individual REE usually displays a unique characteristic. This has resulted in a criticality classification that is based on their importance, lack of comparable and reliable substitutes and the monopolisation of the supply (Golev et al., 2014). The earliest application of REE was traced back in the 1890s in Vienna, with the commercialisation of the first mantles for gas lighting, which consisted of a mix of REO and other metals (Szabadvary, 1988). More than a decade later, in 1903 still in Vienna, Carl Auer patented an alloy called "Auermetal" in which Ce and Fe were utilised for lighter flint (Massari & Ruberti, 2013). However, Eu was the first REE used in pure form as active component of the red cathodoluminescent phosphors in colour television screens (Binnemans & Jones, 2015).

Nowadays, the fields of application for REEs are extensive and mainly include automotive, nuclear, metallurgical, catalytic, electronic, electric, magnetic, and optic. REEs are also used in green technologies such as wind power, efficient lighting, and plug-in hybrid electric vehicles. REEs are also strategic for advanced applications in the military field (cruise missiles, night-vision goggles and other weapons). In the automotive industry, REEs are used mostly to build high efficiency and long lasting catalysts, Nd super-efficient magnets for electric motors, superlight and long lasting La-NiMH batteries (Massari & Ruberti, 2013). Table 2.2. gives some REEs and their main applications reported between 2017 and 2018. It was found that Nd was the most critical REE followed by Tb and Dy. From their initial time of discovery and extraction, the use of REEs has been developing from mischmetal used in lighter flints to high purity separated REE metals that are used in advanced applications. This has resulted in a significant growth in terms of the demand of REOs. For example, in 2000, about 75,500 tons have been reported compared to 123,100 tons in 2016 (Goodenough et al., 2018). In 2017, the total use of REEs based on different applications was estimated at 167,500 tons (Table 2.3.). Of this amount, magnets dominated the global REE utilisation by weight and value

with about 51,000 tons followed by metal alloys and catalyst with 31, 000 tons and
30,000 tons respectively (Mancheri et al., 2019).

Table 2.2: Some applications of REEs and their criticality level between 2017 and
2018 adapted from Binnemans et al., (2018).

REEs	Criticality level	Main applications
La	None	NiMH batteries, catalysts, green lamps phosphors, optical glasses.
Ce	None	Catalysts, polishing compounds, decolorizing agent, Ce-doped glass
Pr	None	Ceramic pigment, decorative glass
Nd	Highest	Nd-Fe-B permanent magnets
Sm	None	Sm-Co permanent magnets
Eu	None	Lamp phosphor
Gd	None	Additive in Nd-Fe-B magnets, Green lamps phosphor
Tb	High	Green lamp phosphor
Dy	High	Additive in Nd-Fe-B permanent magnets
Lu	Low	Medical imaging
Y	Low	Red lamp phosphor, ceramics

Table 2.3: Global demand of REEs by application in 2017 adapted from Mancheri
et al., (2019).

Applications	Amounts (tons)
Magnets	51,000
Metals alloys	31,000
Catalysts	30,000
Polishing	22,000
Glass	9,500
Ceramics	8,500
Phosphors and pigments	5,000
Others	10,000
Total	**167,500**

2.7 Market trading of REEs

The REEs are generally traded as REOs and their prices have been quite volatile for the past decades. The percentage of purity for a single element in these REOs is usually requested based on the applications where either four nine (99.99 %) or five nine (99.999 %) purity is needed (Massari & Ruberti, 2013). The average prices of REOs shot up from about 18 $/Kg to 270 $/Kg in 2011. However, the price fell back to 18.5 $/Kg in 2015 and 7.5 $/Kg in 2017. This falling of the prices for REO was previously attributed to an oversupply (Ganguli & Cook, 2018). It is known that an increased demand for a specific single REE causes an overproduction of less demanded REEs resulting in repricing of other REEs to balance the market (Golev et al., 2014). There are globally less than twenty companies that are currently trading the REEs. Of these few companies, Canada leads with about five (Avalon Rare Metals, Great Western Minerals, Material Technologies, Rare Elements Resources, VMS Ventures). China occupies the second position with four companies (Baotou Steel Rare Earths Hi-Tech, China Rare Earths Holdings, Jiangxi Copper, Aluminium Corporation of China) followed by Australia (Alkane resources, Arafura Resources, Lynas Corporation) and Russia (JSC Sevredmet, Solikamsk Magnesium Works, Irtysh Rare Earths) which have three companies each; India has two companies (Indian Rare Earths, Kerala Minerals & Metals); one in Japan (Showa Denko) and finally one in the US (Molycorp) (Massari & Ruberti, 2013; Seeking Alpha, 2011). However, amongst the aforementioned producers, the Chinese Baotou Steel Rare-Earths Hi-Tech is the largest producer of REOs in the world (Massari & Ruberti, 2013). Recent prices of some REEs in pure form (metal) and their respective oxides recorded between December 2020 and May 2021 are shown in Table 2.4. The REEs such as Ho, Tm, Yb and Lu as well as their respective prices were not available. It can be seen from the tabulated prices that Gd and Sc metals and oxides had the highest prices followed by Tb and Er among all the REEs and in particular the HREEs. LREEs have the lowest prices for both metal and oxides forms.

Table 2.4: REE prices between December 2020-May 2021 (US $/ Kg)

LREEs	Purity	Dec 2020	May 2021	HREEs	Purity	Dec 2020	May 2021
La	> 99 %	4.12	4.27	Eu_2O_3	> 99.5 %	30.38	29.66
La_2O_3	> 99.5 %	1.27	1.41	Gd	> 99.9 %	20, 010	20, 010
Ce	> 99 %	3.98	4.56	Gd_2O_3	> 99.5 %	25.75	27.85
CeO_2	> 99.5 %	1.37	1.45	Tb	> 99.9 %	1,320	1,382
Pr	> 99 %	81.73	102.7	Tb_4O_7	> 99.9 %	470.1	1,150
Pr_2O_3	> 99.5 %	52.44	77.76	Dy	> 99 %	355.9	470.1
Nd	> 99 %	89.69	94.8	Dy_2O_3	> 99.5 %	280.6	368.9
Nd_2O_3	> 99.5 %	73.42	78.41	Er	> 99.9 %	268.2	800
Sm_2O_3	> 99.9 %	1.95	1.66	Er_2O_3	> 99.5 %	24.59	31.46
				Y	> 99.9 %	29.66	31.10
				Y_2O_3	> 99.99 %	2.97	5.14
				Sc	> 99.99 %	520,260	520,260
				Sc_2O_3	> 99.99%	46,200	56,610

Adapted and modified from https://mineralprices.com/rare-earth-metals (access on the 28.07.21)

2.8 REE supply

The REE supply and availability are described to be at risk due the current state of affairs, where China has been controlling over 90 % of REE production worldwide (Golev et al., 2014). It is historically known in respect of the mining of important metals around the world that a much lower level of market concentration can harm manufacturing firms. For example, the Democratic Republic of Congo (DRC) formerly the republic of Zaire had a control of about 48 % of cobalt supply in 1978 worldwide. Yet, political unrest in the DRC resulted in a disruption to global supply that was known as the "Cobalt Crisis" which affected many firms in the world (Charles, 1977, Alonso et al., 2012). To alleviate the shortage of REEs and balance the supply, search for new and mineable REE resources outside China or reopening of former REE mines were suggested. However, searching for new REE deposits or reopening formerly existing REE mines is economically costly. Therefore, alternative sources of REEs to compensate both the current scarcity and cost associated with the conventional mining is needed as the use of REEs is expected to increase and will affect several innovative areas for future decades (Seredin et al., 2013; Canovas et al., 2019).

Recently, studies have been carried out to investigate the feasibility for the extraction of REEs through the recycling of low value waste streams such as bauxite residue, mine tailings, phosphogypsum, slag and waste waters (McLellan et al., 2013; Bandara et al., 2014; Binnemans et al., 2013a, 2013b; Tunsu et al., 2015; Innocenzi et al., 2014). Among the aforementioned waste streams, phosphogypsum (PG) has been identified as a promising secondary source of REEs due to the high content of these elements (Table 2.5.) (Canovas et al., 2017; Kulczycka et al., 2016; Rychkov et al., 2018). Although the concentration of REEs in PG is far lower compared to primary REE bearing minerals such as monazite (Bruckner et al., 2020), the large volumes of PG produced worldwide which is currently estimated to be 200–300 million tons per annum make it a potential source of REEs (Masmoudi-Soussi et al., 2019). Furthermore, the extraction and recovery of REEs

from PG has several advantages over the conventional mining such as the costs for mining and its related infrastructure that are almost absent (Bruckner et al., 2020). The following sections therefore give an overview of PG produced from phosphoric acid processing using sulfuric acid.

Table 2.5: Total REE content from various recycling waste streams (ppm)

Waste streams	Total REEs	REEs available	References
Acid mine drainage	1.43	La, Ce, Pr, Nd, Sm, Eu, Gd, Tb, Dy, Ho, Er, Tm, Yb, Lu	Li et al., (2017)
Fly ash	597	La, Ce, Pr, Nd, Sm, Eu, Gd, Tb, Dy, Ho, Er, Tm, Yb, Lu, Y	Pan et al., (2018)
Mine tailings	5,299	La, Ce, Pr, Nd, Sm, Eu, Gd, Tb, Dy, Ho, Er, Tm, Yb, Lu, Y	Peelman et al., (2018)
NdFeB Magnet	305	Pr, Nd, Dy	Hoogerstraete et al., (2014)
NiMH batteries	340	La, Ce, Pr, Nd,	Maroufi et al., (2014)
Phosphogypsum	5,556	La, Ce, Pr, Nd, Sm, Eu, Gd, Tb, Dy, Ho, Er, Tm, Yb, Lu, Y, Sc	Binnemans et al., (2015)
Phosphor	127	La, Ce, Eu, Gd	Innocenzi et al., (2018)

2.9 Production of phosphogypsum

Phosphate ores, in particular fluoro-apatite are the main feedstock used in a wet process of phosphoric acid (Preston et al., 1996). The reaction stage involves a concentrate of the mineral apatite which is dissolved in a mixture of sulfuric acid (H_2SO_4) to produce phosphoric acid along with other products as described in equation 2.1.

$$Ca_{10}(PO_4)_{6\,(S)}F_2 + 10\,H_2SO_{4\,(a)} + 20\,H_2O_{(a)} \rightarrow 6\,H_3PO_{4\,(a)} + 10\,CaSO_4 \cdot 2H_2O_{(S)} + 2HF_{(a)}$$ Equation 2.1
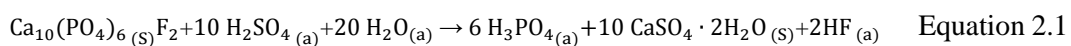
As can be seen in equation 2.1, the main by-product associated with this process is calcium sulfuric hydrate commonly known as gypsum or phosphogypsum (PG)

27

(due to its nature of production) (Habashi, 1985). PG is highly acidic with pH around 1 due to residual acid from phosphoric acid processing, but this acidity usually decreases by dewatering and weathering (Rashad, 2017). Two types of PG namely PG-dihydrate (PGDH) and PG-hemihydrate (PGHH) can be obtained depending upon the process that can be adopted to produce phosphoric acid. These two forms basically differ according to the hydration degree of calcium sulfate which is the main mineral phase of PG (Wu et al., 2018). However, phosphoric acid processing associated with the production of PGDH as described in equation 1, has been the most world widely used in recent years compared to a few processes where PGHH is produced (Wu et al., 2018). In general, for each ton of phosphoric acid produced, approximately 1.7 tons of PGDH can be produced as precipitate (See equation 2.1). Up to date more than a billion tons of PG has been generated and generally stockpiled on land worldwide leading to landfill issues (Li et al., 2008). The main environmental concerns associated with the production of phosphoric acid are the stockpiles of PG, which usually exceed the mass of the product (Binnemans et al., 2013). PG is therefore the main by-product and its environmental concerns include fluorine uptake, ground and surface water pollution and emission of gaseous and radioactive elements (Rutherford et al., 1995; Koopman & Witkamp, 2000; Binnemans et al., 2013).

2.10 Mineralogical and elemental composition of phosphogypsum

The mineralogical composition of phosphate ore is mainly dominated by fluorapatite [$Ca_{10}F_2 (PO_4)_6 \cdot CaCO_3$], quartz and goethite, with minor amounts of other minerals such as magnetite, monazite, barite and anatase; heavy metals and trace elements such as nickel and cadmium; REEs and radioactive elements (uranium and thorium) (Tayibi et al., 2009). The nature and characteristics of the PG produced is strongly influenced by the composition and quality of phosphate ore. Thus, PG is mainly composed of $CaSO_4 \cdot 2H_2O$ but also contains impurities such as $Ca(H_2PO_4)_2 \cdot H_2O$, $CaHPO_4 \cdot 2H_2O$, $Ca_3(PO_4)_2$ and H_3PO_4 and other residual acids; fluorides (NaF, Na_2SiF_6, Na_3AlF_6, Na_3FeF_6 and CaF_2); sulfate ions, trace

28

metals such as Cr, Cu, Zn and Cd; REEs and organic matter as aliphatic compounds of carbonic acids, amines and ketones (adhering onto the surface of gypsum crystals) (Tayibi et al., 2009; Rutherford et al., 1996). Of the aforementioned impurities, the concentration of REEs vary between 0.01 and 0.6 wt% (Table 2.6.) (Binnemans et al., 2015; Lambert et al., 2018). However, REE content also depends upon both the source of phosphate ores and the processing method. For instance, in a process where PGHH is produced, about 90–95 % of the REEs can be transferred to PG whereas only 70–80 % are transferred in the PGDH process (Koopman & Witkamp, 2000; Wu et al., 2018). The present study will mainly focus on PGDH since the phosphoric acid processing associated with the production of PGDH is common.

Table 2.6: REE content from various type of PG (Adapted from Wu et al., 2018)

Origin	Type of phosphogypsum	REO content (% wt)	References
America	DH	0.034	Al-Thyabat et al., (2015)
Belgium	DH+HH	0.55	Li et al., (2008)
Brazil	DH	0.52–0.54	Santos et al., (2006)
Canada	DH	0.02	Walawalkar et al., (2016)
Egypt	DH	0.048	Ismail et al., (2015)
Poland	DH+HH	0.11–0.65	Kulczycka et al., (2016)
Russia	DH	0.47	Lokshin et al., (2013)
Russia	HH	0.40–0.43	Lokshin et al., (2013)
Russia	HH	0.59	Lokshin et al., (2013)
Russia	HH	0.11	Kybartiene et al., (2016)
Russia	HH	0.46	Kybartiene et al., (2016)
Russia	DH+HH	0.3–0.9	Samonov et al.,(2011)
Tunisia	DH	0.022	Hammas-Nasri et al., (2016)

DH: dihydrate

HH: hemihydrate

2.11 Disposal and utilisation of phosphogypsum

There are generally two main routes that exist for the disposal of PG worldwide, the dry and wet technique, the latter being the most common (Fuleihan et al., 2012; Tayibi et al.,2009). In the dry technique, PG is separated from the phosphoric acid by filtration and is disposed using conveying belts or truck. In contrast to dry disposal, the wet processing consists of slurring and pumping the PG filtered cake with waste water from phosphoric acid processing into settling ponds near the acid plant (Fuleihan et al., 2012; Tayibi et al.,2009). The disposal of PG requires large land areas where it can be stacked. In some countries where phosphoric acid is produced such as Morocco, Mexico, Tunisia and South Africa, the PG is directly poured into the ocean (Fuleihan et al., 2012). In attempts to utilise such huge amounts of PG, several studies have focused on transferring it into building materials, ammonia fertilizer and soil amendments (Oliveira et al., 2012). However, of over 85 % of PG annually generated worldwide only 15 % is utilised in the aforementioned recycling processing (Romero-Hermida et al., 2019). This is mainly due to some specific limitations of impurities such as radioactive and REEs elements presents in it (Masmoudi-Soussi et al., 2019).

2.12 REE occurrence in phosphogypsum

A few studies have discussed the phases in which REEs occurred in PG but their conclusions varied depending on the source of the PG (Dutrizac, 2017; Borges et al., 2016; Yang et al., 2019). From these studies, it was found that REEs usually occurred in four main phases namely as carbonates, phosphates, fluorides, and sulphates. The first two phases are usually referred as associated phases and the last two as replacement phases for calcium in the crystal lattice structure of PG. The REEs occurring in carbonates and phosphates are readily soluble in inorganic or organic solutions while those in replacements phases require treatment processes to increase both chemical and physical reactivity of PG (Costis et al., 2019). However,

apart from these phases, REEs can also be found as adsorbed ions in PG. The REE occurrence in PG was recently investigated by Yang et al., (2019) by combining the mineral liberation analysis (MLA) and electron microprobe analysis (EMA) for mineral analysis and ICP-MS for elemental composition. Their results showed that gypsum ($CaSO_4$) was the dominating mineral phase in PG that was carrying over 72 % of REEs presents in the samples.

2.13 REE beneficiation from phosphogypsum

Physical and chemical pre-treatment methods have been used to upgrade the low concentrations of REEs presents in PG prior to hydrometallurgical processing (Yang et al., 2019; 2019a). Yang et al., (2017), conducted physical enrichments of REEs from PG using flotation, mechanical grinding techniques and their results revealed that REE concentration was improved from an initial grade of 0.13 to 7.3 wt%. In another trial, the authors used centrifugal ball milling at 30, 60 and 90 min prior to leaching in a suspension of HCl or HNO_3. Their results clearly showed that the milling had a significant effect on the extractability efficiencies of REEs as, in the samples milled, the extracted REEs increased for all the REEs as the milling time increased. According to these authors, this increase was attributed to the increase of the specific area and decrease in virtual activation energy of the ground material due to interior crystal defects. However, the recovery of individual elements differed because REEs in PG are carried by the gypsum mineral phase which was not completely enriched by the aforementioned physical methods. Therefore, the loss of REEs during the beneficiation process mainly resulted from the portion that remained in the gypsum. Similarly, Rychkov et al., (2018) applied grinding and ultrasonic treatment simultaneously in an attempt to reduce the particle size of PG to between 6 and 8 µm while adding a strong acid cation exchange resin (Purolite C-160) directly to the H_2SO_4 leaching solution, the REE recovery was found to increase by a factor of 4. The proposed process was able to increase REE recovery from 15 % to17 % to over 70 % by physical and chemical reactivity of the PG, which also led to a PG product containing less impurities. Microwave radiation

has also been used by Reid et al., (2017) and Lambert et al., (2018) for enrichment of PG. It was found that microwaving PG resulted in dielectric heating of water molecules present in PG crystals causing the formation of pores in the PG matrix as the water vapour escaped. Chemical enrichment was also reported by Hammas-Nasri et al., (2019). In their study the PG was treated consecutively with solutions of NaCl and Na_2CO_3 in an attempt to enrich the PG with REEs in the final residue prior to the leaching process. The methods consisted of washing PG with 25 or 60 g/L saline Na_2CO_3 solutions, resulting in approximately 81 % and 84 % increased rates of enrichment respectively.

Despite the fact that physical and chemical treatments of PG are promising approaches towards high leaching efficiencies of REEs, they involve additional costs which might compromise the process particularly at large scale. To overcome this, PG could be treated directly through hydrometallurgical processing without physical and chemical pre-treatments due to its smaller particle size (Jordens et al., 2013; Tunsu et al., 2015; Tayibi et al., 2009; Romero-Hermida et al., 2019). Leaching is the first step in a hydrometallurgical process in which the operational parameters such as agitation speed, contact time (residence time), particle size, solid to liquid ratio (S:L), lixiviant type, and temperature are usually varied to obtain optimum conditions (Binnemans et al., 2013; Jyothi et al., 2020). The leaching of PG is mainly possible as most REEs occur as adsorbed secondary phases onto the surface of PG. This surface adsorption suggests that REEs should be relatively susceptible to be extracted through aqueous chemical agents such as inorganic or organic liquids, compared to a case where REE are found incorporated within the crystal lattice of PG (Antonick et al., 2019). A few recent studies in which some of the aforementioned parameters have been varied and the corresponding REE leaching efficiencies are tabulated in Table 2.7.

Table 2.7: Leaching efficiencies of REEs from PG using various leaching agent

Approach	REE content (wt%)	Lixiviant	S:L ratio	Time (h)	Temperature (°C)	Efficiency (%)	References
Inorganic acid leaching	0.041	15 % H_2SO_4	1:3	2	100	60	Masmoudi-Soussi et al., (2019)
	0.035	3 M HNO_3	1:30	8	25	85	Canovas et al., (2019)
	0.17*	2.5 % HNO_3	1:7.5	0.25	25	59	Laurino et al., (2019)
	0.032	1.5 M HCl	1:15	1	85	Nd: 80 Dy: 99 Y: 99	Lambert et al., (2018)
	2.6	H_2SO_4	1:6	4.3	275	95	Brückner et al., (2020)
	0.19	0.01 M H_2SO_4	1:20	20-22	24	15	Laurino et al., (2019)
	0.44	10 % H_2SO_4	1:3	20	2	52	Grabas et al., (2019)
	1.7	1g/L H_2SO_4	1:8	24	-	45-75	Virolainen et al., (2019)
	0.44	10–30 % H_2SO_4	1:7.5	2	50	72	Rychkov et al., (2018)
	0.022	10 % H_2SO_4	1:1.3	1-2	60	50	Hammas-Nasri et al., (2016)
	0.020	1.5 M HCl				51	
		1.5 M H_2SO_4	1:8	0.33	80	23	Walawalkar et al., (2016)
		1.5 M HNO_3				57	
	0.042	36 % HNO_3	1:4	1	72	58	Al-Thyabat et al., (2015)
	0.034	90 % H_2SO_4+10 % H_3PO_4	1:6.7	1	72	49	
	0.048	3 M HNO_3	1:2	3	25	43	Ismail et al., (2015)
		2 M HCl				12	
		4 M H_2SO_4				13	
	0.048	1 M $C_6H_8O_7$	1:5	0.25	85	83.4	Gasser et al., (2019)
Organic acid leaching	0.040	0.7 M TBP–0.9 M TOPO 0.5 M Na_2CO_3+ TPB-TOPO	1:1	2	55	70	El-Didamony et al., (2012; 2013)
			1:1	2	55	80	
Bioleaching	1.3	Spent medium (*Gluconobacter oxydans,* 220 mM gluconic acid) Gluconobacter oxydants NRRL, B85	1:50	24	25	Y: 91.2 Ce:36.7 Nd: 42.8 Sm: 73.2 Eu: 50 Yb: 83.7	Antonick et al., (2018)

33

2.13.1 Direct leaching

As can be seen in Table 2.7, strong inorganic acids such as H_2SO_4, HCl and HNO_3 are the most commonly used lixiviants in direct leaching of PG due to their strength and availability (Wu et al., 2018). In general, H_2SO_4 leaching is economically advantageous due to its much lower cost (Binnemans et al., 2015). However, the key obstacle encountered with direct H_2SO_4 leaching of PG for REE extraction, is the inefficient diffusion of proton, sulphate ions and REE ions between the layers of calcium sulphate crystals to which calcium ions are tightly bonded. This effect is attributed to low solubility of PG in H_2SO_4 solution resulting from the common-ion effect (Walawalkar et al., 2016). For instance, under normal conditions of temperature and pressure, only low leaching efficiencies ranging from 12–40 % have been attained using H_2SO_4 (Wu et al., 2018). Liang et al., (2017) studied the extraction of REEs from PG generated at Mosaic Co. in Florida using 5 % H_2SO_4, at S:L ratio of 1:4 at a temperature of 50 °C and 120 min of residence time. Their results showed that a maximum leaching efficiency of 43 % REE was obtained with increased contact time and S:L ratios. However, the leaching of the impurities such as U, F and P also increased. In order to enhance the leaching efficiency, a few other approaches have been considered. Hammas-Nasri et al., (2016) conducted a study on REE recovery from PG using a double H_2SO_4 leaching steps. Their results showed a high enrichment of REEs of about 86 % in the crystallised solid obtained from the evaporation of the second leachate, which was a mixture of anhydrite-monetite ($CaSO_4$-$CaHPO_4$) phases. Notwithstanding the enrichment of REEs obtained in this approach, the evaporation process was energy consuming when considering scaling up the process. This is because, the evaporation of the leachate exerts a beneficial influence on the isolation of REEs from PG but the incurred costs related to heating of the solution dominates among the production costs rendering the process unprofitable. Lokshin et al., (2010) extended the leaching time to several weeks in an attempt to increase the REE extraction efficiency using a H_2SO_4 solution. In their investigation, PG was leached with H_2SO_4 for 3025 h (18 weeks)

34

using a S:L ratio of 1:2. However, the leaching efficiency of REEs only increased by 3 times compared to the case where 1 h leaching was used under the same conditions. Other methods such as that developed at Prayon SA in Belgium, consisted of extracting the REEs from PG using diluted H_2SO_4 solution while stirring the suspension at a high speed of 6000 rpm to enhance the leaching efficiency (Binnemans et.al, 2015). Valkov et al., (2014) developed a method consisting of bubbling air into the H_2SO_4 pulp of PG at a temperature of 70–100 °C for 1–2 h S:L of 1 to increase the leaching efficiency but no percentage was given.

Similar to H_2SO_4, the leaching of REEs from PG was also found to be moderately low with HCl. The low leaching of HCl was mainly attributed to the relatively low solubility of calcium sulphate in HCl solution because of the salt out effect that is associated with this process (Walawalkar et al., 2016). HNO_3 leaching of REEs from PG seems the most efficient compared to H_2SO_4 and HCl due to the relative higher solubility of PG (calcium sulphate) in HNO_3 solution (Walawalkar et al., 2016; Ismail et al., 2015). The leaching efficiency of REEs with HNO_3 can reach up to 50 % when using low S:L ratio. A study conducted on Egyptian PG by El-Reefy et al., (2008) using 2.0 M HNO_3 for 8 h residence time and varying the S:L ratios showed that the leaching efficiency of REEs increased with increasing S:L ratio. Similar patterns were observed in another study where the temperature effect was investigated (Ismail et al., 2015). Lokshin et al., (2002), reported a high leaching efficiency of REEs up to 90 % using 15 wt% HNO_3 concentration and S:L ratio 1:10. It was found that with high S:L ratio, the leaching efficiency of REEs increased when increasing the concentration of HNO_3 below 15 % wt and decreased gradually with continuously increasing the concentration from 15 % wt and above. However, while leaching REEs and calcium ions from PG obtained at Agrium fertilizer plant, only a slight improvement of 6 % on the leaching efficiency of REEs and 29 % for calcium were reached when increasing the HNO_3 concentration from 1.5 M to 3.0 M (Walawalkar et al., 2016).

Despite that HNO_3 showed moderately high leaching efficiency compared to HCl, the latter is more economical and can be potentially considered as a better leaching agent of REEs from PG from an industrial point of view (Walawalkar et al., 2016). Although a few moderate REE leaching efficiencies have been reported through direct leaching of PG, so far these methods have been deemed uneconomical especially for larger scales (Salo et al., 2020). Furthermore, due to the limited solubility of PG, dissolving it completely in an attempt to recover only REEs is neither economical nor practical feasible as the concentration of REE to be extracted is low (Yahorava et al., 2016). Therefore, exploring technologies that involve indirect leaching of REEs such as carbonation and recrystallization of PG for production of materials that have commercial and industrial utilization with subsequent extraction of REEs is advisable.

2.13.2 Indirect leaching

In contrast to direct leaching, indirect leaching refers here to processes that consist of modifying the microstructure of PG into materials that could find commercial and industrial applications while releasing locked REEs. Processes such as carbonation and recrystallization of PG offer good potentiality to achieve such an approach. Applying such processes can render the extraction of REEs more economical and attractive due to high REE content in PG estimated at about 21 million tons as well as saleable products that can be obtained for industrial and commercial utilisation (Yahorava et al., 2016). Therefore, the following sections mainly discuss the development that has been achieved so far in respect of the aforementioned approaches with a particular attention on the mild acid dissolution and recrystallization of PG for the fabrication of calcium whiskers and subsequent recovery of REEs from PG.

2.13.2.1 Carbonation of phosphogypsum

The carbonation process is one of the approaches that can be explored for the valorisation of PG by converting it to calcium carbonate ($CaCO_3$). The conversion process as indicated in equation 2.2., generally involves the utilization of ammonium carbonate and has been widely described in the literature (Mulopo & Ikhu-Omoregbe, 2013; Kolokolnikov & Kovalev, 2009; Mattila & Zevenhoven, 2015; De Beer et al., 2014).

$$(NH_4)_2CO_3 + CaSO_4 \rightleftharpoons (NH_4)_2SO_4 + CaCO_3 \hspace{3cm} \text{Equation 2.2}$$

Pure $CaCO_3$ can be used in a wide range of commercial and industrial applications such as the manufacturing of concrete (Portland cement) and production of lime (soil stabilization and acid neutralization), water treatment and flue gas desulfurization (Mattila & Zevenhoven, 2015; Kandil et al., 2017). $CaCO_3$ produced from PG processing has been found to be richly concentrated in REEs originally present in the PG waste (Kolokolnikov et al., 2009; Safiulina et al., 2015). This processing is therefore, considered as an interesting method of up-concentrating REE prior to their recovery through dissolution of $CaCO_3$ using mineral acids followed by extraction (Binnemans et al., 2013; Kolokolnikov et al., 2009). Masmoudi-Soussi et al., (2019) recently developed a hydrothermal method that consisted of converting PG to $CaCO_3$ using a high-pressure and high-temperature Parr-reactor. Prior to the conversion, PG was washed with salt water (NaCl/ 25 g/l). The results were obtained at 80–100 °C for 2 h, and showed that the hydrothermal conversion was effective and led to a complete conversion of the sulphate matrix of PG to the corresponding carbonate, which was enriched in REEs at a rate of 66 %. The authors indicated that the enrichment was related to the insertion of the REEs into the gypsum matrix by replacement of calcium ions in the PG as well as the known affinity of REEs towards carbonates in an alkaline pH. The leaching of the obtained carbonate using HCl solution (5–6 %) at 80–90 °C for an hour in the presence of ascorbic acid as a reducing agent, allowed the migration of about 89 % of REEs to the acid liquor (Masmoudi-Soussi et al., 2019). In a

parallel approach, the obtained calcium carbonate can also be dissolved in nitric acid or calcined prior to leaching of REEs with ammonia chloride (Binnemans et al., 2015). Although, the carbonation of PG demonstrated interesting improvement in terms of REE extraction, the main disadvantages remain the high reagent cost and energy consumption as well as the limited market for calcium carbonate and ammonia sulphate, which is a common by-product in this process (Yahorava et al., 2016).

2.13.2.2 Dissolution and recrystallization of phosphogypsum

REEs do not isomorphously co-crystallize with the lattice structure but rather exist in separate phases offering a good opportunity in terms of REE extraction and recrystallization of technically pure PG (Genkin et al., 2017). Although the dissolution and recrystallization of PG is an emerging area of research only a few studies have focused on a combined process of recrystallization and subsequent REE recovery (Koopman & Witkamp, 2000; Valkov et al., 2014; Walawalkar et al., 2016). In view of this approach, a few trials have been performed both at laboratory scale and larger scale. Genkin et al., (2017) described a process where PGDH was recrystallized in the presence of calcium nitrate (in terms of Ca^{2+}) under acidic medium (0.2–8 M, in terms of H^+). Subsequent to this method, REEs reported to the leaching solution. In this process, the solvent extraction method was suggested for subsequent recovery of REEs and further processing. Nevertheless, the proposed process was found to be unattractive from an economical and waste management point of view. Furthermore, although increased concentration of Ca^{2+} ions was favourable in terms of REE recovery, this increase made the formation of the targeted and purified PG less favourable. Another approach described by Koopman & Witkamp (2000), consisted of introducing an ion-exchange resin for the extraction and recovery of REEs leached out during the dissolution and recrystallization of PGHH to PGDH. Their results revealed that the amount of REEs released during this process was up to 53 %. The authors indicated that REE extraction efficiency was mainly influenced by the recrystallization reaction but

individual REEs that had a strong affinity to PGDH crystal lattice were least extracted. The main disadvantage of this process was that, the sulfonic acid resin also extracted calcium ions besides having a preference for trivalent REEs. A method developed at "Mintek" in South Africa by Yahorava et al., (2016) consisted of hydrothermally treating PG containing slurry using an autoclave for the recrystallization of PG and REE extraction. The process was tested on various PG samples and showed that REE recoveries were improved from 5 to 80 % while recrystallizing the PG. Although the process carried a large potential for unlocking valuable REEs encapsulated in PG stock piles, there were still several parameters such as residence time in the autoclave, impact of seeding and solids content which required verification and optimization. Moreover, even though the process claimed to be "chemical free", temperatures of up to 100 °C were required in the autoclave for high release of REEs during the recrystallization process. Similarly, the method developed at "Integra.Ru" Co Ltd in Russia by Kanzel et al., (2017) consisted of decomposing PG while extracting released REEs using sulphuric acid in five consecutive stages. The resulting solid residue (cake) was technically a gypsum that could be used in the production of building materials (e.i. binders) and the liquid waste which was technically an industrial water contained high concentrations of REEs. However, the production of gypsum from PG in such a process is an energy intensive process since the PG binder is burned at higher temperatures than are traditionally used to obtain a binder from natural gypsum stone, hence making the proposed process economically unprofitable, particularly when considering large scale processing (Bouchhima et al., 2017; Campos et al., 2017; Demirel & Caglar, 2017).

The production of calcium sulfate whiskers (CSWs) from PG due to high content of $CaSO_4$ is also an emerging area of research and has been recently discussed (Sheng et al., 2018; Sun et al., 2016). CSWs have been widely used for several applications such as reinforcing materials in plastics, paper mills, rubbers, grafting materials in bone and tissue regeneration, filters, paints and other products (Miao et al., 2015; Qi et al., 2017). So far, efforts in this area have been made following

three directions namely: the synthesis, modification of the crystal morphologies using additives, and the application of CSWs for constructional materials (Wang et al., 2017). Sun et al., (2016) synthesised CSWs from flue gas desulfurization gypsum using atmospheric acidification method. The influence of the concentration of acid (HCl) and leaching temperature on the morphology of CSW was discussed. The results showed that the obtained CSW had high purity and high whiteness and their width and aspect ratio range from 3 to 22 µm and 25 to 80 respectively. CSWs with length diameter ratio of 10 to 100 and 50 to 80 have been also reported (Du & Huang, 2014). However, little effort has been made to develop a combined process in which both the synthesis of CSWs and REEs extraction could be sequentially achieved. CSWs are typically prepared through hydrothermal or atmospheric acidification synthesis. Compared to the hydrothermal synthesis, which is usually carried at high temperatures (> 100 °C) and steam pressures (Qi et al., 2017; Zhou et al., 2021), the atmospheric acidification of PG has advantages since it can be carried out at a mild reaction conditions (temperature < 90 °C and atmospheric pressure) (Sun et al., 2016).

2.13.3 Organic liquid

REE leaching using organic solvents has also been discussed in the literature. This approach is referred to as solvometallurgy in comparison to hydrometallurgy where mineral acids are usually used. The solvometallurgical method allows a high selectivity of metals to be obtained and reduces both the consumption of acids and the volumes of leaching solutions (Binnemans et al., 2015; Canovas et al., 2018). A recent method proposed by El-Didamony et al., (2012, 2013) aimed to remove the radioactive elements (radium, uranium, thorium) and heavy metals (cadmium, chromium) from PG while recovering REEs simultaneously using an organic solution of tri-n-butyl phosphate (TBP), tri-n-octylphosphine oxide (TOPO) and a mixture of TBP+TOPO in kerosene. The results revealed leaching efficiencies of between 66 % and 73 % for radioactive metals and 69 % of total REEs when leaching PG with 0.5 M TBP using S:L ratio of 1 for 2 h at 55 °C. Two successive

leaching steps were found to increase the removal efficiencies of both radioactive elements and REE metals while a third step did not bring any further enhancement. However, in the case of successive steps using a mixture of organic solutions namely TBP and TOPO with molar concentrations of 0.7 and 0.9 respectively, a considerable increase was obtained. Further investigation showed that pre-treating PG with hot sodium carbonate solution (0.5 M) prior to a leaching with a mixture of TBP and TOPO in kerosene had a significant effect on the extractability of these elements with an optimal removal efficiency of 94.6 % and 80.1 % that were achieved for radioactive elements and REE recovery respectively. Although organic solvents have demonstrated relatively high recovery of REEs and other metals present in PG, the loss of organic reagents that were generally adsorbed and entered into the matrix of gypsum may lead to high costs due to the amount of organic solvents used as well as environmental concerns. Organic leaching processes are therefore promising but require more research and development before they can be implemented at large scale (Walawalka et al., 2016).

2.13.4 Bioleaching

Bioleaching for metal extraction is an emerging technology, which is currently considered among other approaches to overcome some of the disadvantages encountered in direct leaching such as high operational cost, generation of both heavy metal pollution and sludge, and poor recovery (Binnemans et al., 2013; Pollmann et al., 2016; Corbett et al., 2017; Hopfe et al., 2018; Reed et al., 2016). Bioleaching processes can be performed using autotrophic or heterotrophic microorganisms and the selection of the latter depends on the type of the bearing mineral. Heterotrophic microorganisms have mostly been reported in the literature for REE extraction via bioleaching and includes the production of organic acids and metal-binding molecules (Dev et al., 2020). The organic acids, namely oxalic, gluconic, acetic, citric, formic and malic acids decrease the pH allowing the leaching of REE while the metal-binding molecules act as chelating agent for separation of the targeted molecule out of the solution (Salo et al., 2020; Hopfe et

al., 2018; Fathollahzadeh et al., 2019). Bioleaching processes are relatively slow, most occur at lower pressures and temperatures and do not require the utilisation of aggressive reagents (Pollmann et al., 2016). Bioleaching has mostly been reported for REE extraction from other secondary REE sources such as bauxite but only a little information is available for PG. Bioleaching of PG for REE recovery is usually achieved using microorganism species such *as gluconobacter, acidithiobacillus, acetobacter or desulfivibrio* and can be achieved through column or heap leaching processes (Fathollahzadeh et al., 2019; Hopfe et al., 2018). A study by Barmettler et al., (2016), has showed that a mixed culture of sulphur-oxidizing bacteria was able to extract 55–70 % of REEs from PG after 30 days of incubation at pH 1.5–1.8. The authors attributed this leaching of REEs to the sulphuric acid generated by sulphur-oxidizing bacteria. In another trial, where a sulphate-reducing bacteria *disulfovibrio desulfuricans* was used, about 80 % extraction was achieved for yttrium using a fixed-bed reactor. The ability of gluconic acid dominated biolixiviant was also examined for the extraction of REEs from synthetic PG. The results indicated that although the biolixiviant was more effective for REE leaching compared to a commercial gluconic acid, its performance was very low in comparison with conventional H_2SO_4 acid leaching. The authors suggested more trials on real PG. However, more studies with regard to the costing and environmental impacts associated are still needed to decide whether or not bioleaching is a suitable option for REE recovery from industrial PG (Barmettler et al., 2016). Compared to conventional chemical leaching which uses strong acids (inorganic or organic) and complexants, bioleaching suffers from lower yield and rates (Rasoulnia et al., 2021). The effectiveness of this process mainly depends on the ability of the microorganisms to oxidize and thus to leach the REEs and also on parameters such as particle size of the REE bearing mineral, the pH of the leaching media and the temperature (Costis et al., 2020).

2.14 Methods of REE recovery

The recovery of REEs from aqueous solutions such as PG pregnant leach solution (PLS) is usually carried out using common techniques as those developed for primary sources of REEs (Fuleihan, 2012). Various techniques such as adsorption, ion exchange, chemical precipitation, electrocoagulation, flotation, membrane filtration, membrane electrolysis, nano-filtration, solvent extraction (liquid-liquid extraction) and solid-liquid extraction (adsorption) have been widely discussed (Hidayah et al., 2017; Pereao et al., 2018). These methods are generally employed in attempts to produce the REEs in a suitable form and purity and some of them, such as solvent extraction is already in application at industrial scale whilst a few are still at research level. Solvent extraction and liquid-solid extraction are two general concepts applied for the extraction and separation of REEs from aqueous solutions (Hidayah et al., 2017). The latter is an extraction process in which the desired element from the liquid phase is attracted towards the reactive solid phase while the former consists of extracting the desired element from one side of the liquid phase (aqueous) towards another liquid phase (organic solvents) (Hidayah et al., 2017). The following sections briefly describe the recent development within these techniques with a particular attention to solid-liquid extraction of REEs from aqueous solutions.

2.14.1 Solvent extraction

Solvent extraction (SX) also known as liquid-liquid extraction is highly selective and has the advantage over the conventional ion-exchange method because it is fast, cost effective and can be used in continuous process where large volumes of solutions are required. SX is the most commonly used commercial method for recovery and extraction as well as the separation and purification of metals ions such as REEs (Peiravi et al., 2020; Salo et al., 2020). The extraction in SX is carried out from the aqueous phase to an organic phase in which the extractant solvate,

exchange or chelate the metal ion. The organic phase impregnated with the metal ions can be scrubbed with suitable aqueous phase in attempts to remove impurities prior to the stripping stage which allows transferring the solutes back from the organic phase into the aqueous phase. In most cases, the organic phase consists of two constituents, an extractant which is generally viscous and difficult to use on its own and its corresponding solvent. The extractant collects the targeted metal ions from aqueous solution and a suitable solvent is used to dissolve the impregnated extractant in turn.

Up to date, several type of organic extractants have been used for the recovery and extraction of REEs from various aqueous media. These organic extractants can be classified as neutral, basic and acidic (Hidayah et al., 2018). Neutral extractants mainly include phosphonate esters, phosphine oxides and phosphate esters. Tributyl phosphate (TBP) is the most known neutral extractant which has been demonstrated to be more efficient in nitrate medium. The main disadvantage of TBP is due to its low separation factors (β) ranging between 1.2 and 2.2 for adjacent REEs. This makes TBP and others neutral extractants less commonly used in separation process compared to acidic and basic extractants. The basic extractants (anion exchanger extractants) are long chain quaternary ammonium salts which usually react with the metal ions through an ionic exchange process. The most widely used basic extractant is Aliquat 336 (A336) which is more suitable for light REE than heavy REE extractions (Xie et al., 2014; Hidayah et al., 2018). Compared to neutral and basic extractants, the acidic extractants have high efficiencies (cation exchanger extractants) and can be found in the forms of carboxylic acids, organophosphorus acids and glycol amide acid (Xie et al., 2014). Organophosphorus acids such as di (2-ethylhexyl) phosphoric acid (D2EHPA) is most efficient and has been widely used for the extraction of REEs in SX (Basualto et al., 2013; Soo Kim et al., 2012). The following section therefore gives a detailed discussion on the D2EHPA extractant with regard to one of the objectives of the current study.

2.14.1.1 Di (2-ethylhexyl) phosphoric acid extractant

Di (2-ethylhexyl) phosphoric acid, commonly known as D2EHPA and traded as P204 (Deqian et al., 2017), is one of the most efficient organophosphorous extractants for the extraction and separation of REEs due to its chemical stability, high selectivity towards REE ions and low solubility in aqueous acidic solutions (Hidayah et al., 2018; Xie et al., 2014). Compared to other organo-phosphorous extractants, D2EHPA is cost effective and thereby regarded as one of the most suitable commercial extractant in the field of SX (Parhi et al., 2015). The presence of requisite sites of atoms O in the structure of D2EHPA (Figure 2.2) allows the binding with metal ions during the solvent extraction process (Pradhan et al., 2020). However, it has been found that D2EHPA preferentially extracts HREEs over LREEs. This has been explained by the fact that the ionic size of REE ions decrease along the period from La through Lu (with increase in atomic number) due to the poor screening effect of electrons in the f-subshell. Thus, HREEs being smaller in ionic size behave as hard acids compared to LREEs. In fact, the presence of the O-atom in D2EHPA as binding site acts as hard base. Therefore, as per the hard soft acid base rule (HSAB), the hard prefers hard and soft prefers soft. This explains the preferential extraction trend of D2EHPA towards HREEs rather than LREEs (Pradhan et al., 2020).
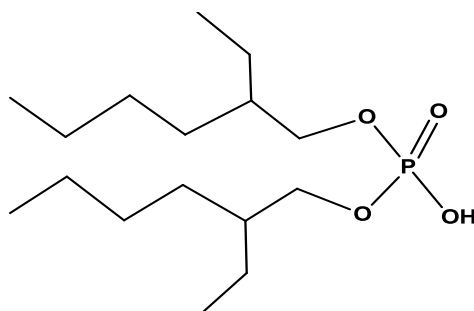
Figure 2.2: Structure of D2EHPA extractant

The earliest studies by Peppard et al., (1957, 1958) found that the extraction mechanism of REEs using D2EHPA involves the formation of dimers (Figure 2.3)

in the organic phase and the REE ions chelate through a cation exchange process. These dimers usually form in non-polar diluents in which the branched alkyl chains and the presence of oxygen donors in its structure favours the dimerization. This mechanism of extraction was further explored and confirmed by Iglesias et al., (1999). Furthermore, according to Swain & Mishra, (2019), the extraction of REE ions with D2EHPA usually proceeds via a complexation process as shown in equation 2.3. where HR is the acidic extractant and Ln^{3+} is the REE ion.

$$Ln^{3+}_{(aq)} + 3(HR)_{2(org)} \rightleftharpoons Ln(HR_2)_{3(org)} + 3H^+_{(aq)} \qquad \text{Equation 2.3}$$
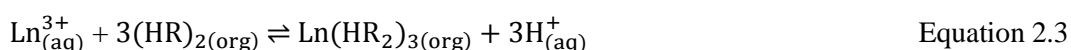
The composition and structure of the complexes formed during the extraction have been studied by various techniques such as IR spectroscopy, small angle neutron scattering and X-ray absorption spectroscopy (Basualto et al., 2013; Gannaz et al., 2006; Jensen et al., 2001; Mohammadi et al., 2015). Basualto et al., (2013) studied the mechanism of adsorption of LREE ions namely La^{3+}, Ce^{3+}, Pr^{3+} and Nd^{3+} with D2EHPA and found that the number of extractant dimers that coordinated with the investigated REEs were in the range of 1.05 (Pr) to 2.45 (Ce) by evaluating the equilibrium concentration. The formation of dimeric ligand bridged 6:2 complexes and multinuclear species was also confirmed in the $[NdC_3]_n$ when extracting Nd^{3+} by D2EHPA (C) using small angle neutron scattering, X-ray absorption spectroscopy and IR spectroscopy measurements (Gannaz et al., 2006; Jensen et al., 2001).
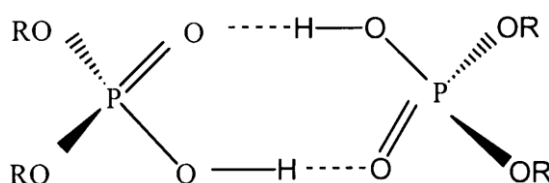
Figure 2.3: Formation of dimers of D2EHPA

The extraction capacities of D2EHPA has been investigated for several aqueous solutions and demonstrated suitable separation factors (β= 2.5) between two

adjacent elements for all the REEs. However, its distribution factor (D) was found to increase with an increase of the atomic number of REEs and decrease with increased temperature during the extraction process. The distribution factor of D2EHPA is also affected by the diluents and increases in the following order: benzene < xylene < tetrachloromethane < cyclohexane < kerosene. Kerosene is therefore the most used diluent for D2EHPA (Peramaki, 2014). Although the extraction of REEs with D2EHPA can be carried out at low pH values, this depends essentially on the equilibrium of equations 2.4 and 2.5 which lies strongly to the right, sometimes making the stripping of loaded metal ions difficult (Xie et al., 2014).

$$D = \frac{[M_{or}]}{[M_{aq}]}$$

Equation 2.4

Where D (sometimes designated as K) is the distribution coefficient of a metal ion (M), $[M_{or}]$ is the molar concentration of M in the organic phase and $[M_{aq}]$ is the concentration in the aqueous phase. The separation factor (β) of two different metal ions, M_1 and M_2 is defined as shown in equation 2.5. Both D and β are usually used to quantitatively describe a SX process and also help to decide on the type of the extractants (Xie et al., 2014).

$$\beta = \frac{DM_1}{DM_2}$$

Equation 2.5

The effectiveness of D2EHPA in the SX process is usually modulated by varying the pH, the equilibrium time, the temperature, the concentrations of metal ions and extractant in the aqueous phase (A) and organic phase (O) respectively, O/A phase volume ratio etc. (Satpathy & Mishra, 2017). Batchu et al., (2018) investigated the effect of diluents using D2EHPA and showed that aliphatic diluents promote higher extraction efficiencies while the aromatic diluents tended to suppress the formation of emulsions or gels. Early studies by Sato et al., (1989) showed that the extraction efficiencies of REEs with D2EHPA increase with increasing atomic number of

47

trivalent elements. The kinetics of REE extraction with D2EHPA was also studied by Geist et al., (1999) and they found that the extraction rate was limited by the diffusion whereas the aqueous phase composition had no effect on the extraction kinetics.

The extraction of REEs by D2EHPA has been investigated in different acid media such as HCl, H_2SO_4 and HNO_3 solutions (Basualto et al., 2013). It was found that the extraction from HCl media and H_2SO_4 is similar while extraction from HNO_3 is poor (Gupta & Krishnamurthy, 2005; Xie et al., 2014). However, Deqian et al., (2017) showed that selectivity order of REEs using D2EHPA extractant from various acid solutions was found to be Lu > Yb > Tm > Er >Y > Ho > Dy > Tb > Gd > Eu > Sm > Pm > Nd > Pr > Ce > La. Battsengel et al., (2018), studied the selective separation and recovery of LREEs and HREEs from a pregnant leach solution obtained from the leaching of apatite ore in 1 M H_2SO_4 using D2EHPA and other related organic extractants. The influences of experimental parameters such as pH, the concentration of D2EHPA, organic to aqueous phase ratio, diluent type, the extraction time and the concentration of the stripping agent were investigated. The results showed that LREEs and HREEs in the pregnant leach solution were selectively recovered via a two-stage extraction process. The authors indicated that, in the first stage up to 90 % of (0.05 g/L) of HREEs was extracted with 1.8 M D2EHPA in kerosene whereas the vast majority of LREEs (up to 95 %) remained in the raffinate. However, in the second stage, it was found that up to 93 % of LREEs (1.01 g/L) was extracted from the raffinate at the same concentration of D2EHPA at a pH 1.6. In the first and second stage, the stripping of the loaded REEs was carried out using 4 M and 1 M of H_2SO_4 solutions respectively. Innocenzi et al., (2018) showed that the pH had positive influence on the extraction process while extracting REEs with D2EHPA and found that the order of extraction of elements under investigation was Y > Tb > Gd > Eu > Ce > La. Khaironiel et al., (2014) studied the extraction of Ce(IV), Nd(III) and La(III) from HNO_3 (0.1 M) and H_2SO_4 (1.0 M) acid solutions using D2EHPA (1.0 M). Their results showed that

48

the extraction ability of these three elements increased in the sequence La < Nd < Ce for both acids.

Despite having a few industrial applications, SX has been described as the most applicable commercial technology for the extraction and separation of REEs since it can handle larger volumes of dilute pregnant liquors (Pereao et al., 2018, Xie et al., 2014). However, the use of large volumes of extractants in this process as well as the time and intensive labour required make it inefficient (Das, 2013; Xie et al., 2014). Furthermore, parameters such as low extraction efficiency, impurity of the final product, loss of extractant into the aqueous phase and low purity are still challenging especially when considering large scale processes (Krishnamurthy & Gupta, 2004, Hidayah et al., 2017). Health and environment concerns due to the emissions of volatile organic compounds to the atmosphere as well as flammable residues resulting from the use of organic diluents are also major issues in SX (Cadore et al., 2019). To overcome these issues, solid-liquid extraction (SLE) methods have been suggested and will be discussed below.

2.14.2 Solid liquid extraction

Solid-liquid extraction (SLE) also known as solid phase extraction (SPE) offers the advantages of having large surface area and better contact between the extractant and metal ions in aqueous phase (Da Silva et al., 2019). SLE is usually achieved through the adsorption concept and has been used long before solvent extraction (SX) ever was commercialised (Hidayah et al., 2017). The adsorption has the ability to extract desired metals such as REEs at high efficiency in particular at low concentration from various solutions (Liu et al., 2012). The adsorption approach occurs by a mass transfer process where the adsorbate is transferred from the liquid phase to the surface of the adsorbent on which a molecular or thin film is formed through physical or chemical bonding interactions (Foo & Hameed, 2009; Ogata et al., 2014). In practice, this involves passing of a solution containing metal ions over the adsorbent material onto which they adsorb and the process continues until

49

saturation of the adsorbent (Keller & Staudt, 2005). The adsorption capacity is crucial in SLE process to estimate the cost of the process. However, the adsorption capacities of two different adsorbents cannot be compared without maintaining similar experimental conditions such as adsorbent dosage; agitation speed; contact time; initial concentration of component; ionic strength of the solution; temperature; the pH solution and volume of the adsorbate (Pereao et al., 2018).

The adsorption process is a highly effective technique as it offers good flexibility in terms of the operational design, reversibility of the process and the ability to regenerate the adsorbent using a suitable desorption process (Fu & Wang, 2011; Lakherwal, 2014; Pereao et al., 2018). In adsorption, an adsorbent should display both good mechanical (strength and resistance to attrition) and kinetics (ability to rapidly transfer adsorbing molecules to the adsorption site) to be considered. Moreover, the adsorbent must be able to be regenerated after the adsorption process without damaging its adsorptive and mechanical properties. The preparation methods of the adsorbent should be ultimately inexpensive for the adsorption to be economically competitive with other existing extraction and recovery processes (Sousa et al., 2013; Olafadehan et al., 2012; Crittenden & Thomas, 1998). Various supporting materials such as polymer, membrane, silica and bio-derived materials have been developed in this regard. The supporting materials are usually selected so that the resulting adsorbents exhibit strong bonding and robust characteristics towards REE extraction. Amongst other supporting materials, polymer materials consist of a good framework to carry positive and negative electric charges, high stability, easy preparation method and good interaction with positive or negative charges (Atanassova et al., 2014, Hidayah et al., 2017).

2.14.2.1 Polymer based adsorbents

Polymer based sorbents have been mainly develop\d to address the limitations of some traditional adsorbents such as silica-based materials. For instance, the presence of residual silanol groups (Si-OH) as well as the instability at extreme pH

of silica-based adsorbents can be overcome using polymer sorbents. Polymer adsorbents are cost effective and abundantly available and mostly found as derivatives of polystyrene-based resin with pendant chloromethyl groups (Zhu et al., 2012; Hidayah et al., 2017); and are available in either gel or macroporous structure which can be activated as ion exchange materials. Macroporous polymers such as polystyrene-divinylbenzene (PS-DVB) is the precursor of polymer adsorbents, which has a specific surface area of up to 800 m^2/g of its hydrophobic structure (Fontanals et al., 2011). The activated polymer materials can be tuned into acid and base exchange resins (Masram, 2013). Acidic resins are divided into strong and weak acid exchange resins. The strong acid resins are usually associated with sulfonic group (SO_3^-) acting similarly to strong acid and active in any pH level. In contrast to strong acid resins, weak acid resins behave in the opposite way by simply releasing H$^+$ due to its weak dissociation. This behaviour makes weak acid resins more favourable for metal ions extraction since they have higher ion exchange capacity compared to strong acid resins. Weak acid resins are generally associated with the carboxylic group (COOH) and are passive in the pH range between 4 and 6 (Masram, 2013).
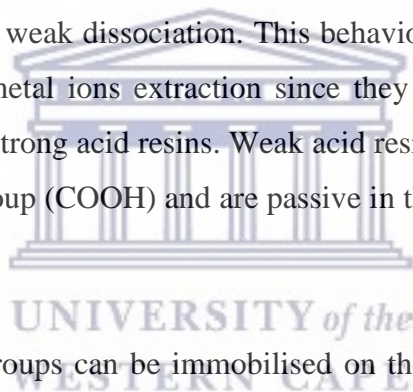
Different functional groups can be immobilised on the polymer through organic reactions and a successful functionalization strongly relies on a suitable solvent that can be used to swell the materials (Pustam & Alexandratos, 2010). The surface modification mainly aims to enhance the adsorption efficiency of the polymers. Functional groups such as carboxylic, sulfonic, amide and amine have been widely developed in this regard (Huang et al., 2012; Lu & Huang, 2007; Dharanivasan et al., 2015; Leonor et al., 2007; Shin et al., 2004; Bahramzadeh et al., 2016). For instance, polymer supported ligands such as EDTA and DTPA (Dupont et al., 2014; Rahal et al., 2015), 8-hydroxyquinoline (8-HQ) (Kajiya et al., 2004; Sohrin et al., 1998), hydroxamic acid, (Agrawal et al., 1999; Kumar et al., 2011), tetramethylmalonamide (TMMA) (Yang & Alexandratos, 2010; Nogami et al., 2003), 2,6-diacetylpyridine (Karadaş et al., 2011) and phosphorus ligands (Wu et al., 2013) have been commonly used for REE recovery and separation. In this

separation, the selectivity is important and can be increased with ligands that can suitably coordinate or chelate with the targeted metal ion. Among other steps involved in polymer-based adsorption, stripping of the metal ions from the ligand is crucial for the process itself whereas regeneration and reuse of the polymer are also important with regard to the economics of the application. The main disadvantage encountered in SLE is the relatively low contact area between the surface of the support with immobilised ligand or organic extractant and the solution containing the metal ions of interest. This low contact area is known to hinder mass transport between the solution and the adsorbent, making this technique less efficient. Therefore, new materials with high contact areas such as polymer nanofibers are needed to overcome this problem. Polymer nanofibers offer a large surface area, enhanced interactions, high porosity, and flexibility (Rathna et al., 2013, Liao et al., 2014; Luo et al., 2015).

2.14.2.2 Polymer nanofibers

The application of polymer nanofibers for adsorption process is an emerging area and has drawn the attention of research in recent decades (Rahmani et al., 2010). Polymer based nanofibers are a novel class of adsorbents possessing larger surface areas which can easily be modified in comparison to microfibers (Pereao et al., 2017; Hiremath et al., 2015). The adsorption process using polymer nanofibers is rapid and its operation is simple. Polymer nanofibers can be produced from natural or blends of polymers or synthetic polymer (Bhardwaj & Kundu 2010; Ramakrishna et al., 2006). Synthetic polymers can be found as semicrystalline or amorphous and are generally named based on the monomer from which they are synthesised (Mohammad, 2007). Semicrystalline polymers consist of regular and repeated units which allow the chain to fold into dense regions known as crystallites. These crystallites act as crosslinks giving the polymer higher tensile strengths and modulus or stiffness compared to the amorphous analog. However, there is no polymer that is completely organised into a fully crystalline material. This means that, amorphous areas will still be available in a semicrystalline polymer

(Middleton & Tipton, 2000). Compared to natural polymers, synthetic polymers offer many advantages as they can be easily tailored to obtain a wider range of properties such as thermal stability, strength, viscoelasticity, degradation rate (Hakkarainen, 2002). Among the synthetic polymers, polystyrene has been widely used as adsorption support or modified polymer adsorbent (Bessbousse et al., 2009; Pereao, 2018). Therefore, the following section briefly discusses this polymer with regard to this study.

2.14.2.2.1 *Polystyrene*

Polystyrene (Figure 2.4) is a hydrophobic-olephilic material and the most popular organic polymer that has been used long before as an adsorption support due its outstanding physical and reactive properties (Bessbousse et al., 2009). Polystyrene has been confirmed as a versatile support because of the large number of ligands that can be covalently bound to it (Alexandratos & Crick, 1996). The immobilisation of these ligands can lead to the synthesis of variety of polymer-supported extractants that can be used for extraction and recovery of metals ions such as REEs from different aqueous solutions (Alexandratos & Crick 1996; Helfferich, 1965).
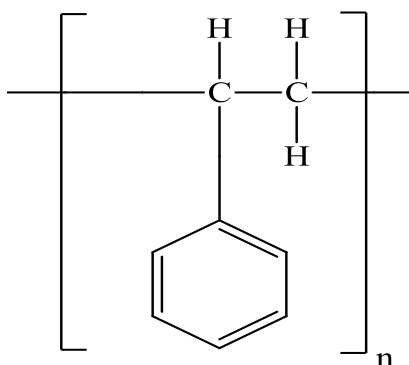
Figure 2.4: Unit of a polystyrene polymer structure

Although polystyrene possesses outstanding chemical and mechanical properties and is not costly, its adsorption efficiency is very low when used unmodified.

Chemical modification of polystyrene is an emerging field and has attracted much attention due to the numerous applications of functionalised polymers (Pereao, 2018). This chemical modification is generally carried out to improve the adsorption efficiency of the polystyrene polymer. Thus, ligands containing functional groups such as amide, amine, carboxylic and sulfonic have been widely discussed in the literature (Bahramzadeh et al., 2016; Dharanivasan et al., 2015; Huang et al., 2012; Leonor et al., 2007; Li et al., 2009; Lü et al., 2007; Shin et al., 2004). Biswas & Chatterjee (1983), modified polystyrene by Friedel-Crafts acylation with cis-1,2,3,6 tertrahydrophthalic anhydride using anhydrous aluminium chloride as catalyst. Their results showed that the electrophilic substitution of polystyrene with the aromatic anhydrides (phthalic anhydride, pyromellitic dianhydride and trimellitic) modified the properties of the parent polystyrene polymer. Esma et al., (2014) synthesised a macroporous cross-linked polystyrene which was functionalised with iminodiacetic and aminomethylphosphonic acid group for adsorption of lanthanum. Among other ligands, the possibility of using diglycolic acid (DGA) as ligand on a polymer support material for REE extraction and recovery has drawn the attention of research in recent years. This ligand is briefly discussed in the following section with regard to this study.

2.14.2.2.2   *Diglycolic acid ligand derivatives*

Oxygen donors such as carboxylic acids, ketones and phosphoric have been reported as the best ligands for extraction and separation of REEs (Florek et al., 2015). Diglycolic acid (DGA) is a tridentate ligand (Figure 2.5) (Ogata et al. 2014; Ogata et al., 2015); which belongs to carboxylic acid groups and can be used as ligand for the extraction and recovery of REEs from various aqueous solutions. Diglycol amic acid (DGAA) is similar to DGA and has also been regarded as a promising ligand for the extraction and recovery of REEs (Selvan et al., 2017). Ogata et al., (2014) chemically immobilised DGAA onto the surface of silica particles in attempts to investigate the adsorption behaviour of REE metal ions (Dy

and Nd) and base metal ions Cu, Fe(III) and Zn. In a similar approach, Suneesh et al., (2015) functionalised iron oxide particles with DGAA for mutual separation of Am(III) and Eu(III) from a diluted solution of nitric acid. Other ligands similar to DGA such as diglycolamides have also been discussed for the extraction of REEs (Horwitz et al., 2005; Suneesh et al., 2012). Thorough analysis of complexes bearing the DGA ligands show that REEs usually bind in a tridentate fashion where each individual metal ion is coordinated by the three oxygen atoms of the DGA ligand (Pereao, 2018). The binding properties of DGA ligand can greatly be affected by the bite angle (Figure 2.6) in the corresponding complexes. The bite angle which is the angle formed by the chelate ligand (or between the metal ions) and the coordinating atoms of the ligands is crucial during the coordination of metal ions and ligands. For instance, a larger bite angle will have a higher affinity for larger metal ions whereas a smaller bite angle favours the coordination of smaller metal ions (Freixa & Van Leeuwen, 2003). Nevertheless, a chelating ligand bound to the solid surface through more than one anchor point is expected to be a rigid conformation which will exhibit less flexibility to adapt itself to the metal electronic requirements than in solution. Thus, a suitable chemical tailoring of the chelating ligands and their grafting on solid supports might allow the functional materials to exhibit selective affinities for both larger or smaller ions (Florek et al., 2015). Similarly, to DGA, the adsorption of REE ions with DGAA also takes place via three oxygen atoms which confers high selectivity. Although this high selectivity is attributed to the chelation of the metal ions by the tridentate framework of DGA or DGAA, the complete adsorption mechanism remains undefined (Pereao, 2018). The adsorption mechanism of REE ions was investigated and elucidated by Ogata et al., (2016) using derivatives of DGA. Their results showed that the adsorbents modified with DGAA were able to adsorb REE ions because DGAA contains ether oxygen atoms whereas glutaramic and succinamic acids did not. This means that the ether oxygen atoms in DGAA framework has a crucial role in the adsorption mechanism of REE ions and other metal ions. In contrast to this result, Nguyen et al., (2016) indicated that the dissociation of the terminal carboxylic acid group of

55

DGAA was responsible for the adsorption of metal ions and that the variation of the pH during the dissociation plays an important role on the adsorption efficiency.
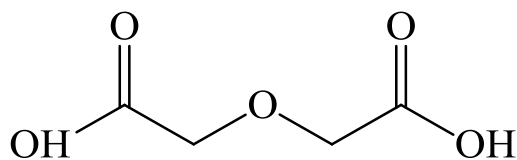
Figure 2.5: Structure of diglycolic acid ligand
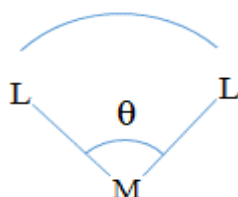
Figure 2.6: Bite angle between the metal ion (M) and the coordinating ligand (L)

2.14.2.3 Preparation of polymer nanofibers

Amongst other techniques used for preparation of nanofibers, electrospinning is a versatile polymer nanofiber production technique (Xu et al., 2015). This technique was patented for the first time in 1900 by Cooley followed by Morton in 1902 (Chipara et al., 2013). Electrospinning consists of placing a polymer solution in a syringe connected to one electrode of a high voltage power supply generating a high voltage difference (5–30 kV) between the syringe needle and the grounded target. Subsequently, the polymer is ejected; the electrical charges on the polymer solution promote solvent evaporation and nanofiber thinning. The formed dry nanofiber (solidified or semi solidified) is deposited on the grounded target in chaotic pattern known as the Taylor cone (Chipara et al., 2013; Liu et al., 2015). The electrospinning setup is very common in vertical or horizontal alignment or orientation and is usually chosen depending upon the properties of the polymer nanofibers that can be produced (Stankus et al., 2006; Kidoaki et al., 2005). The electrospinning set up of a horizontal orientation is shown in Figure 2.7 while the steps towards the electrospinning process are briefly discussed below.
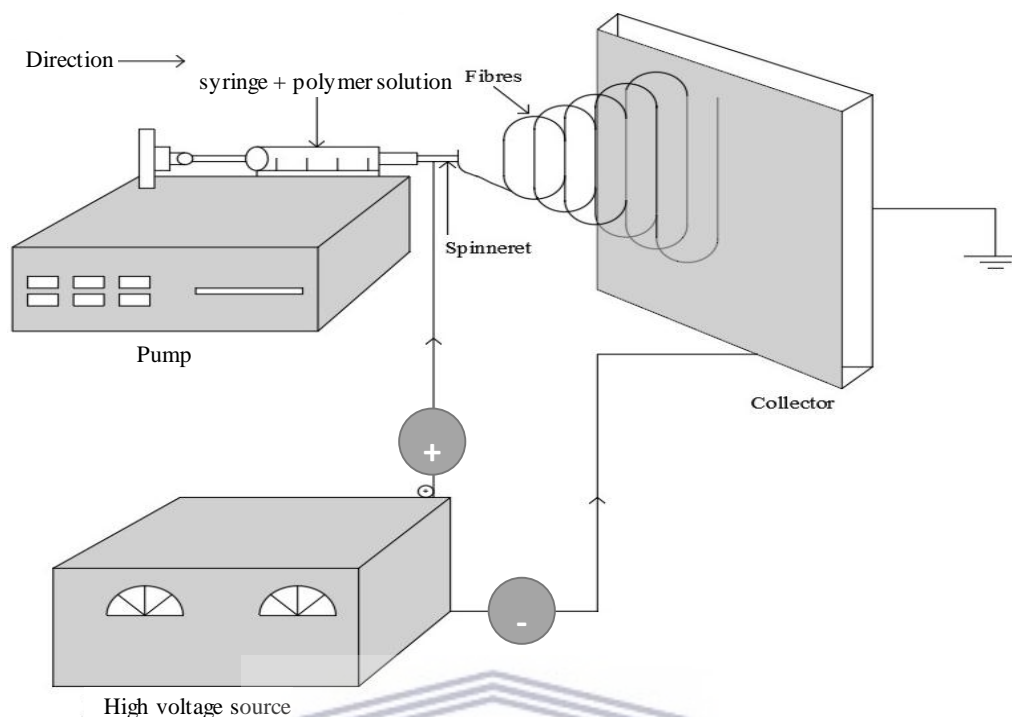
Figure 2.7: Electrospinning set up for the fabrication of nanofibers

The dissolution of the polymer to be electrospun is the first step of the electrospinning process. This step requires that the polymer is completely dissolved in a suitable solvent to form a homogeneous solution and finding a suitable solvent is the main challenge to successfully electrospun and in many cases, a mixture of solvents is usually employed to achieve this (Bhardwaj & Kundu, 2010). The majority of the polymers dissolve at room temperature and atmospheric conditions (Chronakis, 2005; Huang et al., 2003) and solvents used are usually volatile and expected to dry up during the traveling of the polymer jects towards the collector (Nataraj et al., 2012; Yu et al., 2006). This therefore means the peaks of the solvents are not expected to appear when characterising the polymer electrospun nanofibers through techniques such as ATR-FTIR. In some cases, the polymers were electrospun in molten form in attempts to make polymer nanofibers free of solvent or benign. To achieve this, the powdered polymer can be introduced into a syringe followed by the application of heat to melt the polymer and then the electrospinning process is carried out in a vacuum (Lyons et al., 2004). This approach is

57

advantageous compared to a ventilated chamber since both high electric field strength over large distances and high temperatures can be used.

Generally, the electrospinning of the polymer solution can be affected by three main factors namely, the nature of the solution (concentration, conductivity, molecular weight of the polymer and surface tension), the ambient conditions (humidity, temperature and air velocity in the chamber or room) and the process parameters (applied voltage, feed rate, types of collectors, motion of the target screen, distance between the spinneret tip and the collector and needle tip) (Bhardwaj & Kundu, 2010; Huang et al., 2003). A good understanding of the polymer solution, ambient conditions and process parameters prior to electrospinning process is crucial. This allows to obtain polymer nanofibers that can be free of beads (defect-free) and collectable as continuous single fibres having consistent and controllable diameters. However, achieving such targets is by no means easy. It is therefore important to always optimize the three process parameters namely the dissolution of the polymer, as well as process and ambient conditions. The concentrations of the polymer solution are usually expressed in weight percentage (wt%). After identifying the appropriate solvent prior to polymer electrospinning, the following must be known: the weight percentage of the polymer (g) to be dissolved, volume of the solvent to be used (mL) and the density of the solvent (gcm^{-3}).

2.14.2.4 Modification of polymer electrospun nanofibers

Electrospun nanofibers are gaining much attention in recent decades due to their distinctive properties such as high porosity and interconnected pores of their assembled nonwovens; variety of morphology and structure; and most importantly high specific surface area as well as ease of functionality (Liu et al., 2015). The development of nanofibers for adsorption of metal ions is still emerging, and more approaches are expected to increase the knowledge in this field, in particular for adsorption of REEs. Modification of polymer electrospun nanofibers is a field of research that can be carried out by surface chemistry, incorporation of functional materials or coating techniques allowing the removal of small molecules or metal

ions efficiently from a solution (Fang et al., 2008). Various approaches can be used to produce polymer electrospun nanofibers bearing functional groups whilst functionalization of a preformed nanofiber only requires setting the conditions for the functionalization reaction, since the base fibre is the same (Pereao et al., 2018). The preparation of functional fibres can be carried out via three main approaches, namely a pre-electrospinning-synthesis of a functional polymer followed by spinning into a fibre, or blending and co-electrospinning by special spinning techniques, or lastly, post-functionalization-fibre preparation followed by introduction of functional groups (Shimamura et al., 1989, Pereao et al., 2018). The aforementioned techniques are briefly discussed in the subsection below.

2.14.2.4.1 *Pre-functionalisation method*

Pre-functionalisation process consists of chemically modifying the surface of the polymer prior to the electrospinning to enable the adsorption of metal ions from solutions. This process is mainly possible because of the abundance of functional groups available on the surface of some polymers. The modification method is usually carried through direct modification or monomer-grafting which allows the attachment of various groups to the backbone of the nanofibers (Ngah et al., 2008; O'Connell et al., 2008).

2.14.2.4.2 *Blending method*

The blending consists of incorporating molecules into the bulk material of the nanofibers during the fabrication process. This process can be carried either by direct blending (mixing) or co- axial electrospinning. Koh et al., (2008) showed that the direct incorporation technique referred to as blending can allow for a greater amount of molecules to be incorporated and also improved the activity of the polymer in comparison with the surface modification method. Furthermore, the molecules incorporated through this approach are embedded into the bulk material of the nanofibers which can extend the adsorption ability throughout the nanofibers

and not only the surface. However, the method of controlling the surface properties through incorporation of small molecules such as oligometric additives which can migrate to the surface of the polymer and be removed after washing may not be effective. Such small molecules may compromise the physical properties of the bulk of the polymer and since they are not strongly bound to the matrix of the polymer, they may be removed through post-processes such as evaporation, dissolution, wear or leaching out of the adsorbent (Pereao, 2018).

2.14.2.4.3 *Post-functionalisation*

Post-functionalisation makes use of various methods such as plasma treatment (Ladizesky & Ward 1995), UV irradiation and UV–induced grafting polymerisation to modify the surface of polymer nanofibers. The main disadvantage of these surface modifications of polymer nanofibers is due to strong reaction conditions that are used during the process. Such strong reaction conditions should be avoided since polymer nanofibers are ultrafine materials and not as strong as bulk materials to withstand harsh conditions which might lead to their destruction (Ramakrishna et al., 2005). Although some of the methods used in post-functionalisation require strong reaction conditions, this approach remains the most popular due to a variety of functionalised nanofibers that can be produced using suitable chemical reactions that can allow introduction of functional groups on the surface of various polymers. For instance, for the adsorption of REEs and associated metal ions, functional groups or chelating ligands such as iminodiacetic acid, iminodimethylphosphonic acid, phenylarsonic acid and amino acid moieties have been used for the functionalisation of cross-linked polymers (Galhoum et al., 2015). Post functionalisation is a promising approach but requires nanofibers to possess high mechanical strength as a prerequisite.

2.14.2.5 Adsorption of REE ions using modified polymer nanofibers

The adsorption of metal ions can be carried out using either batch or column techniques (Horzum et al., 2012). The batch technique consists of placing the adsorbent (i.e. modified nanofibers) in a vessel containing the metal ions solution and shake them together over a period of time (Neghlani et al., 2011), while in the column technique, the adsorbent is usually placed in a vertical column to form a bed through which the solution containing metal ions runs (Horzum et al., 2012). The mechanisms of adsorption of some modified polymer nanofibers have been investigated for various metal ions and it was found that adsorption proceeds mainly through chelation and ion exchange (Chen et al., 2002; Jin & Bai, 2002). The ion exchange mechanism is mostly favoured by the presence of functional groups such as carboxyl, sulfonic and phosphonic on the surface of the adsorbents while nitrogen containing groups such as amino, thioamide and hydrazine allow metal ions adsorption through chelation mechanisms (Ndayambaje et al., 2016; Chen et al., 2002; Jin & Bai, 2002).

Metal ions such as REEs have been adsorbed using various modified polymer nanofibers (Pereao et al., 2018). For example, Martin et al., (2019) applied polyacrylonitrile (PAN) electrospun nanofiber membranes for the recovery of Eu^{3+} and Y^{3+} as representative of the lanthanides. In their study, PAN nanofibers were impregnated with cyanex 272, a commercial organic extractant in order to increase their affinity towards REEs and metals ions. Their results from batch adsorption demonstrated that the adsorption capacity was high, reaching a maximum of 200 and 400 mg/g for Eu and Y respectively. Further investigations showed that the presence of interfering heavy metals ions, namely Zn^{2+}, Ni^{2+}, Cu^{2+}, Cd^{2+} and Pb^{2+} as well as some anions such as NO_3^-, SO_4^{2-} or PO_4^{3-} did not affect the adsorption process significantly. Pereao et al., (2019) chemically modified a polystyrene nanofiber with diglycolic anhydride (DGA) to produce novel electrospun polystyrene diglycolic acid nanofiber (PS-DGAnf) adsorbents which were

examined for adsorption of Ce^{3+} and Nd^{3+} in the presence of Ni^{2+}, Co^{2+} and Sr^{3+} as interfering ions. Their results showed that the adsorption capacity of PS-DGAnf at pH 6.0 was 152.5 mg/g and 146.2 for Ce^{3+} and Nd^{3+} respectively. Furthermore, the amount of Ce^{3+} adsorbed in the presence of interfering ions (mixture solution) was about 100 mg/g which was only slightly lower than 119 mg/g obtained in single ion solutions. The developed PS-DGAnf also displayed rapid adsorption kinetics for Ce^{3+} and Nd^{3+} ions within 15 min and could be regenerated and reused for 4 cycles without substantial loss to its adsorption abilities. Wang et al., (2016) used a colloid-electrospinning route to prepare a poly (acrylic acid)-silica hydrogel nanofibers (PAA-S HNFs) scaffolds for La^{3+}, Eu^{3+} and Tb^{3+} recovery. The effects of initial solution pH, concentration and contact time on adsorption of La^{3+}, Eu^{3+} and Tb^{3+} were systematically investigated and the maximum equilibrium adsorption capacities of ions of these REEs on PAA-S HNFs were 232.6; 268.8 and 250.0 mg/g respectively at pH 6.0. Furthermore, the FT-IR and XPS revealed that the proposed adsorption mechanism of REEs on PAA-S HNFs scaffold resulted from the formation of bidentate carboxylates groups between carboxylic groups and REEs. Hong et al., (2014) prepared nanofiber mats with blended solution of polyacrylnitril (PAN) and polysulfone (PSF) in N,N'-dimetal acetamide by electrospinning. The nanofiber mats PAN/PSF were coated with polydopamine (PDA) for adsorption of La^{3+} ions from aqueous solution. The effects of initial solution concentration, pH and contact time on the adsorption process were investigated and the results showed that the maximum equilibrium uptake capacity of La^{3+} on PAN/PSF-PDA membrane was 59.5 mg/g and these experimental data well fitted to Langmuir isotherm equation. This membrane was suggested as pre-concentration route for the separation of La in hydrometallurgical processes. Poly (methyl methacrylate)-random-poly (2-(acetoacetoxy) ethyl methacrylate) (PMMA-co-PAEMA) and the hydrophilic polyethylene oxide (PEO) electrospun fibres containing β-ketoester metal binding functionalities were fabricated by electrospinning and evaluated for adsorption of Eu^{3+} from aqueous media. The possibility to incorporate magnetic nanoparticles (Fe_3O_4 NPs) within PMMA-co-PAEMA)/PEO fibres to enhance metal ion adsorption was also investigated for possible magnetic separation. The

results showed that the presence of the β-ketoester functionalities as well as the incorporation of the Fe_3O_4 nanoparticles positively affected the adsorption process and indicated the significance of chemical modification with respect to metal recovery. Furthermore, the experimental data, which were well fitted by the Langmuir isotherm model, indicated increased affinity with increasing pH and reached maximum values (~ 95 %) at pH 6.5 (Panteli et al., 2018). Most of these adsorption studies were carried out by investigating parameters such as the adsorbent dosage, contact time, initial concentration of adsorbate (metal ions), temperature and pH while the efficiency of the adsorption process was determined using adsorption isotherms, kinetics models and thermodynamics parameters. Thus sections below briefly discuss some of these parameters with regards to the adsorption studies.

2.14.2.5.1 *Effect of pH*

The pH is the most highlighted factor in adsorption studies and plays a crucial role on both the adsorbents and the solution containing metal ions. For instance, stabilities tests are routinely carried out on modified nanofibers in different pHs and mostly acidic medium in attempts to make sure that the surface of the modified nanofiber retains its functionality throughout the adsorption process knowing that at certain pH chelating functional groups of the modified nanofibers can undergo dissociation (Bode-Aluko, 2017). On the other hand, the pH of the aqueous solution containing metal ions affects the adsorptive process due to the protonation and deprotonation of the acidic and basic group of the chelating ligands of the modified nanofibers (Horzum et al., 2012; Neghlani et al., 2011; Deng et al., 2003a). At lower pH values, the functional groups or active sites of the adsorbents are less available for metal ions because of the protonation of the active sites at high concentration of protons (H^{3+}). The degree of the protonation of the functional groups on the surface of the adsorbent will gradually reduce and approach zero when the pH increases, indicating a gradual increase in the adsorption. Thus, metal ions are readily available for adsorption as the pH of the solution increases. Nevertheless, high pH

can lead to the precipitation of metal ions and to prevent this, pH higher than 7.0 is not often studied in adsorption processes (Soltanzadeh et al., 2013). Higher adsorptions of metal ions are usually observed at lower pH of the solution (pH < 7.0) (Fu & Wang, 2011). The pH of adsorption is usually adjusted prior to adsorption process using weak concentration of acid (i.e. 0.1 M HCl) or base (i.e. 0.1 M NaOH) for polymer nanofibers (Ndayambaje et al., 2016).

2.14.2.5.2 *Effect of initial metal ions concentration*

Generally, the initial concentration of a model metal ion solution is prepared in mg/L (ppm) prior to effective application of the adsorbents using a real solution. The amount of metal ions adsorbed usually increases with an increase in the initial concentration of the solution containing metal ions until attaining a saturation plateau where there will be no sites available on the adsorbent for further adsorption to occur (Soltanzadeh et al., 2013; Horzum et al., 2012; Deng et al., 2003a).

2.14.2.5.3 *Effect of contact time*

The contact time or residence time is also an important parameter in adsorption studies. There is a usual trend in adsorption studies that as the contact time increases, the amount of metal ions also increases up to a certain point where there will be in sufficient surface area and fully saturated active sites of the adsorbent. According to Wang et al., (2014), the contact time could also be related to protonation time. This is because as the contact time increases, the protonation time also increases while the proton (H^{3+}) takes up the adsorption sites, blocking other metal ions from being adsorbed.

2.14.2.5.4 *Adsorbent dosage*

The adsorbent dosage or the amount of the adsorbent is rarely studied in adsorption process. This is because, an increase in the amount of the adsorbent would mean an

increase in the number of adsorption sites which will result in an increased adsorption of the metal ions. However, this is not always the case. For instance, Soltanzadeh et al., (2013), observed an opposite trend while increasing the adsorbent dosage from 0.1 to 0.3 g and attributed the decrease of sorption capacity to the aggregation of adsorbent particles at high dosage, which reduced the total surface area of the adsorbent resulting in an increase in the diffusion path length. The authors further indicated that with a constant initial concentration, an increase of the adsorbent dosage would lead to a large number of active sites being available for metal ions. This means that a saturation of the active sites would not take place and the excess capacity of the adsorbent would be wasted. Moreover, in adsorption studies it is important not to use too little or too much adsorbent so that equilibrium can easily be observed.

2.14.2.6 Desorption and regeneration

Depending upon the applications, the disposal of the modified adsorbent would be favoured if its cost is low but difficult to regenerate (formation of strong chemical bonding) and the adsorbed products are not of a very high value. However, the disposal of the adsorbent as waste is not an economic option in the majority of processes. Thus, regeneration remains the best option in many application and this can be carried out either in situ or external to the adsorption vessel to the extent that the adsorbent can be recovered or reused (Pereao, 2018). The regeneration of the modified adsorbent such as nanofibers and the stability of any moiety attached to its surface are crucial in the adsorption process in attempts to promote their reusability, potential application as well as improve the process economics. Similarly, to the regeneration process, the desorption aims to elucidate the nature of the adsorption process and importantly to recover the metal ions from the adsorbents. In addition, desorption is crucial to allow the adsorbent to be regenerated so that the adoption process can be repeated. Various methods of regeneration of the adsorbent such as solvent washing, chemical, thermal and electrochemical cycling have been used in adsorption processes (Shah et al., 2007).

However, most of these methods are suitable for a specific application where a particular adsorbate of interest is targeted. Amongst others, solvent washing is very effective and advantageous from the environmental point of view (Velu et al., 2003). The desorption of metal ions from polymer matrix adsorbent is usually carried out in acidic or basic solutions (Jeon & Kwon 2012; Pakade et al., 2011). Desorption and regeneration agents such as NaOH, NaCl, HCl, H_2SO_4, H_3PO_4 and EDTA have been reported for modified nanofibers. For instance, Min et al., (2012), showed that 0.005 M EDTA and 0.05 M of NaOH solutions efficiently desorb heavy metal ions from poly(ether sulfones)/poly(ethyleneimine) nanofibrous membranes.

2.15 Characterisation techniques

This section gives a brief overview on the background and principles of selected techniques used throughout this study to characterise different materials namely PG, liquid solutions and polymer nanofibers and derivatives. These techniques mainly include the ICP-(OES/MS), XRD, FT-IR, SEM, SEM-EDS, XRF, NAA, TGA and PSD.
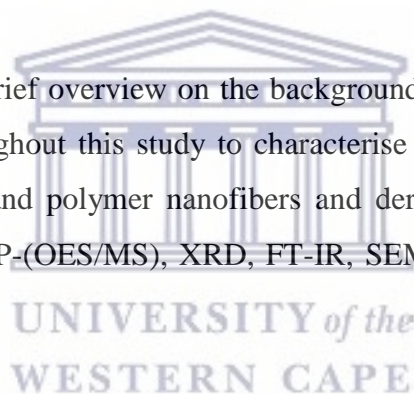
2.15.1 Characterisations of phosphogypsum

This section covers some characterisations techniques that will be used for identification of mineral, chemical bonding, morphology, particle sizes, elemental composition of PG and derivatives.

2.15.1.1 Powder X-ray Diffraction

X-rays Diffraction (XRD) is an analytical technique that has been extensively used for identification, determination and, in some cases for semi-quantification of structures, mineral phases and phase purity in a powder. The relative intensities of peaks and in particular the position of each powder pattern acts as a fingerprint

identifying a particular type of mineral (Treacy & Higgens, 2001). For instance, Mousa, & Hanna, (2013) found only one phase of pure gypsum containing trace of quartz with low intensity characteristic peak at d-spacing value 3.34 Å while characterizing a PG waste. However, Mechi et al., (2016) showed that XRD peaks at 12º indicates the presence of gypsum dehydrate ($CaSO_4 \cdot 2H_2O$) while those at 15º, 30º, 32º and 49º are an indication of the presence of gypsum hemihydrate ($CaSO_4 \cdot \frac{1}{2} H_2O$) and peak at 26.5º is characteristic of gypsum anhydrite ($CaSO_4$).

2.15.1.2 Fourier transformed infrared spectroscopy

Fourier transformed infrared spectroscopy (FTIR) is one of the most widely characterisation techniques that measures vibrational and rotational transitions within chemical bonding to identify organic and inorganic materials (Coates, 2000). Various bonds and functional groups absorb in infrared (IR) region at different wavelengths creating characteristic and unique spectra of molecules (Griffiths & Haseth, 1986). Generally, the absorption bands in the range of 4000–1500 wavenumbers (cm^{-1}) are due to functional groups such as C=O, N-H, OH, CH_3 etc. while the region between 1500–400 cm^{-1} is referred to as the fingerprint region (Cooke, 2005). For instance, the FTIR spectra of PG waste is characterized by broad peak around 1000 cm^{-1} which corresponds to the elongation of sulphate ion within the network and another less intense peak at 600 cm^{-1} corresponding to the deformation of the sulphate ion. The presence of water is usually characterized by two peaks located around 1620 cm^{-1} and 3590 cm^{-1} which are an indication of the two states in which water can be found (hydrated or dihydrated) (Mechi et al., 2016).

2.15.1.3 Scanning electron microscopy

Scanning electron microscopy (SEM) is a useful technique for unveiling characteristics such as morphology, particle size, pore structure as well as identifying the presence of different phases in a given material (Goldstein et al.,

2003). Examination of the PG through SEM technique by Mechi et al., (2016) showed that PG particles had tubular shapes or hexagonal having lengths between 0.2 and 180 µm and 50 µm median. Stacking arrangement of homogenous and prismatic PG crystalline structure and well-developed euhedral structure, monoclinic with a tabular aspect of rhomboidal and orthorhombic crystals were also observed by Romero-Hermida et al., (2019). SEM coupled to Energy Dispersive Spectroscopy (SEM-EDS) is a semi qualitative technique used to obtain information about the chemical composition of the sample. Walawalkar et al., (2016) were able to observe REE content on a cross-section polished PG particle using EDS mapping technique.

2.15.1.4 Particle size distribution

Particle size distribution (PSD) analysis is an important tool to determine the effectiveness of grinding in order to ascertain the degree of liberation of economic elements from the gangue (Wills, 2006). PSD is usually presented as the percentage of the total dry weight occupied by a given size fraction (Di Stefano et al., 2010). Walawalkar et al., (2016) found that the average particle size of PG was about 71 µm which eliminated the need for crushing and grinding during their leaching process.

2.15.1.5 Thermogravimetric analysis

Thermogravimetric analysis (TGA) is one of the most common thermal analysis techniques used to measure the changes in weight as temperature or time vary in a controlled atmosphere (Prime et al., 2009). According to Mechi et al., (2016), weight loss below 300 ºC in PG corresponds to the evaporation of water related to the residual moisture whereas temperature higher than 300 ºC is attributed to the degradation or decomposition of PG into other phase such as anhydrite.

2.15.1.6 X-Ray fluorescence spectroscopy

X-ray fluorescence spectroscopy (XRF) is a rapid quantitative technique, which allows determining the elemental composition of both majors and traces (bulk composition) of powdery samples (Bekkum et al., 1991). XRF analysis of PG showed that Ca and S are the main component of PG and weight loss on ignition (LOI) due to the dehydrated gypsum was about 18 % (Romero-Hermida et al., (2019).

2.15.1.7 Inductively coupled plasma spectroscopy

Inductively coupled plasma (ICP) spectroscopic technique is extensively used to quantitatively determine the concentrations of elements in aqueous samples. Although ICP-OES has the advantage over other atomic spectroscopic techniques such as atomic absorption spectroscopy (AAS) in terms of detection limit (low), ICP-mass spectroscopy (MS) provides lower detection limits and simpler spectra than ICP-OES (Zawisza et al., 2011). In a study by Walawalkar et al., (2016), ICP-OES was used to determine the concentrations of calcium and REE in the leached solutions of PG.

2.15.1.8 Neutron activation analysis

Neutron activation analysis (NAA) is a valuable technique that can allow to obtain both qualitative and quantitative measurement of elements (major, minor and trace) in a solid sample. According to Hibstie et al, (2013), NAA can measure and detect all the elements in a sample irrespective of their chemical form or oxidation state in which they can be found.

2.15.2 Characterisations of polymer nanofibers

The assessment of the parent polymer to the polymer nanofiber is usually carried out in attempts to understand the entire electrospinning process. The characterizations of these polymer materials and in particular the electrospun nanofibers generally aim to understand the geometry, physical and structural, mechanical, chemical, crystallinity, properties (Lyons & Ko, 2005). These characterisations are briefly discussed in the following sections.

2.15.2.1 Geometric assessments

The geometry of polymer nanofibers can be carried out through characterisation techniques such as atomic force microscopy (AFM), scanning electron microscopy (SEM) and transmission electron microscopy (TEM). These characterisations enable understanding of the properties of the polymer nanofibers such as its diameter, diameter distribution, orientation and morphology (Demir et al., 2002; Li et al., 2002). Among other techniques, SEM is the quickest method for obtaining the information about the structure or surface morphology and diameters of the polymer nanofibers. The diameters of the nanofibers can also be obtained through TEM which is an alternative method especially for extremely small fibres in the range below 300 nm. Regarding the sample preparation, TEM has a slight advantage compared to SEM since it does not require the sample to be in dry state as it is for SEM. This means that, the electrospun polymer nanofiber from the polymer solution can directly be analysed by TEM. However, the two techniques require a small amount of the sample for analysis. In addition to SEM and TEM, AFM is another method and actually the best for observing any type of surface morphology with exact description of polymeric fibres. Furthermore, AFM can also be used for the characterisations of roughness of the polymer nanofibers (Demir et al., 2002).

70

2.15.2.2 Chemical assessments

Fourier transform infra-red, in particular attenuated total reflectance (FTIR-ATR) and X-ray photoelectron spectroscopy (XPS) are commonly carried out to assess the molecular structure or chemical properties on the surface of the polymer nanofibers. IR is usually described as the quickest method for observing the information of the polymer nanofibers or any type of samples. For instance, the molecular components present on the polymer nanofibers would appear as peaks in the IR spectra (Huang et al., 2000). The IR technique plays a major role for the characterisation of parent polymer and modified nanofibers in assessing for the surface and intramolecular interactions (Huang et al., 2001). XPS is mainly used to observe the formation of bonds on the surface of parent and modified nanofibers (Kampalanonwat & Supaphol in 2011; Deng et al., 2003a). Besides, the two aforementioned techniques, the chemical properties of polymeric nanofibers can also be evaluated using the water contact angle analysis by measuring their hydrophilicity (Huang et al., 2003; Deitzel et al., 2002).

2.15.2.3 Physical and mechanical assessments

Physical properties of polymer nanofibers can be carried out using techniques such as thermal gravimetric analysis (TGA) (Kim & Lee, 2000), capillary flow porometer (Li et al., 2002; Schreuder-Gibson et al., 2002) and Brunauer, Emmett and Teller (BET) (Brunauer, et al., 1938). BET has been the most frequent method for determination of the surface area of porous materials and other related materials such as polymer nanofibers. Jing et al., (2016) analysed polymer nanofibers using BET method before and after modification with diethylammonium dihydrogen phosphate. The results showed that the specific surface area of the modified fibres increased from 9.4 m^2g^{-1} to 12.3 m^2g^{-1}. This increase in the surface area was attributed to an increase in the roughness of the modified polymer nanofibers. Unlike the physical assessments which are carried to analyse the characteristics such as the pore sizes, porosity, specific surface area and weigh loss of the polymer

nanofibers, mechanical assessments deal with the properties such as tensile strength and strain at the break (Yee et al., 2008; Shields et al., 2004). However, carrying out mechanical characterisations on individual nanofibers is difficult and challenging to achieve due to their small dimensions. Therefore, the existing methods and standards for assessing the mechanical behaviour of polymer nanofibers are not adequate.

2.16 Chapter Summary

This chapter has provided the relevant information concerning the rare earths elements (REEs), their indispensability in current advanced technologies, supply, scarcity and more specifically the possible extraction and recovery of REEs from phosphogypsum waste feedstock. Despite the fact that there exist some applications of phosphogypsum, the rate of its production exceeds the rate of reuse worldwide, hence offering a good opportunity for long term REE recovery to alleviate the supply and scarcity. It was noted that the extraction of REEs from phosphogypsum stands out as one of the most attractive ways of REE beneficiation through hydrometallurgical processes but the leaching efficiency is still not well established and no study was found that combined the extraction of REE with subsequent synthesis of phosphogypsum whiskers. This means that there is a need for further work in that direction.

Considering the gaps identified in the literature review, the research presented in this thesis aims at developing new efficient pre-treatment methods through dissolution and recrystallization of phosphogypsum with subsequent extraction of REEs, modifying the polystyrene polymer support with the most known REE ligands (D2EHPA and DGA) and developing new nanofiber adsorbents using electrospinning technique for REE recovery and testing their applicability.

The literature review therefore informed the formulation of the hypothesis and research questions presented in Chapter 1.

The next chapter describes the detailed experimental procedures and instrumental set-ups that were conducted in an attempt to achieve the research objectives set in this thesis.

73

3. EXPERIMENTAL AND ANALYTICAL TECHNIQUES

3.1 Introduction

The present chapter gives a detailed description of materials and chemicals reagents used throughout the study. The experimental procedures, equipment set-ups for each characterization technique as well as the schematic design of the research approach are given in this Chapter.

3.2 Experimental diagram

In an attempt to answer the research questions laid out in Section 1.2 of Chapter 1 and to achieve the objectives set in this study, a schematic diagram representing three main sections was designed as shown in Figure 3.1. These three sections make up the core of the current study and correspond to chapters (four, five and six) that involve the presentation and discussion of data obtained from various experiments.

3.3 Material and sampling

The as-received phosphogypsum (PG) feedstock was a representative sample collected at a dump of Omnia Phosphates located in Rustenburg, North-West province of South Africa (Figure 3.2). This PG is originally wet when it comes from the production line of phosphoric acid. Thus, the water associated with it, is usually collected in dams from the heap on which it is disposed. This is mainly done to avoid the dispersion of the dry PG over the surrounding areas. However, in the experimental tests, the as-received PG sample (15 kg) was dried for four days at a temperature of 60–70 °C in a hot air oven prior to the utilisation.

74
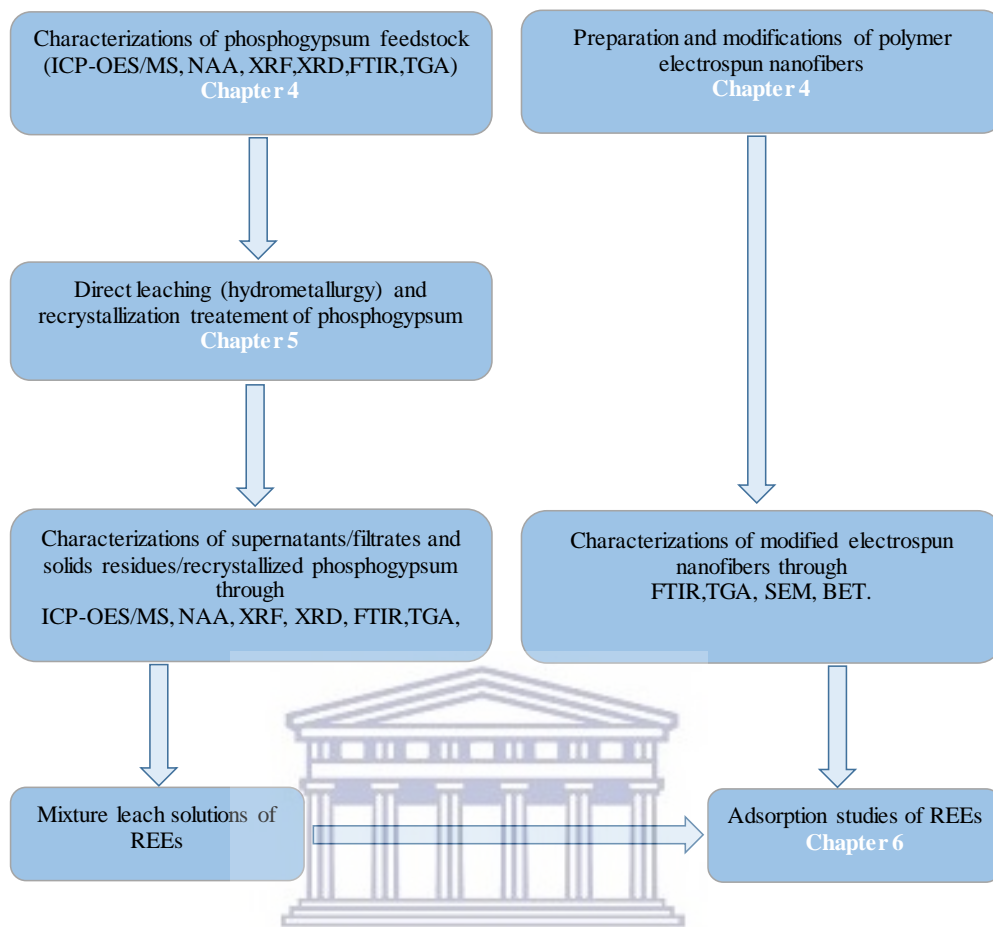
Figure 3.1: Schematic diagram of experimental study

Figure 3.2: Phosphogypsum stockpile at Omnia Phosphates located in Phokeng near Rustenburg, North-West province of South Africa.

3.4 Reagents

The chemical reagents that have been used throughout the experimental sections of this study, their sources and purities are respectively listed in Table 3.1. Some of these reagents were used as received whereas other required specific preparations such as dilution in the case of mineral acids or dissolution of salts.

Table 3.1: Chemical reagents, suppliers and purity

Reagents	Suppliers	Purity (%)
Calcium sulfate dihydrate (commercial gypsum)	Science world	99.00
Cerium(III) nitrate hexahydrate	Sigma-Aldrich	99.90
Diglycolic acid	Sigma-Aldrich	90.00
Di(2-ethylhexyl) phosphoric acid	Sigma-Aldrich	97.00
Hydrochloric acid	Science world	65.00
Neodymium(III) nitrate hexahydrate	Sigma-Aldrich	99.90
Nitric acid	Science world	99.80
N,N-dimethylformamide	Sigma-Aldrich	≥ 99.00
Polystyrene	Sigma-Aldrich	-
Tetrahydrofuran	Sigma-Aldrich	≥ 99.00
Sulfuric acid	Merck	95–98
Ethylenediaminetetraacetic acid (EDTA)	Kimix	95.90
Ethanol	Sigma-Aldrich	96.00

3.5 Total acid digestion

The total acid digestion of the as-received PG and related solid samples was adopted and modified from Al-Thyabat & Zhang, (2015). In this study, approximately 0.5 g of the solid sample was obtained using a weighing boat. The weighed sample was added to 10 mL of concentrated 6 M HNO_3 initially measured in a 25 mL beaker. The resulting mixture was poured into a 100 mL flask and heated on a hot plate for approximately 20 min. The flask was afterwards filled up to the mark with deionized water and filtered using 0.45 µm syringe filter prior to elemental analysis.

For major elements, in particular calcium content and REEs analysis, the aqueous samples from the digestion were respectively diluted 20 and 10 times. The analysis of major elements was obtained through ICP-OES while ICP-MS was used for REEs composition throughout the study.

3.6 Theoretical water content

The theoretical water content of the as-received PG was calculated by weighing certain grams of the feedstock thereafter recording the weight, the sample was air dried in an oven for 24 h at a temperature of 60–70 °C. The dried PG sample was reweighed and theoretical water content (%) was calculated as illustrated in equation 3.1. This was carried out in an attempt to know the moisture content of the as-received PG prior to the leaching process as much water content can affect the concentration of the leaching agent.

$$\text{water content (\%)} = \frac{(W_i - W_d) \times 100}{W_i}$$
Equation 3.1

Where W_i and W_d are respectively weights of the as-received and dried PG.

3.7 Direct leaching of phosphogypsum

The leaching method used in this study was adopted and modified from the existing literature. In this study, three acids that are commonly used in leaching processes at small scale (laboratory) and large scale (industry) namely HCl, HNO_3 an H_2SO_4 were selected to achieve this task. These three inorganic acids are all strong acids but HCl is the strongest among the three followed by H_2SO_4 and HNO_3 (Van der Hagen & Järnberg, 2009). The effects of these acids were investigated for direct leaching of REEs and other elements from the as received phosphogypsum by varying the parameters such as concentration, reaction time, temperature, solid liquid ratio and stirring speed. These parameters were investigated by varying one parameter a time while the rest were kept constant as shown respectively in Tables 3.2 through 3.7. The leaching process was carried out under a reflux system in a

77

double neck round bottle as shown in Figure 3.3. The double neck bottle was used for sampling purpose of aliquot.

Table 3.2: Effect of concentration

Lixiviant	constant				variable
	S\L ratio	Temperature (°C)	Reaction time (min)	Stirring (rpm)	Concentration (M)
HCl	0.1	80	120	300	
HNO$_3$	0.1	80	120	300	0.5; 1; 1.5; 2; 2.5; 3; 3.5
H$_2$SO$_4$	0.1	80	120	300	

Table 3.3: Effect of reaction time

Lixiviant	constant				variable
	Concentration (M)	S\L ratio	Temperature (°C)	Stirring (rpm)	Reaction time (min)
HCl	2	0.1	80	300	
HNO$_3$	2	0.1	80	300	20; 40; 60; 80; 100; 120
H$_2$SO$_4$	1.5	0.1	80	300	

Table 3.4: Effect of temperature

Lixiviant	constant				variable
	Concentration (M)	Reaction time (min)	S\L ratio	Stirring (rpm)	Temperature (°C)
HCl	2	60	0.1	300	
HNO$_3$	2	60	0.1	300	30; 40; 50; 60; 70; 80
H$_2$SO$_4$	1.5	120	0.1	300	

Table 3.5: Effect of solid to liquid (S\L) ratio

Lixiviant	constant				variable
	Concentration (M)	Reaction time (min)	Temperature (°C)	Stirring (rpm)	S\L ratio
HCl	2	60	50	300	
HNO$_3$	2	60	60	300	0.1; 0.12; 0.18; 0.22
H$_2$SO$_4$	1.5	120	50	300	

Table 3.6: Effect of stirring

| Lixiviant | constant | | | | variable |
	Concentration (M)	Reaction time (min)	Temperature (°C)	S\L ratio	Stirring speed (rpm)
HCl	2	60	50	0.1	
HNO$_3$	2	60	60	0.1	300; 600
H$_2$SO$_4$	1.5	120	50	0.1	

Table 3.7: Identified optimum conditions

Lixiviant	Concentration (M)	Reaction time (min)	Temperature (°C)	S\L ratio	Stirring (rpm)
HCl	2	60	50	0.1	600
HNO$_3$	2	60	60	0.1	600
H$_2$SO$_4$	1.5	120	50	0.1	600
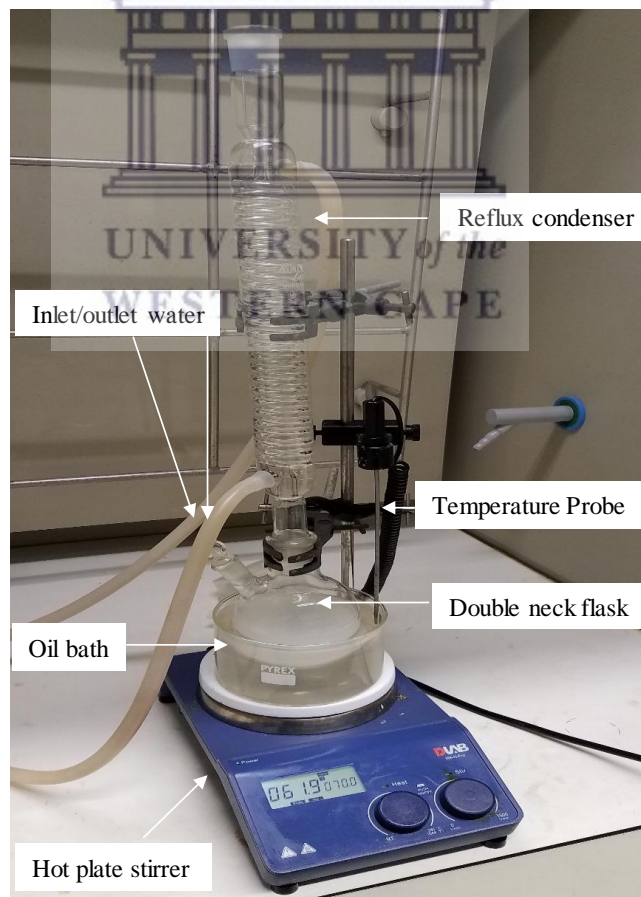
Figure 3.3: Setup of the leaching experiments

79

3.8 Recrystallization of phosphogypsum

The recrystallization of the as-received PG for up concentration of REEs was developed from a few studies with some changes. Prior to recrystallization, about 10 g of the as-received PG was weighed and mixed with 50 mL solution of 2 M HCl or 2 M HNO_3 and then the mixture was stirred at 600 rpm in a reflux system for 1 h at 60 °C. Thereafter, the resulting solution was directly centrifuged for 5 min at 1500 rpm. The supernatant was placed in an Erlenmeyer flask to allow the recrystallization process to take place for about 3 h at an atmospheric pressure until no further sign of recrystallization was observed from the supernatant. The precipitate (recrystallized gypsum) was separated from the mixture through filtration. The obtained recrystallized gypsum was washed with deionised water until neutral pH 7.0 and dried in an air oven at 60 °C for overnight. Then, the obtained material was later characterized by XRD, FTIR, SEM and TGA. The supernatant (filtrate) obtained from the first cycle was used for two more cycles making a total of three for each process. The final supernatant was diluted 10 and 20 times for determination of REEs and major elements content. The final concentration is considered as an accumulated content of three cycles. Figure 3.4 shows a schematic diagram of the dissolution and recrystallization of PG with subsequent REE recovery step that was developed in this study.
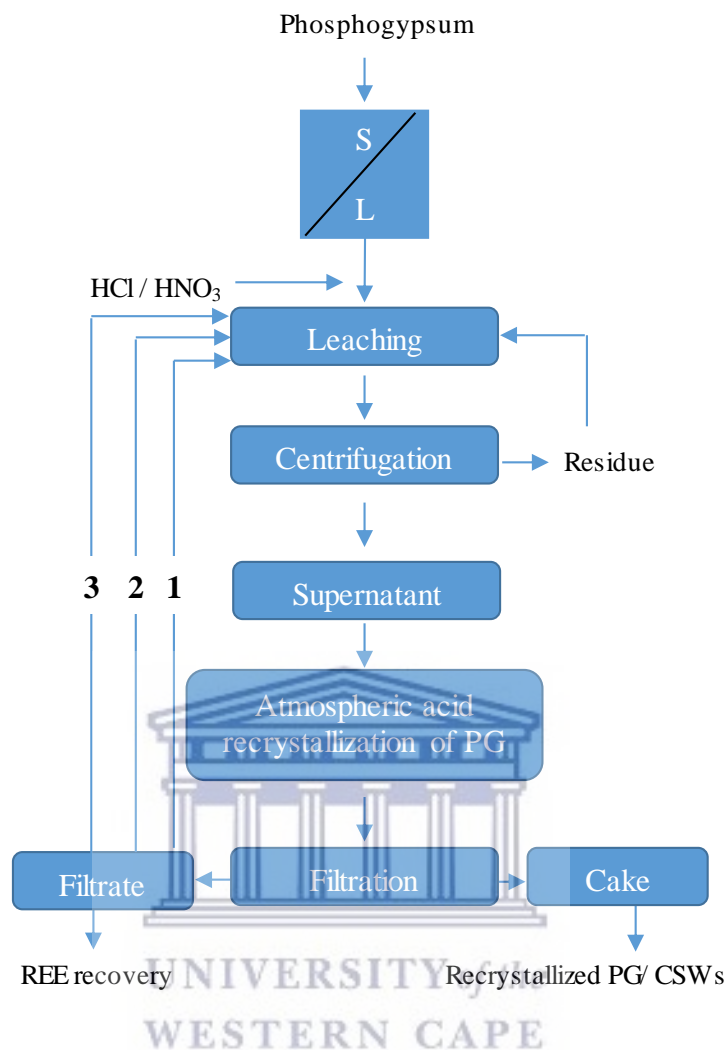
Figure 3.4: Developed schematic diagram of atmospheric acid recrystallization of PG combined with REE recovery

3.9 Electrospinning process

The electrospinning technique was used to fabricate nanofiber based adsorbent membranes. In this study the setup was a horizontal double nozzle spinning setup. The apparatus is shown in Figure 3.5. The electrospinning conditions for the preparation of the nanofiber support were modified from the available literature (Pereao et al., 2020). Prior to the electrospinning process, the polymer solution was prepared by dissolving an appropriate mass (wt%) of the polystyrene beads (PS) using a mixture of solvents DMF:THF (3:1) making up a total volume of 10 mL in each case.

81
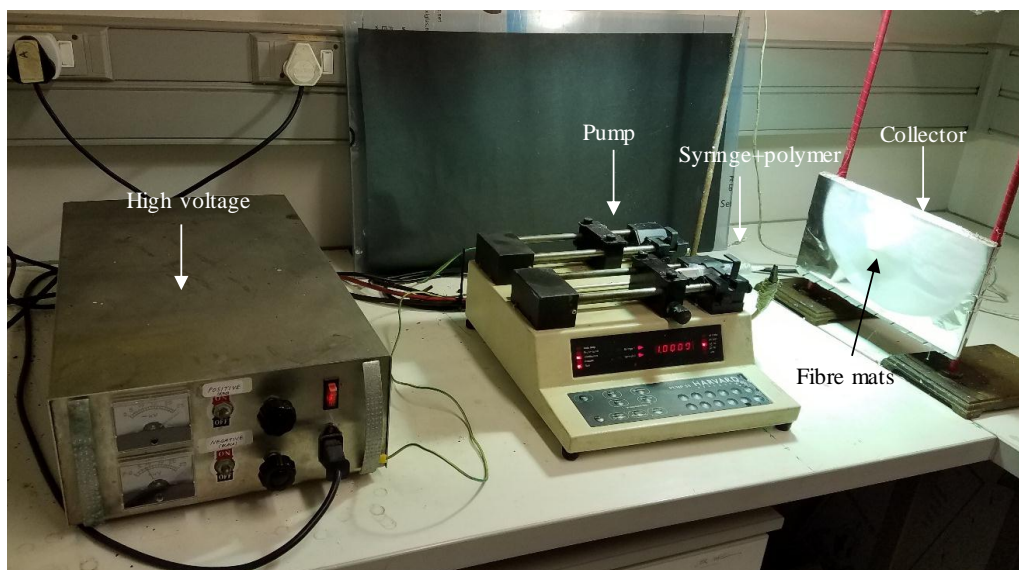
Figure 3.5: Horizontal apparatus of the electrospinning used in this study

In this study only the weight % (wt%) of the polymer was investigated during the preparation of the nanofiber supports and the rest of the parameters which are related to instrument setup were kept constant as can be seen in Table 3.8. In each case, the obtained polymer solution was filled in a 10 mL syringe that was fitted with a needle with inner diameter of 0.8 mm. Then the syringe was placed on a programmable syringe pump situated at about 15 cm distance from a rectangular glass plate covered with aluminium foil that acted as the counter electrode and collector of the nanofiber mats. All samples were spun for 6 h to allow sufficient deposition of fibre mats on the aluminium foil. The deposited fibre mats were thereafter air-dried at room temperature for 24 h in order to remove the residual solvent prior to further treatment.

Table 3.8: Preparation of PS solutions at different concentrations (wt%)

samples	constant					varied
	voltage (kV)	flow rate (mL/h)	collector distance (cm)	deposition time (h)	DMF: THF ratio	PS (wt%)
PS8	25	1.0	15	6	3:1	8
PS10	25	1.0	15	6	3:1	10
PS12	25	1.0	15	6	3:1	12
PS14	25	1.0	15	6	3:1	14

3.9.1 Modification of PS polymer

The modifications of PS polymer solution or PS nanofiber mats were undertaken in order to improve the sorption capacities of the PS electrospun nanofibers for metal ions extraction. In this study post-functionalization and direct blending methods have been used depending upon the type of the ligands. The following subsections briefly describe these two approaches.

3.9.1.1 Direct blending of PS with D2EHPA ligand

Direct blending of the PS polymer solutions with di-(2-ethylhexyl) phosphoric acid (D2EHPA) ligand was carried out using the polymer concentration of 14 wt% (1.47 g) as set in Section 3.8 and discussed in Section 4.2.1.1 of Chapter 4 at different concentrations of D2EHPA ligand of 5 wt% (0.49 g), 10 wt% (0.98 g, 15 wt% (1.46 g) and 20 wt% (1.95 g) in a mixture of solvents DMF:THF (3:1) by keeping the total volume of the final solution to 10 mL in each case. The resulting modified polymer solution was stirred for approximately 4 h at temperature of 30 °C and thereafter transferred into a syringe for electrospinning process. The direct blending used in this study was modified and adopted from a recent procedure described by Da Silva et al., (2019) who modified nylon-6 polymer with D2EHPA ligand for zinc and nickel extraction.

Table 3.9 gives the main conditions that were used during the modification of PS polymer with D2EHPA ligand whereas Figure 3.6 shows a macroscopic image of the unmodified polymer solution and after the modification of with D2EHA ligand.

83

The colour changed from a cloudy aspect (A) to clear solution (B) indicating that the reaction took place between the PS polymer and the added ligands. The proposed mechanism for the modification of PS polymer with D2EHPA ligand was an addition reaction as illustrated in Figure 3.7. The reaction is suggested to occur through the attack of the proton of the hydroxyl group leading to a strong bond in an addition fashion under DMF and THF as medium using a mild temperature of 30 °C.

Table 3.9: Modification of PS polymer solution at different concentrations (%) of D2EHPA

samples	voltage (kV)	flow rate (mL/h)	collector distance (cm)	PS (wt%)	DMF: THF ratio	D2EHPA (%)
DH-PS5	25	1.0	15	14	3:1	5
DH-PS10	25	1.0	15	14	3:1	10
DH-PS15	25	1.0	15	14	3:1	15
DH-PS20	25	1.0	15	14	3:1	20
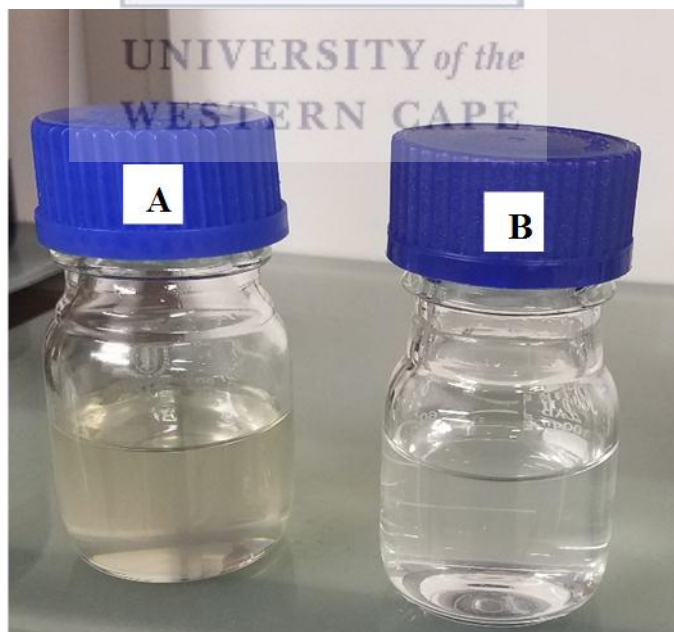
Figure 3.6: Polymer solution of unmodified (A) and modified polymer solution with D2EHPA ligand (B).
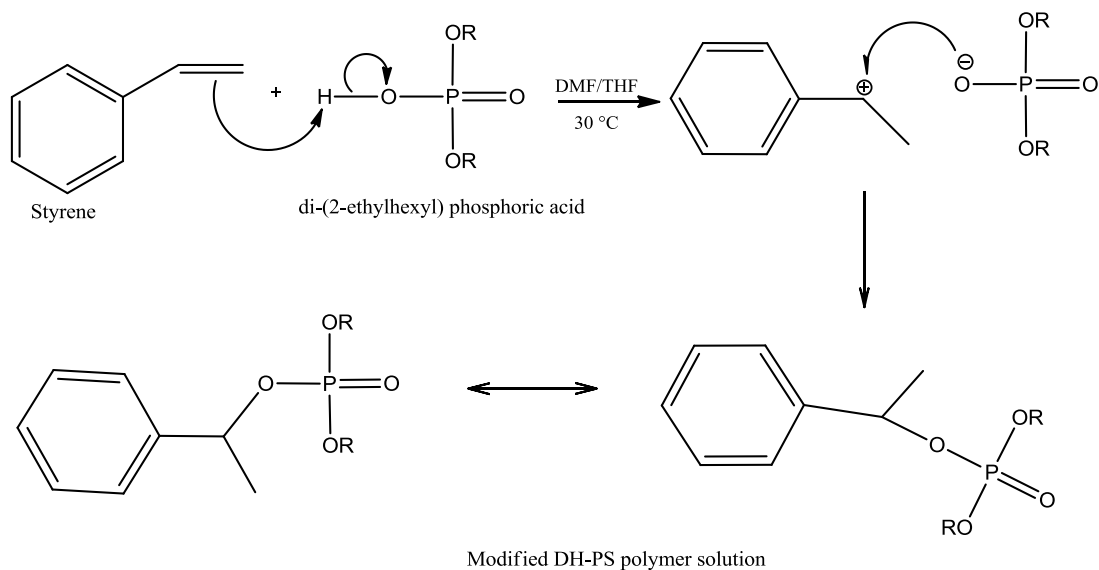
Figure 3.7: Addition reaction mechanism of D2EHPA and styrene (polystyrene backbone)

3.9.1.2 Surface modification with DGA ligand

The surface modifications of the PS14-nfs selected and discussed in Section 4.2.1.1 of Chapter 4 was mainly performed in attempts to generate a new carbon-carbon bond. Approximately 0.1 g of PS14-nfs mats was cut in square shape and attached to homemade polymer sample holder and thereafter immersed in different concentrations of diglycolic acid (DGA) of 0.75 g (0.0056 mole), 1.5 g (0.0112 mole), 2.25 g (0.017 mole) and 3 g (0.0224 mole) using a mixture of 5 % acetic acid (10 mL) and 20 mL methanol. Thereafter the PS14-nfs was held under stirring of the solution mixture for 4 h at temperature between 40–45 °C. Table 3.10 gives the main conditions used during the modification of PS14-nfs with DGA ligand while Figure 3.8 shows the set of the modification experiment. The surface modification of PS14-nfs carried out in this study was adopted and modified from recent studies by Pereao et al.; (2019) and Repo et al., (2010). The proposed mechanism for the modification of PS14-nfs with DGA ligand was an electrophilic aromatic substitution as illustrated in Figure 3.9.

Table 3.10: Surface modification of PS14-nfs at different concentrations (g) of
DGA

sample	voltage (kV)	flow rate (mL/h)	collector distance (cm)	PS (wt%)	DGA (g)
DG-PS0	25	1.0	15	14	0.5
DG-PS1	25	1.0	15	14	1.0
DG-PS15	25	1.0	15	14	1.5
DG-PS2	25	1.0	15	14	2.0
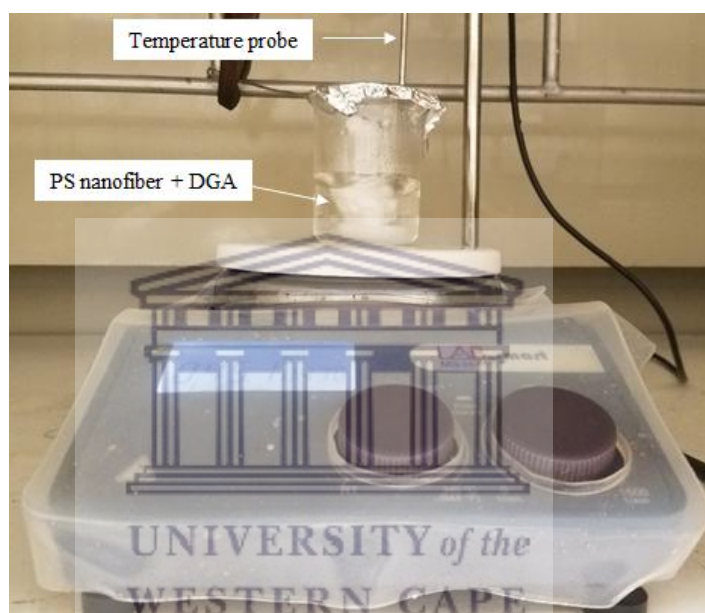
Figure 3.8: Surface modification set up of PS14-nfs mats in DGA solutions

The oxygen of the carbonyl group is first protonated to form a strong reactive intermediate electrophile which is in turn attacked by the benzene ring of the PS which acts like a nucleophile. This attack occurs from a pair of π-electrons of the benzene ring which led to the destruction of the aromaticity the PS molecule. The positive charge created after the attack is delocalized over the ortho and para positions (resonance). To restore the aromaticity of the benzene ring, a pair of π-electrons of the hydroxyl group assist to eliminate the now-extraneous proton on the benzene ring. The backbone of the ligand was thereafter restored with elimination of the hydronium which decomposed in acid medium as the reaction was acid catalysed.

86
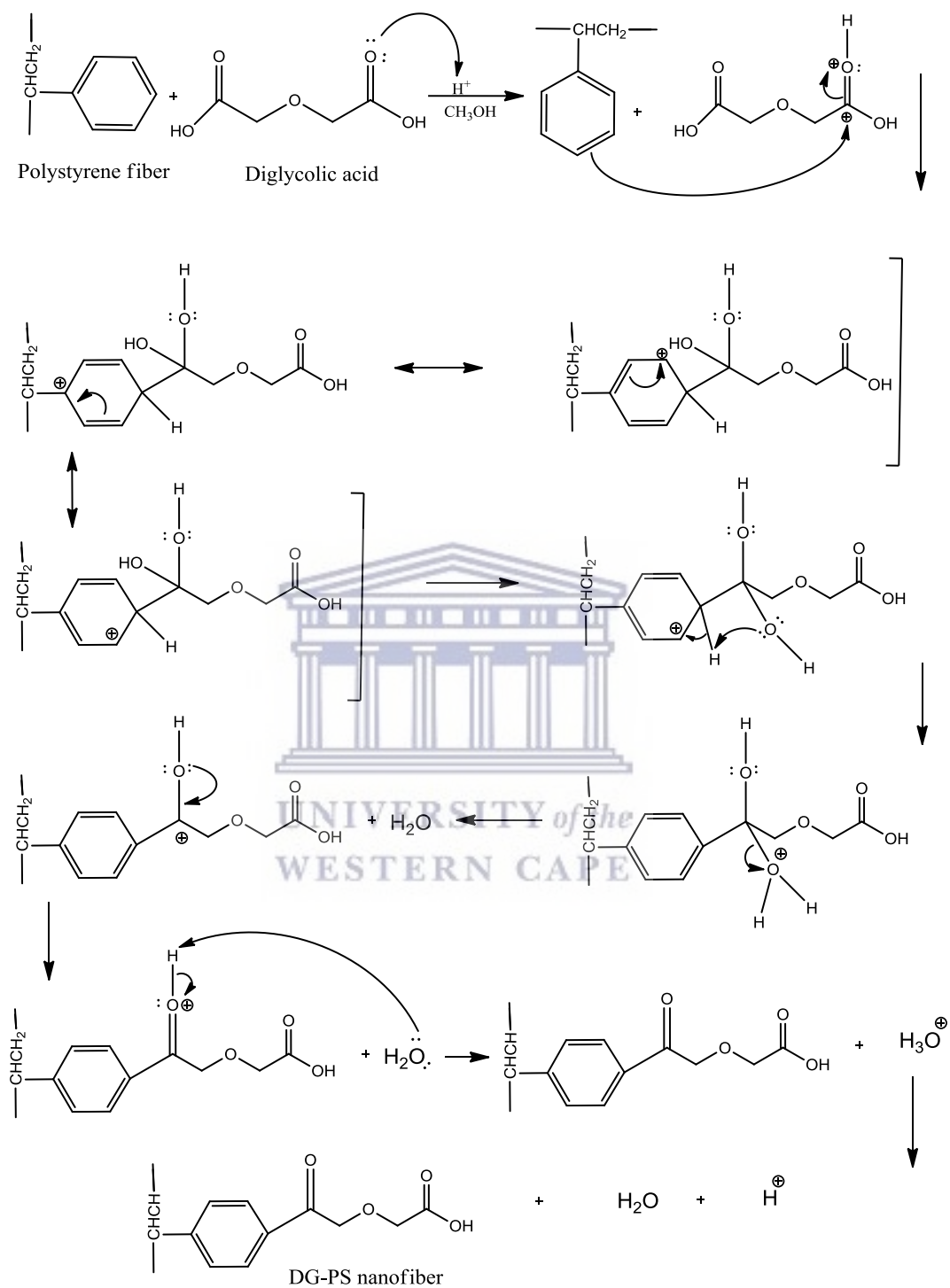
Figure 3.9: Proposed electrophilic aromatic substitution reaction

3.10 Adsorption studies

3.10.1 Preparation of the stock solutions

Simulated solutions (model solutions) of Ce^{3+}, Nd^{3+} and Ca^{2+} having the concentrations of 1000 ppm each were prepared by weighing certain grams of their respective salts namely, $Ce(NO_3)_3 \cdot 6H_2O$; $Nd(NO_3)_3 \cdot 6H_2O$ and $CaCl_2 \cdot 2H_2O$ into separate 1000 mL volumetric flasks in which about 200 mL of deionised water was initially measured. The solution was then shaken until complete dissolution of the weighed salt and then 800 mL of deionised waster was added to fill the volumetric flask to the 1000 mL mark. The stock solutions were kept in the fridge.

In the case where lower concentrations were needed, the initial concentration of 1000 ppm was diluted in order to get some specific concentrations. In the case of the PG, the stock solutions from the filtrates were first filtered using a 0.45 μm syringe filter then diluted to specific concentrations based on the initial concentrations of Ce^{3+}, Nd^{3+} and Ca^{2+} obtained from the total digestion experiments as described in Section 3.4.
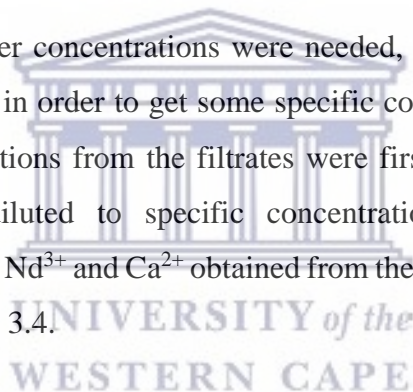
3.10.2 Stability of the adsorbents

DH-PS20 or DG-PS2 nanofibers were tested in solutions of HNO_3 (0.25; 0.5; 1 M) or EDTA (0.05; 0.1;1.5 M) to evaluate their stabilities prior to the adsorption studies. This step was important as it helps to study the possible regeneration of DH-PS or DG-PS. The experiments were carried out using 0.01–0.02 g of DH-PS20 or DG-PS2 nanofiber that was shaken in 10 mL of HNO_3 or EDTA at 25 °C for 1 h. The nanofibers mats were then washed with deionised water and air dried in an oven at 35 °C overnight and then characterized using FTIR.

3.10.3 Batch experiments

The adsorption experiments were carried out to investigate the capacities of various adsorbents prepared in Section 3.8 for the extraction of REEs from the real solution (PG pulp solution) or model solution. The real solution was obtained from acid leaching or filtrate solution after recrystallization of the as-received PG. The adsorption of REEs was conducted through batch studies. Prior to the adsorption using the real solution, the optimization of the process parameters namely initial pH solution, initial concentration of metal ion and contact time was carried out on model solutions of selected REEs (Ce, Nd) and Ca. The steps for the optimization of the aforementioned parameters for DH-PS20 and DG-PS2 nanofiber samples are given in Tables 3.11; 3.12; 3.13 and 3.14. The rest of the parameters such as adsorbent weight, adsorption temperature, solid to liquid ratio and stirring or shaking speed were kept constant throughout the study. The batch adsorption was typically carried out by immersing a certain amount of DH-PS20 or DG-PS2 nanofiber adsorbent (0.01–0.02 g) in 10 mL of a solution containing metal ion (i.e. Ce^{3+}, Nd^{3+} or Ca^{2+}) at a specific pH. The resulting mixture was shaken on the MRC (TOS-4030FD) for a certain contact time at room temperature (~25 °C). After each selected contact time, the adsorbent was removed from the solution and the remaining solution was filtered prior to analysis using ICP-OES/MS to determine the amount of metal ions remaining in the solution and the amount adsorbed was calculated using equation 3.2 below.

$$q_e = \frac{(C_0 - C_e)V}{M}$$ Equation 3.2

In this formula, q_e is the amount of metal adsorbed on the adsorbent in mg/g; C_0 and C_e are respectively initial and equilibrium concentrations of metals in the aqueous solution in mg/L; V and M are volume of the aqueous solution (L) and weight of the adsorbent (g).

89

Table 3.11: Effect of initial pH solution

adsorbent	constant		variable
	contact time (min)	initial conc.(mg\L)	initial pH solution
DH-PS20/DG-PS2	120	80	1;2;3;4;5;6

Table 3.12: Effect of contact time

adsorbent	constant		variable
	initial pH solution	initial conc. (mg\L)	contact time (min)
DH-PS20/DG-PS2	4/5	80	20;40;60;80;100;120

Table 3.13: Effect of initial metal ion concentration

adsorbent	constant		variable
	initial pH solution	contact time (min)	initial conc. (mg\L)
DH-PS20/DG-PS2	4/5	60	40;80;120;160;200;240

Table 3.14: Identified conditions

adsorbent	initial pH solution	contact time (min)	initial conc. (mg\L)
DH-PS20/DG-PS2	4/5	60	160

3.10.4 Adsorption isotherms and kinetics modelling

The experimental data obtained from the adsorption process were compared and studied using the isotherms and kinetics modelling in attempts to describe the mechanisms, performances and practicability design of the adsorption process. For adsorption isotherms, this study only covered the Langmuir and Freundlich systems. The principles behind these two types of adsorption isotherms are briefly described below.

Langmuir is commonly used to explain the adsorption process by assuming that the adsorption takes place through a monolayer system onto a homogenous surface having finite number of identical sites (Liu et al., 2019). This adsorption isotherm

and its linearized form can mathematically be expressed as illustrated below in equations 3.3 and 3.4 respectively.

$$q_e = \frac{q_m b C_e}{1 + b C_e}$$
Equation 3.3

$$\frac{1}{q_e} = \frac{1}{q_m} + \frac{1}{b q_m} \frac{1}{C_e}$$
Equation 3.4

where q_e (mg/g) represents the adsorption capacity at the equilibrium, C_e (mg/L) is concentration of metal ions in the solution at the equilibrium, q_m (mg/g) is the maximum monolayer adsorption capacity and b (L/mg) is the Langmuir constant which also indicates the energy of adsorption. The values of q_m and b are usually obtained from the slope and the intercept respectively of the straight line of the linearized form of the Langmuir equation (Yang et al., 2011). In addition to the aforementioned parameters, R_L is another important parameter that can be obtained from the Langmuir isotherms. R_L is a factor that determines the tendency between the adsorbents and adsorbate during the adsorption process and can be calculated from equation 3.5 (where b is the Langmuir constant and Co is the initial concentration of solute). The values of R_L help to classify the adsorption process (Neghlani et al., 2011) as follow: R_L=0: Irreversible; R_L=1: Linear; $0 > R_L < 1$: Favourable; $R_L > 1$: Unfavourable.

$$R_L = \frac{1}{1 + b C_o}$$
Equation 3.5

In contrast to the Langmuir isotherm, the Freundlich isotherm allows the empirical relationship between the surface of the adsorbent and the concentration of the adsorbate to be explained. Freundlich isotherm can be applied by assuming that the surface of the adsorbent onto which the adsorbate adsorbs is heterogeneous. This isotherm and its linearized form can mathematically be expressed as shown in equation 3.6 and 3.7 respectively.

$$q_e = K_F C_e^{1/n}$$

Equation 3.6

$$\ln q_e = \ln K_F + \frac{1}{n} \ln C_e$$

Equation 3.7

Where q_e and *Ce* are respectively the adsorption density and the concentration of the adsorbate in solution at the equilibrium. *KF* and *n* are Freundlich constant (or adsorption capacity) and adsorption intensity of the adsorbent respectively. The value of *n* helps to predict the adsorption process and values between 1–10 indicate that the sorption is favourable. According to Uddin et al., (2009), the values of *KF* and *n* can be calculated from the intercept and slope of the linearized form of the Freundlich equation respectively.

3.10.5 Kinetic models

The kinetic models allow evaluation of the rate of the adsorption process and potential rate-controlling step. The kinetic performance of an adsorbent is utmost important for the application. The kinetic analysis determines the rate of solute (adsorbate) uptake which invariably indicates the reaction time required to complete an adsorption process. In this study, the kinetic experimental data obtained from the batch adsorption were analysed using pseudo-first order and pseudo-second order models. These two models can be expressed as illustrated in equations 3.8 and 3.9 respectively.

$$\frac{dq_t}{dt} = k_1(q_e - q_t)$$

Equation 3.8

$$\frac{dq_t}{dt} = k_2(q_e - q_t)^2$$

Equation 3.9

Where q_e et q_t indicate the amount of the solute adsorbed (mg/g) at the equilibrium and time *t* respectively. k_1(min^{-1}) and k_2 (g/mg/min) are respectively the rate constants of the pseudo first-order and second-order adsorption models.

92

3.10.6 Desorption and regeneration experiments

Desorption experiments are important in an adsorption study as it allows an estimation of the reusability of the adsorbent and amount of the adsorbate adsorbed. In this study, DH-PS20 or DG-PS2 nanofiber (0.01–0.02 g) was first transferred into 10 mL of 160 mg/L of Ce^{3+} or Nd^{3+} at the optimum pH as identified in Section 3.9.3, and the mixture was shaken for 1 h at room temperature (~25 °C). Thereafter, the resulting solution was filtered and the amount of the metal ions adsorbed was determined through ICP-OES/MS. DH-PS20 or DG-PS2 nanofibers were thereafter washed with deionised water to remove excess of metal ions that were not adsorbed and then air dried in an oven overnight at temperature of 35 °C (slightly higher than room temperature). The dried metal loaded DH-PS20 or DG-PS2 fibres were then transferred again into 10 mL of 1.0 M HNO_3 and shaken for 1 h at 25 °C for desorption of the metal ions loaded. The obtained solutions after the desorption were analysed by ICP-OES/MS and the regenerated DH-PS20 or DG-PS2 fibres were used again in three another cycles of adsorption.

3.11 Characterization techniques

3.11.1 Fourier Transformed Infra-Red spectroscopy

Fourier Transformed Infra-Red (FT-IR) required minimal sample preparation and only a small amount of sample. Prior to FT-IR analysis, a background was first run on the instrument (Model: PerkinElmer UATR Two). Thereafter a small amount of either PG, polymer nanofibers or other samples (liquid or solid) generated in this study was placed on the crystal of an attenuated total reflectance (ATR) where a certain Gauge force was applied (for solid sample) within the range. In the case of liquid samples, no Gauge force was applied during the analysis. The full set-up conditions of the FT-IR instrument is tabulated below.

Table 3.15: Set-ups conditions on the PerkinElmer UATR Two

Gauge force	40–50
Number of scans	5
Resolution	4 cm^{-1}
Scan range	4000–400 cm^{-1}

3.11.2 Thermogravimetric analysis

Thermogravimetric analysis (TGA) was done using a Simultaneous Thermal Analyzer (PerkinElmer STA 8000). The TGA was used to determine the thermal stability of PG and derivatives, unmodified and modified polymer nanofibers. TGA for adsorbents was mainly conducted in an attempt to examine the thermal behaviour of the nanofiber composite adsorbents before and after the adsorption. Prior to the analysis, the TGA instrument was calibrated in order to obtain stable baseline. Thereafter, about 2–3 mg of the sample were placed in a ceramic pan and heated from 30–1000 °C, at heating rate of 10 °C/ min under nitrogen flow and each analysis was done in triplicate for reproducibility.

3.11.3 X-ray Diffraction analysis

The X-ray diffraction (XRD) for qualitative analysis of the as-received PG and other solid samples generated in this study was carried out on a wide-angle instrument (Model: PW3830 X-ray generator, PANalytical). The set-up parameters of the instrument are given in Table 3.16. The XRD technique requires a little sample preparation prior to the analysis. In the current study, all solid samples were thoroughly packed onto the sample holder using a spatula. Thereafter, the surface of the powdered sample was rendered smooth or flat, and the sample holder was placed in the X-ray diffractometer for analysis.

The quantitative analysis for the determination of mineral phases of the as-received PG was carried out on a PANalytical X'Pert Pro powder diffractometer with X'Celerator detector and variable divergence and fixed receiving slits with Fe

94

filtered Cu-Kα radiation. Thereafter, the mineralogical phases were identified using X'Pert Highscore plus software and relative phase amounts in weight % were estimated using the Rietveld method.

Table 3.16: Instrumental conditions on PW3830 X-ray generator, PANalytical.

First angle	3.015
Generator current	25 mA
Radiation	Cu-Kα
Scan type	Continuous
Scan range	60 °
Step-width	0.03°
Time per step	0.50 min
Voltage	40 kV
Wavelength	λ: 1.54056
2θ	38.98

3.11.4 Scanning electron microscopy analysis

The high-resolution scanning electron microscopy (HR-SEM) analysis was carried out on Zeiss Auriga for both morphological imaging and the electron dispersive X-ray spectroscopy (EDS) for semi-quantitative elemental analyses. All samples (solids) were prepared prior to SEM analysis by sprinkling a small amount of powder onto an aluminium stub covered with double-sided sticky carbon discs. The samples were coated using carbon evaporated by either electric arc method or by metal heating method using an EmiTech K950X coater. After the pre-treatment process, the samples were then imaged. A similar sample pre-treatment was also used on the same instrument for the EDS analysis. The EDS data were collected from an average of five spots mapping on the sample specimen. The instrumental conditions of the HR-SEM-EDS coupled are presented in Table 3.17.

Table 3.17: Instrumental set-up conditions on the Zeiss Auriga

Accelerating voltage	5.00 kV
Exposure time	2–5 min
Imaging particle size	1μm–200 nm
Magnification	5.00–100 kX
Resolution	High
Signal A	inLens
Working distance (WD)	3.5–6.5 mm

3.11.5 Neutron Activation Analysis

Neutron activation analysis (NAA) was used for elemental composition of the as-received PG and related solid samples to determine the REE content. This analysis was carried out at the Joint Institute for Nuclear Research (JINR) at IBR-2 reactor in Dubna, Russia. Samples preparation was done at Franck Laboratory of Neutron Physics (FLNP) in which two channels of the IBR-2 reactor are used for NAA. Prior to analysis (irradiation), all samples were oven dried for 24 h. About 100 mg was placed in a small polyethylene bag (3x1 cm) and aluminium foil cups (diameter 0.5 cm) for short and long irradiation respectively. All PG based samples were first pelletized after weighing using a manual single pellet press machine. This step was particularly done in order to prevent the spilling over of the samples during the irradiation process. All pellets were reweighed again and then placed in polyethylene bags and aluminium cups for short and long analysis respectively. Samples for short-lived analysis were irradiated for 1 min to determine the short-lived isotopes and placed in HPGe gamma-ray detectors to be counted for 3 min, 2 min after being irradiated then for 15 min after 10 min of decay. Long-lived analysis was carried at 100 h in the Cd-shielded channel 1. Samples were repacked after irradiation and measured after 4–5 days (short long-lived isotopes) and 20–23 days (long-lived isotopes) for 30 min and 90 min respectively. The concentration of elements was determined based on gamma spectra using Genie 2000^{TM} (Canberra) or GammaVision (ORTEC) software at FLNP computer lab.

3.11.6 Inductively coupled plasma optical emission spectroscopy

The Inductively coupled Plasma-Optical Emission spectroscopy (ICP-OES) was done using a Varian 720 equipped with an axial-view plasma, a cooled cone interface, CCD detector and Expert II software for data collection. The ICP-OES instrument was calibrated before the measurements with certified standards to check the accuracy and reliability of the analysis. The instrument was thereafter used for elemental composition of liquid samples. Prior to the measurements, the aqueous samples were filtered through a 0.45 μm membrane paper to remove suspended solids and then diluted with deionized water or 2 % HNO_3 depending on the source of the samples. For instance, samples from HNO_3 leaching were diluted with deionized water while 2 % HNO_3 was used for the rest of the samples. Then the samples were diluted 20 and 10 times for majors and traces respectively. The sample was introduced through a high sensitive glass, single-pass cyclone spray chamber and conical nebulizer using argon gas. All measurements were done in triplicate for reproducibility check of the analysis.

3.11.7 X-ray fluorescence spectroscopy

The X-ray fluorescence spectroscopy (XRF) was mainly used for bulk elemental composition of solid samples. 5 g of the solid samples was mixed with approximately 1 g of the binder (wax). The resulting mixture was thoroughly ground and placed in a mould, thereafter it was pelletized under high pressure. The Loss on ignition (LOI) was carried out in a furnace. Table 3.18 gives the set-ups conditions of the XRF instrument.

Table 3.18: XRF instrument set-up conditions on Philips PW 1480
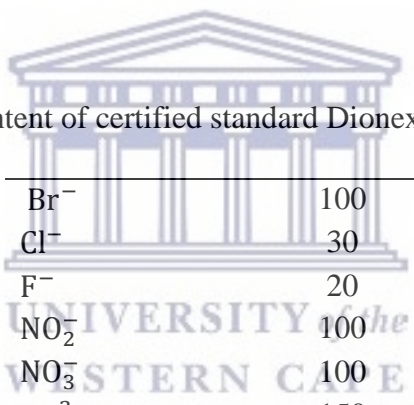
Current	50 mA
Crystal analysers (x5)	LIF 200, LIF 220, GE, PE, PX
Spectrometer tube	Chromium
Voltage	40 kV

3.11.8 Ion chromatography analysis

Ion chromatography (IC) was used to determine the concentration of anions present in the as-received PG. Prior to the measurements, a pulp of the as-received PG was prepared using S\L ratio 1:50. The resulting supernatant was filtered through a 0.45 µm membrane filter to remove the suspended solids and then diluted with deionised water to obtain EC values within a range of 50–100 µS/cm. The final measurements were carried out on a Dionex ICS-16000 instrument equipped with an Ion Pac AS14A colomn and AG14-4 mm guard column. In this measurement, a Dionex SEVEN ANION certified standard was used to check the efficiency of the IC instrument. The concentrations of the seven anions presents in Dionex SEVEN are tabulated below.

Table 3.19: Anion content of certified standard Dionex SEVEN ANION (mg/L)

Br^-	100
Cl^-	30
F^-	20
NO_2^-	100
NO_3^-	100
PO_4^{3-}	150
SO_4^{2-}	150

3.11.9 pH measurements

The pH measures the hydrogen ion [H^+] concentration in a solution to define the acidity or alkalinity of the solution. The pH of all liquid samples generated throughout the study was measured on a SevenCompac pH/ion (Mettler Toledo) instrument. Prior to the measurements, the instrument was calibrated with buffer solutions of pH 4.0 and pH 7.0 at room temperature.

3.11.10   Particle size distribution

Particle size distribution of the as received-PG was conducted using a Malvern Zetasizer ZS (Westborough, MA, USA). The sample was dispersed in ethanol and sonicated for about 15 min then allowed to settle for 5–10 min prior to the measurement (RI of the PG as gypsum was 1.52 and 1.361 for ethanol used as dispersant, relative viscosity:1.1140). The results were recorded as particle per volume percent and the average of a triplicate was used to produce the particle size distribution. The particle size distribution was carried to confirm the gravimetric sieving of the dried PG.

UNIVERSITY of the
WESTERN CAPE

CHAPTER 4

4. CHARACTERIZATIONS OF MATERIALS

4.1 Introduction

The present chapter discusses the results obtained from the characterizations of the materials used or generated throughout the study. These characterizations aimed to give insight on various characteristics of the materials such as mineral phase, surface morphology, chemical and physical properties, thermal properties and chemical composition. The main characterization techniques used for that purpose included the X-ray fluorescence spectroscopy (XRF), Inductively coupled plasma (ICP-OES/MS), Neutron activation analysis (NAA), X-ray diffraction (XRD) analysis, FT-IR analysis, High-resolution scanning electron microscopy (HR-SEM), Energy dispersive spectroscopy (EDS) and particle size distribution.

4.2 Characterization of phosphogypsum and derivatives

The characterizations of the as-received phosphogypsum (PG) and derivatives were carried out to give insight on characteristics and properties of PG. These characterizations were performed by XRD XRF, ICP-OES/MS, NAA, FT-IR, SEM, SEM-EDS, and PSD techniques.

4.2.1 Bulk chemical composition for major elements in PG

Bulk chemical composition of the as-received PG was carried out in triplicate by XRF analysis as described in Section 3.10.8. As can be seen from Table 4.1, the average masses (wt%) of the oxides indicated that CaO and SO_3 were the major oxides making up a cumulative (CaO+SO_3) weight mass of 92.32 wt% followed by P_2O_5 (1.3 wt%) and the rest were present in traces (< 1 wt%). The high mass content of CaO and SO_3 as expected, is characteristic for PG material and represents different forms of calcium

sulphate which, depending upon the amount of water molecules, might be dihydrate ($CaSO_4 \cdot 2H_2O$), hemihydrate ($CaSO_4 \cdot 0.5H_2O$), and anhydrate ($CaSO_4$). The minor proportion of P_2O_5 originates from the residual mineral phosphate ore used during the production of phosphoric acid and is indicative of the degree of acidity. For instance, the pH of the as-received PG was found to be between 3.4 and 4.0 (Table 4.2) indicating a mild acidity and was in good agreement with the acidity reported by Moalla et al., (2018). The measurement of the Loss On-Ignition (LOI) was 6.51 % and could indicate a combined effect emanating from the loss in weight and impurities of the as-received PG (Romero-Hermida et al., 2019). However, Smadi et al., (1999) reported that LOI of PG was solely related to the loss in weight after dehydration rather than due to the loss of impurities during the ignition process.

Table 4.1: Composition of major oxides of as-received PG (mass %)

Oxides	PG1	PG2	PG3	Average	St. Dev
Fe_2O_3	0.04	0.05	0.04	0.04	0.00
MnO	0.01	0.01	0.02	0.01	0.00
Cr_2O_3	0.01	0.01	0.01	0.01	0.00
TiO_2	0.01	0.02	0.40	0.14	0.22
CaO	38.89	39.02	39.41	39.11	0.27
K_2O	0.01	0.01	0.01	0.01	0.00
SO_3	52.88	52.01	51.73	52.21	0.60
P_2O_5	1.30	1.35	1.24	1.30	0.06
SiO_2	0.31	0.31	0.27	0.30	0.02
Al_2O_3	0.05	0.03	0.05	0.04	0.01
MgO	0.07	0.70	0.66	0.48	0.35
Na_2O	0.01	0.01	0.01	0.01	0.00
LOI	6.51	6.59	6.44	6.51	0.08
Total	100.10	100.12	100.29	100.15	

In addition to the major elements shown in Table 4.1, fluorine, phosphate and sulphates were found to be the main anions presents in the as-received PG as can be seen in Table 4.2. Nevertheless, sulphates and phosphates were present in higher concentration compared to fluorine. The molar ratios between sulphates and phosphates was about 12:1. This molar ratio corresponds to weigh masses (wt%) of

101

SO_3 and P_2O_3 obtained from the XRF results discussed in Section 4.1.1. where SO_3 was about 40 fold higher than P_2O_3.

Table 4.2: Anions, acidity and water content of the as-received PG

Anions	mg/kg
Fluorine	99.52 ± 10
Phosphate	1423.53 ± 148.2
Sulphate	18110.18 ± 126.5
Acidity (pH)	3.69 ± 0.27
Water content	20 %

The high amount of sulphates is due to the presence of high content of gypsum in the as-received PG which exists as the main anions while phosphates are an indication of residual phosphoric acid present in the as-received PG. This confirmed the acidity of the as-received PG as shown in Table 4.2. The presence of fluorine is due to an impurity from apatite ore which was initially used for production of phosphoric acid. Apatite ore is generally described as fluoroapatite ($Ca_{10}(PO_4) F_2$) due to the presence of fluorine (Canovas et al., 2019). It can therefore be deduced that the as- received PG obtained from Omnia originated from $Ca_{10}(PO_4) F_2$ rocks.

4.2.2 REE content in the as received PG (minor elements)

The elemental composition analysis of the as-received PG with particular attention on REE content was carried as described in Sections 3.10.6 and 3.10. The elemental analysis was first performed using three techniques namely ICP-OES, ICP-MS and NAA in an attempt to evaluate the efficiency and reliability of each instrument. The results obtained from these three techniques are shown in Table 4.3. As can be seen, of the 15 REEs, La, Ce, Nd, Sm, Eu, Tb, Gd and Yb were repeatedly detected through the three techniques. La, Ce and Nd which are part of the light REEs group (La-Eu) were the most abundant REEs found in the as-received PG with concentrations ranging between 400 to 600 mg/Kg; 1100 to 1500 mg/kg and 600 to 850 mg/kg respectively. In contrast, among the heavy REEs (Gd–Y), only Gd and Y dominated in this group but their concentrations were far lower compared to that of LREEs and ranged between

102

45 to 85 mg/Kg. The trend in terms of REEs content, with LREEs tending to have high concentrations compared to HREEs, is common for PG material and is believed to reflect their respective composition in the earth's crust as discussed in Section 2.2. Table 4.3 furthermore indicated that all 15 REEs were detected using ICP-MS followed by ICP-OES in which only a few REEs (Pr, Tm and Lu) were not detected compared to NAA. However, although, NAA could not detect all REEs, it revealed the highest amounts of REEs in particular for La, Ce and Nd compared to ICP-MS and OES.

Table 4.3: REE content of as-received PG by different instruments (mg/Kg)

REEs	ICP-OES	ICP-MS	NAA
La	405 ± 8	488.1 ± 5	612 ± 9
Ce	1121 ± 12	1243 ± 9	1520 ± 21
Pr	*	165.2 ± 4	*
Nd	604 ± 10	743 ± 6	862 ± 16
Sm	171 ± 6	121.7 ± 3	138 ± 3
Eu	28 ± 3	26.9 ± 3	29.9 ± 2
Gd	45 ± 3	82.4 ± 3	12.5 ± 0.6
Tb	11 ± 2	8.1 ± 1	8.7 ± 1
Dy	28 ± 3	30 ± 4	*
Ho	4 ±1	3.5 ± 1	*
Er	10 ± 2	5.7 ± 1	*
Tm	*	0.4 ± 0.1	0.9 ± 0.2
Yb	2 ± 0.6	1.7 ± 0.2	1.7 ± 0.02
Lu	*	0.2 ± 0.01	*
Y	76 ± 5	85.7 ± 3	*

*: Not detected

This might be as a result of its simpler and easier sample preparation where no digestion nor dilutions steps are required compared to ICP-OES and MS in which these steps entail loss of more elements during the sample preparation. However due to the time of waiting as well the use of a nuclear reactor that is required to carry out NAA analysis and also its deficiency in detection for the full range of REEs, ICP-OES and MS are preferable. Therefore, ICP-MS and OES were used throughout the study for further elemental composition determination of REEs.

4.2.3 Qualitative mineral analysis

Figure 4.1 compared the qualitative mineralogy of the as-received PG and a commercial PG material (PGcom) by XRD technique that was carried out following the procedure described in Section 3.10.4. Understanding the mineralogy of the as-received PG was crucial in order to foresee further treatment such as recrystallization and its leachability for REE recovery.
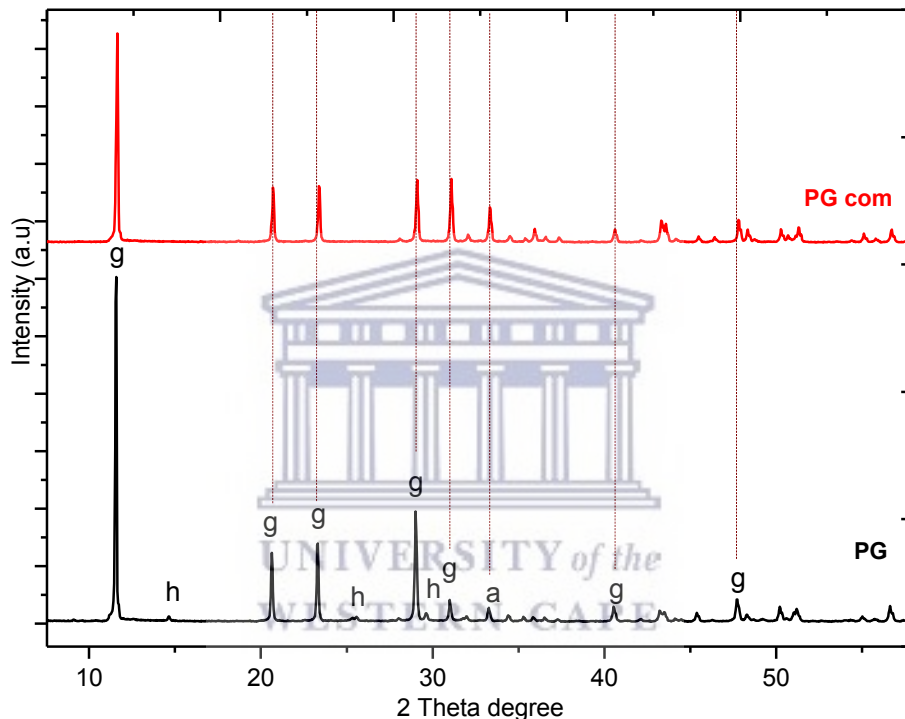
Figure 4.1: Mineral phases of as-received PG and commercial PG (PG com). **g:** CaSO$_4$·2H$_2$O; **h:** CaSO$_4$·0.5H$_2$O; **a:** CaSO$_4$.

As can be seen from Figure 4.1, the X-ray diffraction patterns of both PG and PGcom are identical indicating similar crystalline phases being present. Furthermore, it was found that both the as-received PG and PG com were mainly made of mineral phases gypsum (g) with minor traces of bassanite (b) and anhydrite (a) which were dominant in the as-received PG rather than in the commercial PG with peaks identified at 2θ: 14.8, 25.7, 29.9 and 33.7. These three mineral phases namely, gypsum (CaSO$_4$·2H$_2$O), bassanite or hemihydrate (CaSO$_4$·0.5H$_2$O) and anhydrate (CaSO$_4$) are different forms of calcium sulphate in which only the degree of hydration differs. As also discussed in

104

Section 2.9. depending upon the production technique of PG, a high proportion of $CaSO_4 \cdot 2H_2O$ or $CaSO_4 \cdot 0.5H_2O$ or $CaSO_4$ can be generated. It is therefore evident that the process used to generate the as-received PG favoured high production of gypsum. The high weigh mass (wt%) of CaO and SO_3 obtained by XRF discussed in section 4.1.1. could also justify the presence of high content of $CaSO_4 \cdot 2H_2O$ observed in the XRD patterns of the as-received PG.

For further analyses, only the as-received PG was used in this study after confirming its mineral phases by comparing its XRD patterns to those of the commercial PG (Pcom).

4.2.4 Quantitative mineral analysis

The quantitative analysis of mineral phases of the as-received PG was carried out as described in Section 3.10.4 and the results are shown in Figure 4.2. These data corroborated with the qualitative X-ray diffraction analysis discussed in section 4.2.3 and revealed that the as-received PG was made up of about 87 % of $CaSO_4 \cdot 2H_2O$ (gypsum), 9 % of $CaSO_4 \cdot 0.5H_2O$ (bassanite or hemihydrate) and 4 % of $CaSO_4$ (anhydrite). The high amount of gypsum phase found in the as-received PG is in a good agreement with the findings of Walawalkar et al., (2016) who reported 84 % of gypsum present in their PG material. However, compared to the PG under investigation in this study, their results indicated high anhydrite content as well as the presence of calcium phyllo-tetra phosphate in a fairly significant amount of 8 % each. According to these authors, the high content of anhydrite and the presence of calcium phyllo-tetra phosphate was associated with the process and source of phosphate ores.

The results further indicated that no solid phases based on other metals than calcium, in particular for REEs, were identified in the as-received PG by X-ray diffraction. This could be justified by the low concentration of REEs as seen in Table 4.1 making them undetectable through the XRD technique. The knowledge of these phases is crucial and helps to decide on the appropriate method of treatment for recovering the REEs.
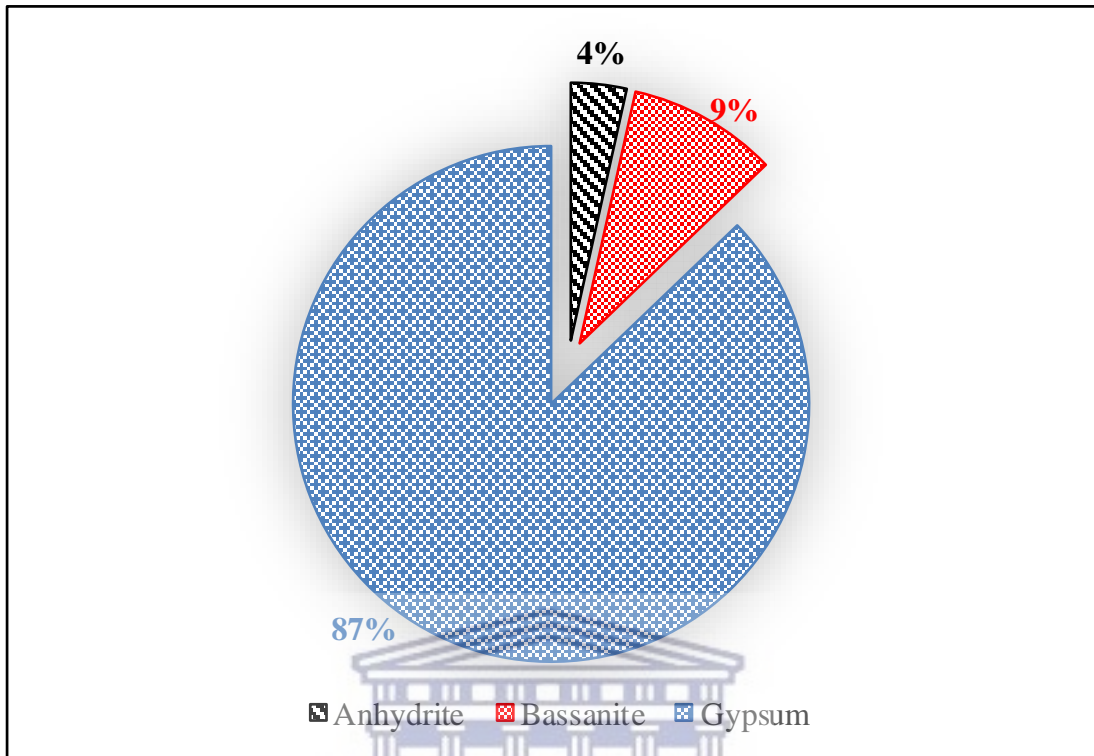
Figure 4.2: Quantitative mineral phase content of as-received PG (Anhydrite: $CaSO_4$; Bassanite: $CaSO_4 \cdot 0.5H_2O$; Gypsum: $CaSO_4 \cdot 2H_2O$)

For instance, Genkin et al., (2013) reported that a bassanite based PG ($CaSO_4 \cdot 0.5H_2O$) requires recrystallization to anhydrite or dihydrate to best extract the REEs. This is because the REEs in bassanite form a solid solution with the main phase of calcium sulfate, making their recovery inefficient without changing the structure of bassanite. Unlike bassanite, a gypsum ($CaSO_4 \cdot 2H_2O$) based PG forms a separate mineral phase with REEs in the form of sulfates.

4.2.5 Morphological analysis

The imaging analysis with SEM was carried out as described in Section 3.10.5 and allowed observation of different physical and morphological properties such as size and texture of the as-received PG particles at different sizes and magnifications. The EDS analysis was performed on the images to gain more information concerning the distribution of elements that make up the PG material.
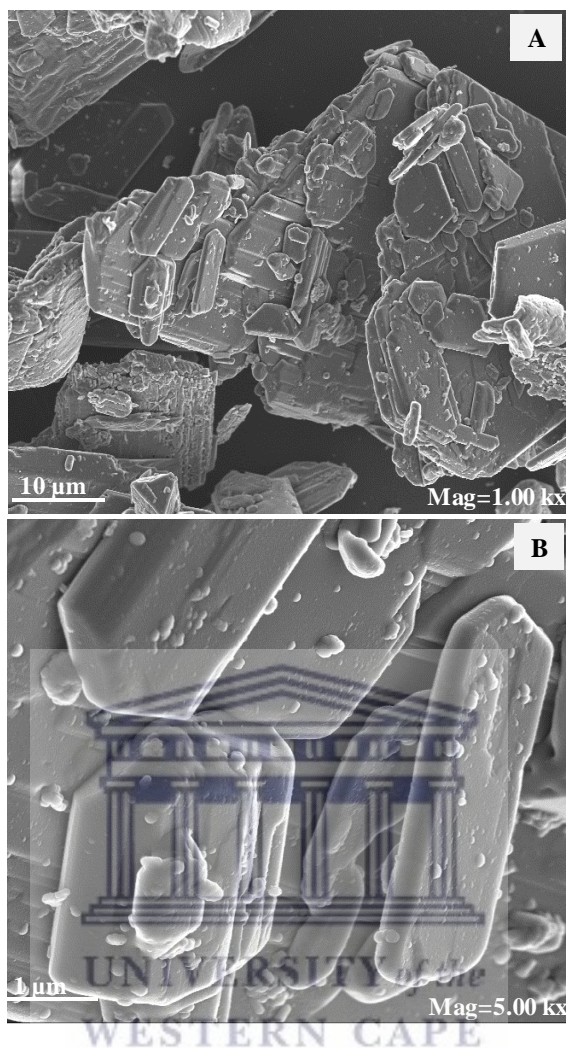
Figure 4.3: SEM imaging of as-received PG at magnifications 1.00 Kx , 10 µm (A)
and 5.00 Kx, 1 µm (B).

Thus, the micrographs images of the as-received PG as shown in Figure 4.3 revealed
the presence of agglomerates (Figure 4.3.A), prismatic PG (Figure 4.3.B) and well-
developed euhedral structures, monoclinic in a tubular habit of rhombic and
orthorhombic crystals. These morphological aspects were in a good agreement with
those reported by Romero-Hermida et al., (2019) and Grabas et al., (2019). The
agglomeration of crystals in the as-received PG as observed in Figure 4.3.A might be
as a result of impurities on the surface adhering on the surface of PG crystals. This
effect was also reported by Singh et al., (1999). Furthermore, the semi quantitative
analysis conducted on the as-received PG using EDS (Figure 4.4. and Table 4.4.)
showed mainly high contents of Ca, S and O which are the main elements making up

107

the structure of the as received PG (calcium sulfate). The presence of C resulted from the coating material that was used during the analysis of PG sample.
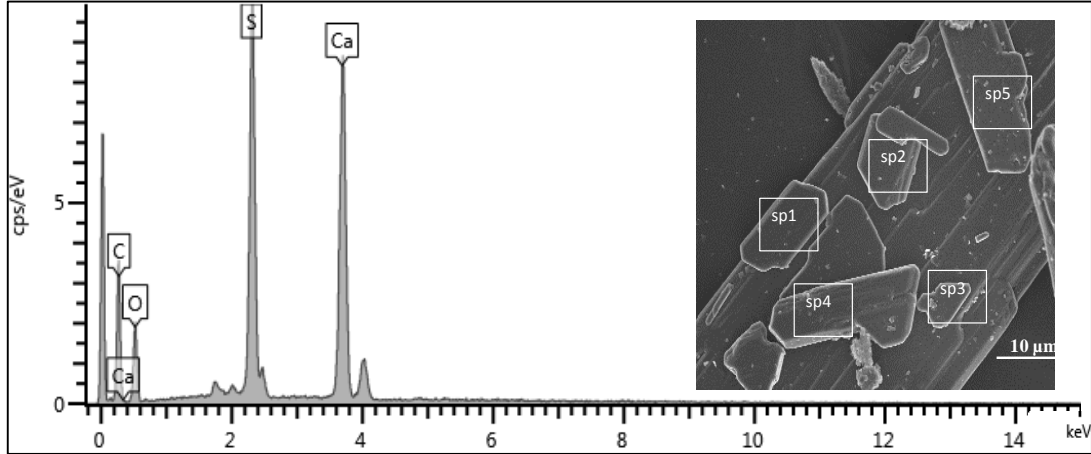
Figure 4.4: Semi quantitative elemental composition of as-received PG by EDS (n=5)

As expected, no REEs were detected by EDS/SEM indicating that their trace concentrations were below the detection limit and suggesting that REEs do not occur at the surfaces but rather might be co-crystallizing within the inner framework of the as-received PG. This might be in agreement with the findings of Yahorava et al., (2016), who performed a microprobe analysis on individual grains of PG using backscattered electron image and showed that REEs were contained within the structure of PG and their content varied from grain to grain. However, in another approach reported by Walawalkar et al., (2016) some of the REEs in PG were detected using a cross-section analysis on individual PG grain.

Table 4.4: Elemental composition of as-received PG by EDS analysis (n=5)

Element	Wt %
C	18 ± 0.8
O	15.7 ± 1
S	34.6 ± 0.4
Ca	31.7 ± 1
Total	100 ± 3.2

108

4.2.6 Structural and thermal analysis

Thermal analysis of the as-received PG was conducted as described in Section 3.10.3. to evaluate its thermal stability prior to various treatment and the result is shown in Figure 4.5.
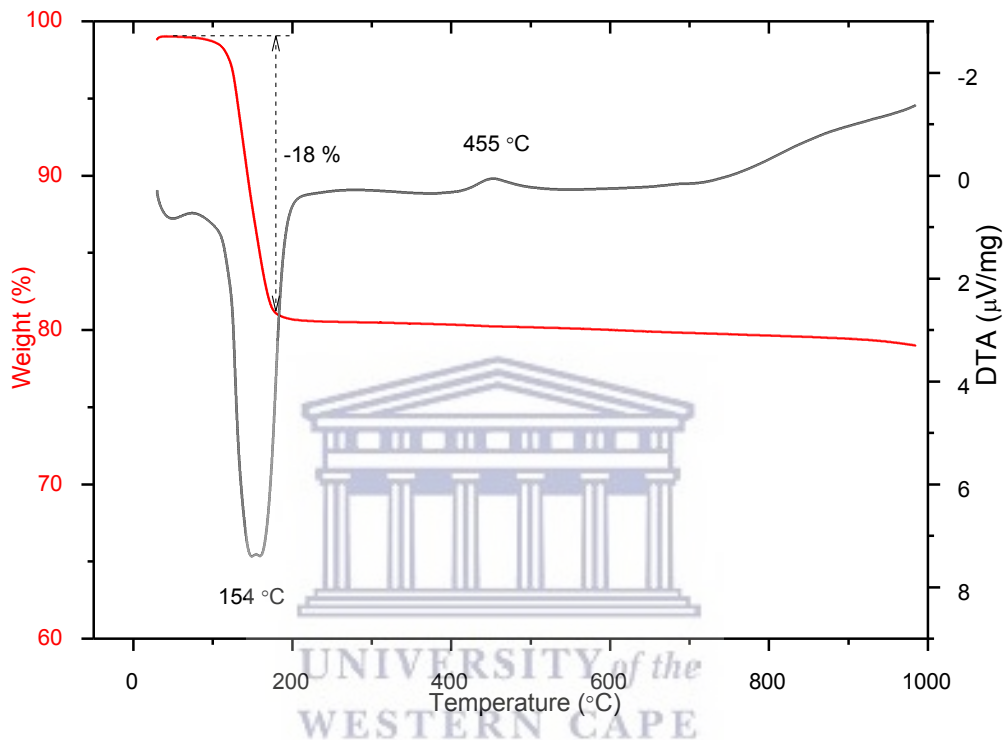
Figure 4.5: Mass loss behaviour of the as-received PG

As can be seen from Figure 4.5., the thermal profile of the as-received PG was a one-step decomposition process. The as-received PG started losing its thermal stability around 100 °C up to 200 °C with an approximately weight loss of 18 % which was essentially due to the loss of both free and structural water present in the PG crystal. This finding was in good agreement with the results of Grabas et al., (2019) who have reported a weigh loss of about 20 % from PG waste within the same range of temperature. The dehydration observed at 154 °C is related to structural water and might be due to the endothermic reaction of the hemihydrate ($CaSO_4 \cdot 0.5H_2O$) formation. This might be in agreement with the findings of Ma et al., (2018) who attributed a peak at 141.5 °C to crystal water removal (dihydration). The peak observed at 455 °C corresponds to the crystalline transition of anhydrite III to anhydrite II

109

through an exothermic reaction. This result is in good agreement with Schaefer et al., (2017) who reported a similar peak around this temperature in PG. Above all, the thermal behaviour of the as received PG is associated with its origin as mineral ore (phosphate rocks).

4.2.7 Particle sizes distribution (dry and wet analysis)

The dry-sieving analysis of the as-received PG was carried out as described in Section 3.10.11 and the results are presented as weight passing percentage versus the diameter of the sieves in Figure 4.6.
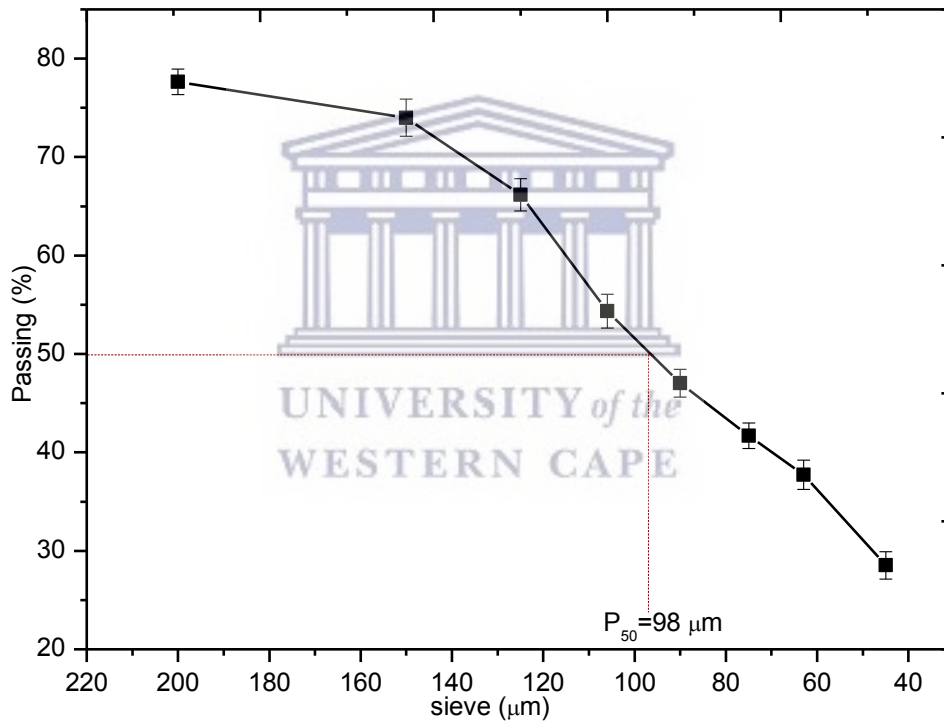
Figure 4.6: Dry sieving analysis of as received PG

The results showed that the highest proportion of the particles in terms of weight passing (%) are within particle sizes fractions < 200 μm (77 wt%) followed by < 106 μm (54 wt%), < 90 μm (47 wt%), < 75 μm (42 wt%), < 63 μm (38 wt%) and < 45 μm (29 wt%). It was further deduced from these results that the cumulative dry passing weight of the as-received PG contained particle fractions that were between 90 μm and 106 μm as indicated by P_{50} which was found to be 98 μm. In addition to the dry-sieving

110

analysis, the particle size distribution of PG was also carried out as described in Section 3.10.11 and the results are presented in Figure 4.7 in terms of the frequency curve of the volume percent versus the logarithm of particle sizes. This result revealed a single population of particle size in which 10 % measured 64.8 µm. The slight tail observed at the left of the curve indicated the presence of fine particles in the as-received PG. These findings are consistent with previous findings by Walawalkar et al., (2016) who obtained a particle size distribution of 76 µm for PG. The slight discrepancy in these two findings might be attributed to the type of the PG.

Thus, combining both the dry and wet analyses, it can be deduced that the as-received PG required no pre-treatment prior to the leaching process as the leaching agent can easily penetrate the small particle size of the PG resulting in short reaction time and fast kinetics. However, since one of the main objectives of this study is to up concentrate the REEs from PG feedstock, a granulometric test was carried out in order to determine if REEs had preference for a particular particle size distribution. In order to achieve that, four granulometric sizes smaller and bigger than P_{50}=98 µm namely 45, 75, 125 and 150 µm were examined using total acid digestion as described in section 3.4.
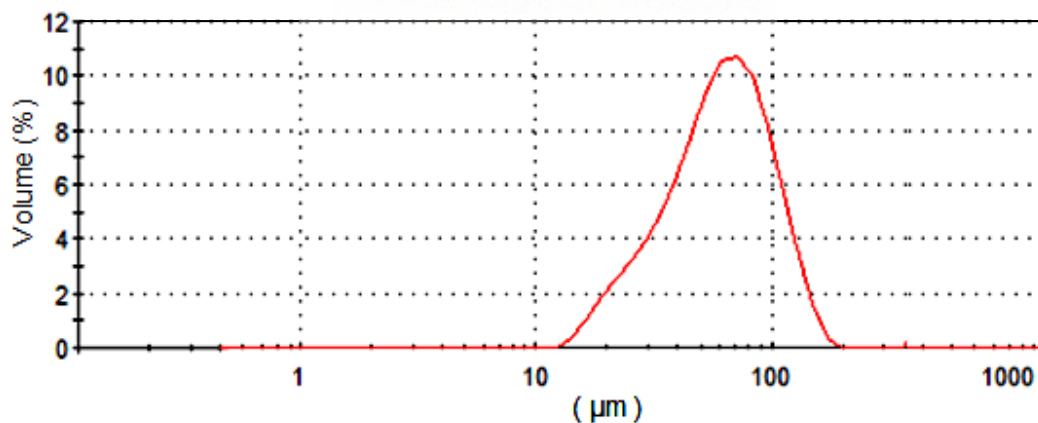
Figure 4.7: Particle size distribution of as received PG (wet analysis in ethanol)

The results as shown in Figure 4.8 surprisingly revealed that REEs were fairly evenly distributed among the four particle size fractions. It was found that finer or coarser particle sizes of the as-received PG showed a similar trend in terms of REEs content

111

(LREEs and HREEs). This equivalent distribution might be as a result of REEs released from the inner matrix of each particle size rather than on the surface of PG particles. This result is in line with the results reported by Hammas-Nasri et al., (2016) who evaluated the granulometric composition of five fractions (80, 100, 180, 300 and 600 μm) of PG and found a uniform distribution of REEs regardless the size of the fractions of PG analysed. Therefore, the rest of the experiments in this work were directly performed using the rough particle size of the as-received PG.

	Rough	φ < 75	φ < 90	φ < 106	φ < 150
LREEs	2200.25	2339.3	2299.45	2279.95	2258
HREEs	134.05	142	135.3	137.45	132.3
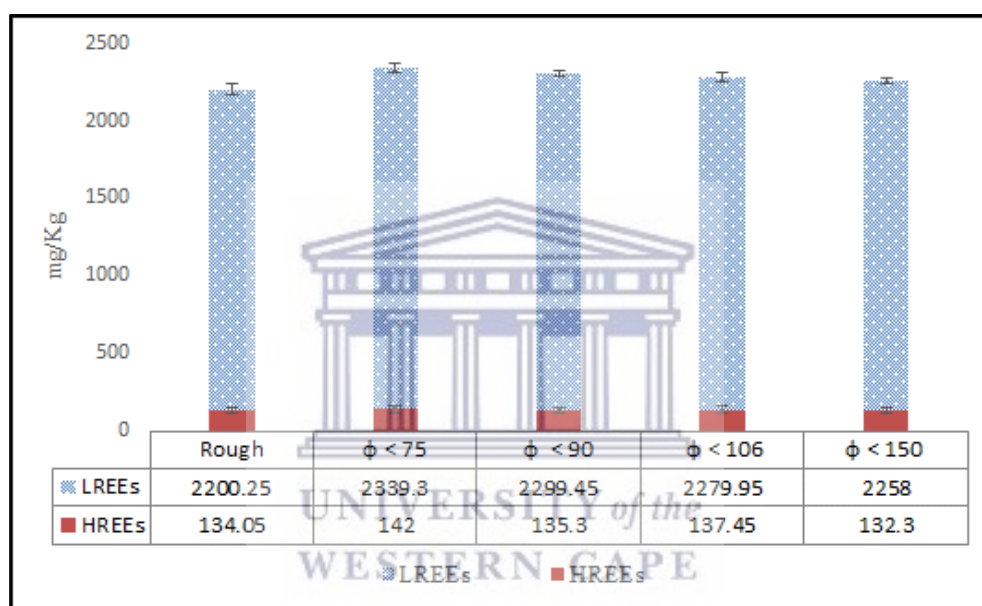
Figure 4.8: Distribution of LREEs (La, Ce, Pr, Nd, Sm, Eu, Gd) and HREEs (Tb, Dy, Ho, Er,Tm, Yb,Lu, Y) in as-received PG (rough) and after sieving analysis.

4.3 Characterization of polymer nanofibers

This section mainly covers the characterizations of polymer electrospun nanofibers that were performed using the ATR-FTIR, SEM and TGA. These characterizations aimed to give insight on chemical bonding, surface morphology and thermal stability respectively of these materials.

4.3.1 Unmodified polystyrene nanofibers

The unmodified polystyrene (PS) nanofibers were prepared as described in Section 3.8. of Chapter 3.

4.3.1.1 Surface morphology

The surface morphology of PS electrospun nanofiber was investigated at different concentrations of the polymer solutions as described in Section 3. The experiment aimed to determine the best concentration for formation of nanofibers prior to the modification process and was conducted at different polymer weigh percentage (wt%) of 8, 10, 12 and 14 wt%. The rest of the parameters (solvent mixture: DMF:THF (3:1) and deposition time: 6 h) as well the electrospinning instrument setup (voltage: 25 kV; collector distance: 15 cm; flow rate: 1.0 mL/h) were constant (Section 3.8). Figure 4.9 and 4.10 respectively show the morphological changes and diameters of PS nanofibers at different concentrations of the polymer solutions.

It can be observed from Figure 4.9 that the surface of the electrospun nanofibers tended to generate bead-on-string structure at polymer solutions of 8 wt% and 10 wt% while concentrations of 12 wt% and 14 wt% led to nanofibers free of bead structures. Although the spherical beaded structures were present at concentrations of 8 wt% and 10 wt% these beaded structures were intense at lowest concentration of 8 wt%. These beaded structures might be as a result of surface tension as low concentrations of polymer solutions which tended to form droplets during the electrospinning process. This finding is consistent with the findings of Koski et al., (2004) who showed that low concentration of the polymer solution could lead to insufficient entanglement of the polymer chains resulting in the polymer solution breaking down into droplets and not initiating fibre formation. Overall, all the electrospun PS nanofibers exhibited cylindrical aspects with various diameters at different concentrations of the polymer solutions. It was also found that the alignment of the electrospun nanofibers was more noticeable at higher concentrations of 12 wt% and 14 wt% in which the fibres also increased dimeter owing to increasing of the polymer solution concentration due to

stable interfacial conditions during the electrospinning process. The increase in fibre size was evidenced through the average fibre diameter as illustrated in Figure 4.10, which was higher at 14 wt% (749 nm) than the rest of the concentrations in particular at 8 wt% (262 nm) and 10 wt% (384 nm). The diameters of the nanofibers were further found to increase with the increase in the concentration of the polymer solutions as shown in Figure 4.11.
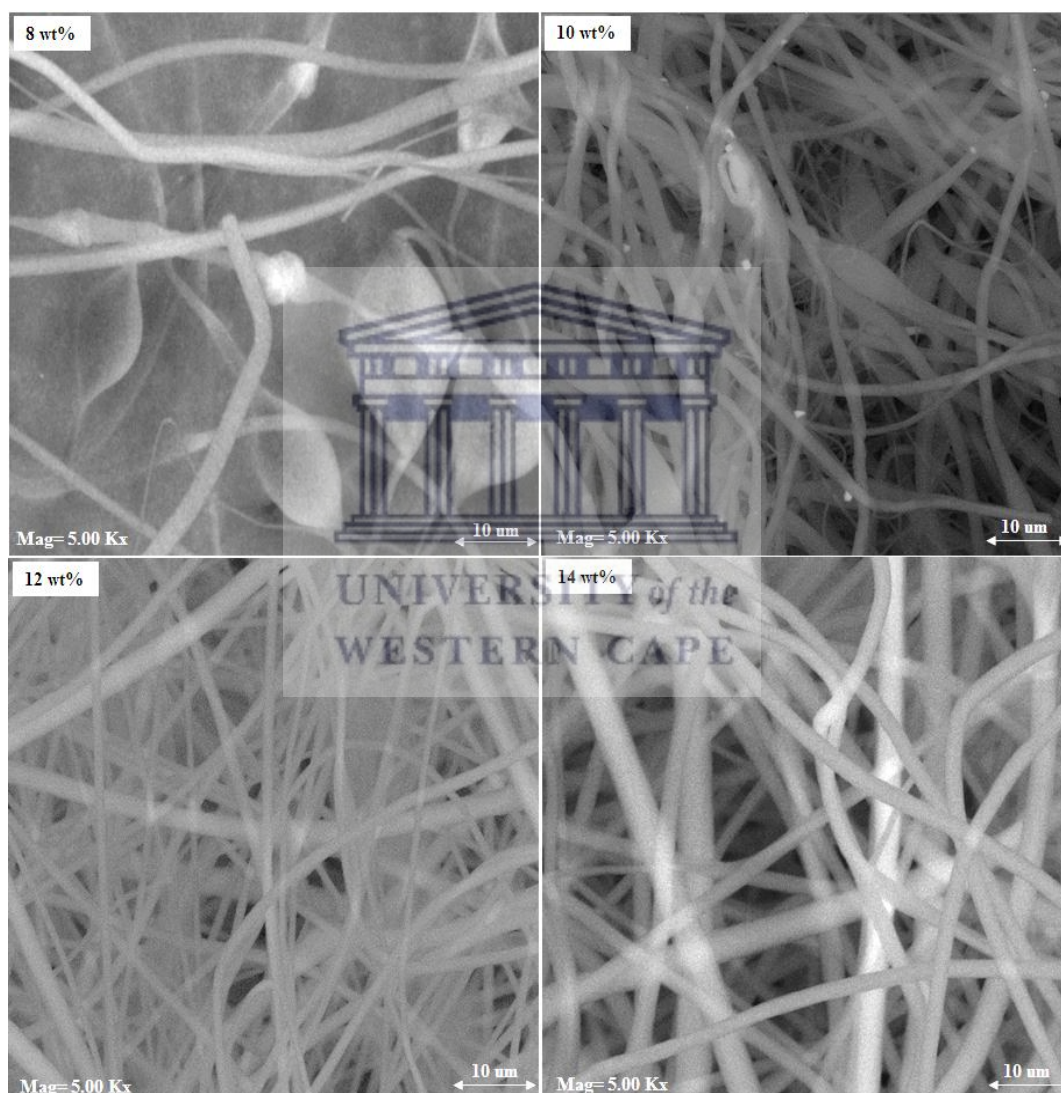
Figure 4.9: Micrograph images of PS electrospun nanofibers obtained from different concentrations of polymer weight solutions (8, 10, 12 and 14 wt%) in DMF:THF (3:1).

Despite that, the increased concentrations of the polymer solution tended to reduce the formation of beads, it also led to an increase in the average fibre diameter. This increase in the average fibre diameter might be as a result of insufficient elongation and stretching of the ejected jets being viscous during the electrospinning process. The characteristic of the fibre mats obtained at 14 wt% was found to be consistent with recent findings by Pereao, (2018) who reported bead free PS nanofibers at high concentrations of the polymer solutions. Therefore, in this study the concentration of 14 wt% was selected as the best concentration for the preparation of the PS nanofiber support for further surface modification which is one of the objectives of this part of the study. The sections below further characterize the PS nanofibers obtained at 14 wt% referred to as PS14 sample.
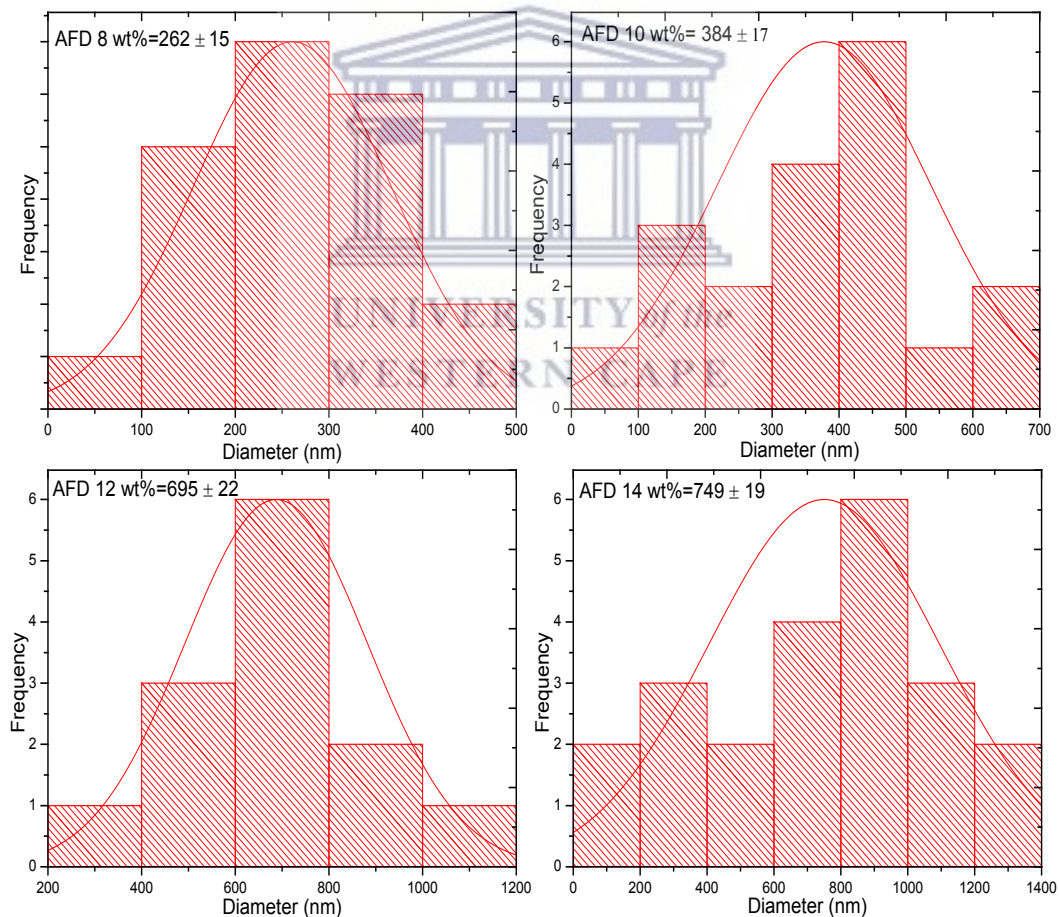
Figure 4.10: Average fibre diameters of PS electrospun nanofibers at different polymer weight concentrations in DMF:THF (3:1).
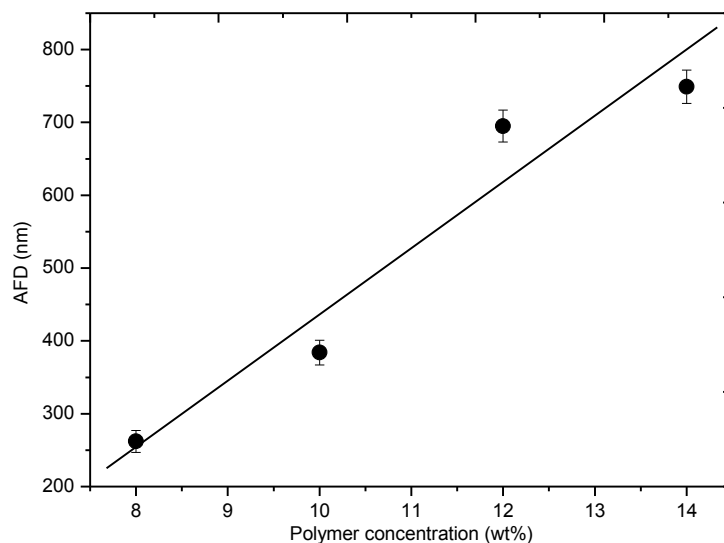
Figure 4.11: Correlation between polymer solution concentration and the diameter of PS electrospun nanofibers

4.3.1.2   FTIR analysis

The ATR-FTIR technique was used to compare and understand the chemical composition of PS14-nfs selected in Section 4.2.1.1 and the as-supplied PS beads. This analysis was carried out as described in section 3.10.2 using a wavenumber range of 400 to 4000 cm^{-1}. The results from the FTIR-ATR analysis are displayed in Figure 4.12 in terms of the transmittance (%) versus the wavenumber (cm^{-1}).

The results shown in Figure 4.12 exhibited three characteristic vibration bands of PS. The strong and intense vibration bands located between 780–650 cm^{-1} are attributed to mono-substituted benzene ring of PS while the bands at 1600–1400 cm^{-1} are ascribed to the bending vibration and the lower intensities between 3000–2800 cm^{-1} are attributed to C-H symmetric and asymmetric vibration (Huan et al., 2015). The similarities in the FTIR spectrum of PS beads and PS14-nfs as indicated by the characteristic vibration bands, implied that the dissolution of PS and the electrospinning process led to no chemical reaction or alteration in the obtained fibre. In attempts to understand furthermore the structure of the obtained PS14-nfs, TGA analysis was also carried out and the results are presented in Figure 4.13.

116
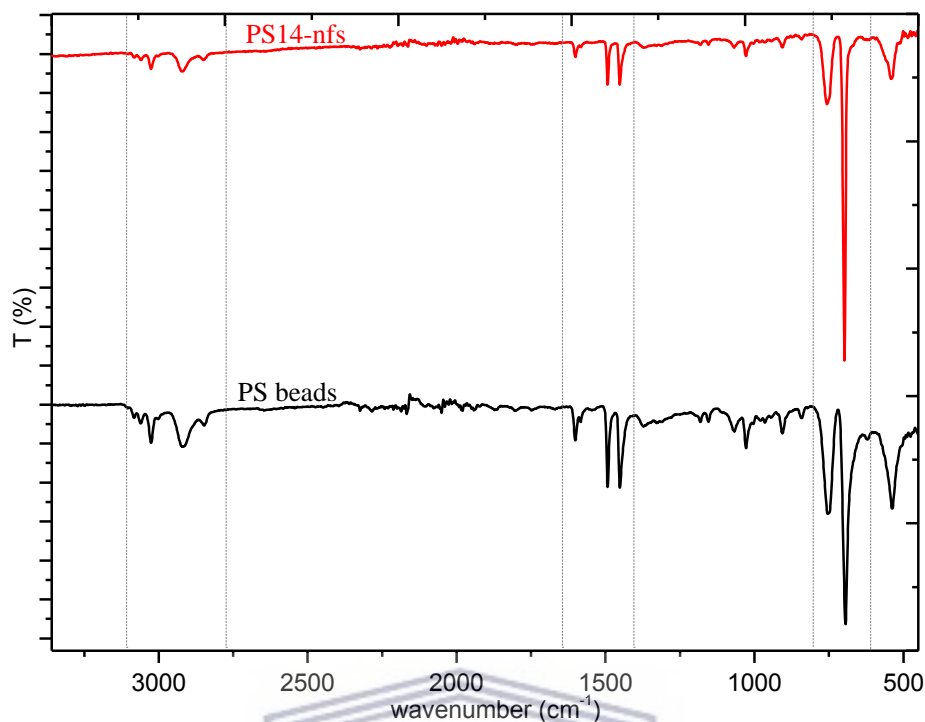
Figure 4.12: FTIR of PS beads and PS electrospun nanofiber (PS14-nfs)

4.3.1.3 Thermal profile

The TGA profile was obtained on PS14 electrospun nanofibers (PS14-nfs) as described in Section 3.10.3. This analysis was carried out in attempts to understand and investigate the thermal stability of PS14-nfs. The result of the TGA analysis is shown in Figure 4.13 in which it is plotted as the weight percentage loss versus the temperature of decomposition.

The PS14-nfs exhibited a single stage decomposition profile with weight loss of 95.6 % in which PS14-nfs started to lose its stability around 380 °C and thereafter gave off volatile gases at 470 °C. This implies that the obtained electrospun nanofibers are thermally stable up to 380 °C. The above findings are in good agreement with recent findings by Pereao et al., (2018) who have reported a weight loss of 98 wt% between 392 °C and 487 °C for PS-nfs.

117
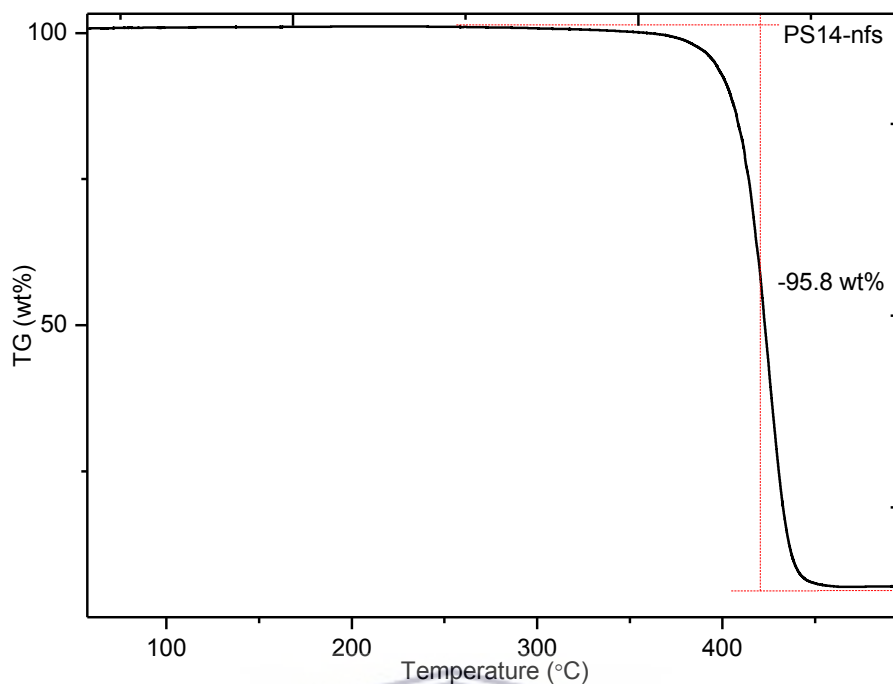
Figure 4.13: Thermal profile of PS14-nfs.

4.3.2 Modified nanofibers

The modified nanofibers were obtained through two approaches namely direct blending and post-functionalization using D2EHPA and DGA ligands, respectively. The modification experiments were carried out as described in Sections 3.8.1.1 and 3.8.1.2 using the PS polymer concentration of 14 wt% as discussed in Section 4.2.1.1. These modifications were performed in attempts to improve the sorption ability of the PS based adsorbents for REE metal ion extraction. The characterizations of these modified nanofiber mats were carried out by FTIR, SEM and TGA for chemical bonding analysis, surface morphology and thermal stability respectively.

4.3.2.1   Modification by direct blending with D2EHPA ligand

The schematic reaction proposed for the direct blending modification of PS polymer with D2EHPA ligand was illustrated in Section 3.8.2. The experiments were carried out to investigate the effect of D2EHPA concentration in PS polymer solution (14 wt%) to identify the best concentration. The section below briefly and systematically

118

presents characteristics and discusses the results obtained after the direct blending modification.

4.3.2.1.1   *ATR-FTIR analysis*

The ATR-FTIR technique was used to evaluate the chemical composition of the electrospun nanofiber mats obtained after the direct blending modifications with attention to functional groups assigned to the D2EHPA ligand. The ATR-FTIR spectra of D2EHPA ligand, unmodified PS14-nfs (14 wt%) and modified electrospun nanofiber mats at different concentrations of D2EHPA are shown in Figure 4.14.
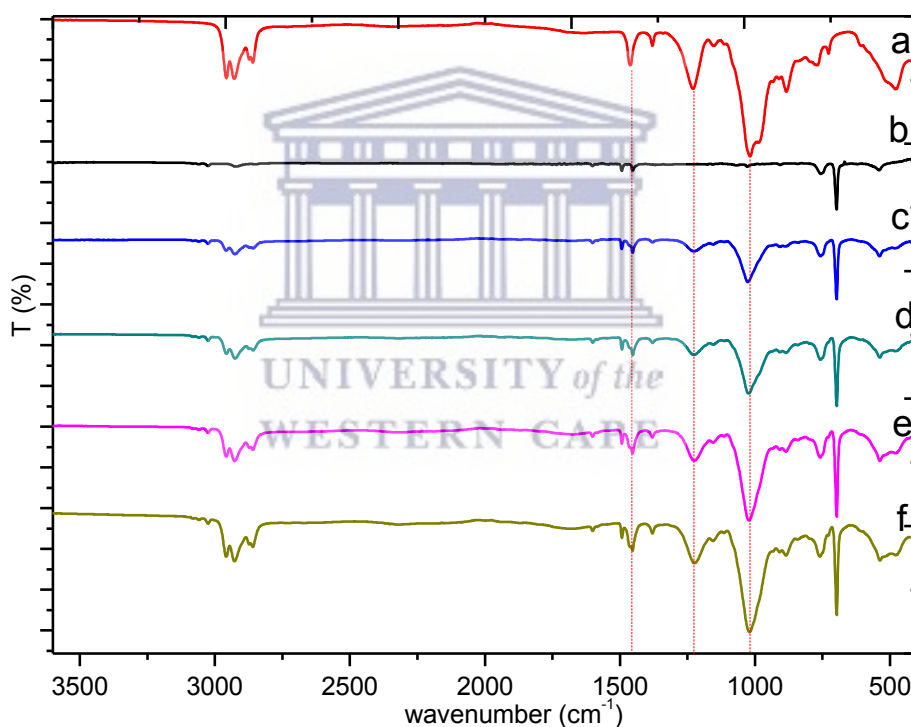
Figure 4.14: FTIR spectra of D2EHPA ligand (a), unmodified PS14-nfs (b), modified electrospun fibres at different concentrations of D2EHPA: c) 5 wt %, d) 10 wt %, e) 15 wt % and f) 20 wt %

Figure 4.14 (a) shows the characteristic vibration bands of D2EHPA ligand at 1460, 1230 and 1032 cm^{-1}. These vibration bands were assigned to O-H stretching, P=O stretching and P-O-H (or P-O-C) stretching respectively and were in a good agreement with those identified in recent studies by Da Silva et al., (2019) and Cadore et al.,

119

(2019). The presence of these functional groups is crucial for interaction with metal ions in solutions. Figure 4.14 (c-f) confirmed the presence of P=O and P-O-H or P-O-C functional groups originated from the ligand onto the backbone support of the polymer (Figure 4.14b) and these bands were intense with increased concentrations of D2EHPA ligand. The increase at vibration band of 1460 cm^{-1}, which was attributed to stretching of the O-H, could also be an indication of the formation of new carbon-carbon bonding between the ligand and the polymer support.

Although all the characteristic bands of the D2EHPA ligand were present in the modified nanofibers (Figure 4.14 (c–f)) at different intensities depending upon the concentrations, the highest concentration of 20 wt% of D2EHPA in PS exhibited relatively intense peaks. This suggested a good functionalization at this concentration and intense peaks in particular at 1032 cm^{-1} is preferable as it is an indication of an effective presence of P=O and P-O-H or P-O-C functional groups where metal ions can bind. Therefore, the concentration of 20 wt% was used for effective modification of the PS polymer nanofibers for further experiments in this study and will be referred to as DH-PS20-nfs in the following sections.

4.3.2.1.2   *Morphological analysis*

The surface morphology of blended DH-PS20-nfs was carried out as described in Section 3.10.5 to evaluate and monitor the morphological changes of electrospun nanofibers after the modification with D2EHPA ligand. Figure 4.15 shows the micrograph images of the unmodified PS (PS14-nfs) and modified nanofiber (DH-PS20-nfs).
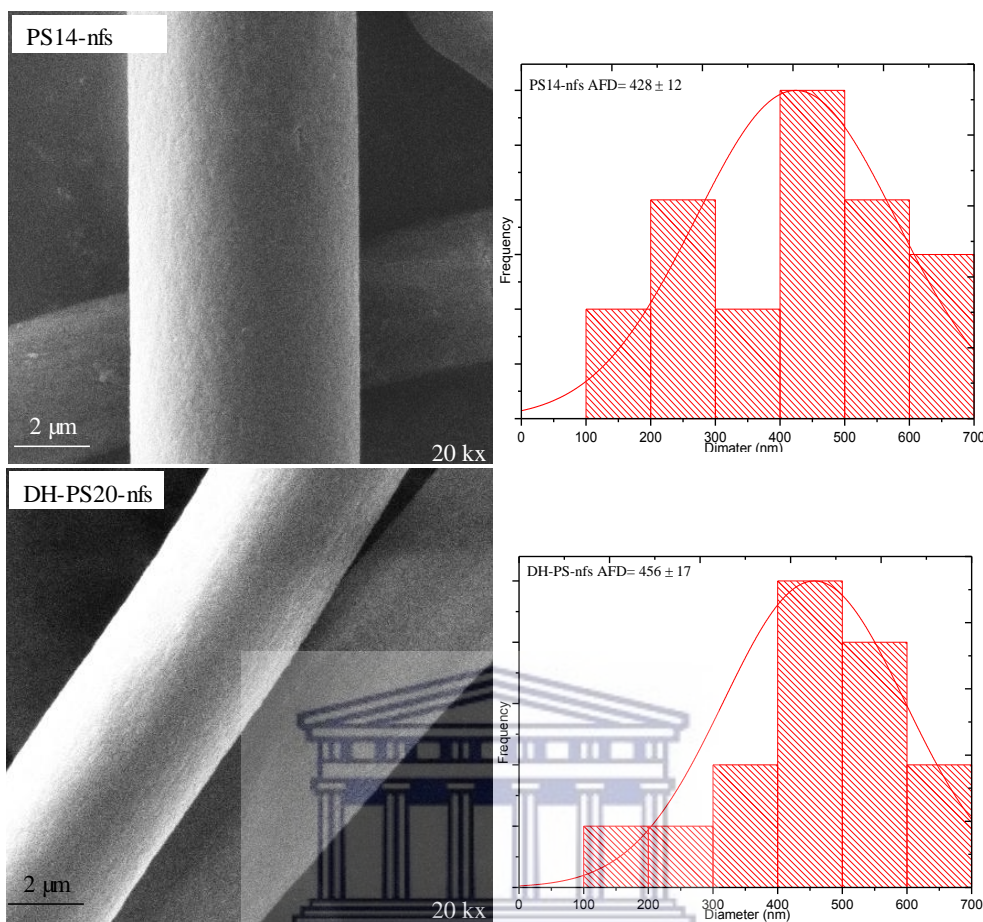
Figure 4.15: SEM images of unmodified PS-nfs 12 wt % and modified PS blended with 20 wt % of D2EHPA

These micrograph images were obtained at the magnifications of 20 kx to best examine the impact of the modification on the surface of the fibres. The results showed that the surface of DH-PS20-nfs had no morphological changes and was smooth as the neat PS14-nfs. This indicated that the introduction of 20 wt% D2EHPA ligand during the blending process led to no surface change. However, the average diameter of the modified fibre mats slightly increased with a coefficient of variation of approximately 25 nm. This increase might be as a result of the addition of D2EHPA ligand to PS polymer solution causing an increase in viscosity leading to DH-PS20 nanofibers with greater diameters. The increase in diameters for polymer solution modified with D2EHPA ligand was also reported by Mahalingam & Edirisinghe, (2013) and Da Silva et al., (2019). Since, the SEM technique could not fully support the ATR-FTIR results so as to confirm the presence of D2EHPA ligand onto the PS backbone, other

121

characterizations such as TGA analysis was further considered and the results are briefly discussed below.

4.3.2.1.3   *Thermal analysis*

Thermal analysis of the modified DH-PS20 and unmodified PS14 electrospun nanofiber mats was carried out as described in Section 3.10.3. Figure 4.16 shows the comparative thermal profiles of 20 wt% blended DH-PS20 nanofibers and unmodified PS14 nanofiber mats. The thermal profile of PS14-nfs as discussed in Section 4.2.1.3 occurred in a one-step degradation, whereas DH-PS20-nfs decomposed via a two steps process, which is an indication of the decomposition of independent components.

Figure 4.16: Thermal profile of unmodified PS and modified DH-PS20-nfs

The modified DH-PS20-nfs started first by losing the thermal stability around 235 °C up to 295 °C and thereafter it continues decomposing from 404 °C 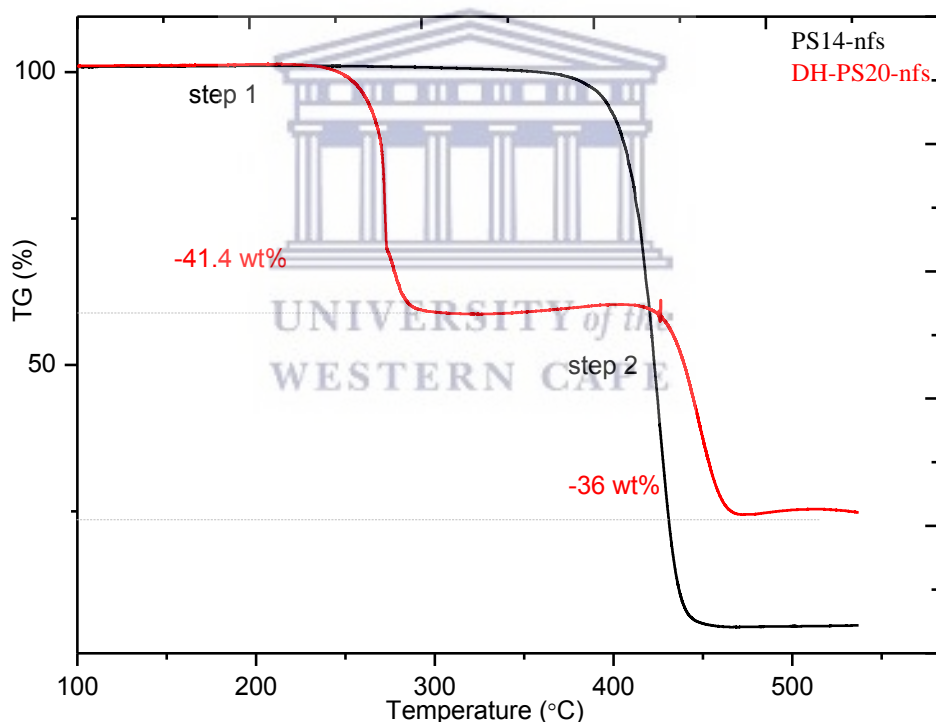up to 482 °C. The first degradation between 235 °C and 295 °C is related to decomposition of the solvent and functional groups of the D2EHPA ligand where a weight loss of about 41.4 wt%

122

was recorded. The decomposition of D2EHPA ligand within the range of temperature between 235–295 °C was in good agreement with the findings of Yadav et al., (2013); da Silva et al., (2019) who reported the degradation of D2EHPA ligand in a similar range of temperatures. However, the second degradation (404–482 °C) corresponds to the decomposition of the PS polymer support with a weight loss of 36 wt%. It therefore clear that the results from TGA technique combined to those obtained from ATR-FTIR and SEM confirmed the presence of D2EHPA ligand in the modified DH-PS20 nanofiber mats.

4.3.2.2   Surface modification with DGA ligand

The schematic reaction proposed for the surface modification of PS nanofiber mats obtained at the concentration of 14 wt% (PS14-nfs) as detailed in Section 3.8 with the DGA ligand was illustrated in Section 3.8.2. The experiments were carried out to investigate the effect of the concentration of DGA ligand during the chemical grafting of PS14-nfs to identify the best concentration as detailed in Section 3.8.1.2. The section below briefly discusses the results obtained after the surface modification process.

4.3.2.2.1   *FTIR analysis*

The ATR-FTIR technique was used to investigate the formation of new bonds in the backbone structure of the unmodified PS14-nfs after the surface modification at different concentrations of DGA ligand. The ATR-FTIR spectra of the DGA ligand, unmodified PS14-nfs and modified nanofiber mats at different concentrations of DGA ligand are presented in Figure 4.17.
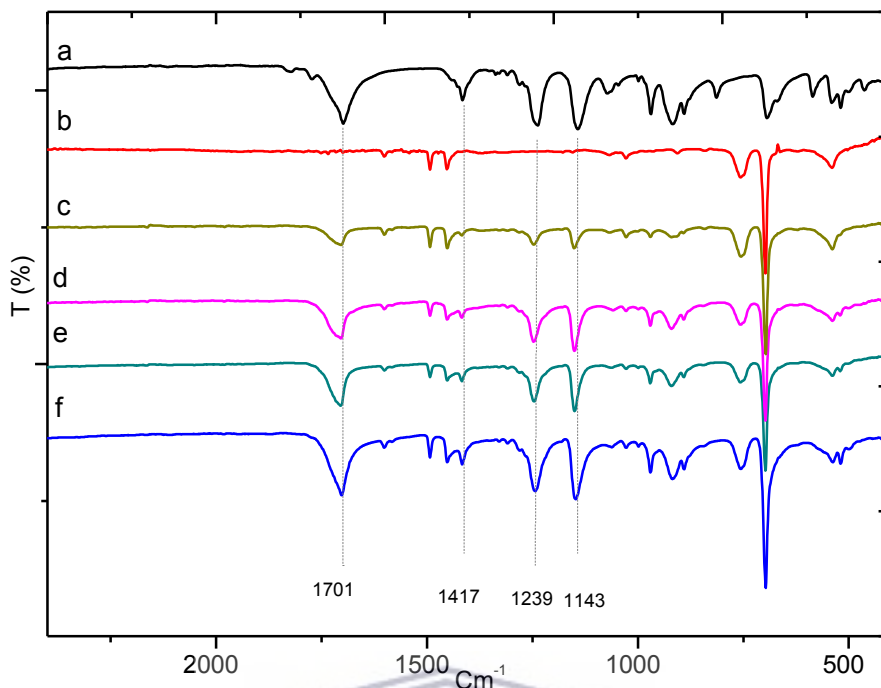
Figure 4.17: FTIR spectra of: a) DGA ligand, b) unmodified PS14 (weight mass: 0.1 g), modified PS14 nanofibers at c) 0.5 g, d) 1 g, e) 1.5 g, f) 2 g of DGA in 5 % acetic acid (10 mL), 20 mL methanol

The characteristic bands of the DGA ligand located at 1700 cm^{-1} was ascribed to the stretching vibrations of the two carbonyl group (C=O) present in the DGA ligand while the band at 1417 cm^{-1} is due to scissoring vibrations of the -CH$_2$- group (Figure 4.17a). These bands are the main characteristic of the DGA ligand and were in a good agreement with recent studies by Pereao et al., (2018). Figure 4.17b shows the spectra of the unmodified PS14-nfs and its characteristic vibration bands which were previously discussed in Section 4.2.1.2. Figure 4.17(c-f) show the spectra of the modified PS14-nfs at different concentration of DGA ligand. It can be seen from these spectra that the major alterations occurred between 1800–1600 cm^{-1} and 1300–1100 cm^{-1} indicating the formation of new bonds within these regions of the backbone of the PS14-nfs during the ligand attachment. The vibration band at 1700 cm^{-1} which was ascribed to the C=O group was identified in all the modified PS14-nfs at different intensities. The variation in intensities of this band was dependent upon the concentration of the ligand and increased with increased concentration of the DGA ligand. The presence of the C=O functional group in the modified PS14-nfs is crucial

124

as it is the main site of interaction between the metal ion and the adsorbent. In addition to this band, bands at 1239 cm^{-1} and 1144 cm^{-1} also confirmed the stretching of C=O group in the matrix of PS14-nfs. The intensity of the vibrations also increased with increased concentration of the DGA ligand. The FTIR spectra of the modified nanofiber mats further showed that the backbone was conserved as evidenced by the vibration bands located between 1600–1400 cm^{-1} as well as those between 800–600 cm^{-1} which are attributed to -CH$_2$- bending and benzene ring of PS present in the unmodified PS14-nfs respectively. This means that the introduction of the DGA ligand into the matrix of the PS14-nfs led to no significant alterations. The presence of C=O group in the structure of the modified PS14-nfs confirmed that the DGA ligand was chemically grafted onto the matrix of PS as these bonds were initially not existent in the structure of the unmodified PS14-nfs (Figure 4.17b).

In this study, to allow the DGA ligand to be grafted efficiently onto the PS14-nfs mats, the concentration of 2 g (0.015 mole) was selected for effective surface modification of PS14-nfs and further experiments. The modified PS14-nfs mats will therefore be referred to as DGA-PS2 in the following sections.

4.3.2.2.2 *Morphological analysis*

The surface morphology of DGA-PS2 nanofibers was carried out as described in Section 3.10.5 to evaluate the effect of DGA ligand on the surface of PS14-nfs. This was crucial also to determine if the morphological structure of the PS14-nfs was retained after the surface modification process. Figure 4.18 shows the micrograph images of the unmodified PS (PS14-nfs) and modified DGA-PS2 nanofiber at the concentration of 2 g of DGA ligand. The micrograph images were obtained at the magnifications of 20 kx to best examine the surface of the modified nanofiber mats.
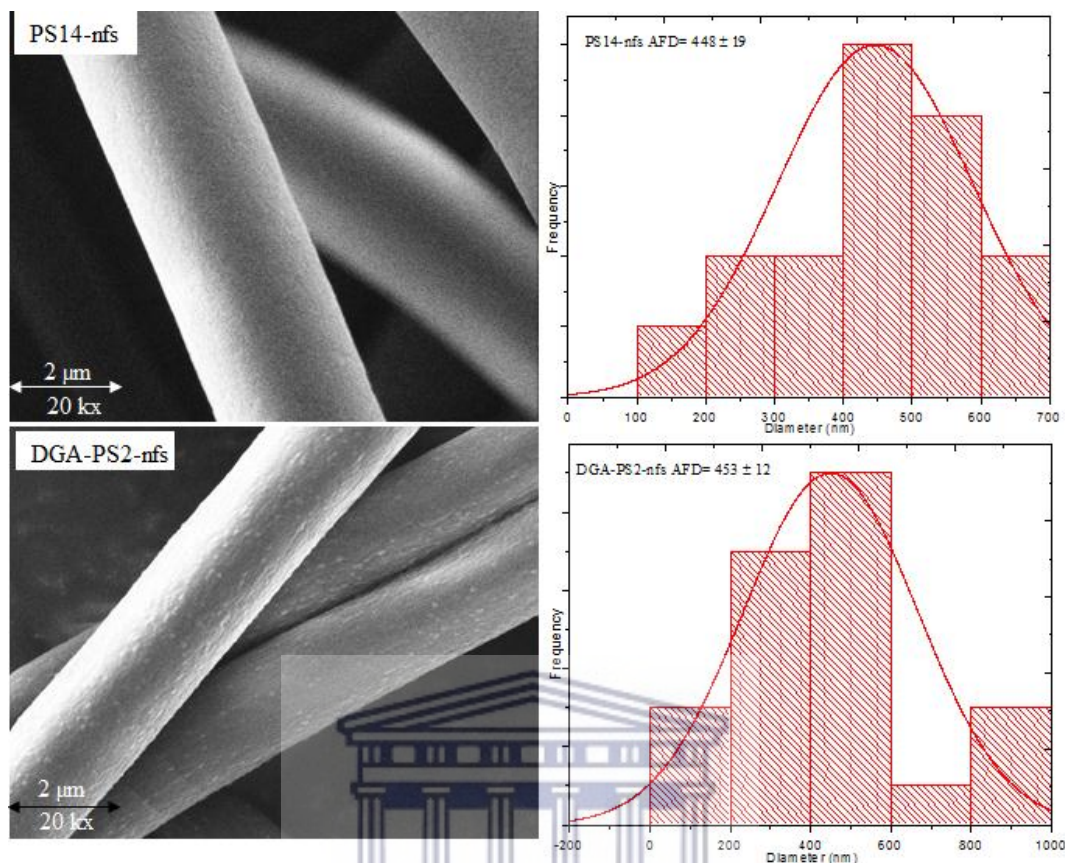
Figure 4.18: Micrograph images of unmodified PS14 and modified DGA-PS2-nfs.

The results showed that the surface of DGA-PS2 nanofibers compared to that of PS14-nfs tended to adhere. This adherence of the modified DGA-PS2 nanofibers might be as a result of chemical reactions that occurred between the surface of adjacent nanofibers mats during the modification. Furthermore, the average fibre diameter of DGA-PS2 nanofibers slightly increased compared to that of the neat PS14-nfs with a coefficient of variation of approximately 5 nm. This slight increase in the average diameter can be attributed to DGA ligand swelling the nanofiber during the modification. The increase of the average diameter of modified polystyrene nanofibers was also recently reported by Pereao et al., (2018) but their studies showed no major changes on the surface of the modified fibre. To confirm the attachment of the DGA ligand onto the PS support, TGA analysis was also carried on the fibre mats and the results are shortly discussed.

4.3.2.2.3 *Thermal analysis*

Thermal analysis of the unmodified PS14-nfs and modified DGA-PS2-nfs was carried out as described in Section 3.10.3. Comparative thermal profiles of these samples indicating the weight loss in percentage are given in Figure 4.19.
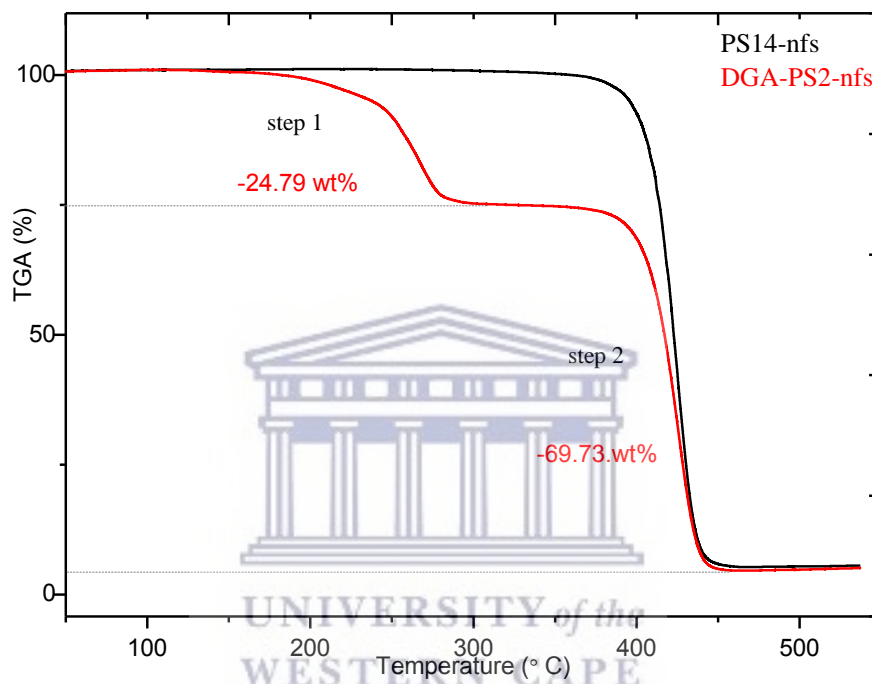
Figure 4.19: Thermal analysis of unmodified PS and modified DGA-PS2-nfs

The thermal profile of PS14-nfs as discussed in Section 4.2.1.3. occurred in a one-step degradation at above 400 °C whereas the modified DGA-PS2 thermal degradation occurred as a two-steps process which is an indication of the decomposition of independent components. DGA-PS2-nfs started losing their thermal stability around 155 °C up to 300 °C and thereafter it again continued degrading from 364 °C up to 458 °C, losing weights of 25 % and 75 % respectively. The first degradation of DGA-PS2 nanofibers corresponds to the decomposition of oxygen functionalities (i.e. CO, CO_2) and the second to that of the PS chain. These findings are consistent with the findings of Roghani-Mamaqani (2015) who reported a similar observation for graphene supported PS having oxygen containing groups. These results therefore

127

confirmed the successful attachment and thermal stability of the modified DGA-PS2 nanofibers and were in a good agreement with the recent findings by Pereao et al., (2018).

4.3.3 Stability test of DH-PS20 and DG-PS2 nanofibers

The stability test of DH-PS20 and DG-PS2 nanofiber mats discussed in Sections 4.3.2.1 and 4.3.2.2 respectively was crucial prior to the desorption process. This stability test was carried out in this study in HNO_3 or EDTA media as described in section 3 of Chapter 3. To recall, the purpose of this test is to determine to which extent the adsorbent nanofibers could be regenerated during the adsorption and desorption process. Thus, the adsorbent stability was tested by shaking 0.1 g of DH-PS20 and DG-PS2 nanofiber mats in 10 mL of different concentrations (1.0, 1.5, 2 M) of HNO_3 or EDTA for 1 h at a room temperature to determine the concentration that was ideal for regeneration of the modified DH-PS20 and DG-PS2 nanofibers without detaching their respective functional groups. The FTIR results obtained after the stability tests are shown in Figures 4.20-4.23. Figures 4.20 and 4.21 show the stability test of DH-PS20 nanofiber mats in HNO_3 and EDTA respectively.

As can be seen from the FTIR results, DH-PS20 nanofiber mats remained somewhat stable and intact in different concentrations of HNO_3 solutions as shown in Figure 4.20 (b-d) with a slight variation in terms of peak intensities which decreased as the concentrations of HNO_3 increased. This slight decrease in peak intensities might be attributed to the acid washing treatments of DH-PS20 nanofiber mats. The treatments of DH-PS20 nanofiber mats in HNO_3 solutions compared to that of EDTA solutions showed that EDTA was not favourable for regeneration of the DH-PS20 nanofiber mats as it tended to remove the ligand (Figure 4.21(b-c)) and also modified the PS support (Figure 4.21d).

Figure 4.20: FTIR spectra of a) DH-PS20-nfs and treated DH-PS20-nfs in 10 mL of different concentrations of HNO_3: b) 1.0 M, c) 1.5 M and d) 2.0 M (1 h, 200 rpm)

Figure 4.21: FTIR spectra of a) DH-PS20-nfs and treated DH-PS20-nfs in 10 mL of different concentrations of EDTA: b) 1.0 M, c) 1.5 M and d) 2.0 M (1 h, 200 rpm)

The impact of EDTA solutions were mainly observed between 750–1600 cm^{-1} where functional group are located. Therefore, for regeneration of DH-PS20 nanofiber adsorbents during the desorption process, only the HNO$_3$ solutions were considered at the lowest concentration of 1.0 M as ideal regenerant concentration. Figure 4.22 and 4.23 respectively show the results obtained from the treatments of DG-PS2 nanofiber mats in solutions of HNO$_3$ and EDTA.
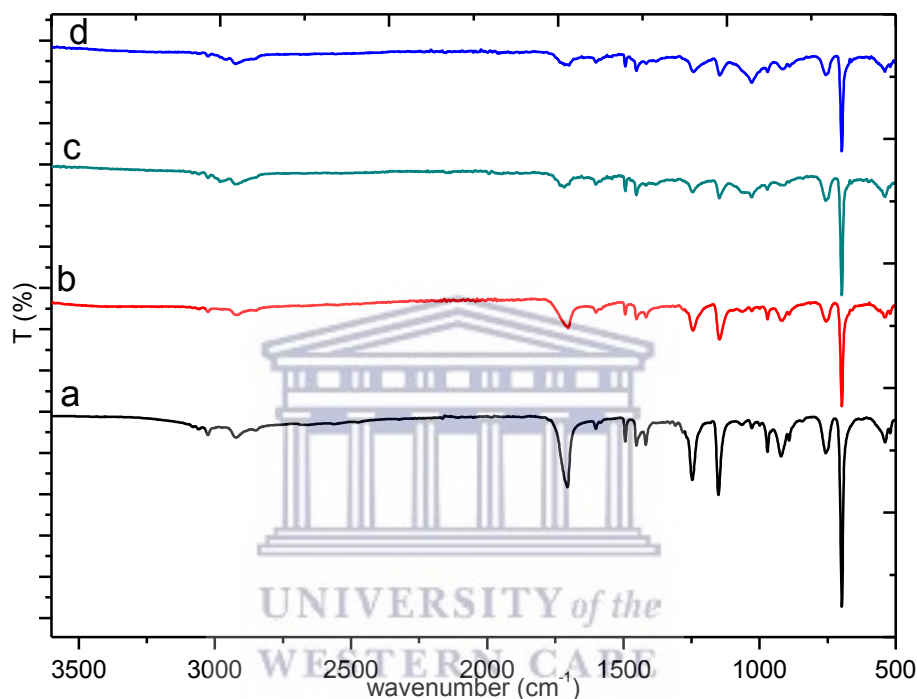
Figure 4.22: FTIR spectra of a) DG-PS2-nfs and treated DG-PS2-nfs in 10 mL of different concentrations of HNO$_3$: b) 1.0 M, c) 1.5 M and d) 2.0 M (1 h, 200 rpm)

It can be seen from Figure 4.22, that increasing the concentrations of HNO$_3$ solutions tended to remove the ligand from the PS support as indicated by reduced peak intensity of the functional groups located at 1700, 1239 and 1144 cm^{-1}in DG-PS2 nanofiber mats (Figure 4.22 (b-d)). This suggested that higher concentrations of HNO$_3$ above 1.0 M were not suitable for regeneration of DG-PS2 nanofibers as the material integrity was not preserved. These results compared to those obtained from the treatments in EDTA solutions, showed that the removal of the ligand on the PS supports was very significant and the carbonyl groups (1700 cm^{-1}) somewhat eroded off at their initial position and shifted towards lower wavenumbers (Figure 4.23 (c-d)). It was clear that

130

EDTA solutions were not suitable as regenerants for DG-PS2 nanofiber mats. Therefore, HNO$_3$ solution at a concentration of 1.0 M was used as a regenerant for desorption since at this concentration the integrity of the ligand was retained only to some extent.
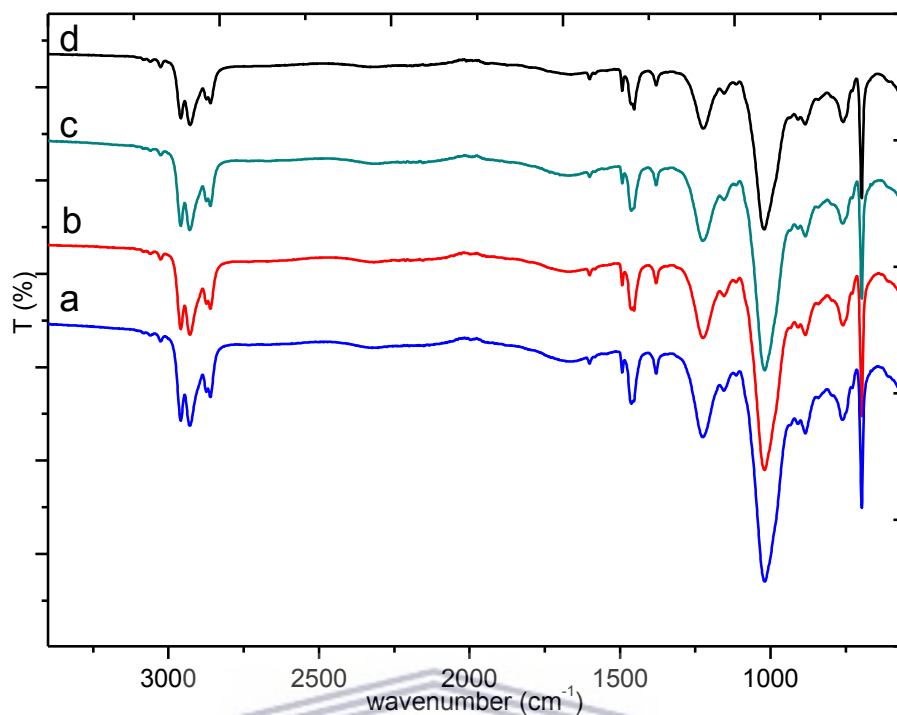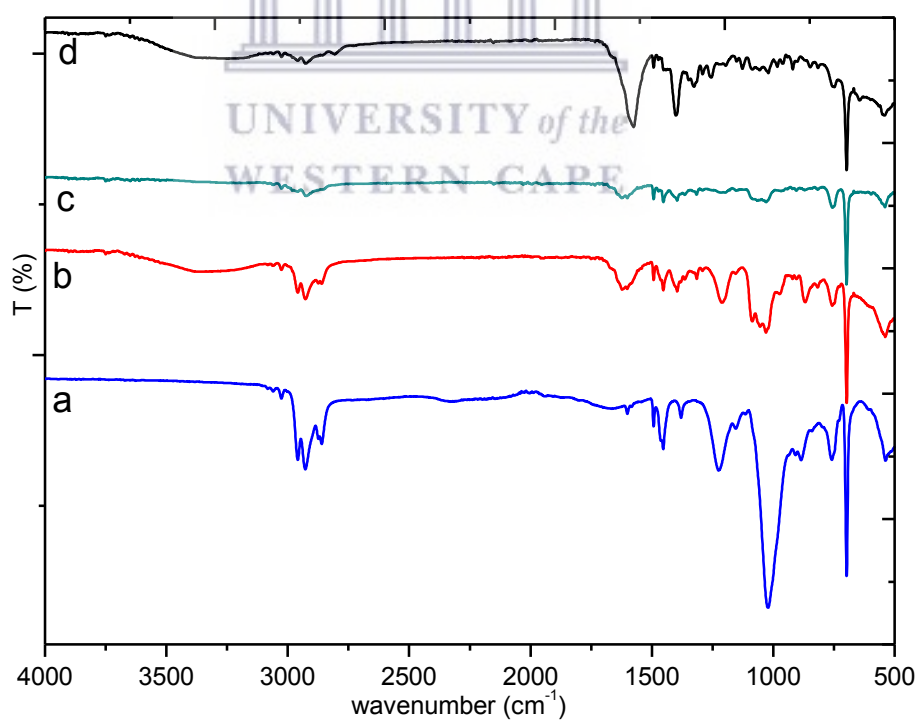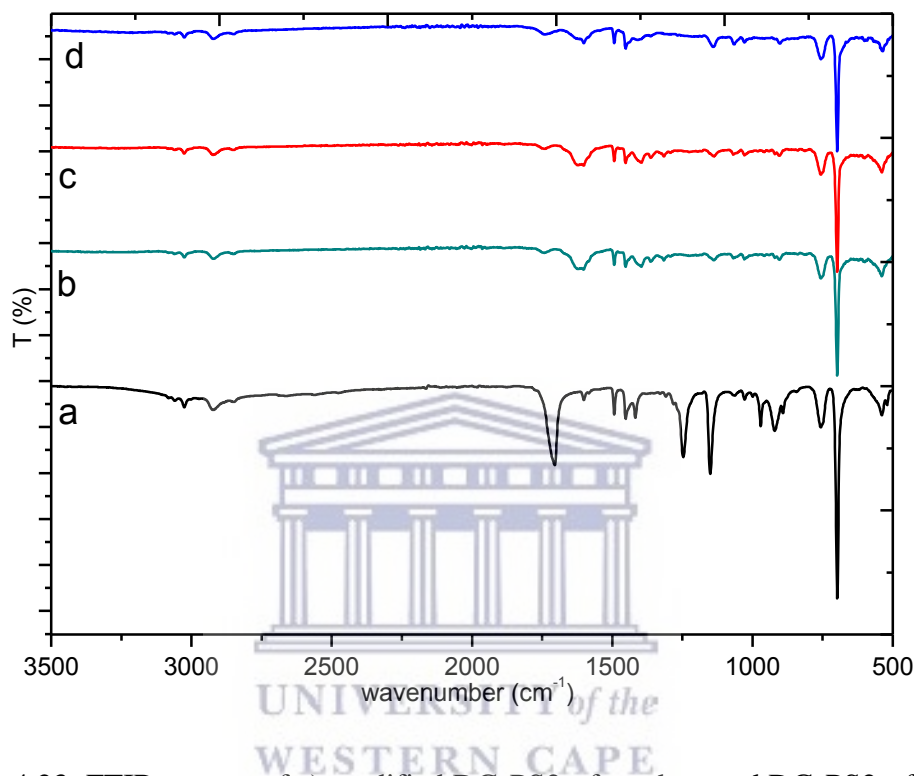

Figure 4.23: FTIR spectra of a) modified DG-PS2-nfs and treated DG-PS2-nfs in 10 mL of different concentrations of EDTA: b) 1.0 M, c) 1.5 M and d) 2.0 M (1 h, 200 rpm)

4.4 Chapter summary

This chapter presented the results obtained after the characterizations of the as-received PG and derivatives as well as the prepared nanofiber materials. This chapter intended to answer to objectives 1, 3 and 4 as set in Chapter 3 and comprised two main sections which dealt with the characterizations of the as-received PG with regard to REE content and nanofibers materials respectively.

The characterizations of the as-received PG was carried out using different analytical techniques such as XRF, ICP-OES/MS, NAA, XRD (qualitative and quantitative),

131

SEM-EDS, TGA and PSD. The results from these characterizations were compared and discussed based on the existing data in the literature. The XRF results showed that, CaO and SO_3 were the major oxides present in the as-received PG. This XRF results correlated to qualitative and quantitative XRD and TGA confirmed that the as-received PG was a calcium sulphate dihydrate ($CaSO_4 \cdot 2H_2O$) produced from fluoroapatite ore. Dry sieving and wet analysis (ethanol) for the particle size distribution of the as-received PG suggested that no pre-treatment was required as the particle size distribution was find to be below 98 µm. With regard to REE content, elemental analysis using ICP-MS was found to be more effective compared to ICP-OES and NAA as it was able to detect the full range of the fifteen (15) REEs series. However, highest concentrations of the REEs were obtained through NAA. This was attributed to its simpler and easier sample preparation which does not require steps such as digestions of the sample which generally lead to loss of the elements. Overall, it was found that La, Ce and Nd dominated among all the REEs in the as-received PG with concentrations ranging from 400–600 mg/kg; 1100–1500 mg/kg and 600–850 mg/kg respectively.

The characterizations of polystyrene (PS) support and modified nanofibers (blended with D2EHPA and surface modified with DGA ligands) were done using mainly SEM, ATR-FTIR, and TGA techniques. SEM technique conducted on the unmodified PS nanofibers obtained at different concentrations of PS solutions showed that the concentration of 14 wt% was suitable for further experiments as it led to electrospun nanofiber mats free of beads having an average diameter of 750 nm. The comparative ATR-FTIR spectra of PS beads (pristine) and PS nanofiber mats obtained at a concentration of 14 wt% (PS14-nfs) revealed that the mixture of the solvents DMF:THF (3:1) that was used to dissolve PS beads did not alter the structure of PS in the obtained PS14-nfs mats as was evidenced through the similarity of the characteristic vibrations bands. PS polymer concentration of 14 wt% was further used for the modifications processes with D2EHPA and DGA ligands for direct blending and surface modification respectively at different concentrations of the ligands. The ATR-FTIR spectra of the modified fibres supported by the TGA and SEM results

confirmed the presence of the main functional groups of the ligands onto the PS backbone.

Beside the two main sections of characterizations summarized above, the last experiments were conducted on the selected modified nanofiber mats to check their stability in solutions of HNO_3 or EDTA at different concentrations prior to desorption process (Chapter 6). The results showed that HNO_3 solution at concentration of 1 M was suitable as regenerant compared to EDTA which significantly affected the integrity of the materials in particular the functional groups onto the PS backbone.

The following chapter (Chapter 5) presents the experimental results obtained from direct leaching and indirect leaching (recrystallization) of the as-received PG for REE up concentration.

CHAPTER 5

5. LEACHABILITY OF RARE EARTHS ELEMENTS VIA RECRYSTALLIZATION OF SOUTH AFRICAN PHOSPHOGYPSUM WASTE

Chapter 5 presents a short background on valorisation of phosphogypsum into various materials with attention to possible extraction of REEs from the resulting leachates or filtrate solutions. The chapter further gives a detailed discussion on the leachability of REEs and other associated elements in direct leaching and indirect leaching (recrystallization) from phosphogypsum. The chapter thereafter ends with a summary.

5.1 Introduction

Phosphogypsum (PG) is a chemical gypsum generated during the processing of phosphate ores for the production of phosphoric acid. Phosphate ore used in this process usually contains 20–40 % of phosphate and the balance constitutes of the impurities that mainly include aluminium dioxide, calcium oxide, carbon dioxide, fluorine, silicon dioxide, sodium dioxide, sulphur trioxide, iron oxide, magnesium oxide; heavy metals, U, Th and rare earths elements (REEs). Of these impurities, REE content varies between 0.1–2 wt% of which 70–95 % gets concentrated into PG (Binnemans et al., 2015; Wu et al., 2019). This REE content is far lower compared to primary REE bearing minerals such as monazite (Bruckner et al., 2020), but the large volumes of PG produced worldwide with an estimated amount of 200–300 million tons per annum make it a potential source of REEs to compensate the current scarcity and supply (Masmoudi-Soussi et al., 2019). Although a few moderate REE leaching efficiencies have been reported through direct leaching of PG, so far these methods have been deemed uneconomical especially for larger scales (Salo et al., 2020, Mukaba et., 2021). Therefore, exploring technologies that involve indirect leaching of REEs such as recrystallization of PG for production of materials that have commercial and industrial utilization with subsequent extraction of REEs is advisable.

The recrystallization of certain types of PG for enhanced recovery of REEs is an emerging area of research and, in view of this approach, a few studies have been performed at laboratory scale and larger scale. For instance, Genkin et al., (2017) described a process where PG-dihydrate ($CaSO_4 \cdot 2H_2O$) was recrystallized in the presence of calcium nitrate under acidic medium (0.2–8 M). Subsequent to this method, over 98 % of the REEs reported in the leaching solution. However, the proposed process was found to be unattractive from an economical and waste management point of view. Furthermore, although increased concentration of Ca^{2+} ions was favourable in terms of REE recovery, this increase made the formation of the targeted and purified PG less favourable. Koopman and Witkamp, (2000) described a method consisting of introducing an ion-exchange resin for the extraction and recovery of REEs leached out during the recrystallization of PG-hemihydrate ($CaSO_4 \cdot 0.5H_2O$) to PG-$CaSO_4 \cdot 2H_2O$. Their results showed that the REEs in the final PG-$CaSO_4 \cdot 2H_2O$ residue and the amount of REE released during the recrystallization process was found to be up to 53 %. The main disadvantage of this process was the low recovery of REEs and the sulfonic acid resin used also extracted calcium ions besides having a preference for trivalent REEs.
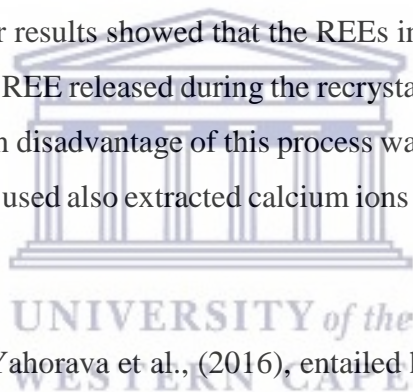
A method developed by Yahorava et al., (2016), entailed hydrothermally treating PG containing slurry using an autoclave for the recrystallization and recovery of REEs. The process was tested on various PG samples and showed that REE recoveries were improved from 5 % to 80 % while recrystallizing the PG. Although the process carried a large potential for unlocking valuable REEs encapsulated in PG stock piles, there were still several parameters such as residence time in the autoclave, impact of seeding and solids content which required verification and optimization. Moreover, even though the process claimed to be "chemical free", temperatures of up to 100 °C were required in the autoclave for high release of REEs during the recrystallization process. Kanzel et al., (2017) developed a method which consisted of decomposing PG while extracting released REEs using sulphuric acid in five consecutive stages. These authors found that the resulting solid residue was technically a gypsum which was converted into binders whereas the liquid waste contained high concentrations of REEs.

135

However, the production of binders from PG in such a process was found to be an energy intensive process since the PG binder is burned at higher temperatures than are traditionally used to obtain a binder from natural gypsum stone. This makes the proposed process economically unprofitable particularly when considering large scale processing.

The synthesis of calcium sulphate whiskers (CSWs) from PG has also recently been reported due to high content of $CaSO_4$ in PG waste (Sheng et al., 2018). CSWs have been widely used for several applications such as reinforcing materials in plastics, paper mills, rubbers, grafting materials in bone and tissue regeneration, filters, paints and other products (Miao et al., 2015; Qi et al., 2017). Up to date, efforts in the area of CSWs synthesis have been made following three directions, namely: the method of synthesis, modification of the crystal morphologies using additives, and the application of CSWs for constructional materials (Wang et al., 2017). However, little effort has been made to develop a combined process in which both the synthesis of CSWs and REEs extraction could be sequentially achieved. CSWs can typically be synthesized through hydrothermal or atmospheric acidification synthesis or recrystallization. Compared to the hydrothermal synthesis, which is usually carried out at high temperatures (>100 °C) and steam pressures (Zhou et al., 2021), the atmospheric acidification of PG has advantages since it can be carried out at a mild reaction conditions (temperature < 90 °C and atmospheric pressure) (Sun et al., 2016). These conditions are relatively similar to those used in direct leaching of REEs from PG where HCl, H_2SO_4 or HNO_3 are commonly used due their strength and availability Mukaba et al., (2021). This can allow the CSWs synthesis and REE recovery in a combined process. The scope of this chapter is therefore to evaluate the leachability of the REEs during the dissolution and recrystallization of South African PG waste for prospective combined REE recovery and CSWs synthesis (Objective 2 of Chapter 1).

5.2 Materials and experimental

Details of the materials and the experimental protocol for direct leaching and the recrystallization of the as-received PG are described in Sections 3.6 and 3.7 of Chapter 3. The characterizations of the materials were carried out as described in Section 3.10 of Chapter 3. Prior to the recrystallization (indirect leaching process) of the as-received PG, the direct leaching process was optimized using HCl, HNO_3 and H_2SO_4 solutions and the parameters investigated were described in Section 3.6. All the experiments were performed in triplicate for reliability and the average values were plotted and discussed for each case.

5.3 Results and discussion

The elemental composition of the materials in the following sections was determined by ICP-OES or MS and NAA while XRD, FTIR, TGA, and SEM were used to elucidate the mineral phase, structural changes, thermal profile and morphology of the materials.

5.3.1 Total acid digestion analysis

Total acid digestion analysis of the as-received PG was carried out as described in Section 3.4 and was used as reference for the evaluation of the leaching efficiencies throughout this Chapter. As can be seen in Table 5.1, the majority of REEs present in the as received PG were light REEs (LREEs) which predominated with a cumulative total concentration that was approximately 20 fold higher than for the heavy REEs (HREEs). However, the major LREEs were La, Ce and Nd, whereas Dy and Y made up the weight of the HREEs group. The large discrepancy between the concentrations of LREEs and HREEs might be as a result of the Oddo-Harkins rule as discussed in Section 2.2 of Chapter 2 (Massari & Ruberti, 2013).

137

Table 5.1: Total acid digestion of the as-received PG (mg/Kg) for REEs content.

LREEs		HREEs	
La	488 ± 59	Tb	8 ± 0.7
Ce	1243 ± 76	Dy	30 ± 1.4
Pr	165 ± 7	Ho	4 ± 0.3
Nd	743 ± 48	Er	6 ± 0.5
Sm	122 ± 24	Tm	0.4 ± 0.02
Eu	27 ± 3	Yb	2 ± 0.3
Gd	82 ± 6	Lu	0.2 ± 0.01
		Y	86 ± 7
Total	**2870 ± 223**	**Total**	**136.6 ± 10.23**

5.3.2 Effect of the concentration

Figure 5.1. shows the results of the total REE (ΣREEs) concentrations presented as the leaching efficiencies (%) obtained from HCl, HNO$_3$ and H$_2$SO$_4$ solutions at different concentrations (0.5; 1; 1.5; 2; 2.5; 3 and 3.5 M) while the rest of the parameters (i.e., the contact time, temperature, the agitation and S\L ratio) were constant at 90 min, 80 °C, 600 rpm and S\L ratio. 0.1 respectively.

As can be observed from these results, the concentration had an important effect on the leaching efficiency of ΣREEs from PG. It was found that the leaching efficiencies of HCl and HNO$_3$ steadily increased as the concentrations increased reaching an equilibrium point between 1.5–2.5 M while H$_2$SO$_4$ reached a maximum at 1.5 M then decreased as the concentrations increased. At the concentrations of 2.5, 2 and 1.5 M about 45 %, 56 % and 29 % leaching efficiencies of ΣREEs were respectively obtained in HCl, HNO$_3$ and H$_2$SO$_4$ solutions. The leaching efficiencies of 56 % and 29 % obtained in 3 M HNO$_3$ and 0.5 M H$_2$SO$_4$ solutions respectively were relatively lower compared than those reported by Canovas et al., (2019) who found 80 % and 50 % respectively. This discrepancy may be attributed to the type of PG and also the preferential partitioning of REEs in gypsum crystals over other mineral phases. However, the leaching efficiencies obtained in this study at 1.5 M for H$_2$SO$_4$ was twofold higher than those obtained by Rychkov et al. (2018) at the same concentration.
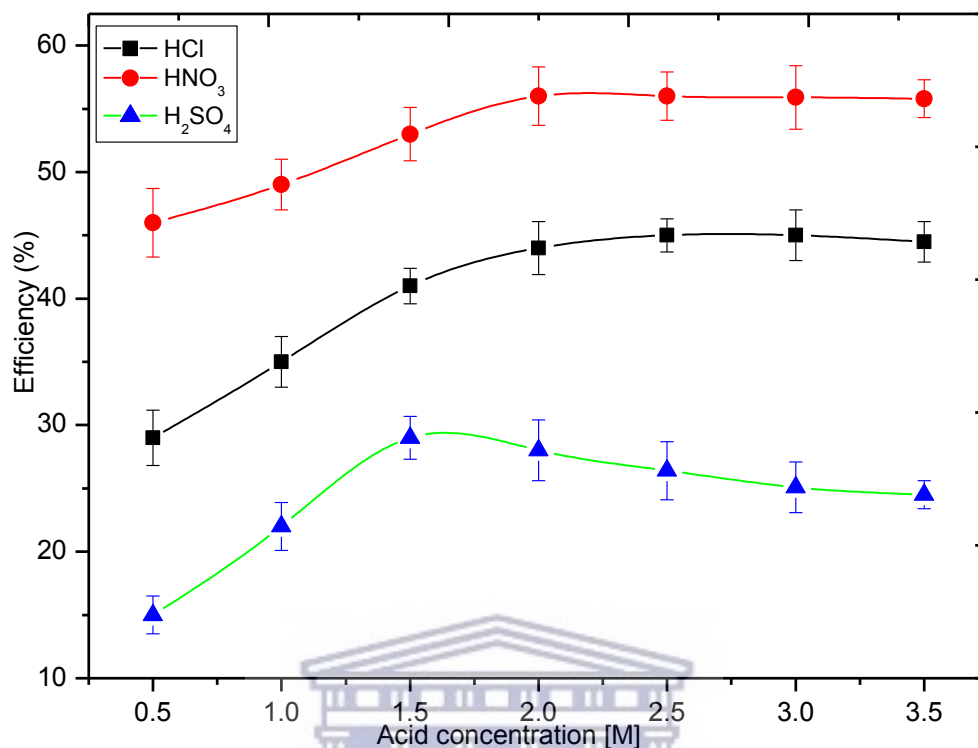
Figure 5.1: Effect of acid concentration (0.5; 1; 1.5; 2; 2.5; 3 and 3.5 M) at 120 min, 80 °C, S/L. 0. 1, 300 rpm on the leaching of REEs from PG.

The leaching efficiencies of ΣREEs in H_2SO_4 initially increased from 0.5 to 1.5 M where it reached the maximum then decreased as the concentration increased. This decrease at high concentrations of H_2SO_4 could be attributed to the adverse effect of the common SO_4^{2-} anions in the solution hindering further dissolution of the gypsum particles and thus resulting in a lower liberation of ΣREEs. This trend might be in good agreement with the results of Liang et al., (2017) who showed that the leaching efficiencies of REEs in H_2SO_4 decreased as the concentration increased. Despite that, all leachants had a similar trend from the concentrations of 0.5 to 1.5 M, overall, HNO_3 exhibited the highest performance followed by HCl and H_2SO_4. The lowest leaching efficiencies obtained in H_2SO_4 compared to HCl and HNO_3 might be attributed to the low solubility of gypsum in H_2SO_4 which might have resulted in a significant decrease in the leaching efficiency of ΣREEs. The solubility of gypsum in H_2SO_4 or HCl was reported by Azimi et al., (2008) who showed that it was 40 times lower in H_2SO_4 compared to HCl. For further investigation of other parameters, the concentrations of

139

2 M HCl, 2 M HNO$_3$ and 1.5 M H$_2$SO$_4$ were found to be ideal since a minor increase or decrease were observed after the aforementioned concentrations. Therefore, the following subsection briefly discussed the effect of residence time on the leaching.

5.3.3 Effect of reaction time

To investigate the leaching kinetic of REEs, the concentrations of 2 M HCl, 2 M HNO$_3$ and 1.5 M H$_2$SO$_4$ were used at different contact times (20, 40, 60, 80, 100 and 120 min) while the temperature, S\L ratio and stirring were kept constant at 80 °C, 0.1 and 300 rpm respectively.
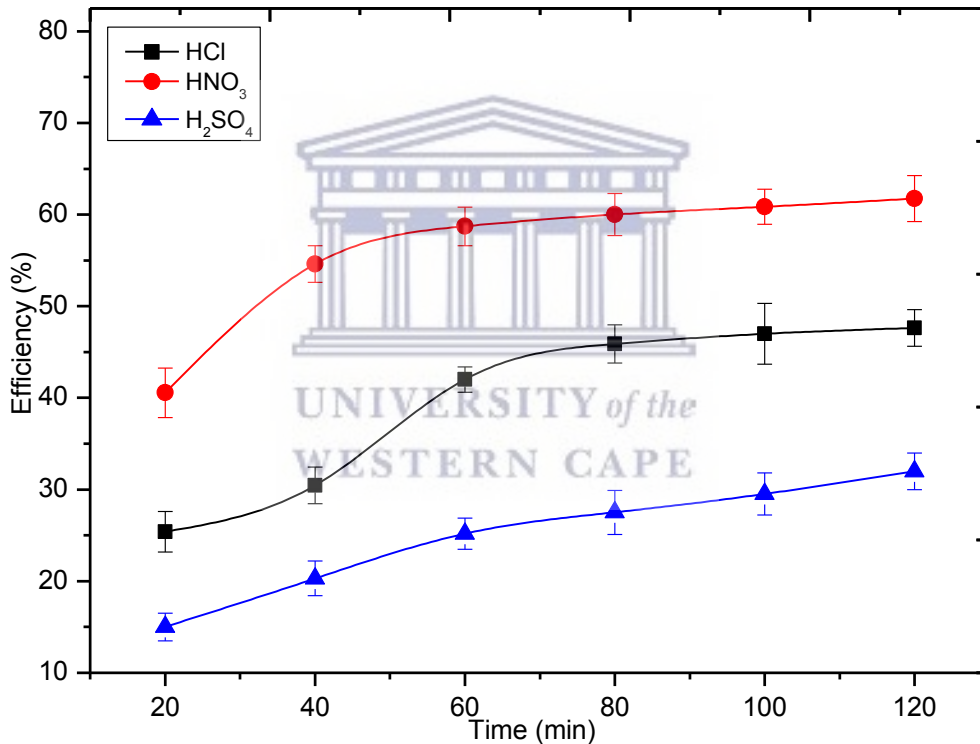
Figure 5.2: Effect of reaction time (20, 40, 60, 80, 100 and 120 min) in 2 M HCl, 2 M HNO$_3$ and 1.5 M H$_2$SO$_4$ at 80 °C, S/L ratio. 0.1, 300 rpm on the leaching of REEs from PG.

It can be observed from the results displayed in Figure 5.2. that the residence time played a crucial role regarding the leaching of total REEs. The leaching efficiencies of ΣREEs rapidly increased between 20 min and 60 min and thereafter showed a gradual increase with minor increments from 60 min to 120 min as the residence time increased

140

for 2 M HCl and 2 M HNO_3 whereas it gradually increased from 20 min to 120 min in 1.5 M H_2SO_4 solution. Although extending the leaching time slowly increased the leaching efficiencies from 20 min to 60 min, the degree of increment was little after 60 min in particular for 2 M HCl and 2 M HNO_3. This small increment observed at prolonged leaching time is in agreement with the results reported by Jin et al., (2017), who observed a small increment of leaching efficiencies after 90 min of prolonged leaching time. The small increment in the leaching efficiencies at prolonged leaching times indicated that the leaching of REEs tended to reach an equilibrium after 60 min. Furthermore, this leaching trend might be attributed to co-crystallization of REEs with the PG which might have led to low leaching efficiencies as the time increased. This is believed to be caused by the similarity of the ionic radius of REEs and calcium ions which can be found in isomorphous substitution within the PG lattice (Al-Thyabat & Zhang, 2015a). The leaching efficiencies values obtained at 60 min for 2 M HNO_3 (59 %) and 2 M HCl (45 %) and 120 min in the case of 1.5 M H_2SO_4 (32 %) were slightly higher than those reported by Ismail et al., (2015) who reported 44 %, 20 % and 7.5 % efficiencies for 3 M HNO_3, 2 M HCl and 4 M H_2SO_4 respectively at approximately 60 min. Although in their study, the concentrations of HNO_3 and H_2SO_4 solutions were higher (3 M and 4 M) respectively, their leaching efficiencies were lower than in the current study. This discrepancy might be due to the difference in terms of the leaching temperatures which was 25 °C in their study as well as the distribution of REEs within the crystal of gypsum. The effect of the temperature will shortly be discussed in Section 5.3.4 for further understanding. Overall, HNO_3 showed the highest performance followed by HCl and H_2SO_4 and the identified contact time of 60 min (HNO_3 and HCl) and 120 min (H_2SO_4) were used to investigate the effect of the temperature on the leaching efficiencies of REEs.

5.3.4 Effect of temperature

The conditions identified in Sections 5.3.2 and 5.3.3 were applied at different temperatures of 30, 40, 50, 60,70 and 80 °C while keeping the S\L ratio constant and stirring at 0.1 and 300 rpm respectively. The results are graphically presented in Figure 5.3 as a relation between the leaching efficiencies of ΣREEs and temperatures.
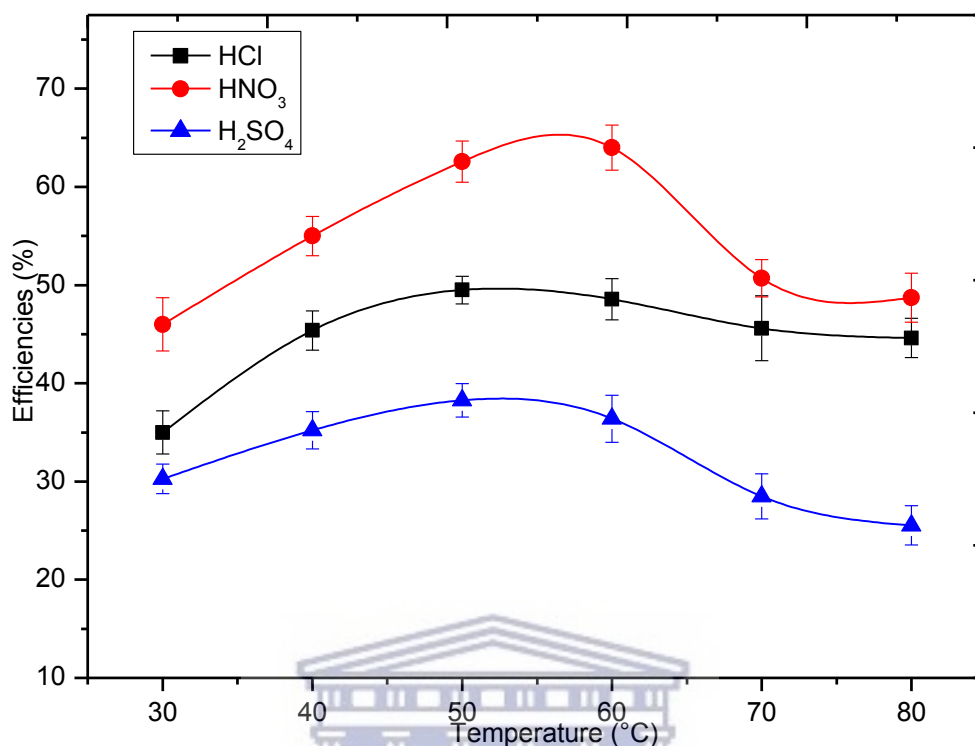
Figure 5.3: Effect of temperature (30; 40; 50; 60; 70 and 80 °C) at 60 min (2 M HCl and 1.5 M HNO₃) and 120 min (1.5 M H₂SO₄), S/L ratio. 0.1, 300 rpm on the leaching of REEs from PG.

From Figure 5.3, it can be seen that the leaching efficiencies of the REEs exhibited a similar trend for all the leachants. The leaching efficiencies increased from 30 °C to 60 °C for HNO₃ then drastically dropped at 70 °C and 80 °C whereas in the case of HCl and H₂SO₄, the efficiencies increased from 30 °C to 50 °C and decreased from 60 °C to 80°C. These leaching trends, especially for HCl and H₂SO₄ differ from those obtained by Ismail et al., (2015) who found no drop between temperatures 50 °C and 60 °C but constant temperatures throughout 60 °C and 25 °C for HCl and H₂SO₄ respectively. The leaching efficiencies reached maxima at 60 °C for HNO₃ and 50 °C in the case of HCl and H₂SO₄. It can be concluded that below the aforementioned temperature maxima, the dissolution of REEs from PG phases was favourable leading to high leaching efficiencies. In other words, the solubility of gypsum at these maxima was high compared to the highest temperatures of leaching. Therefore, the decrease in the leaching efficiencies observed at high temperatures might be due to a decreased dissolution of the gypsum. The leaching trend observed at higher temperature was in

142

good agreement with the result reported by Liang et al., (2017) who showed that at a temperature above 50 °C, the decrease of the gypsum solubility was as a result of the overwhelming factor causing a decrease in the leaching efficiencies of the REEs from the PG. The leaching efficiencies of ΣREEs in HNO_3 solution remained higher than HCl and H_2SO_4 at equilibrium temperatures due to high gypsum solubility. Therefore, in an attempt to obtain high leaching efficiencies, the leaching temperature was set at 60 °C for HNO_3 and 50 °C for HCl and H_2SO_4 to assess the rest of the factors influencing the leachability of the REEs such as solid to liquid ratio.

5.3.5 Effect of solid to liquid ratio

After identifying the leaching concentration, contact time and temperature, it was crucial to investigate the effect of the solid to liquid on the leaching efficiency of the ΣREEs from PG. Figure 5.4 displays the effect of solid to liquid ratio (S\L) on the leaching efficiencies of REEs from the as-received PG.
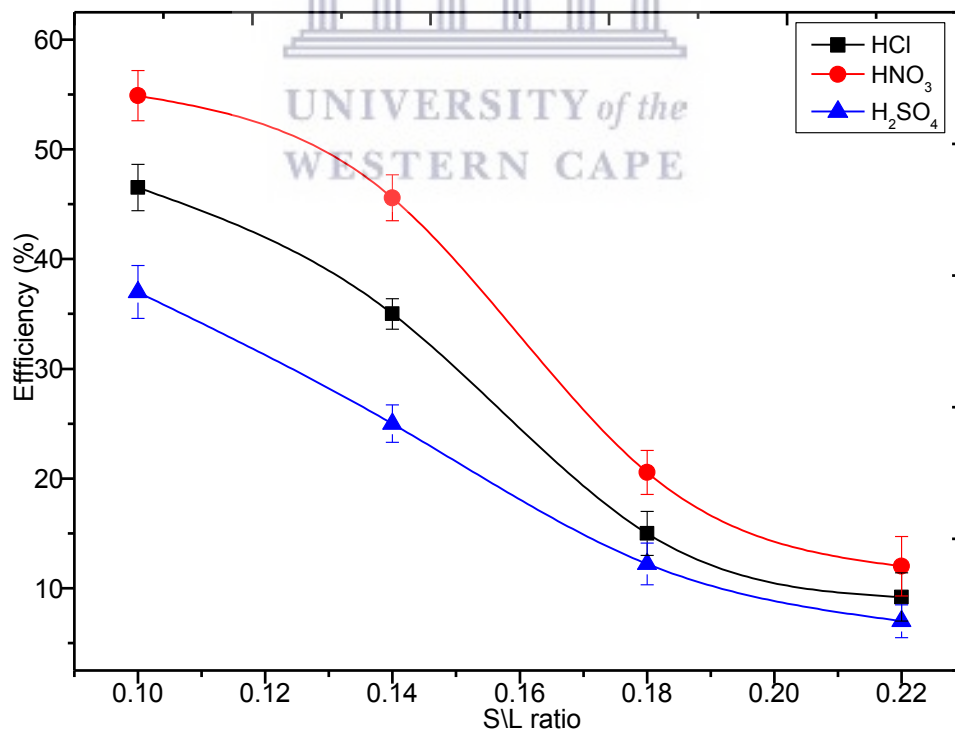

Figure 5.4: Effect of S\L ratios (0.1, 0.14, 0.18, 0.22) on leaching of REEs from PG at 300 rpm in 2 M HCl (60 min, 50 °C), 2 M HNO_3 (60 min, 60 °C) and 1.5 M H_2SO_4 (120 min, 50 °C).

143

The results showed that the leaching efficiencies of ΣREEs decreased from 55 % to 12 % (HNO_3), from 47 % to 9 % (HCl) and from 37 % to 7 % (H_2SO_4) as the S\L ratios increased from 0.1 to 0.22. The lowest S\L ratio of 0.1 led to high leaching efficiencies of REEs for all the leachants, indicating that the solubility of the as-received PG was high at this ratio, which resulted in a high concentration of the REEs in the leaching solution. S\L ratio higher than 0.1 in particular at S\L ratio 0.14 appeared to be economical due to a reduced amount of the liquid (leachant) but showed poor leaching efficiencies especially in the case of HCl and H_2SO_4. This was possibly due to incomplete dissolution of the PG at this S\L ratio. Further increase of the S\L ratios to 0.18 and 0.22 was not practical and tended to generate a denser pulp rendering the leaching of REEs in solution difficult and challenging. Therefore, the lowest S\L ratio 0.1 was used for subsequent experiments to investigate the effect of the stirring during the leaching process.

5.3.6 Effect of stirring

The effect of stirring was also investigated at S\L ratio of 0.1 using 2 M HCl (60 min, 50°C), 2 M HNO_3 (60 min, 60 °C) and 1.5 M H_2SO_4 (120 min, 50 °C) as identified in previous sections.

As can be seen in Figure 5.5, enhancing the stirring speed to 600 rpm from the initial value of 300 rpm tended to have a positive impact on the leaching efficiencies of ΣREEs. These leaching efficiencies approximately showed increments of 4 %, 6 % and 9 % of REE release in H_2SO_4, HCl and HNO_3 solutions respectively. These increments were attributed to the breaking down of PG particles in motion which resulted in high release of REEs from the framework in the leaching solutions. The relatively high performances of HCl and HNO_3 compared to H_2SO_4 might be associated to their higher abilities to dissolve the PG. However, as was found for other parameters discussed above, HNO_3 dominated in terms of the performance followed by HCl and H_2SO_4. Since the average gap based on the increment value of each

144

leachant was approximately 6 %, 600 rpm was set to be convenient for the rest of experiments in this study.
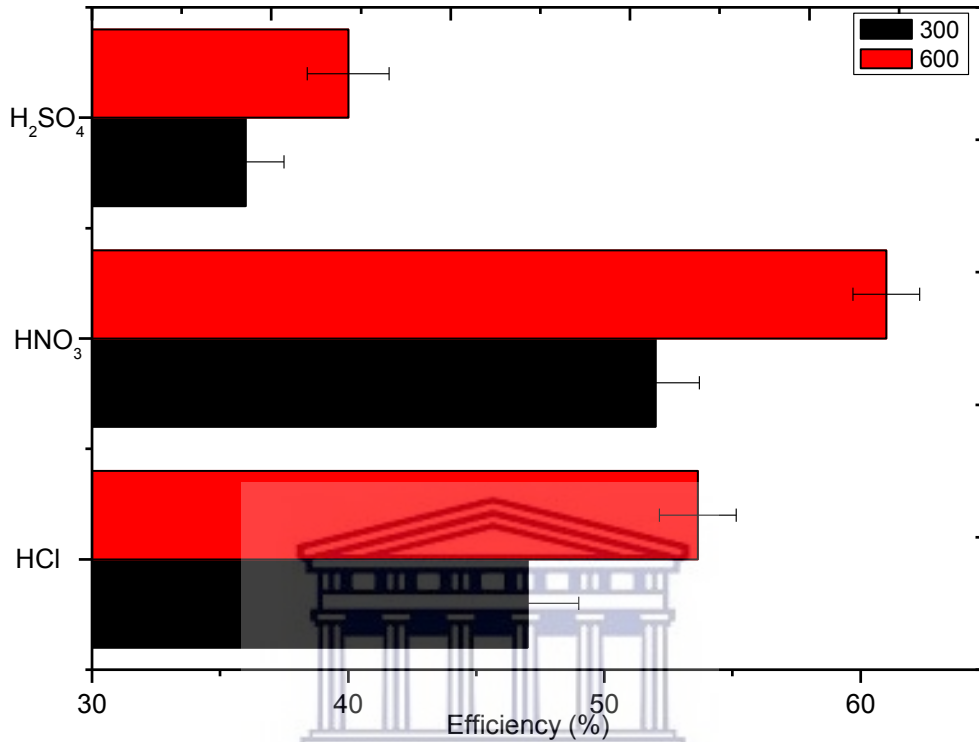
Figure 5.5: Effect of agitation on REE leaching (300, 600 rpm) using 2 M HCl (60 min, 50°C), 2 M HNO_3 (60 min, 60 °C) and 1.5 M H_2SO_4 (120 min, 50 °C).

5.4 Direct leaching trend of individual elements

After identifying the optimum conditions in which the leaching efficiencies of elements were studied in terms of total REEs (ΣREEs), the present subsection further investigated the leaching trends of individual REEs and other associated elements namely Sc, Th and U. The first is usually classified among the REEs due to its physicochemical properties as discussed in Section 2.1 but the last two are the most common radioactive elements associated with REEs and help to classify a PG material. This was carried out in attempts to understand the individual behaviour of these elements in HCl, HNO_3 and H_2SO_4 solutions as shown in Figures 5.6, 5.7 and 5.8.

145

Figure 5.6: Leachability trend of individual LREEs at 600 rpm using 2 M HCl (60 min, 50 °C), 2 M HNO$_3$ (60 min, 60 °C) and 1.5 M H$_2$SO$_4$ (120 min, 50 °C)

Figure 5.7: Leachability trend of individual HREEs at 600 rpm using 2 M HCl (60 min, 50 °C), 2 M HNO$_3$ (60 min, 60 °C) and 1.5 M H$_2$SO$_4$ (120 min, 50 °C).

146

As can be seen in Figures 5.6 and 5.7, none of the individual element among the LREEs (La–Gd) or HREEs (Tb–Y) exhibited a complete leaching efficiency (100 %) from PG. The leaching efficiencies varied between 65–78 %, 75–84 % and 45–54 % for LREEs and remained somewhat constant in the case of HREEs at 78 %, 84 % and 54 % in HCl, HNO_3 and H_2SO_4 solutions respectively. The leaching of LREEs slightly tended to increase from Ce to Sm. This gradual increase trend somewhat remained constant throughout the HREEs and might be as a result of the variation in terms of REE ionic radii due to the lanthanides contraction as discussed in Section 2.1. This might be explained by the fact that, as the ionic radii decreases with the increase of the atomic mass, smaller ions were easily leached compared to elements with higher ionic radii, such as La and Ce, which showed in most of the cases fairly low leaching efficiencies. The high leaching efficiencies observed for HREEs might also be attributed to their lower content than the LREEs and unevenly distribution in PG. It can be seen from Figure 5.8, that the leaching of Sc and U were somewhat similar in HCl and HNO_3 solutions reaching up to 85 % and 65 % respectively but lower in H_2SO_4. Furthermore, HCl was favourable for the leaching of Th in which over 85 % efficiencies could be reached compared to HNO_3 and H_2SO_4 solutions. The variation in the leaching efficiencies of Sc, Th and U might be attributed to the difference in ionic radii which could have imparted their leachability.
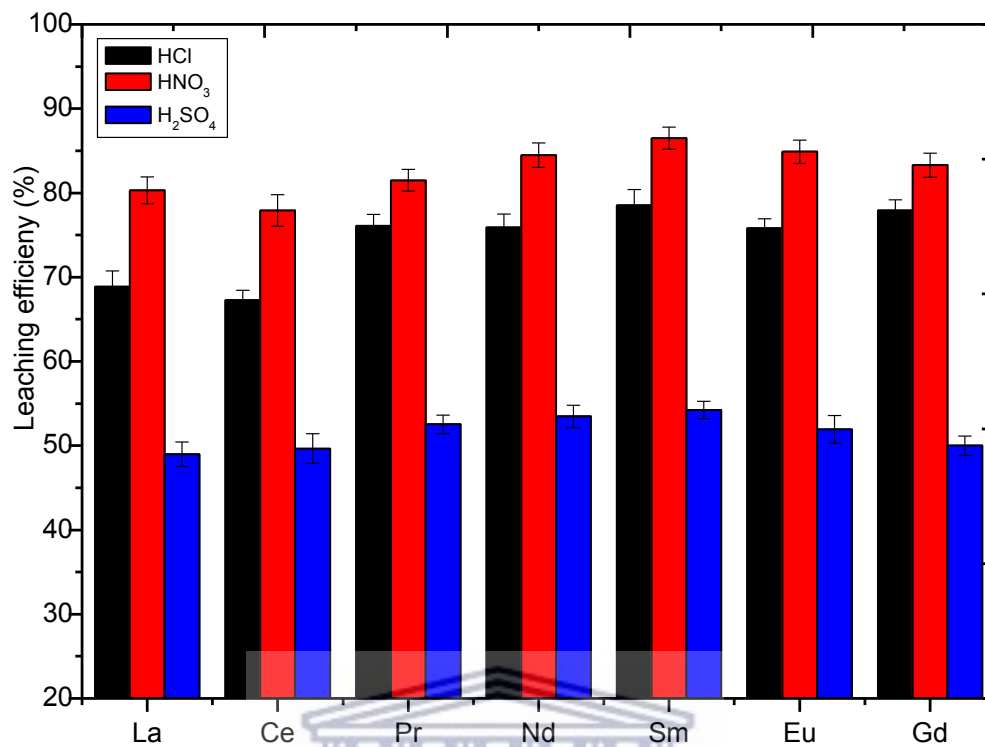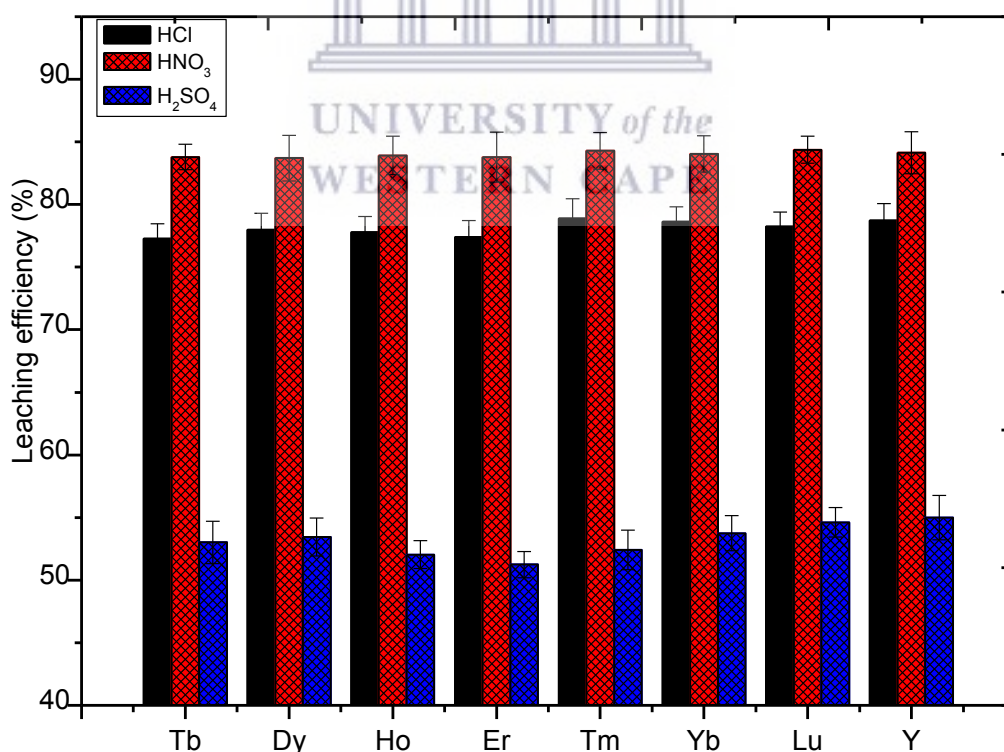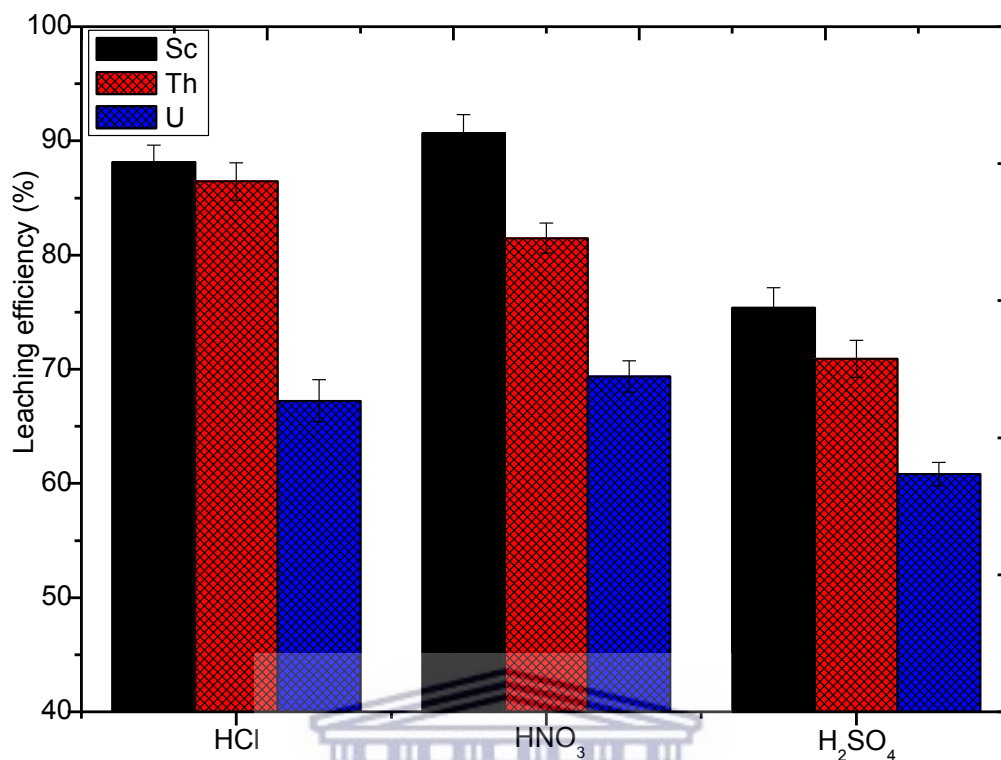
Figure 5.8: Leachability trend of Sc, Th and U at 600 rpm using 2 M HCl (60 min, 50 °C), 2 M HNO$_3$ (60 min, 60 °C) and 1.5 M H$_2$SO$_4$ (120 min, 50 °C).

5.5 Indirect leaching: Recrystallization of PG

One of the disadvantages of the direct acid leaching is the waste residue generated after the leaching which may be an environmental issue in particular when considering large scale process. An approach that could lead to high REE release in the leachate solution while retaining the structural matrix of PG is advantageous. Therefore, this subsection focuses on the dissolution and recrystallization of PG in attempts to obtain a high REE release and a purified gypsum that will be referred in this subsection as calcium sulphate whiskers (CSWs) or recrystallized gypsum. The recrystallization of PG was carried out as described in Section 3.7 of Chapter 3.

5.5.1 Solubility test of PG

Prior to the recrystallization process, a solubility test of PG was carried in HCl, HNO$_3$ and H$_2$SO$_4$. It can be seen from Figure 5.9 that the solubility of PG (in terms of Ca^{2+}

148

release) was higher in HNO_3 followed by HCl and H_2SO_4. This trend corresponded to the leaching performances of HCl, HNO_3 and H_2SO_4 as discussed in section 5.3 in which the high leaching efficiencies were explained as resulting from high solubility of the PG. The significantly lower solubility in H_2SO_4 was attributed to the effect of the common sulphate ion as also discussed in Section 5.3.2. These results were in a good agreement with those reported by Walawalkar et al., (2016) who studied the solubility of gypsum ($CaSO_4$) as a representative phase of PG and showed using simulations and measured experimental data that the solubility of $CaSO_4$ was higher in HNO_3 solutions compared to HCl and H_2SO_4. In this Section, H_2SO_4 was not further used due to the adverse effect of sulphate ions which led to lowest solubility of PG compared to HCl and HNO_3.
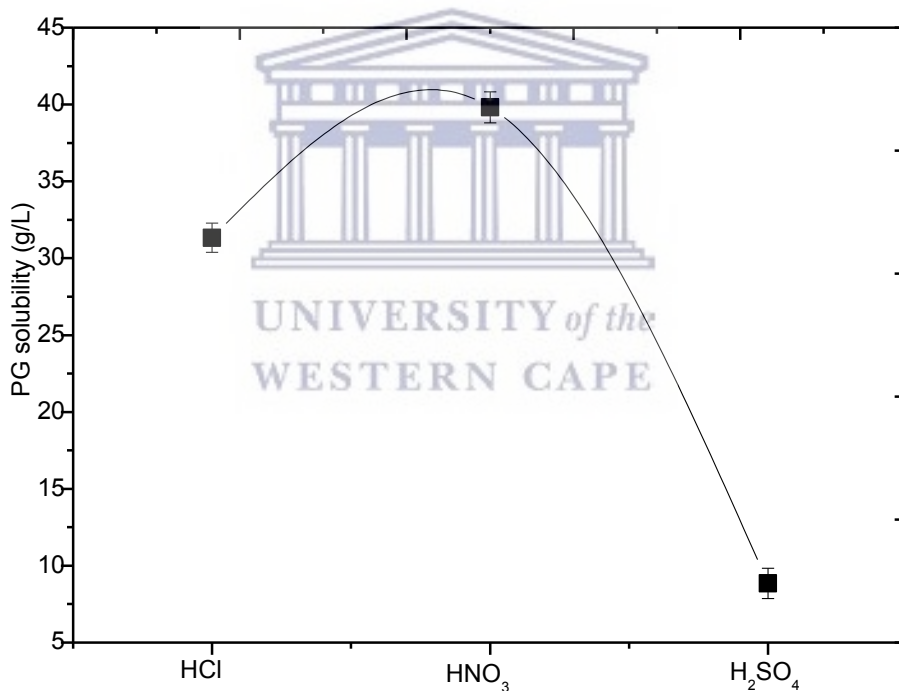
Figure 5.9: Solubility of PG (in terms of Ca^{2+}) in 2 M HCl, 2 M HNO_3 and 1.5 M H_2SO_4

5.5.2 REE release via dissolution and recrystallization of PG

The results displayed in Figures 5.10 and 5.11 were obtained after the dissolution and recrystallization of PG. These results compared to those discussed in section 5.3 regarding the direct leaching of REEs with a particular attention on HCl and HNO_3

149

solutions, revealed that the dissolution and recrystallization significantly improved the REE release in the solution (filtrate). LREE and HREE efficiencies in HCl and HNO_3 solutions were over 90 % with a slight difference in HNO_3 solution. This relatively high performance of HNO_3 could be due to the effect of the conjugated acid ions and acid strength which seemed to dictate the dissolution and recrystallization of the as received PG bringing more REEs in solution of nitrate than chloride solution.
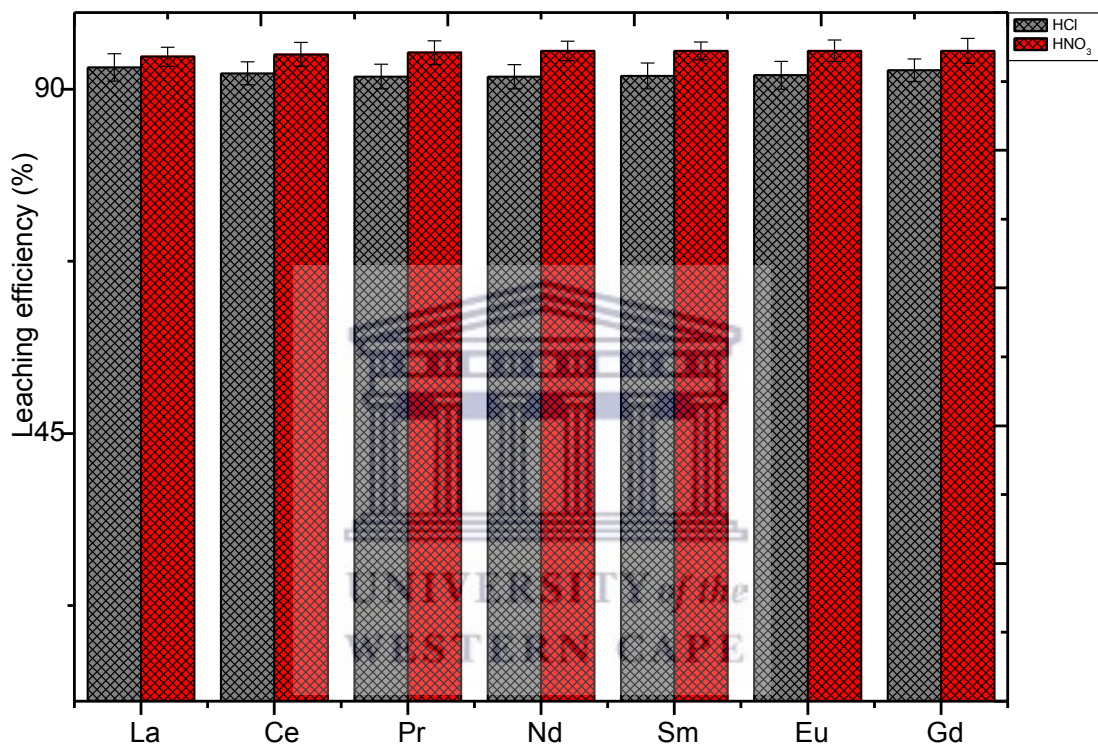
Figure 5.10: LREE release efficiency after recrystallization of PG in 2 M HCl and 2 M HNO_3 solutions

Thorough examination of the results, indicated that the efficiencies of LREEs were somewhat lower than those of HREEs. As also explained in Section 5.3 this slight small difference might be as a result of small ionic radii in HREEs due to lanthanide contraction which might influence their leachability during the dissolution and recrystallization. Although the dissolution and recrystallization method led to high leaching efficiencies of REEs in the solutions, no complete leaching efficiency (100 %) of LREEs or HREEs was found for HCl and HNO_3 solutions. This was evidenced

through a thorough assessment of the REE distribution of dry filtrate (DF), recrystallized PG (CSWs) and PG residue (PGR) all obtained in one batch experiment.
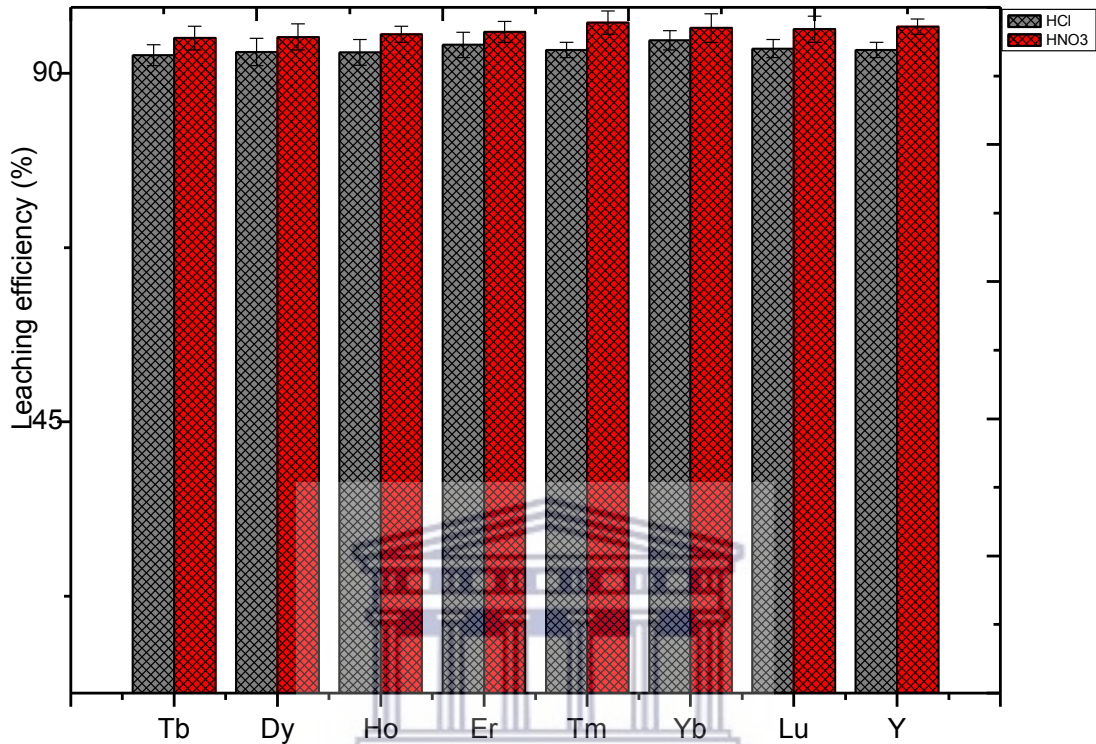
Figure 5.11: HREE release efficiency after recrystallization of PG in 2 M HCl and 2 M HNO_3 solutions.

As can be seen from Figures 5.12 and 5.13 for HCl and HNO_3 processes respectively, these results showed that about 3–5 % of REEs could be detected in both CSWs and PGR after the recrystallization while the majority of the REEs 95–97 % were found in DF. The presence of REEs in the obtained CSWs is inevitable and might be explained by the fact that as REE ions usually substitute with calcium ions within the lattice of gypsum, some of the REEs possibly ended up back in the CSWs but these amounts were far lower compared to those that were found in DF. On the other hand, the REEs detected in the PGR generated from HCl and HNO_3 processes are possibly as a result of the undissolved gypsum particles during the dissolution and recrystallization process.

151

Figure 5.12: Distribution of LREEs and HREEs after recrystallization of PG in 2 M HCl solution.
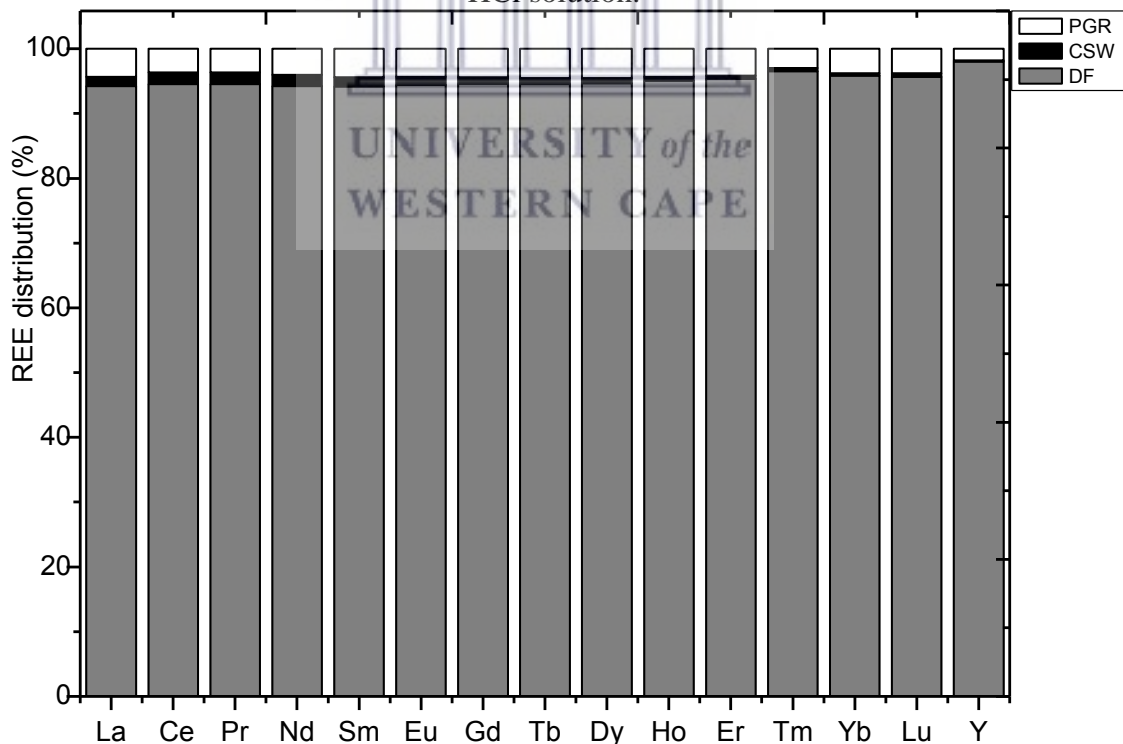
Figure 5.13: Distribution of LREEs and HREEs after recrystallization of PG in 2 M HNO₃ solution.

Although the two processes showed similar trends in terms of REE distribution in CSWs, the HNO_3 process tended to generate CSWs with lower distribution (efficiency) than HCl. This might be attributed to high solubility of the PG in HNO_3 as discussed in Section 5.5.1 which led to more REEs into the DF than in CSWs and PGR. Although the HCl process could be economically cheaper compared to HNO_3, if a high purity CSWs is required, HNO_3 process might be more favourable as less REEs and other elements were found in this process. The release efficiencies of Sc, Th and U as shown in Figure 5.14 compared to the leaching efficiencies obtained from the direct leaching method also showed a significant improvement for the three elements and in particular for U which remarkably increased from 65 % in direct leaching to over 90 % after dissolution and recrystallization method. However, as also discussed in Section 5.3, none of the three elements was completely released in HCl or HNO_3 solutions.
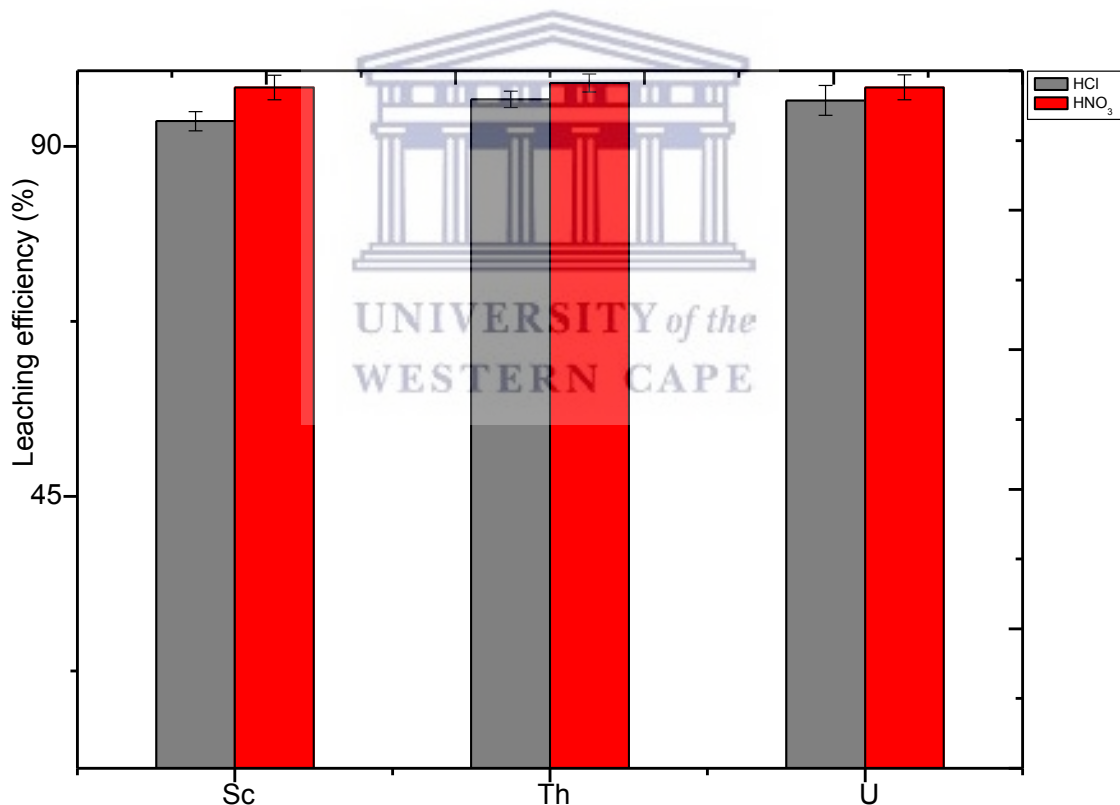
Figure 5.14: Sc,Th and U release efficiency after recrystallization of PG in 2 M HCl and 2 M HNO_3 solutions.

The distribution of Sc, Th and U in DF, CSWs and PGR are shown in Figures 5.15 and 5.16 respectively for HCl and HNO_3 processes. It can be seen from these results that the distributions of Sc, Th and U varied between 95–98 %, 2–5 %, and 0.02–0.08 %

in DF, PGR and CSWs respectively for both HCl or HNO$_3$ processes but the highest removal of these elements with attention to CSWs was found in HNO$_3$ process (Figure 5.16). The lower distribution of Th and U that was found through the dissolution and recrystallization method was of utmost importance, as higher concentrations of Th and U are not favourable when considering the reutilization of the purified gypsum.
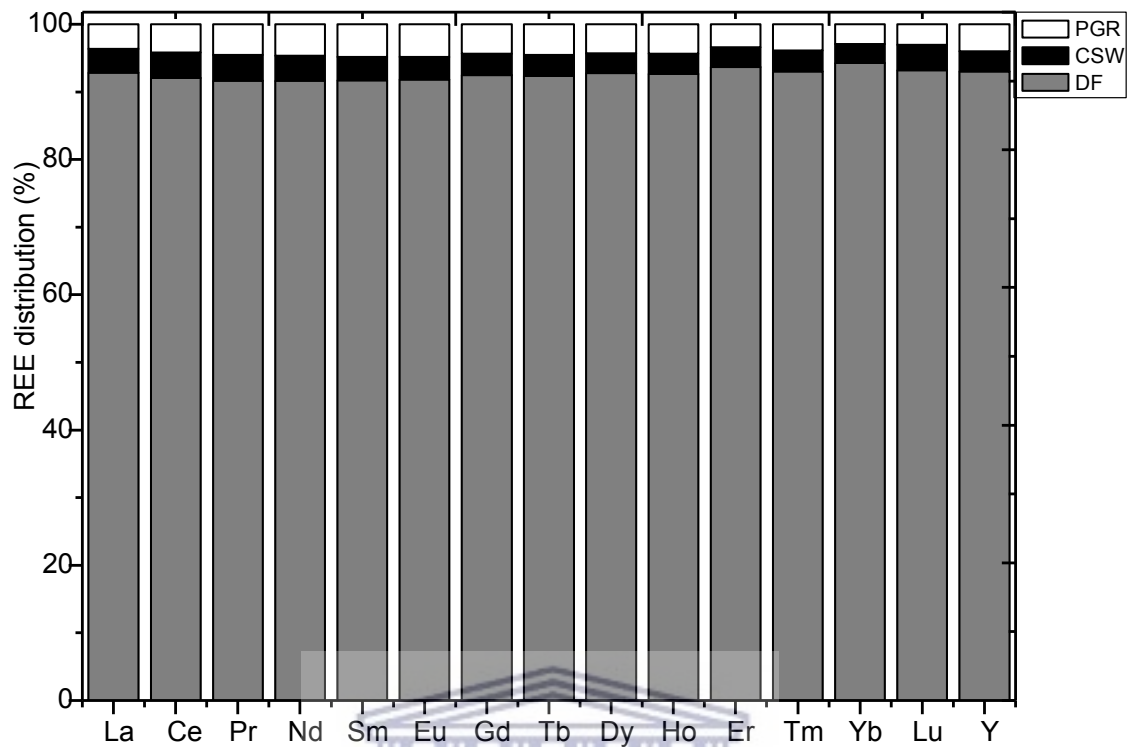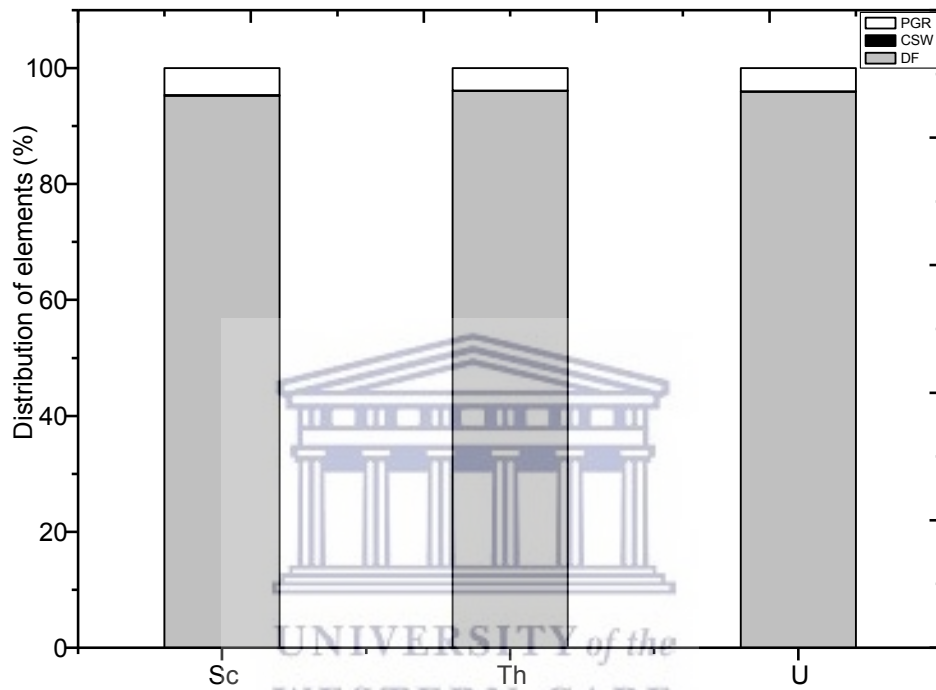

Figure 5.15: Distribution of Sc,Th and U after recrystallization of PG in 2 M HCl solution.
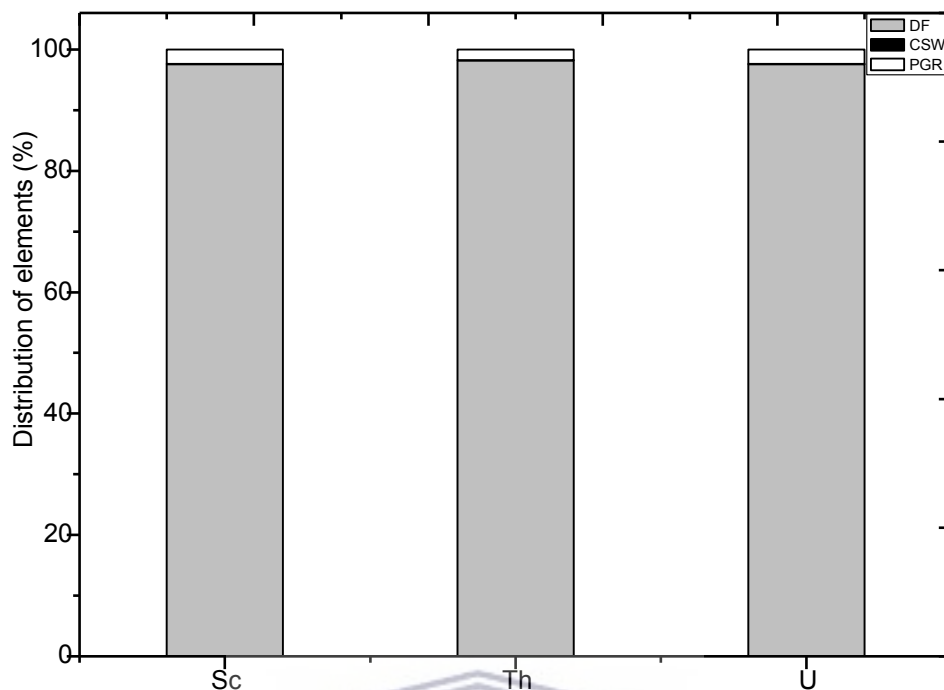
Figure 5.16: Distribution of Sc,Th and U after recrystallization of PG in 2 M HNO₃ solution.

5.5.3 Structural characterization of the recrystallized PG

In attempts to understand the structural changes of the recrystallized PG obtained from 2.0 M HNO₃ (CSW-NO₃) or 2.0 M HCl (CSW-Cl) solutions, a few characterizations were carried out. This was carried out through FTIR, XRD, SEM and TGA for structural composition, mineral phase, morphology and thermal profile respectively.

5.5.3.1   Chemical bonding by FTIR

Figure 5.17 displays overlapping IR spectra of the untreated PG (PGu) and, CSW-Cl and CSW-NO₃ obtained from HCl and HNO₃ solutions. As can be seen, the spectra of PGu, CSW-Cl and CSW-NO₃ were somewhat similar. The similarities of these spectra are emphasized by the presence of the characteristic vibration bands at 3500–3400 cm⁻¹ (stretching mode) and 1680–1618 cm⁻¹ (bending modes) which are related to the OH group of water (as moisture) content in PGu, CSW-Cl and CSW-NO₃. The weak vibrations observed between 2400–2000 cm⁻¹ were attributed to stretching modes of O-S-O whereas the strong band located between 1104–1096 cm⁻¹ was attributed to the

155

stretching vibration of S=O from the sulphate groups present in calcium sulphate which makes up the PGu and CSW-Cl or CSW-NO$_3$. The bands located in the lower region between 750–450 cm^{-1} were assigned to bending vibrations of sulphate anions. The new band which arose at 1733 cm^{-1} was more intense in CSW-NO$_3$ than in CSW-Cl and might be as a result of the deformation of the band at 1680 cm^{-1}. This vibration might be attributed to structural change that might have occurred within the bending mode regions after the dissolution and recrystallization process. Another new band which was also more intense in CSW-NO$_3$ was found at 1366 cm^{-1}. This band might be as a result of the deformation in the vibration region of S=O. The relatively higher intensity of the new bands at 1733 cm^{-1} and 1366 cm^{-1} in CSW-NO$_3$ than CSW-Cl might be related to intrinsic behaviour of nitrate or chloride solutions during the recrystallization process.
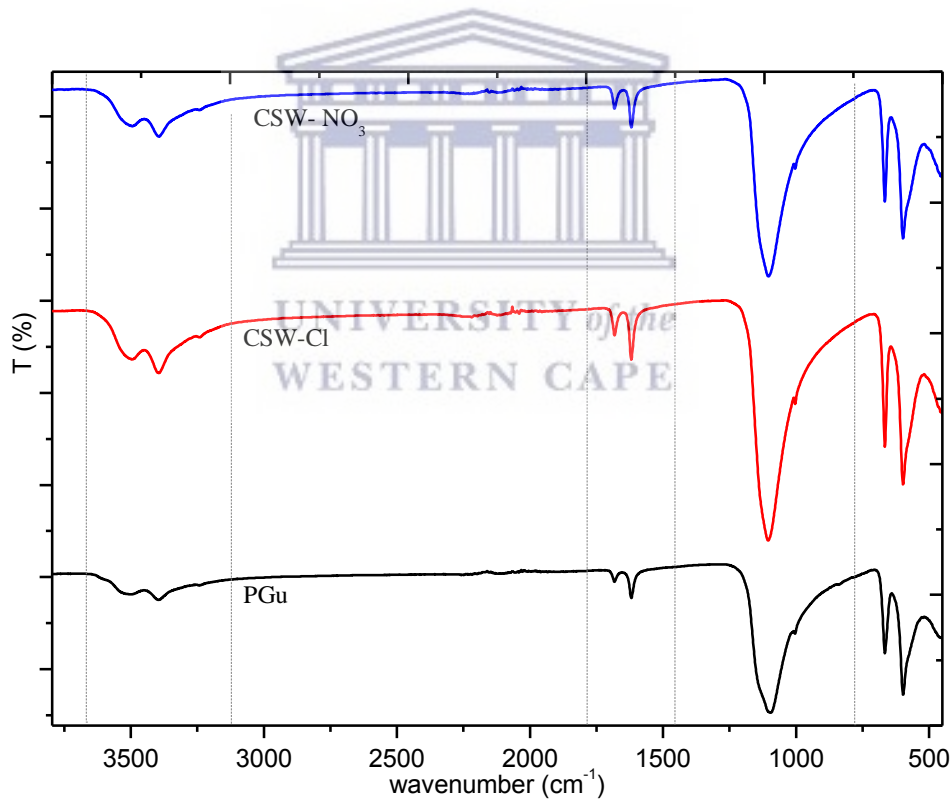
Figure 5.17: IR spectra of untreated PG (PGu), CSW-NO$_3$ and CSW-Cl.

Except the aforementioned new vibration bands which were particularly identified in CSW-NO$_3$ or CSW-Cl, the rest of the bands were in good agreement with those found by Hammas et al., (2013) and Bouhlassa et., (2016) when assessing the bands of

156

untreated PG material. CSW-Cl and CSW-NO$_3$ were also characterized by XRD for further understanding.

5.5.3.2 Mineral phase, morphological and thermal analysis

It can be observed from Figure 5.18, that the diffraction patterns of PGu, CSW-Cl and CSW-NO$_3$ were also somewhat similar. The similarities of the materials are underlined by the characteristic diffraction peaks of calcium sulphate observed between 2θ=10 and 30. No new peak was identified in the diffraction patterns of CSW-Cl and CSW-NO$_3$ materials indicating a pure or single phase of calcium sulphate. These diffraction patterns of CSW-Cl and CSW-NO$_3$ were found to be in a good agreement with those reported by Sun et al., (2016) who prepared the calcium sulphate whiskers from flue gas desulphurization gypsum. However, a slight shifting toward higher 2θ values was observed in CSW-NO$_3$ and CSW-Cl but this shifting was more significant in CSW-NO$_3$ than CSW-Cl. This effect might be in correlation with new IR bands located at 1733 cm^{-1} and 1366 cm^{-1} that tended to be more intense in CSW-NO$_3$ than CSW-Cl.

The diffraction patterns of CSW-NO$_3$ and CSW-Cl compared to that of the parent PGu showed a slightly broader peak which might indicate a structural deformation that might have occurred after the dissolution and recrystallization process as also discussed in Section 5.4.3.1 of the IR results. The XRD patterns also revealed relatively intense peaks in CSW-Cl than in CSW-NO$_3$ and PGu as evidenced in particular at 2θ=11.58 where the intensity tended to be two fold higher. This might be attributed to the effect of chloride or nitrate anion during the recrystallization process which may also explain the slight morphological differences between CSW-Cl and CSW-NO$_3$ (Figure 5.19). The increment in the XRD peak intensity and peak shifting as a result of changes in the morphology of the obtained whiskers was also reported by He et al., (2014). Microscopic SEM images shown in Figure 5.19, further revealed that PGu somewhat differs from CSW-NO$_3$ and CSW-Cl and, mainly consisted of agglomerates, prismatic and euhedral structure whereas CSW-NO$_3$ and CSW-Cl showed whisker like shapes. The whisker like aspects of CSW-NO$_3$ and CSW-Cl

corresponded to those reported by Miao et al., (2015) and Sun et al., (2016) but in their studies, flue gas desulfurization gypsum was used as a feedstock instead of PG in HCl solution and mixture $CaCl_2$-H_2SO_4 solution respectively.
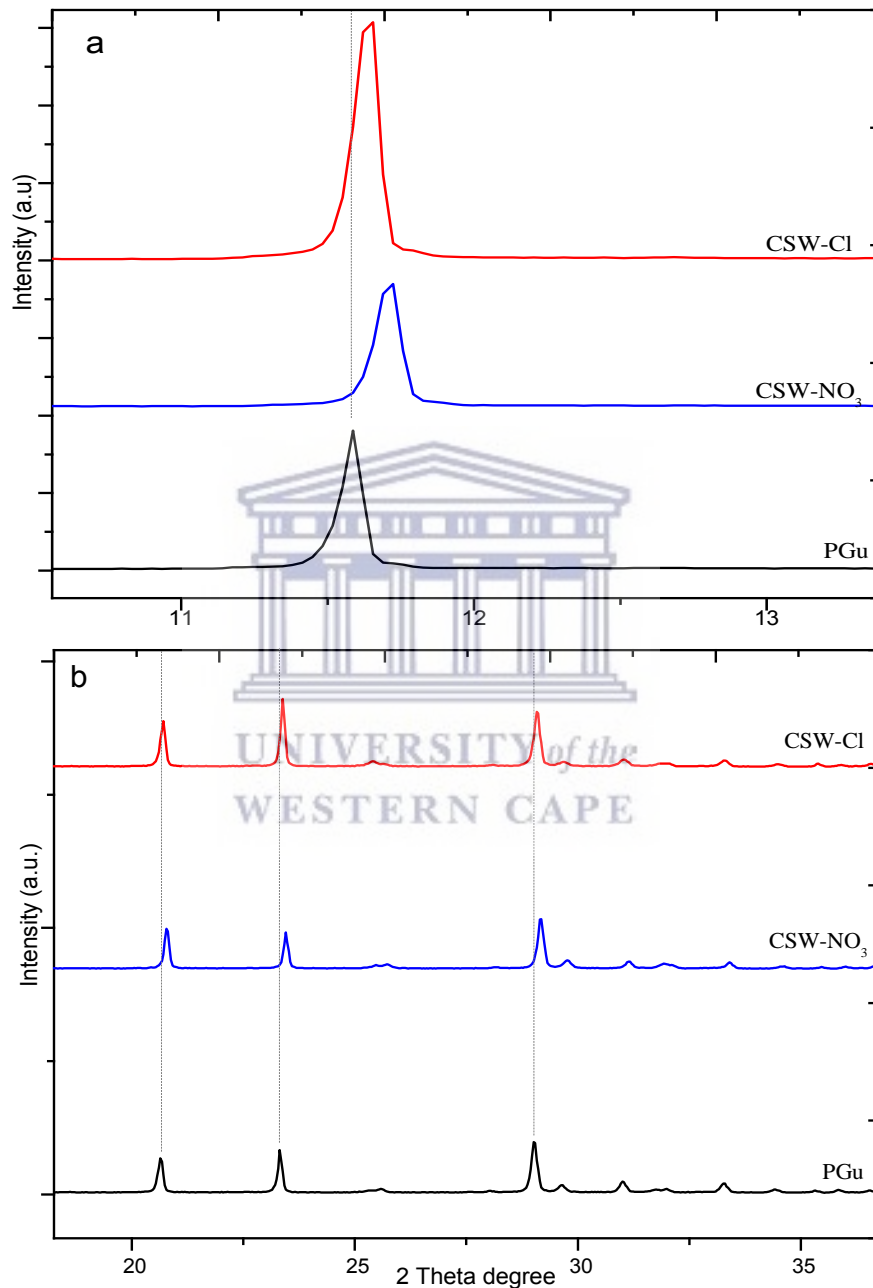
Figure 5.18: Diffraction patterns of untreated PG (PGu), CSW-NO$_3$ and CSW-Cl at low (a) and high (b) 2 Theta degree.
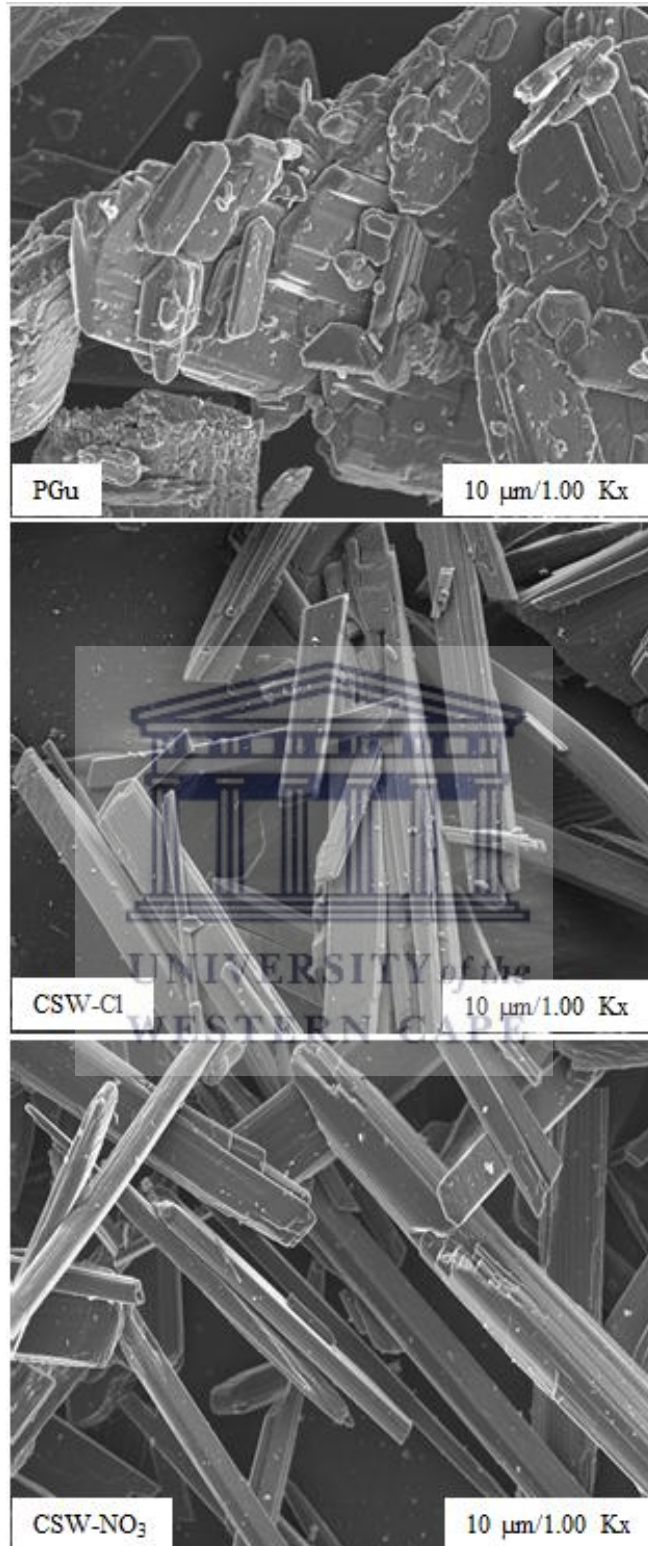
Figure 5.19: Microscopic SEM images of untreated PG (PGu), CSW-Cl and CSW-NO_3

The agglomeration of crystals in PGu might be as a result of impurities on the surface adhering on the surface of PGu crystals. This effect was also reported by Singh et al., (1999). In addition to the changes observed at microscopic level, the macroscopic images as shown in Figure 5.20 also confirmed these changes through the physical aspect of CSW-NO$_3$ or CSW-Cl which was found to be white fibres, and importantly, with whiteness far higher than the untreated PGu. High whiteness of the obtained whiskers was in a good agreement with Sun et al., (2016).
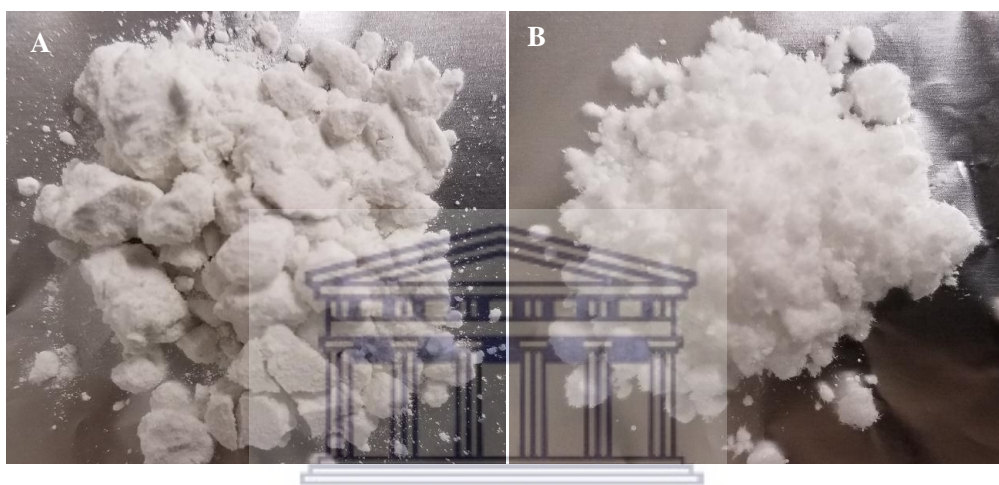
Figure 5.20: Macroscopic images of untreated PG (A) and recrystallized calcium whiskers (B) representing CSW-NO$_3$ or CSW-Cl.

The FTIR, XRD and SEM were not able to fully confirm the structure of CSW-NO$_3$ or CSW-Cl, in particular identifying whether the obtained CSW-NO$_3$ and CSW-Cl were hemihydrate or dihydrate. Therefore, TGA-DTA analysis was performed. The TGA-DTA thermograms (Figure 5.21) showed a one-step profile between 100 °C and 200 °C which is characteristic for the dehydration of calcium sulphate dehydrate (CaSO$_4$·2H$_2$O). The weight loss in PGu was about 17 % and 20 % for CSW-NO$_3$ or CSW-Cl. This weight loss in particular for CSW-NO$_3$ or CSW-Cl confirmed that the obtained materials were CaSO$_4$·2H$_2$O based whiskers and it corresponded to the theoretical weight loss of PG discussed in Section 4.1.5. of Chapter 4.
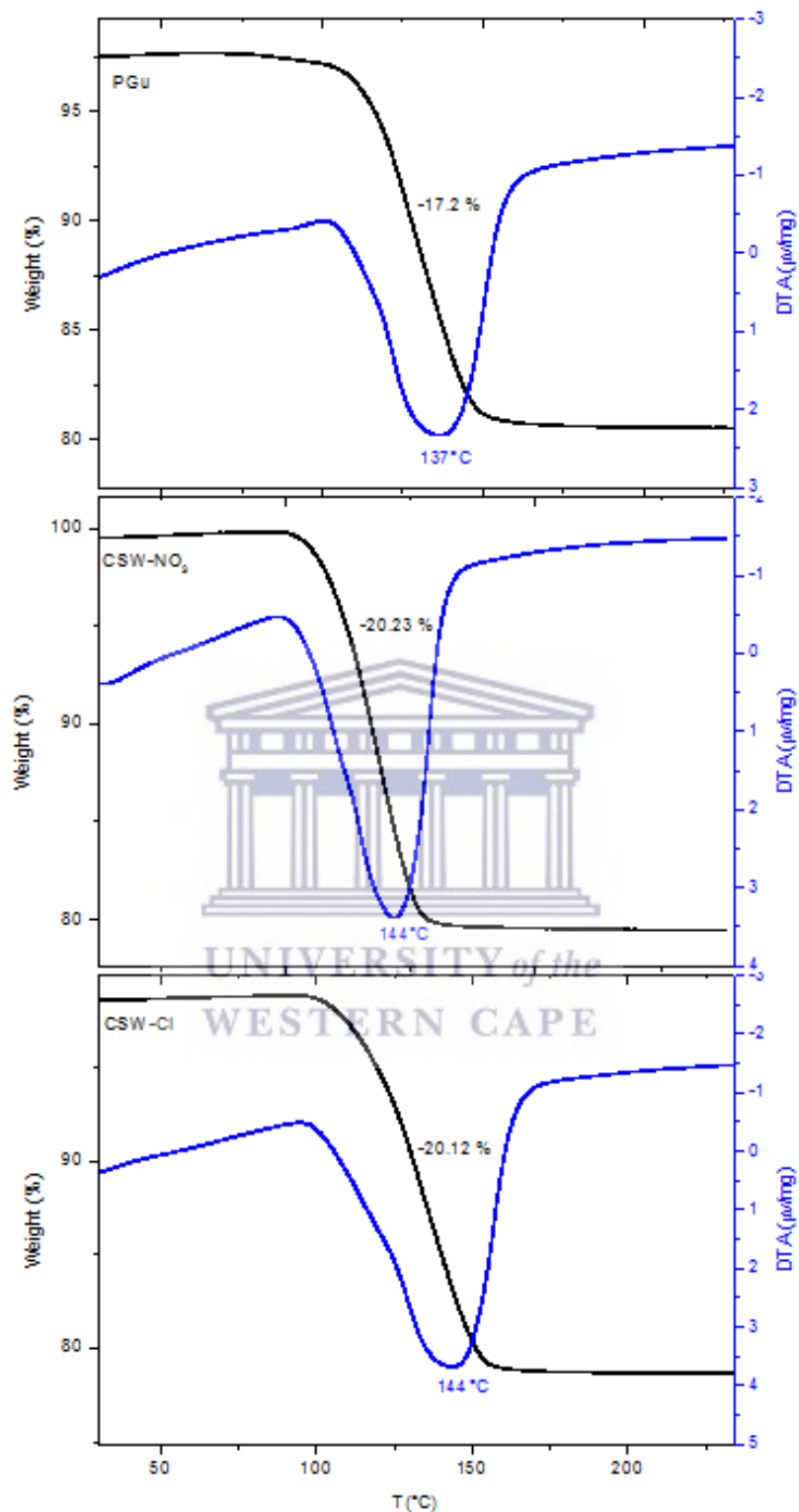
Figure 5.21: TGA-DTA profiles of untreated PG (PGu), CSW-NO$_3$ and CSW-Cl.

The similarity in the TGA-DTA profiles indicated that the obtained CSW-NO$_3$ or CSW-Cl was a single phase of CaSO$_4$·2H$_2$O confirming the FTIR and XRD results

161

discussed in Sections 5.5.1 and 5.5.2. However, the decomposition temperature of PGu was 137 °C, slightly lower than 144 °C found in CSW-NO$_3$ or CSW-Cl. This slight discrepancy could be attributed to the presence of residual phosphoric acid in PGu which might also explain the low weight loss of 17 % as well as the lower XRD peak intensities in PGu. A decrease of the decomposition temperature between 100 °C and 200 °C associated with the presence of residual acid was also reported by Hammas et al., (2013) when studying an old and fresh PG wastes.

5.6 Chapter summary

The leaching efficiencies of REEs from PG in HCl, HNO$_3$ and H$_2$SO$_4$ solutions were more favourable in HCl and HNO$_3$ than H$_2$SO$_4$ in which the effect of the common ion was a limiting factor. It was found that moderately high concentrations of 2 M HCl, 2 M HNO$_3$ and 1.5 M H$_2$SO$_4$; contact time of 60 min for HCl and HNO$_3$ and 120 min for H$_2$SO$_4$; temperature of 50 °C for HCl and H$_2$SO$_4$ and 60 °C for HNO$_3$; S\L ratio 0.1 and stirring at 600 rpm were favourable conditions for the leaching of REEs, Sc, Y, Th and U from PG waste. Direct leaching of PG further showed that 65−78 %, 75−84 % and 45−54 % leaching efficiencies for REEs, Sc, Y, Th and U could be reached in 2.0 M HCl, 2 M HNO$_3$ and 1.5 M H$_2$SO$_4$ solutions respectively. However, the dissolution and recrystallization method (indirect leaching) using 2 M HCl and 2 M HNO$_3$ allowed the up-concentration of the REEs, Sc, Y, Th and U in the filtrate from which the efficiencies were found ranging between 90−97 %. Moreover, the FTIR, XRD, SEM and TGA analysis confirmed that the recrystallized calcium sulphate, referred to as calcium sulfate whiskers (CSWs), were gypsum dihydrates (CaSO$_4$·2H$_2$O). Macroscopic images of CSWs-CaSO$_4$·2H$_2$O further revealed a white fibre like aspect with whiteness higher than the raw PG.

The following chapter (Chapter 6) presents the experimental results obtained from the adsorption studies of Ce^{3+}, Nd^{3+} and Ca^{2+} as representative elements of the as-received PG using modified nanofiber materials.

162

CHAPTER 6

6. ADSORPTION STUDIES OF CE^{3+}, ND^{3+} AND CA^{2+} USING DH-PS20 AND DG-PS2 MODIFIED NANOFIBERS

6.1 Introduction

Chapter 6 presents the results obtained from batch adsorption studies of REEs (Ce^{3+}, Nd^{3+}) and Ca^{2+} using DH-PS20 and DG-PS2 nanofiber mats prepared according to the method detailed in Section 3.9.1. These nanofibers were presented and discussed in Section 4.3.2. The experiments on the adsorption studies were carried out as set in Section 3.10.3. These experiments aimed to investigate the adsorption performance of DH-PS20 and DG-PS2 modified nanofibers for REEs (Ce^{3+}, Nd^{3+}) and Ca^{2+} uptake and their reusability. In these experiments, the effect of the initial concentration of the metal ions, the initial pH solution and contact time were investigated. In each case, ICP-MS was used to analyse the concentrations of the resultant solutions after filtration using 0.45 µm syringe filter. The present chapter intends to cover the objective 5 and 6 as set in Chapter 1.

6.2 Adsorption studies of Ce^{3+}, Nd^{3+} and Ca^{2+} on DH-PS20 and DG-PS2 modified nanofibers

This section presents and discusses the results obtained from the adsorption experiments using DH-PS20 and DG-PS2 nanofiber mats. The main parameters that were investigated in this sections were the initial pH, initial concentration of metal ions and contact time. The adsorbent dosage was not investigated in this section. The adsorption experiments were carried out using synthetic solutions of Ce^{3+}, Nd^{3+} and Ca^{2+} to mimic the solution of phosphogypsum (PG) leachate and details of the experiments were described in Section 3.10.3. The concentrations of Ce^{3+}, Nd^{3+} and Ca^{2+} used throughout the adsorption experiments were the diluted solutions prepared from the 1000 ppm stock solutions as described in Section 3.10.1. The following

163

section discusses the effect of the initial pH of the solutions with fixed initial concentration and contact time. The adsorption experiments were performed in triplicate ran in parallel for each individual metal ion and it was therefore not a competitive adsorption test.

6.2.1 Effect of solution pH

Investigating the effect of solution pH is important in adsorption studies since the metal ions to be adsorbed are known to compete with the protons from the acid medium. Therefore, in this section, the pH of metal ion solutions of Ce^{3+}, Nd^{3+} and Ca^{2+} were investigated in batch mode in attempts to determine the best condition for adsorption capacity. Prior to adsorption experiments, the pH values of the solutions were manually adjusted to the desired values (pH 1.0; 2.0; 3.0; 4.0; 5.0; and 6.0) using 0.1 M HNO_3 or NaOH solution. These experiments were carried out in 10 mL of 80 mg/L of Ce^{3+}, Nd^{3+} and Ca^{2+} solutions containing 0.0106 g of the adsorbent (neat PS14-nfs or DH-PS20-nfs or DG-PS2-nfs) which was shaken at stirring speed of 200 rpm for 2 h at 25 ºC. The obtained solutions were filtered with 0.45 μm and analysed using ICP-OES/MS as described in Section 3.11.6, while the adsorption capacities (q_e) were evaluated using equation 3.2 given in Section 3.10.3. The results obtained from these experiments showing the adsorption capacities vs. the initial pH of solutions for the neat PS14-nfs, DH-PS20-nfs and DG-PS2-nfs are displayed in Figures 6.1.
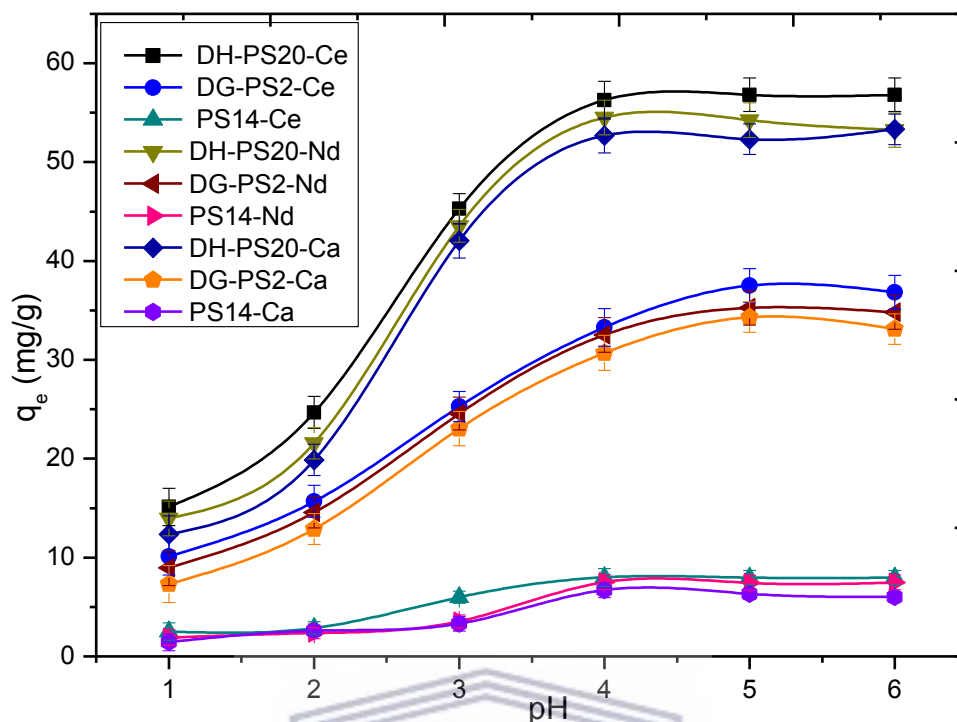
Figure 6.1: Adsorption capacities of unmodified PS (PS14-Ce; PS14-Nd; PS14-Ca) and modified PS with 20 wt% D2EHPA (DH-PS20-Ce; DH-PS20-Nd; DH-PS20-Ca) and with 2.25 g DGA (DG-PS2-Ce; DG-PS2-Nd; DG-PS2-Ca) in different pH solutions (1.0; 2.0; 3.0; 4.0; 5.0; 6.0) of 80 mg/L of Ce^{3+}, Nd^{3+} and Ca^{2+} (2 h, 25 ºC, 200 rpm, adsorbent weight 0.0106 g, volume=10 mL)

Figure 6.1 shows that Ce^{3+}, Nd^{3+} and Ca^{2+} uptakes were relatively low at pH value less than 3. This was attributed to the interference of the hydronium ions (H^+) being in high concentration at low pH values reducing the availability of the active sites for Ce^{3+}, Nd^{3+} and Ca^{2+} on the surface of the nanofiber mats. The presence of high concentration of H^+ ions might have created an electrostatic repulsion effects between the surface of the nanofiber and the metal ions reducing the uptake at lower pH values. The adsorption capacities of DH-PS20 nanofibers increased as the pH values increased from 1.0 to 4.0 and showed steady increase after the pH 4.0 with minor increments. The highest adsorption capacities were reached at pH 4 with the maximum adsorbed amounts of approximately 56; 54 and 53 mg/g for DH-PS20-Ce, DH-PS20-Nd and DH-PS20-Ca respectively. In contrast to DH-PS20 nanofibers, the adsorption capacities of DG-PS2 nanofibers somewhat increased as the pH values increased from 1.0 to 4.0 until reaching an equilibrium around pH 5.0 corresponding optimum adsorption capacities of 38; 35 and 34 mg/g for DG-PS2-Ce, DG-PS2-Nd and DG-

165

PS2-Ca respectively. The discrepancy in the adsorption capacities of DH-PS20 and DG-PS2 nanofibers was obvious and might be due to the difference of the functional groups from their respective ligands. Although the adsorption capacities of DG-PS2 nanofibers were relatively smaller compared to those obtained in DH-PS20 nanofibers, these were far higher compared to those obtained from the unmodified PS nanofibers (PS14-Ce; PS14-Nd; PS14-Ca) on which approximately 7.9; 7.5 and 6.7 mg/g were the highest adsorption capacities achieved between pH 4.0–5.0 for PS14-Ce, PS14-Nd and PS14-Ca nanofibers respectively. The difference in the adsorption capacities between PS14 and DH-PS20 or DG-PS2 nanofibers as aforementioned above is clearly as a result of the presence of the D2EHPA and DGA ligands in the PS nanofiber support. This confirmed that the blending of D2EHPA ligand with PS14 polymer or the surface modification of PS14-nfs with DGA ligand was able to create active sites onto the obtained DH-PS20 and DG-PS2 nanofibers due to the presence of functional groups from D2EHPA and DGA ligands. The slightly higher uptake of Ce^{3+} observed at all the pH values for DH-PS20 and DG-PS2 nanofibers compared to Nd^{3+} and Ca^{2+} might be attributed to its higher ionic radius which could be part of the driving force during the adsorption process of these metals onto the nanofibers.

For the rest of the experiments, the pH values 4.0 and 5.0 were respectively selected as the equilibrium pH values of DH-PS20 and DG-PS2 nanofibers in an attempt to investigate the rest of parameters such as the initial concentration and contact time. Therefore, the following section discusses the effect of initial concentration of Ce^{3+}, Nd^{3+} and Ca^{2+} on DH-PS20 and DG-PS2 nanofibers. It is important to note that these parameters were not investigated for unmodified PS14-nfs in the following sections due to lowest adsorption capacities achieved on these materials at different pH values as discussed above.

6.2.2 Effect of initial concentration

The effect of the initial concentration in adsorption studies is important as it allows to determine the maximum capacity of an adsorbent (optimum concentration of the metal ion). Therefore, in this section, the initial concentration was investigated as described

166

in Section in 3.10.3. To recall, the experiments were carried out by immersing 0.0106 g of DH-PS20 or DG-PS2 nanofiber in 10 mL of 40; 80; 120; 160; 180 and 200 mg/L solutions of Ce^{3+}, Nd^{3+} and Ca^{2+} at pH 4.0 and 5.0 for DH-PS20 and DG-PS2 mats respectively. Each resulting mixture was shaken for 1 h at a stirring speed of 200 rpm and 25 °C. The solutions obtained from the adsorption experiments were first filtered with 0.45 µm syringe filter and thereafter analysed through ICP-MS for metal content. The results from these analyses were used to determine both the optimum concentration and the adsorption isotherms for Ce^{3+}, Nd^{3+} and Ca^{2+} on DH-PS20 and DG-PS2 nanofibers. Figure 6.2 shows the results from these analyses which were plotted as the adsorption capacity (q_e) of DH-PS20 and DG-PS2 nanofiber mats vs. the initial concentrations of metal ions.
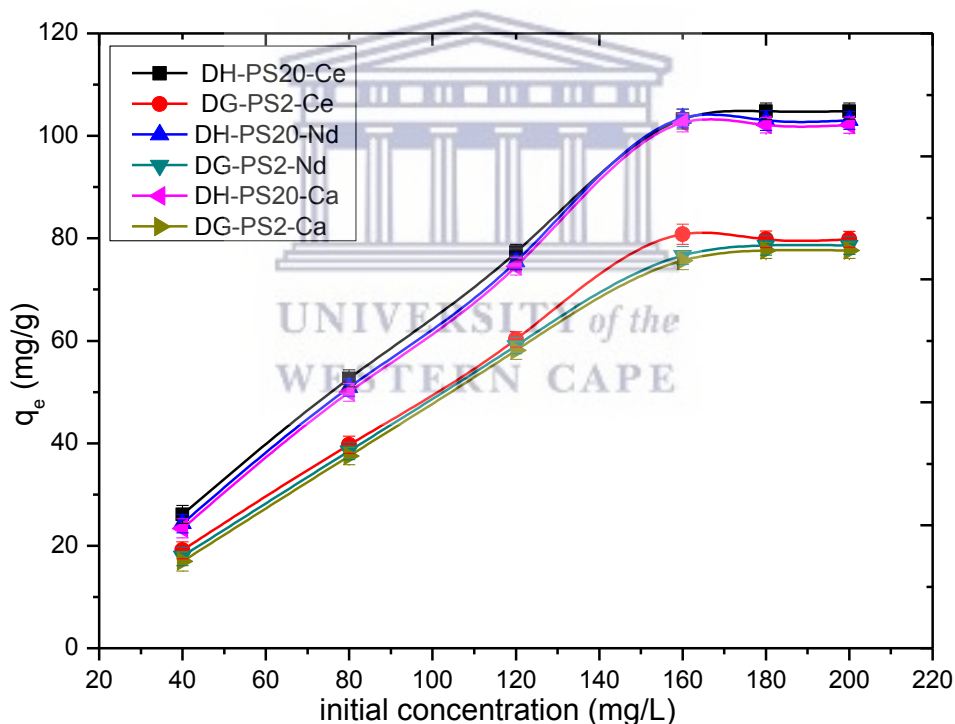
Figure 6.2: Capacity uptake of DH-PS20 and DG-PS2 nanofibers at pH 4.0 and 5.0 respectively (2 h, 25 °C, 200 rpm, adsorbent weight 0.0106 g, volume=10 mL) in different initial concentrations of Ce^{3+}, Nd^{3+} and Ca^{2+} (40; 80; 120; 160; 180; 200 mg/L).

As can be seen from Figure 6.2, the results showed a rapid surge in adsorption capacities of DH-PS20 and DG-PS2 nanofiber mats from 40 mg/L to 160 mg/L as the

167

initial concentrations increased and thereafter remained relatively constant up to the concentration of 200 mg/L. This suggests that below the concentration of 160 mg/L DH-PS20 and DG-PS2 nanofiber materials had more available active sites to accommodate Ce^{3+}, Nd^{3+} and Ca^{2+} and these sites decreased as the concentration was reaching 160 mg/L and upwards. The equilibrium capacities of DH-PS20 and DG-PS2 nanofibers were reached at approximately 160 mg/L. At this concentration the optimum capacities on DH-PS20 mats were 105.3; 103.5 and 102.7 mg/g respectively for DH-PS20-Ce, DH-PS20-Nd and DH-PS20-Ca. However, at the same equilibrium concentration, the adsorption capacities of Ce^{3+}, Nd^{3+} and Ca^{2+} on DG-PS2 mats were somewhat lower with the amounts of 80.8; 78.6 and 77.4 mg/g respectively reached for DG-PS2-Ce, DG-PS2-Nd and DG-PS2-Ca. The difference in the adsorption capacities of DH-PS20 and DG-PS2 nanofiber materials might be attributed to the functional groups that are present in each modified nanofiber as also discussed in Section 6.2.1. The relatively constant trend observed after the equilibrium concentration of 160 mg/L indicated that both DH-PS20 and DG-PS2 nanofibers reached their saturations after this concentration and there were no available active sites to uptake the Ce^{3+}, Nd^{3+} and Ca^{2+}. Therefore, the initial concentration of 160 mg/L was selected as the best concentration to investigate the effect of the contact time during the adsorption experiments of which the results will be presented and discussed in Section 6.3 after the adsorption isotherms shortly discusses in the following section based on the experimental data of the equilibrium pH and concentration.

6.2.3 Isotherms of the adsorption studies

The isotherms of the adsorption process were determined using Langmuir and Freundlich models. This was performed in an attempt to draw the relationship between the concentration of the adsorbate in the solution and the adsorbed amounts onto the nanofiber materials at an equilibrium pH. These two models have been selected since they are the most commonly used in adsorption studies for solid-liquid phase. The theoretical assumptions behind these two types of isotherms were described in Section 3.10.4 and in this section the linearized form of their respective expressions were used in order to compare the experimental results and modelling data.

Figures 6.3 and 6.4 show the results obtained from the experimental equilibrium data and theoretical equilibrium data using Langmuir and Freundlich isotherms for Ce^{3+}, Nd^{3+} and Ca^2 onto DH-PS20 and DG-PS2 nanofiber mats respectively. These two isotherms were used in an attempt to determine the best fit model for the adsorption studies of these selected metals. The linearized form of Langmuir and Freundlich equations were used to analyse or fit the experimental data. These equations were previously described in Section 3.10.4. The results are presented as the equilibrium adsorption capacities q_e (mg/g) vs. the initial concentration (mg/L).

From Figure 6.3 and 6.4, it was found that the experimental data of Ce^{3+}, Nd^{3+} and Ca^{2+} onto DH-PS20 and DG-PS2 nanofiber mats were somewhat well fitted with the Langmuir model compared to the Freundlich model. This was evidenced by the values of the correlation coefficient R^2 which were relatively closer to 1.000 in Langmuir isotherms fitting (0.9678–0.9989) than those of the Freundlich isotherms (0.4917–0.8203) for both DH-PS20 and DG-PS2 nanofiber mats (see Appendix A–F). This therefore suggested that the adsorption process of the aforementioned metals was due to monolayer formation occurred on the homogenous surfaces of DH-PS20 and DG-PS2 nanofibers and no further adsorption could take place after the active sites were occupied (Chen et al., 2009). Moreover, the calculated values of Langmuir R_L according to equation 3.5 illustrated in Section 3.10.4 which are presented in Table 6.1 and 6.2 for DH-PS20 and DG-PS2 nanofibers respectively, indicated that these values were lower than 1.0 and ranged between 0.6239–0.8479 and 0.5163–0.8442 for metal ions adsorption onto DH-PS20 and DG-PS2 mats respectively. This suggests that the adsorption of Ce^{3+}, Nd^{3+} and Ca^{2+} onto DH-PS20 or DG-PS2 mats was favourable and took place.
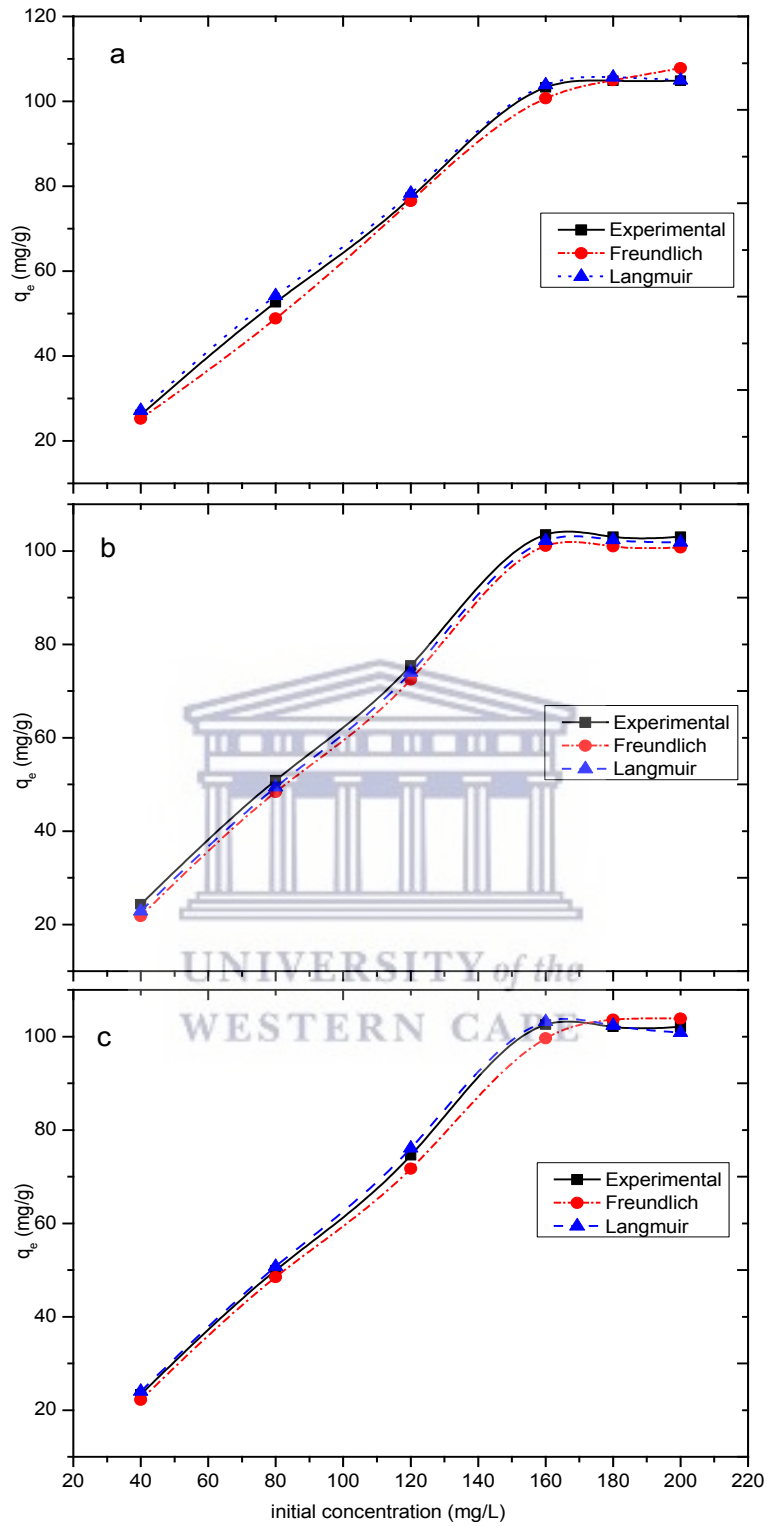
Figure 6.3: Equilibrium isotherms of Ce^{3+}(a), Nd^{3+} (b) and Ca^{2+} (c) adsorption on DH-PS20 nanofibers
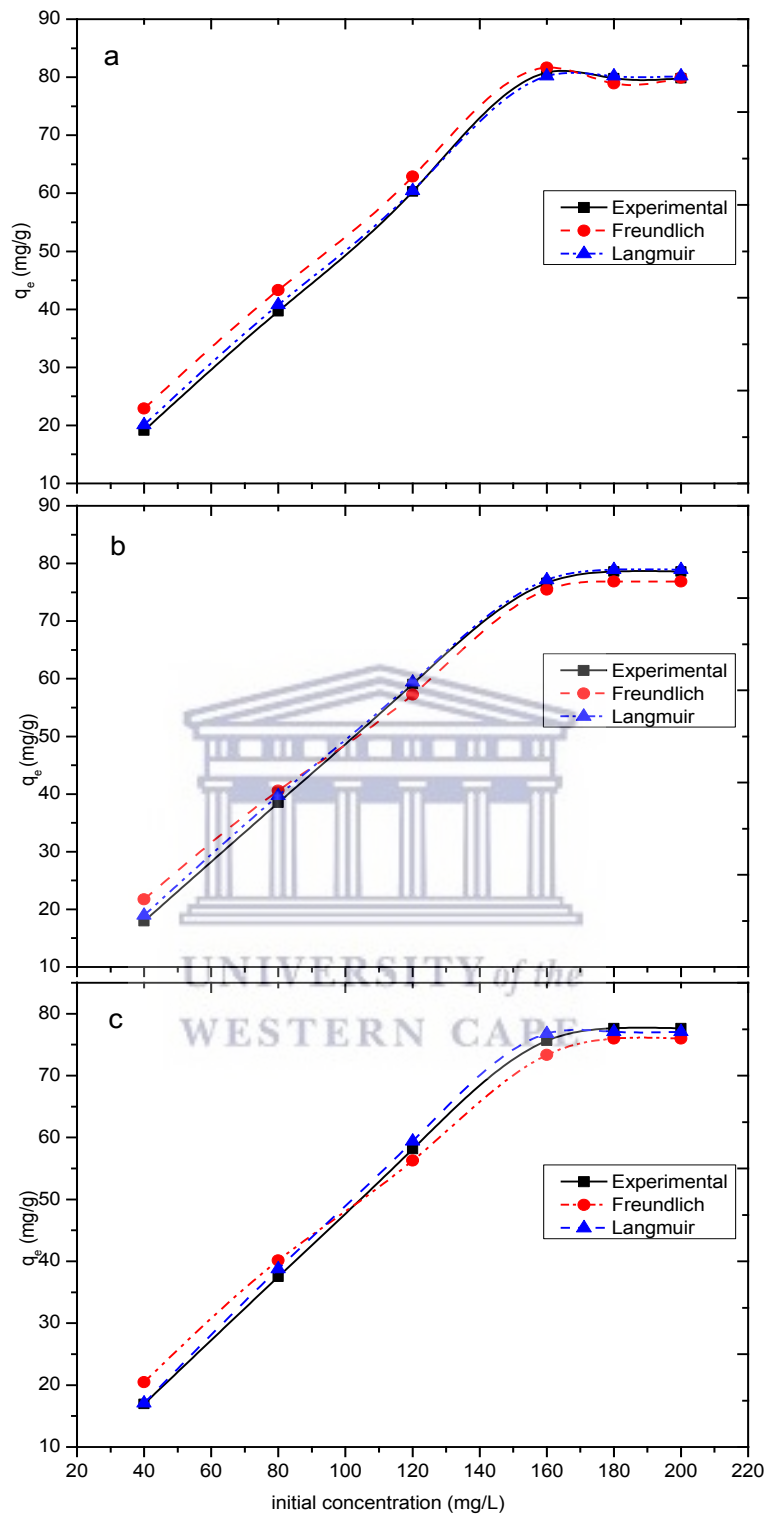
Figure 6.4: Equilibrium isotherms of Ce^{3+}(a), Nd^{3+} (b) and Ca^{2+} (c) adsorption on DG-PS2 nanofibers

171

Table 6.1: R_L values based on Langmuir linearized equation for DH-PS20 nanofibers

initial concentration (mg/L)	Langmuir R_L values		
	Ce^{3+}	Nd^{3+}	Ca^{2+}
40	0.7342	0.7195	0.8479
80	0.7208	0.7075	0.8231
120	0.7073	0.6956	0.7983
160	0.6805	0.6717	0.7487
180	0.6536	0.6478	0.6991
200	0.6268	0.6239	0.6495

Table 6.2: R_L values based on Langmuir linearized equation for DG-PS2 nanofibers

initial concentration (mg/L)	Langmuir R_L values		
	Ce^{3+}	Nd^{3+}	Ca^{2+}
40	0.6051	0.8442	0.7079
80	0.5940	0.8092	0.6865
120	0.5829	0.7742	0.6652
160	0.5607	0.7042	0.6224
180	0.5385	0.6341	0.5796
200	0.5163	0.5643	0.5368

6.3 Effect of contact time

Investigating the effect of the contact time in adsorption studies is important as this allows to determine how fast the metal ions can bind onto the surface (functional groups) of the adsorbent. These experiments were conducted at equilibrium pH 4.0 and 5.0 respectively for DH-PS20 and DG-PS2 nanofibers and initial concentration of 160 mg/L identified in section 6.2.2. at different contact time of 10; 30; 50; 70; 90 and 120 min. The experiments were performed by shaking 0.0106 g of DH-PS20 or DG-PS2 nanofibers in 10 mL containing 160 mg/L of Ce^{3+}, Nd^{3+} and Ca^{2+} at stirring speed of 200 rpm and 25 ºC. The resultants solutions were first filtered with 0.45 μm syringe filter and thereafter analysed using ICP-MS. The results from these analyses were calculated as illustrated in Section 3.10.3 and are presented in Figure 6.5 as the adsorption capacity (q_e) vs the contact time (min). These results were also compared

172

to those obtained from the kinetic studies using adsorption models (pseudo first-order and second-order) based on the mathematical formulas illustrated in equations 3.8 and 3.9.
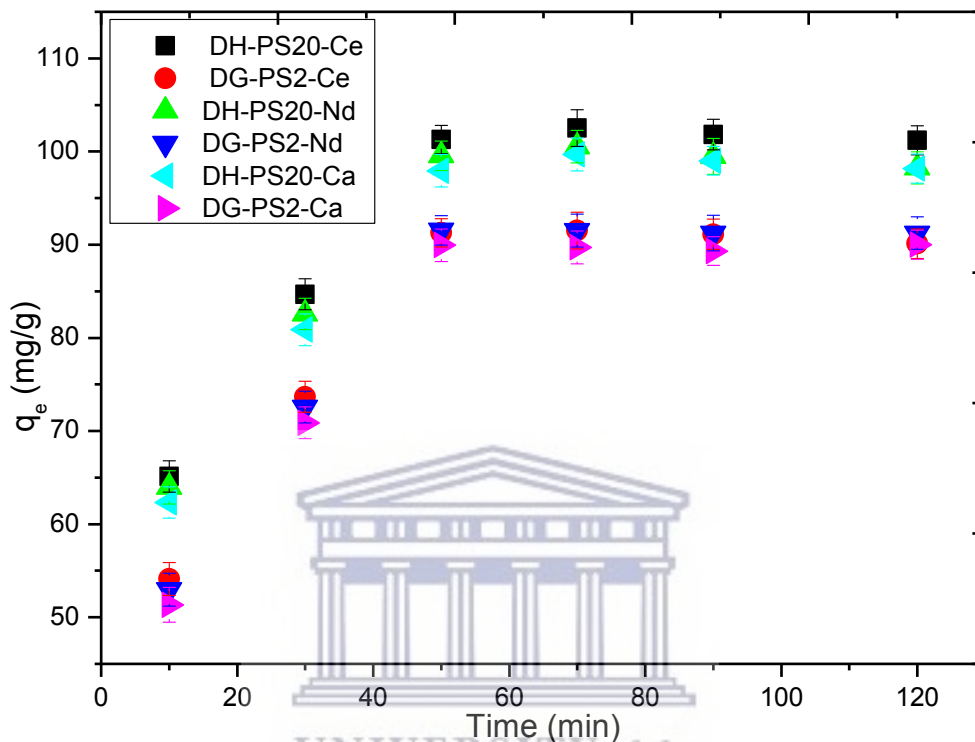
Figure 6.5: Capacity uptake of Ce^{3+}, Nd^{3+} and Ca^{2+} at different contact time (10; 30; 50; 70; 90; 120 min) and pH 4.0 and 5.0 for DH-PS20 and DG-PS2 nanofibers respectively (160 mg/L, 25 °C, 250 rpm, adsorbent weight 0.0106 g, volume=10 mL)

As can be observed from Figure 6.5 the equilibrium uptake was attained at contact time of about 50 min for DH-PS20 and DG-PS2 nanofibers. The adsorption degree first exhibited a rapid surge from 10 to 50 min and thereafter slightly remained steady as the contact time increased. The relatively constant trend observed from 50 min indicated that DH-PS20 and DG-PS2 nanofibers were saturated with Ce^{3+}, Nd^{3+} and Ca^{2+} and increasing the contact time could not add more metal ions onto the active sites of these adsorbents. The slightly decrease observed after the contact time of 70 min might be as a result of desorption of initially adsorbed metal ions onto the adsorbents with extended contact times. Besides that, both DH-PS20 and DG-PS2 nanofibers showed a similar trend in terms of the rate of adsorption of Ce^{3+}, Nd^{3+} and Ca^{2+}, the former exhibited highest adsorption performance for these metal ions as also

173

discussed in Sections 6.2.1 and 6.2.2. For further experiments, the contact time of 60 min was selected as the equilibrium time for effective adsorption capacities of Ce^{3+}, Nd^{3+} and Ca^{2+} in this study. This equilibrium contact time and the corresponding q_e values for adsorption Ce^{3+}, Nd^{3+} and Ca^{2+} onto the DH-PS20 and DG-PS2 nanofibers were used for calculations of kinetics models which will be briefly discussed in Section 6.3.1.

6.3.1 Adsorption kinetics models

The kinetics models of the adsorption process are important as they allow to determine the rate of sorption of an adsorbate onto the adsorbent. In this study, two most commonly known models namely pseudo first-order and pseudo-second order have been used to examine the experimental data obtained from the batch adsorption studies of Ce^{3+}, Nd^{3+} and Ca^{2+} onto DH-PS20 and DG-PS2 nanofibers according to equations 3.8 and 3.9. Figures 6.6 and 6.7 display the results obtained from pseudo first-order and second order plots of the adsorption of Ce^{3+}, Nd^{3+} and Ca^{2+} onto DH-PS20 and DG-PS2 nanofibers respectively. The pseudo first-order plot is presented as *ln (q_e-q_t)* against the time while the pseudo second-order is *t/q_t* vs. the time and details of these equations are illustrated in Section 3.10.5.

174
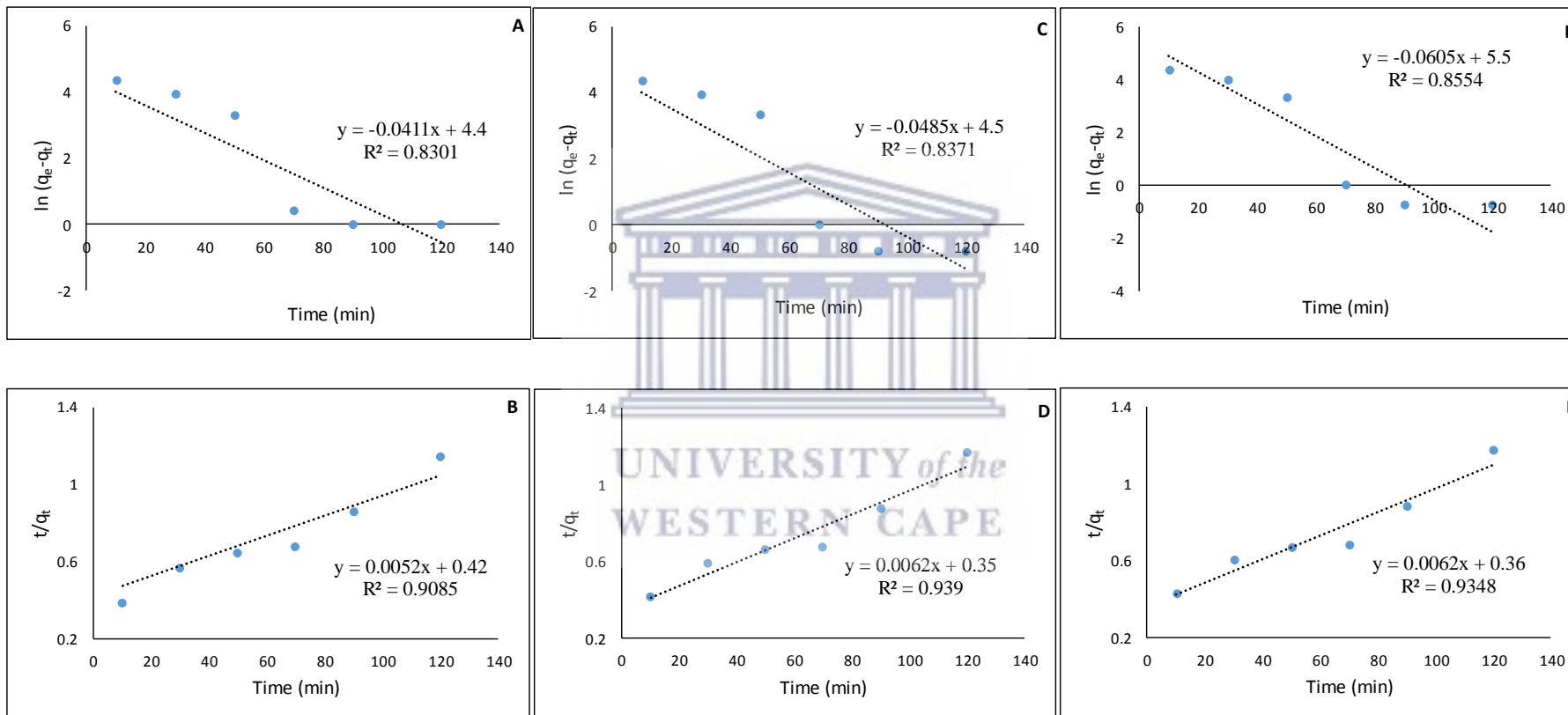
Figure 6.6: Pseudo first-order and pseudo second-order rate equation plots respectively of Ce^{3+} (A and B); Nd^{3+} (C and D) and Ca^{2+} (E and F) adsorption onto DH-PS20 nanofibers.
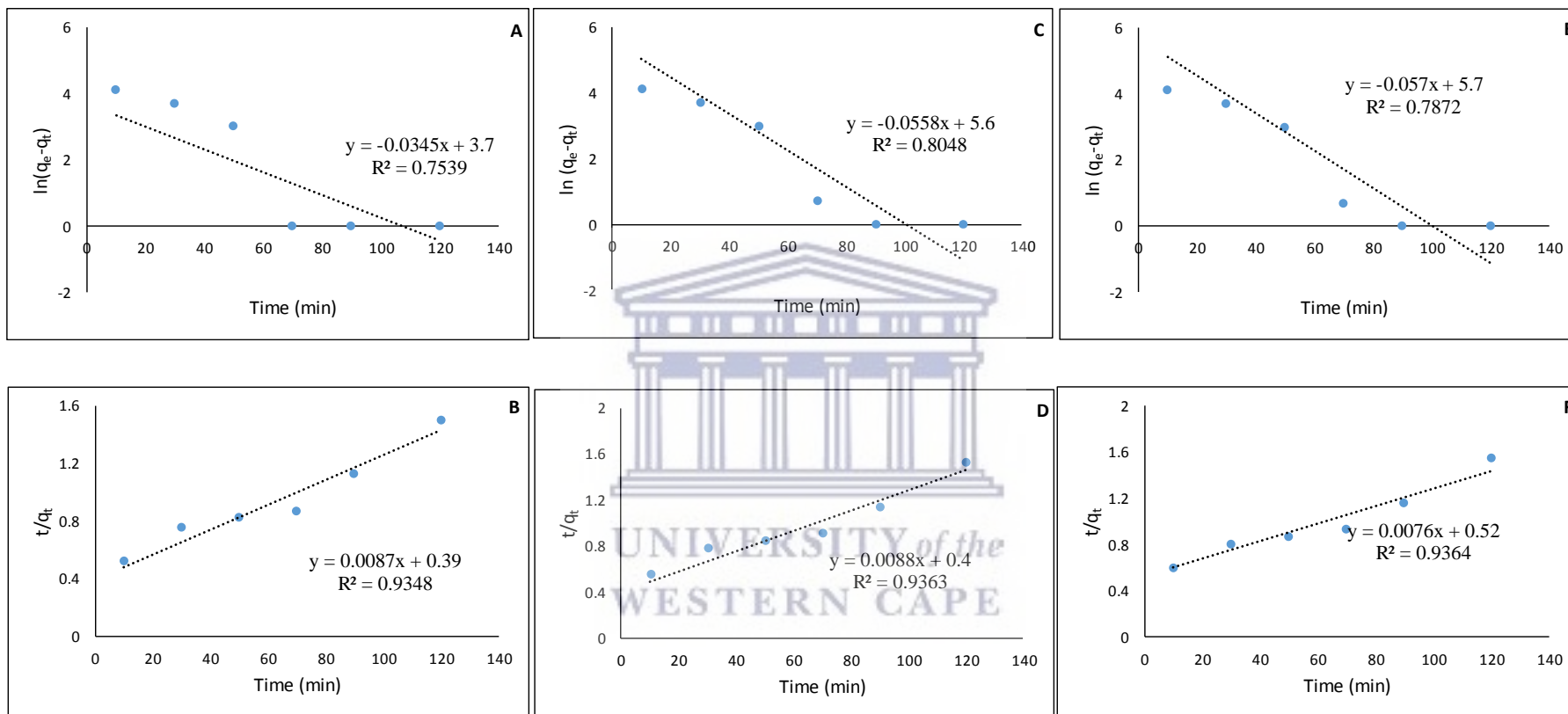
Figure 6.7: Pseudo first-order and pseudo second-order rate equation plots respectively of Ce^{3+} (A and B); Nd^{3+} (C and D) and Ca^{2+} (E and F) adsorption onto DG-PS2 nanofibers.

It can be seen from Figure 6.6 and 6.7 (B, D and F) that for both DH-PS20 and DG-PS2 nanofibers the R^2 values obtained from pseudo second-order kinetics model were relatively closer to 1.000 for Ce^{3+} (0.9085–0.9348), Nd^{3+} (0.9363–0.9390) and Ca^{2+} (0.9348–0.9364) when compared to those obtained from the pseudo first-order models (Figure 6.6 and 6.7: A, C and E) for Ce^{3+} (0.7539–0.8301); Nd^{3+} (0.8048–0.8371) and Ca^{2+} (0.7872–0.8554). This suggests that the pseudo second-order kinetic model is more appropriate to describe the adsorption kinetic data obtained in this study for the aforementioned metal ions onto DH-PS20 and DG-PS2 nanofibers.

6.4 Desorption and reusability studies

The desorption and reusability studies of DH-PS20 and DG-PS2 nanofiber mats after the adsorption process was crucial as it helps to determine the stability of D2EHPA and DGA ligands attachments onto the surface of the PS support. These experiments were also important in order to determine the degree of reusability of the modified nanofiber materials for further sorption studies. The desorption experiments were carried out by shaking DH-PS20 and DG-PS2 nanofiber mats previously used for adsorption of Ce^{3+}, Nd^{3+} and Ca^{2+} in 10 mL of 1.0 M HNO_3 for 1 h at stirring speed of 200 rpm and 25 ºC (Section 3.10.6). In these experiments only HNO_3 was used as regenerant as discussed in Section 4.3.3. The results from these experiments are displayed in Figure 6.8 and 6.9 in terms of adsorption and desorption capacities of Ce^{3+} or Nd^{3+} or Ca^{2+} onto DH-PS20 and DG-PS2 nanofibers respectively.
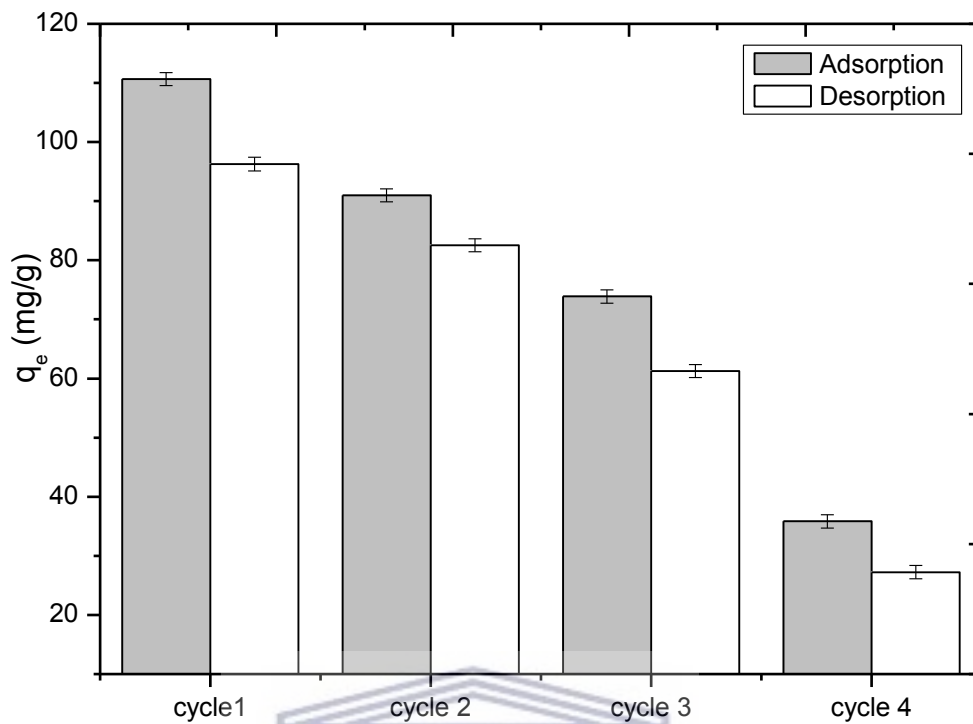
Figure 6.8: Desorption and reusability of DH-PS20 nanofibers
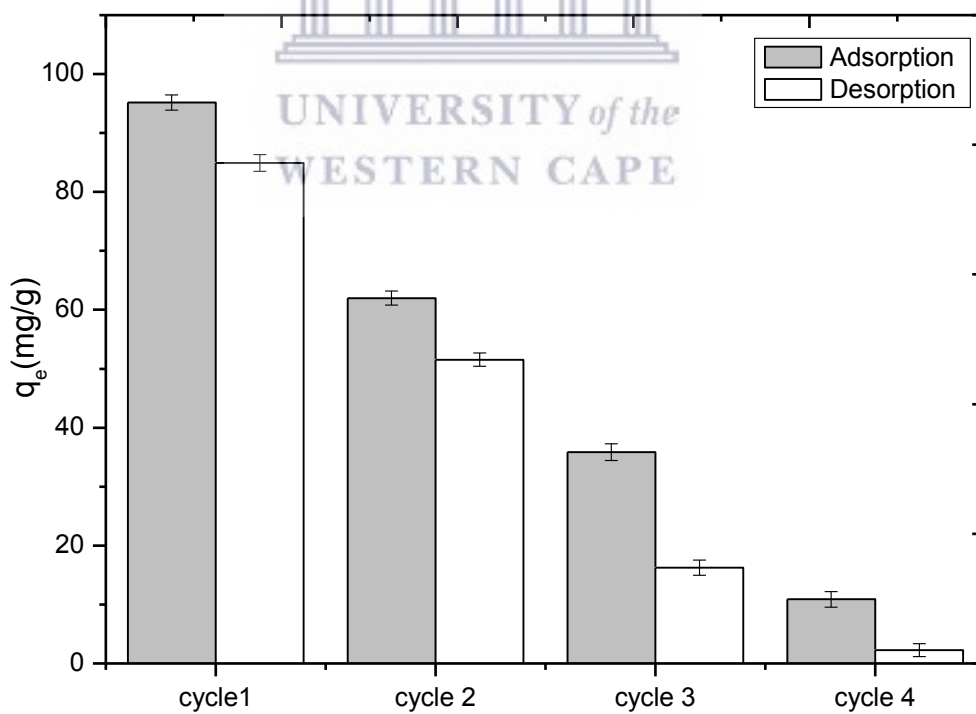
Figure 6.9: Desorption and reusability of DG-PS2 nanofibers

As can be observed from Figure 6.8 and 6.9, the results revealed that both DH-PS20 and DG-PS2 nanofiber mats can be regenerated using 1.0 M HNO_3 after sorption process and be reused for subsequent adsorption process for at least four cycles. However, their adsorption capacities decreased with increased number of the cycles from cycle 2 up to cycle 4. This decrease might be attributed to gradual loss of the ligands on the PS support or to the irreversibility of adsorbed metal ions onto the nanofiber mats. This was evidenced through the ATR-FTIR analysis of DH-PS20 and DG-PS2 nanofibers obtained before the adsorption and after recycling processes as shown in Figure 6.10 and 6.11. From these results, it was clearly confirmed that the loss in capacities of DH-PS20 and DG-PS2 nanofibers was due to the loss of ligands onto the surface of the PS support. From Figure 6.10 it can be noticed that the characteristic peaks of D2EHPA ligand located at 1230 and 1032 cm^{-1} previously assigned to P=O stretching and P-OH stretching respectively shifted toward lower wavenumbers and widen from their initial narrow aspect. The widening and change observed at 1032 cm^{-1} might be as a result of metal ion adsorption and desorption. The widening of this peak due to metal ion adsorption was also reported by Satpathy and Mishra, (2017). However, the change and shifting of the vibration band at 1230 cm^{-1} could be due to the participation of P=O oxygen in complex formation which involved a coordinate bond. This finding was in good agreement with the findings of Jin et al., (2014) and Wilson et al., (2014). It furthermore found that the intensities of these peaks decreased as the number cycles increased. Alike to DH-PS20 nanofibers, DG-PS2 fibres did not exhibit shifting of the characteristic peaks of the DGA ligand but a decrease in these peaks as the number of cycles increased was observed and was very significant at the fourth cycle in which the ligand was merely washed out on the PS support. This could explain the lowest adsorption capacities observed at fourth cycle during the adsorption and desorption process.
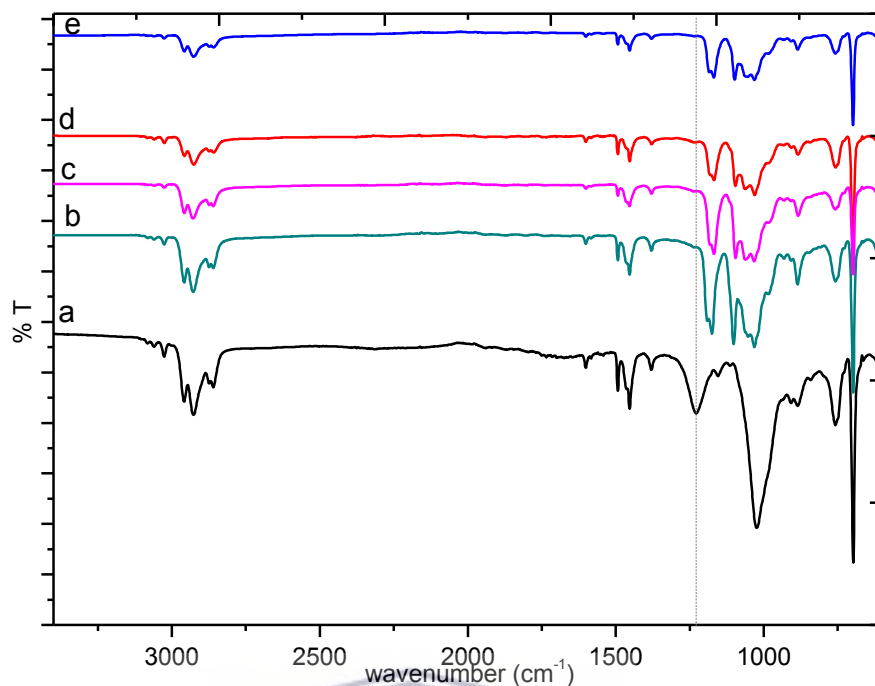
Figure 6.10: Spectra of DH-PS20 nanofibers as made (a) and after 1st (b), 2nd (c), 3rd (d) and 4th (e) cycle using 1.0 M HNO₃.
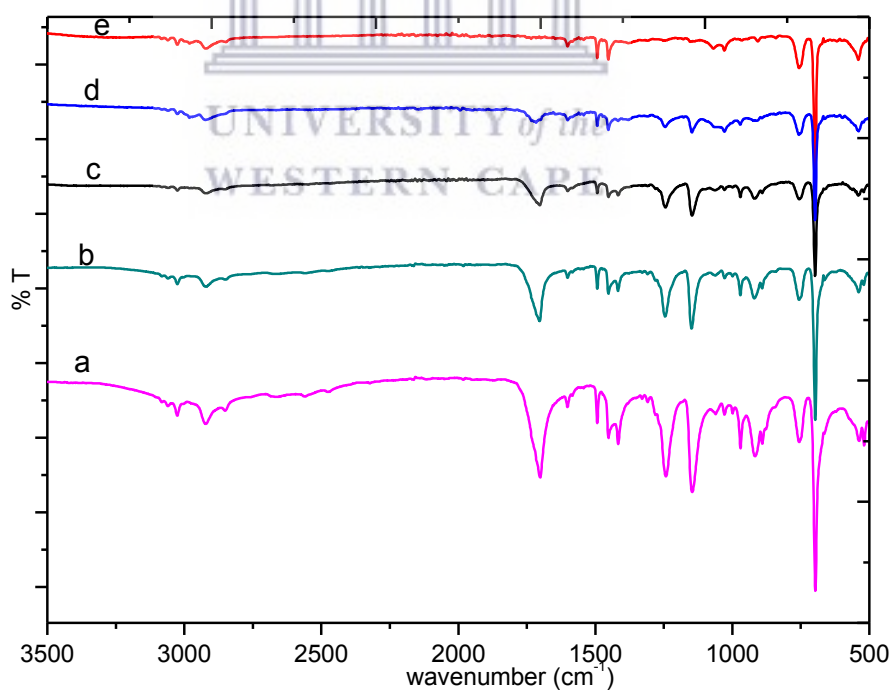
Figure 6.11: Spectra of DG-PS2 nanofibers as made (a) and after 1st (b), 2nd (c), 3rd (d) and 4th (e) cycle using 1.0 M HNO₃.

6.5 Separation of REEs (Ce^{3+}, Nd^{3+}) and Ca^{2+}

The separation of REEs (Ce^{3+}, Nd^{3+}) from Ca^{2+} is utmost important since Ca^{2+} is the major and main interfering cation contained in PG leachate solution. Therefore, this investigation was carried out in an attempt to determine the separation of REEs with Ca^{2+} in a mixture of real solutions after the total digestion (RSAD) and after recrystallization (RSAR) of the as received-PG discussed in Section 5.5.2. RSAD and RSAR solutions were used in this experiment for comparative purpose as the former contained high concentration of Ca^{2+} (Table 4.1 in Section 4.2.1) than the latter. Prior to the adsorption experiments, the initial concentrations of RSAD (298415 mg/L of Ca/ 30 mg/L of ΣREEs) and RSAR (49.74 mg/L of Ca/ 208 mg/L of ΣREEs) solutions were diluted to the concentration of 160 mg/L which was previously identified as the optimum initial concentration for synthetic solutions of Ce^{3+}, Nd^{3+} and Ca^{2+}. These experiments were carried out as described in Section 3.10.3 at the adjusted pH 4.0 and 5.0 for DH-PS20 and DG-PS2 nanofibers, respectively, by immersing 0.0106 g of each adsorbent in 10 mL of diluted solution (160 mg/L) of RSAD or RSAR. The resulting mixture was shaken at stirring speed of 200 rpm, 25 ℃ for 1 h. The obtained solutions were first filtered with 0.45 μm syringe filter and thereafter analysed by ICP-MS for metal content and the adsorption capacity (mg/g) was calculated according to equation 3.2 illustrated in Section 3.10.3 and the results are shown in Figure 6.12 for DH-PS20 (A) and DG-PS2 (B) nanofibers.

	Ce3+	Nd3+	Ca2+
RSAD	0.04	0.01	92.34
RSAR	27.4598	19.224	3.45

	Ce3+	Nd3+	Ca2+
RSAD	0.01	0.008	79.19
RSAR	21.36	18.41	1.87
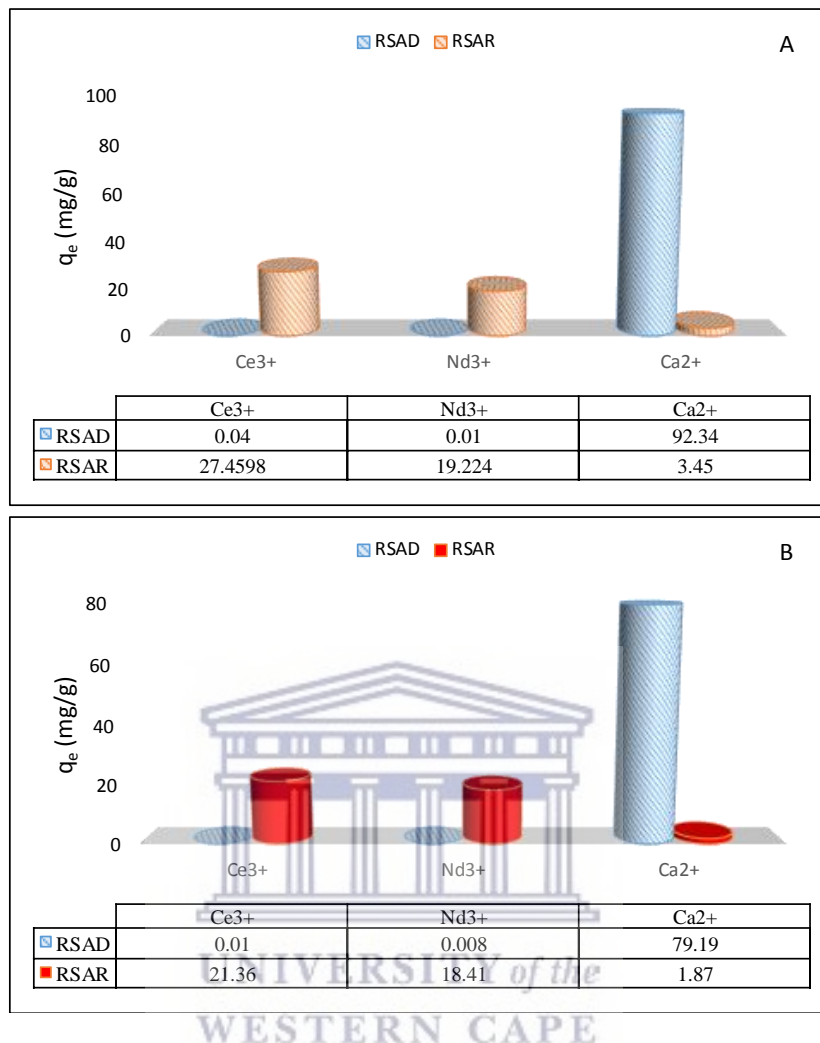
Figure 6.12: Selective adsorption of Ce^{3+}, Nd^{3+} and Ca^{2+} using RSAD and RSAR solutions on DH-PS (A) and DG-PS (B) mats at an initial concentration of 160 mg/L, 25 °C, 200 rpm, 60 min.

From Figure 6.12 (A and B), it can be noticed that Ca uptake largely predominated using RSAD sample for DH-PS20 and DG-PS2 nanofiber mats with the equilibrium adsorption capacities of 92.34 mg/g and 79.19 mg/g respectively. This high uptake of Ca from RSAD sample could possibly be attributed to high Ca content from the original RSAD liquor in which the concentration of Ca^{2+} was about 10000-fold higher than the ΣREE content. However, REEs (Ce^{3+}, Nd^{3+}) uptakes were significantly improved when using the RSAR sample from 0.04 to 27 mg/g for Ce^{3+} and 0.01 to 19 mg/g for Nd^{3+} on DH-PS20 nanofiber and 0.01 to 21 mg/g for Ce^{3+} and 0.008 to 18 mg/g for Nd^{3+} on DG-PS2 nanofiber. These results indicated that

182

REE-Ca separation was more favourable from RSAR than RSAD for DH-PS20 and DG-PS2 nanofibers mats prepared in this study. However, the selectivity of REE-Ca could not be determined because it was difficult to establish an equivalent concentration of REE-Ca in a mixture solution of RSAR and RSAD samples in batch adsorption study. In order to confirm the availability of REEs and Ca on DH-PS20 and DG-PS2 mats, the surface morphology was performed with SEM-EDS mapping after the adsorption experiments using RSAR solution only. The DH-PS20 and DG-PS2 mats were first dried overnight at 40 ℃ and thereafter analysed in an attempt to determine the availability of REEs or Ca^{2+} across the surface of these mats. The results from these SEM-EDS mapping are shown in Figure 6.13 and 6.14 for DH-PS20 and DG-PS2 nanofibers respectively.
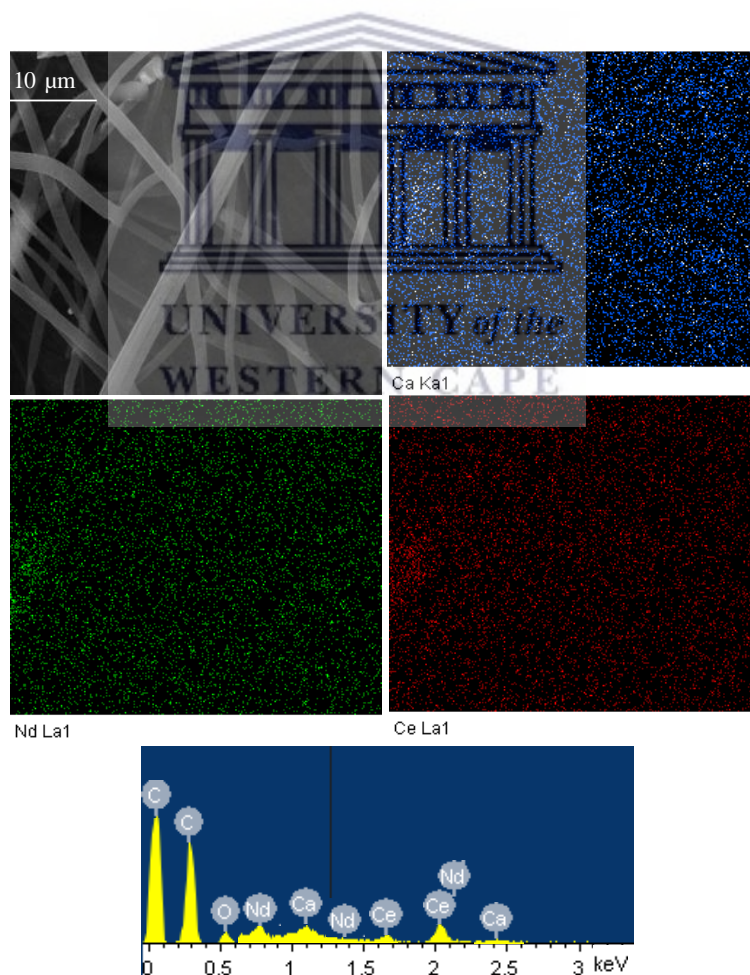
Figure 6.13: SEM-EDS mapping of REEs (Ce^{3+}, Nd^{3+}) and Ca^{2+} on DH-PS20 nanofiber.
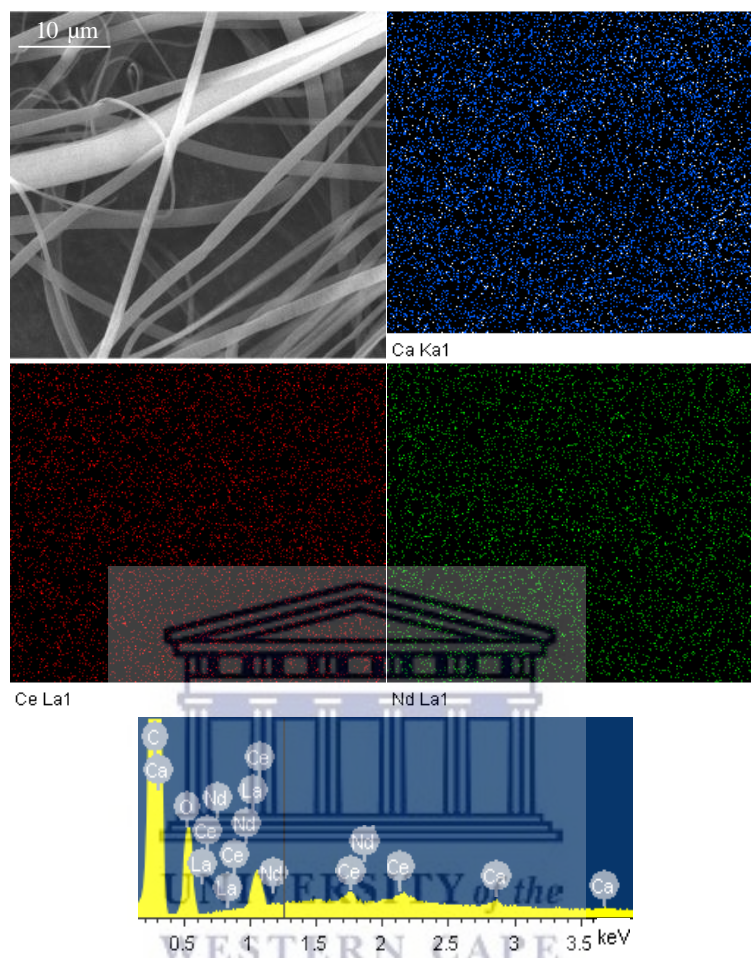
Figure 6.14: SEM-EDS mapping of REEs (Ce^{3+}, Nd^{3+}) and Ca^{2+} on DG-PS2 nanofiber

Figure 6.13 and 6.14, showed that REEs (Ce^{3+}, Nd^{3+}) and Ca^{2+} were available onto the surface of DH-PS20 and DG-PS2 nanofiber mats after the adsorption process from RSAR sample. The difference in terms of the relative intensities of these metals on DH-PS20 and DG-PS2 nanofibers could be attributed to the type of the ligand grafted onto each adsorbent as also discussed in Sections 6.2.1 and 6.2.2. The EDS mapping also confirmed the presence of metals on the DH-PS20 and DG-PS2 nanofiber mats after the adsorption process.

184

6.6 Chapter summary

The results discussed in this chapter have shown and proven that the D2EHPA and DGA ligands were able to increase the adsorption capacity of PS for REEs (Ce^{3+}, Nd^{3+}) and Ca^{2+} as representative metal ions of PG leachate. The optimum adsorption capacities of DH-PS20 and DG-PS2 nanofiber mats were respectively 107 mg/g and 89 mg/g at pH values 4.0 and 5.0 using an initial concentration of 160 mg/L and contact time of 60 min. The discrepancy observed in terms of the adsorption capacities at these conditions was attributed to unique characteristic of each ligand grafted onto the PS support. The experimental data obtained from the adsorption study better fitted the Langmuir isotherms than the Freundlich model suggesting that the adsorption of REEs (Ce^{3+}, Nd^{3+}) and Ca^{2+} took place as a monolayer process occurring on homogeneous surface of DH-PS20 and DG-PS2 nanofibers. On the other hand, the kinetic rate was best described with the pseudo second-order model. The results furthermore showed that the modified nanofibers were able to be regenerated using 1.0 M HNO_3 and to withstand up to 3 cycles. The selective adsorption of REEs (Ce^{3+}, Nd^{3+}) and Ca^{2+} from the real solutions of PG leachates indicated that REEs-Ca^{2+} could be separated from RSAR rather than RSAD solutions. SEM-EDS mapping on the surface of the DH-PS20 and DG-PS2 nanofibers confirmed the availability of the REEs (Ce^{3+}, Nd^{3+}) and Ca^{2+} on the surface of DH-PS20 and DG-PS2 nanofibers after adsorption from RSAR solutions.

185
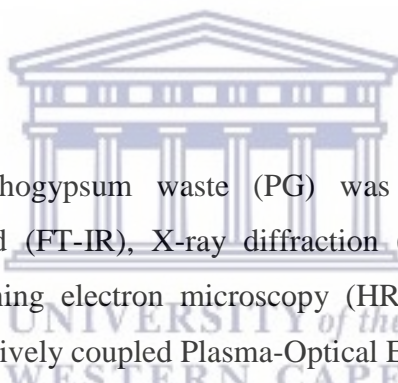
7. CONCLUSIONS

7.1 Introduction

The present chapter gives a general summary on the significance of the research findings based on the objectives that were outlined in Chapter 1. Moreover, the findings highlighted herein is an overview that elucidate the contribution to the knowledge of the research. Furthermore, this chapter outlines recommendations or suggestions for future research in line with the present work.

7.2 Conclusions

In this study, phosphogypsum waste (PG) was characterized by Fourier Transformed Infra-Red (FT-IR), X-ray diffraction (XRD), Thermogravimetric analysis (TGA), scanning electron microscopy (HR-SEM), Neutron activation analysis (NAA), Inductively coupled Plasma-Optical Emission spectroscopy (ICP-OES), X-ray fluorescence spectroscopy (XRF), Ion chromatography (IC) and particle size distribution (PSD). This research has also reported on PG recrystallization for up concentration of rare earth elements (REEs). The characterizations of recrystallized PG using SEM, XRD, FTIR and TGA showed a successful conversion of PG into calcium sulphate whiskers (CSWs) with high REE content reported in the leachates. The research further reported on direct blending and surface modification for obtaining modified polystyrene (PS) based nanofiber via electrospinning process. PS polymer was modified with D2EHPA and DGA ligands before and after electrospinning process respectively to obtain nanofiber adsorbents namely DH-PS20 and DG-PS2 nanofibers. These fibres were ccharacterized by SEM, ATR-FT-IR, TGA techniques. Thereafter, DH-PS20 and DG-PS2 nanofibers were used in batch adsorption studies for extraction of REEs (Ce^{3+}, Nd^{3+}) and Ca^{2+} from solutions. DH-PS20 and DG-PS2 nanofibers were

186

regenerated using HNO_3 but not EDTA solutions. The research questions of this study were answered as followed:

Question 1: What are (is) the most prevailing REEs of the untreated PG under investigation?

- The ICP-OES, MS and NAA results revealed that light REEs group (La–Eu) are the most abundant elements in the as-received PG. However, among the light REEs, La^{3+}, Ce^{3+} and Nd^{3+} make up the weight distribution of these elements with concentrations ranging between 400 to 600 mg/kg; 1100 to 1500 mg/kg and 600 to 850 mg/kg respectively. In contrast, among the heavy REEs (Gd–Y) only Gd^{3+} and Y^{3+} prevailed but their concentrations were far lower than that of light REEs and ranged between 45 to 85 mg/kg. This means that PG could be a good source the light REEs rather than heavy REEs.

Question 2: What will the most feasible and efficient approach be between the direct and indirect acid leaching (recrystallization) for up concentration of REEs from PG waste?

- The results from ICP-MS revealed that direct leaching of REEs from PG waste in HCl, HNO_3 and H_2SO_4 solutions was more favourable in HCl and HNO_3 than H_2SO_4 in which the effect of the common ion was a limiting factor. It was further found that the leaching efficiencies of ΣREEs were 65–78 %, 75–84 % and 45–54 % in 2.0 M HCl, 2 M HNO_3 and 1.5 M H_2SO_4 solutions respectively. However, the dissolution and recrystallization method (indirect leaching) using 2 M HCl and 2 M HNO_3 allowed the up concentration of the ΣREEs in the filtrates from which the efficiencies were found ranging between 94–97 %. This indicated that the recrystallization of PG was the most feasible and efficient method for up concentration of REEs. No study has systematically investigated the above two approaches with attention to REEs.

Question 3: Is it possible to recrystallize the phosphogypsum?

- The results obtained from the FTIR, XRD, SEM and TGA analyses after atmospheric mild acid experiments, confirmed that phosphogypsum waste was successfully converted into new form of calcium sulphate referred to as calcium sulphate whiskers (CSWs). Macroscopic images of the obtained CSWs revealed a white fibre like aspect with whiteness higher than the raw phosphogypsum. This recrystallization was important as it allowed not only to add value to the PG waste but also to up concentrate the REEs in the resulting filtrates.

Question 4: Can D2EHPA or DGA ligand be doped or grafted on polystyrene support?

- The characterizations of polystyrene (PS) support and modified nanofibers (blended with D2EHPA and surface modified with DGA ligands) were done using mainly SEM, ATR-FTIR, and TGA techniques. The obtained results from ATR-FTIR analysis of the modified nanofibers supported by the TGA and SEM analysis confirmed the presence of the main functional groups of the D2EHPA and DGA ligands onto the PS backbone.

Question 5: Can DH-PS20 and DG-PS2 nanofibers adsorb REEs (Ce^{3+}, Nd^{3+}) and Ca^{2+} better than unmodified PS14-nfs?

- The batch adsorption studies revealed that direct blending and surface modification of PS with D2EHPA and DGA ligands for fabrication of DH-PS20 and DG-PS2 nanofibers respectively were able to increase the adsorption capacity of PS support for REEs (Ce^{3+}, Nd^{3+}) and Ca^{2+} from solutions. This increase in adsorption capacity was attributed to unique characteristic of each ligand grafted onto the PS support whereas poor adsorption capacity of PS14-nfs was due to the lack of functional group on it.

Question 6: Are DH-PS20 and DG-PS2 nanofiber mats reusable and how many times will it be possible to reuse each?

- The reusability study of DH-PS20 and DG-PS2 nanofiber mats have demonstrated that these materials can be reused for about four desorption cycles using HNO_3. However, the adsorption capacity of DH-PS20 and DG-PS2 nanofibers decreased with increased number of cycles and was very significant after the second cycle. This decrease in adsorption capacity for both DH-PS20 and DG-PS2 nanofibers is as a result of loss of D2EHPA or DGA ligand on the surface of PS support and this was evidenced through FTIR analyses. The development of such reusable nanofibers offers the potential to be selective adsorbents for PG leachate solutions and other related industrial waste water treatment applications.

7.3 Novelty

This research is reporting the use of atmospheric mild acid recrystallization of PG waste with subsequent up concentration of REEs in the filtrates for the first time. The results from this combined process have shown that pure gypsum materials referred as CSWs was obtained with improved concentrations of REEs in filtrates. This process was unique to this study and has not been carried out in another study, especially with attention to REEs up concentration. This research is reporting furthermore the use of electrospinning technique for fabrication of PS and D2EHPA ligand based nanofibers for extraction of REEs from solutions. The obtained nanofiber materials have not been discussed or reported in another study. This research was therefore able to contribute new knowledge in terms of the valorisation of PG waste into CSWs which have promising potential use in area such as construction and also the use of electrospun nanofibers as supports for extraction of REEs.

7.4 Recommendations

This research recommends the up scaling of the atmospheric acid recrystallization of PG waste for the fabrication of CSWs with subsequent extraction of REEs. Further study should be carried out to investigate the stability of the ligands onto the polymer support to improve the reusability of the materials. This study therefore recommended that more optimization of surface modification and direct blending with ligands should be carried out so that the obtained adsorbents can be regenerated and reused for over four cycles. Thorough studies should be also carried out to investigate the selectivity of electrospun modified nanofibers in a complex mixture solution with more than one competing cation other than Ca^{2+}.

190

REFERENCES

Abramov, Y.K., Veselov, V.M., Zalevsky, V.M., Argunov, N.D., Bogdanova, L.P., Gukasov, N.A., Evdokimov, V.D., Tamurka, V.G. and Motovilova, L.V., Twin Trading Co. (2013). Method for extracting rare earth elements from phosphogypsum. U.S. Patent 8,470, 270.

Abreu, R. D., & Morais, C. A. (2010). Purification of rare earth elements from monazite sulphuric acid leach liquor and the production of high-purity ceric oxide. *Minerals Engineering*, *23*(6): 536-540.

Agrawal Y., H. Kaur, S. Menon. (1999). Poly (styrene-p-hydroxamic acids): synthesis, and ion exchange separation of rare earths, *React. Funct. Polym.*, 39, 155–164.

Al-Thyabat, S.; Zhang, P. (2015). REE extraction from phosphoric acid, phosphoric acid sludge, and phosphogypsum. *Min. Proc. Ext. Met.*, 124, 143–150.

Al-Thyabat, S. and Zhang, P. (2015a). In-line extraction of REE from Dihydrate (DH) and HemiDihydrate (HDH) wet processes. *Hydrometallurgy*, *153*, 30-37.

Alexandratos SD and Crick DW. (1996). Polymer-supported reagents: Application to separation science. Industrial & Engineering Chemistry Research 35(3):635-44.

Alonso, E., Sherman, A.M., Wallington, T.J., Everson, M.P., Field, F.R., Roth, R. and Kirchain, R.E. (2012). Evaluating rare earth element availability: A case with revolutionary demand from clean technologies. *Environmental science & technology*, 46(6), 3406-3414.

Antonick, P.J.; Hu, Z.; Fujita, Y.; Reed, D.W.; Das, G.; Wu, L.; Shivaramaiah, R.; Kim, P.; Eslamimanesh, A.; Lencka, M.M.; Jiao, Y. (2019). Bio-and mineral acid leaching of rare earth elements from synthetic phosphogypsum. *J. Chem. Thermodynamics*. 132, 491-496.

Atanassova, M., Kurteva, V., Lubenov, L., Billard, I., (2015). Solvent extraction and separation of light lanthanoids with mixtures of two chelating extractants: Benzene vs. ionic liquid. *Sep. Sci. Technol.* 51 (2), 290–299.

Azimi, G., Papangelakis, V.G., Dutrizac, J.E., (2008). Development of an MSE-based chemical model for the solubility of calcium sulfate in mixed chloride–sulfate solutions. *Fluid Phase Equilib*. 266, 172–186

Bahramzadeh A., P. Zahedi, M. (2016). Abdouss, Acrylamide-plasma treated electrospun polystyrene nanofibrous adsorbents for cadmium and nickel ions removal from aqueous solutions, *J. Appl. Polym. Sci*., 133, 42944–42953.

Bandara, H.M.D., Darcy, J.W., Apelian, D., Emmert, M.H., (2014). Value analysis of neodymium content in shredder feed: toward enabling the feasibility of rare earth magnet recycling. *Environ. Sci. Technol*. 48, 6553-6560.

Battsengel, A., Batnasan, A., Haga, K. and Shibayama, A. (2018). Selective separation of light and heavy rare earth elements from the pregnant leach solution of apatite ore with D2EHPA. *Journal of Minerals and Materials Characterization and Engineering*, *6*(05), p 517.

Batchu, N.K. and Binnemans, K., (2018). Effect of the diluent on the solvent extraction of neodymium (III) by bis (2-ethylhexyl) phosphoric acid (D2EHPA). *Hydrometallurgy*, *177*,146-151.

Basualto, I.C., Valenzuela, F.I., Molina, I., Munoz, J.P., Fuentes, E., Sapag, J., (2013). Study of the solvent extraction of the lighter lanthanide metal ions by means of organophosphorus extractants. *J. Chil. Chem. Soc*. 58 (2), 1785–1789.

Barmettler, F.; Castelberg, C.; Fabbri, H.; Brandl. (2016). Microbial mobilization of rare earth elements (REE) from mineral solids—A mini review. *AIMS Microbiology*. 2, 190–204.

Bessbousse H, Rhlalou T, Verchere J, Lebrun L. (2009). Novel metal-complexing membrane containing poly (4-vinylpyridine) for removal of Hg (II) from aqueous solution. *The Journal of Physical Chemistry B*. 113 (25):8588-8598.

Bhardwaj N and Kundu SC. (2010). Electrospinning: A fascinating fiber fabrication technique. Biotechnology advances 28(3):325-347.

Binnemans, K., Jones, P.T., Müller, T. and Yurramendi, L., (2018). Rare earths and the balance problem: how to deal with changing markets? *Journal of Sustainable Metallurgy*, 4(1): 126-146.

Binnemans, K., Pontikes, Y., Jones, P. T., Van Gerven, T., & Blanpain, B. (2013). Recovery of rare earths from industrial waste residues: a concise review. In Proceedings of the 3rd International Slag Valorisation Symposium: *The Transition to Sustainable Materials Management*. 191-205.

Binnemans, K., Jones, P.T., Blanpain, B., Van Gerven, T., Yang, Y., Walton, A., Buchert, M., (2013a). Recycling of rare earths: a critical review. *J. Clean. Prod.* 51,1-22.

Binnemans, K., Jones, P. T., Blanpain, B., Van Gerven, T., & Pontikes, Y. (2015). Towards zero-waste valorisation of rare-earth-containing industrial process residues: a critical review. *Journal of Cleaner Production*, *99*, 17-38.

Biswas M and Chatterjee S. (1983). Chemical modification of polystyrene—IV. electrophilic substitution of polystyrene with cis-1, 2, 3, 6 tetrahydrophthalic anhydride. *European Polymer Journal*. 19(4):317-320.

Blench Trevor (2018), https://steenkampskraal.com/wp-content/uploads/steenkampskraal-information-memorandum-january-2018.pdf. tblench@steenkampskraal.com. Access 13/07/21.

Blissett, R. S., Smalley, N., & Rowson, N. A. (2014). An investigation into six coal fly ashes from the United Kingdom and Poland to evaluate rare earth element content. *Fuel*, *119*, 236-239.

Bouhlassa, S., Salhamen, F. and Elyahyaoui, A., (2016). Calcium sulphate hydrates formation in aqueous sulpho-phosphoric media containing rare earth impurity beyond 80° C. *Fluid Phase Equilibria*, *423*, 93-100.

Bode-Aluko, C.A., (2017). Functionalisation of polymer nanofibres and track-etched membrane removal of organic and and inorganic pollutants from water. (PhD. Thesis, UWC).

Bouchhima, L.; Rouis, M.J.; Choura, M. (2017). A study of phosphogypsum-crushing sand based bricks grade negligible weathering. *Rom. J. Mater*. 47, 316–323.

Borges, R.C., Favaro, D.I.T., Caldas, V.G., Lauria, D.C. and Bernedo, A.V.B. (2016). Instrumental Neutron Activation Analysis, Gamma Spectrometry and Geographic Information System Techniques in the Determination and Mapping of Rare Earth Element in Phosphogypsum Stacks. *Environmental Earth Sciences*, 75, 1-15.

Brunauer, S., Emmett, P. H. and Teller, E. J. (1938). Adsorption of gases in multimolecular layers, *Journal of the American Chemical Society*, 60 (2), 309- 319.

Brückner, L., Elwert, T. and Schirmer, T., (2020). Extraction of rare earth elements from phospho-gypsum: concentrate digestion, leaching, and purification. *Metals*, 10(1), p.131.

Bunzli, J.C.G., (2014). Lanthanide coordination chemistry: from old concepts to coordination polymers. *Journal of Coordination Chemistry*. 67(23-24), 3706-3733.

Cadore, J.S., Bertuol, D.A. and Tanabe, E.H., (2019). Recovery of indium from LCD screens using solid-phase extraction onto nanofibers modified with Di-(2-ethylhexyl) phosphoric acid (DEHPA). *Process Safety and Environmental Protection*, *127*, 141-150.

Campos, M.P.; Costa, L.J.P.; Nisti, M.B.; Mazzilli, B.P. (2017). Phosphogypsum recycling in the building materials industry: assessment of the radon exhalation rate. *J. Environ. Radioact*. 1, 232–236.

Canovas, C.R.; Chapron, S.; Arrachart, G.; Pellet-Rostaing, S. (2019). Leaching of rare earth elements (REEs) and impurities from phosphogypsum: A preliminary insight for further recovery of critical raw materials. *J. Clean. Prod*. 219, 225–235.

Canovas, C.R.; Macias, F.; Perez-Lopez, R.; Basallote, M.D.; Millan-Becerro, R. (2018). Valorization of wastes from the fertilizer industry: Current status and future trends. *J. Clean. Prod*. 174, 678-690.

Canovas, C.R., P_erez-L_opez, R., Macías, F., Chapron, S., Nieto, J.M., Pellet-Rostaing, S., (2017). Exploration of fertilizer industry wastes as potential source of critical raw materials. *J. Clean. Prod*. 143, 497-505.

Cardoso, D.S.P., Santos, D.M.F., Sljukic, B., Sequeira, C.A.C., Maccio, D., Saccone, A., (2016). Platinum-rare earth cathodes for direct borohydride-peroxide fuel cells. *J. Power Sources.* 307, 251–258.

Charles River Associates (1977); United States Office of Minerals Policy and Research Analysis, Implications of the War in Zaire for the Cobalt Market. Rev. ed.; *Charles River Associates*: Cambridge, Mass; p 42.

Charalampides, G., Vatalis, K.I., Apostoplos, B. and Ploutarch-Nikolas, B., (2015). Rare earth elements: industrial applications and economic dependency of Europe. *Procedia Economics and Finance*. *24*, 126-135.

Chen, Z., (2011). Global rare earth resources and scenarios of future rare earth industry. *Journal of Rare Earths* 29 (1), 1–6.

Chi, R., Xu, S., Zhu, G., Xu, J., Qiu, X., (2001). Beneficiation of rare earth ore in china. In: Metals, Light. (Ed.): Technical Sessions at the 130th TMS Annual Meeting. TMS Aluminum Committee, New Orleans,1159–1165.

Chen, J., Hong, L., Wu, S. and Wang, L. (2002). Elucidation of interactions between metal ions and Ca-alginate-based ion-exchange resin by spectroscopic analysis and modeling simulation, *Langmuir*, 18 (24): 9413-9421.

Coates, J., (2000). Interpretation of infrared spectra, a practical approach.

Chronakis, I. S. (2005). Novel nanocomposites and nanoceramics based on polymer nanofibres using electrospinning process—A review, *Journal of Materials Processing Technology*, 167, 283-293.

Chipara, D.M., Macossay, J., Ybarra, A.V., Chipara, A.C., Eubanks, T.M. and Chipara, M., (2013). Raman spectroscopy of polystyrene nanofibers—Multiwalled carbon nanotubes composites. *Applied surface science*, *275*, 23-27.

Corbett, M.K.; Eksteen J.J.; Niu, X.Z.; Croue J.P.; Watkin, E.L.J. (2017). Interactions of phosphate solubilising microorganisms with natural rare-earth phosphate minerals: a study utilizing Western Australian monazite. *Bioprocess Biosyst. Eng*. 40, 929–942.

195

Costis, S.; Mueller, K.K.; Coudert, L.; Neculita, C.M.; Reynier, N.; Blais, J.F. (2020). Recovery potential of rare earth elements from mining and industrial residues: A review and cases studies. *J. Geochem. Explor*. 106699.

Da Silva, F.N., Bassaco, M.M., Bertuol, D.A. and Tanabe, E.H., (2019). An eco-friendly approach for metals extraction using polymeric nanofibers modified with di-(2-ethylhexyl) phosphoric acid (DEHPA). *Journal of Cleaner Production*. *210*,786-794.

Das N., D. Das, Recovery of rare earth metals through biosorption: an overview, J. Rare Earths., 31 (2013) 933–943.

Deqian, L.I., (2017). A review on yttrium solvent extraction chemistry and separation process. *Journal of Rare Earths*, *35*(2), 107-119.

Deitzel, J.M., Kleinmeyer, J., Harris, D. and Tan, N.C.B. (2001). The effect of processing variables on the morphology of electrospun nanofibers and textiles, *Polymer*, 42, 261-272.

Demir, M.M., Yilgor, I., Yilgor, E. and Erman, B. (2002). Electrospinning of polyurethane fibers, *Polymer*, 43, 3303-3309.

Deng, S., Bai, R. and Chen, J. (2003a). Aminated polyacrylonitrile fibers for lead and copper removal, *Langmuir*, 19, 5058-5064.

De Beer, M.; Maree, J.P.; Liebenberg, L.; Doucet, F.J. (2014). Conversion of calcium sulphide to calcium carbonate during the process of recovery of elemental sulphur from gypsum waste. *Waste Manag*. 34, 2373–2381.

Demirel, Y.; Caglar, Y. (2017). Recovery of phosphogypsum in the economy in building material waste. *J. Fac. Eng. Archit. Gazi Univ*. 30, 743–750.

Dev, S.; Sachan, A.; Dehghani, F.; Ghosh, T.; Briggs, B.R.; Aggarwal, S. (2020). Mechanisms of biological recovery of rare-earth elements from industrial and electronic wastes: A review. *Chem. Eng. J*. 397,124596.

Dharanivasan G., T. Rajamuthuramalingam, D.M.I. Jesse, N. Rajendiran, K. Kathiravan, (2015). Gold nanoparticles assisted characterization of amine

functionalized polystyrene multiwell plate and glass slide surfaces, Appl. Nanosci., 5, 39–50.

Di Stefano, C., Ferro, V. and Mirabile, S., (2010). Comparison between grain-size analyses using laser diffraction and sedimentation methods. *Biosystems engineering*, *106*(2), 205-215.

Du, B.X. and Huang, K., (2014). The Research on Comprehensive Utilization of Phosphogypsum. In *Advanced Materials Research*. 850, 1368-1371.

Dupont D., W. Brullot, M. Bloemen, T. Verbiest, K. (2014). Binnemans, Selective uptake of rare earths from aqueous solutions by EDTA-functionalized magnetic and nonmagnetic nanoparticles, *ACS Appl. Mater. Interf.*, 6, 4980–4988.

Dushyantha, N., Batapola, N., Ilankoon, I.M.S.K., Rohitha, S., Premasiri, R., Abeysinghe, B., Ratnayake, N. and Dissanayake, K., (2020). The story of rare earth elements (REEs): Occurrences, global distribution, genesis, geology, mineralogy and global production. *Ore Geology Reviews*. *122*, p.103521.

Dutrizac, J.E. (2017) The Behaviour of the Rare Earth Elements during Gypsum (CaSO4・2H2O) Precipitation. *Hydrometallurgy*, 174, 38-46.

Du, X., & Graedel, T. E. (2011). Global in-use stocks of the rare earth elements: a first estimate. *Environmental Science & Technology*. *45* (9): 4096-4101.

Eggert, R., Wadia, C., Anderson, C., Bauer, D., Fields, F., Meinert, L. and Taylor, P., 2016. Rare earths: market disruption, innovation, and global supply chains. *Annual Review of Environment and Resources*. *41*, 199-222.

El-Didamony, H.; Ali, M. M.; Awwad, N. S.; Fawzy, M. M.; Attallah, M. F. (2012). Treatment of phosphogypsum waste using suitable organic extractants. *J. Radioanal. Nuclear Chemistry*. 291, 907-914.

El-Didamony, H.; Gado, H.S.; Awwad, N.S.; Fawzy, M.M.; Attallah, M.F. (2013). Treatment of phosphogypsum waste produced from phosphate ore processing. *J. Hazardous. Materials*. 244, 596-602.

El-Reefy, S.; Nayl, A.; Aly, H. (2008). Leaching and group separation of lanthanides from phosphogypsum. *In Proceedings of the 9th. International Conference for Nuclear Sciences and Applications, Sharm Al Sheikh, Egypt, 11–14 February 2008; 11–14*.

Esma B, Omar A, Amine DM. 2014. Comparative study on lanthanum (III) sorption onto lewatit TP 207 and lewatit TP 260. Journal of Radioanalytical and Nuclear Chemistry 299(1):439-46.

Fang J., H. Niu, T. Lin, X. Wang, (2008). Applications of electrospun nanofibers, *Chinese Sci. Bull*., 53, 2265–2286.

Fathollahzadeh, H.; Eksteen, J.J.; Kaksonen, A.H.; Watkin, E.L.J. (2019). Role of microorganisms in bioleaching of rare earth elements from primary and secondary resources, *Appl. Microbiol. Biotechnol*. 103, 1043–1057.

Fimognari, R., Cinninger, L.M., Lynch, V.M., Holliday, B.J., Sessler, J., (2018). Copper selective polymeric extractant synthesized by ring-opening metathesis polymerization. *Inorg. Chem*. 57, 392-399.

Florek, J., Mushtaq, A., Larivière, D., Cantin, G., Fontaine, F.G. and Kleitz, F., (2015). Selective recovery of rare earth elements using chelating ligands grafted on mesoporous surfaces. *RSC advances*, *5* (126), 103782-103789.

Foo K., B. Hameed. (2009). An overview of landfill leachate treatment via activated carbon adsorption process. *J. Hazard. Mater*., 171, 54–60.

Fontanals N., R.M. Marcé, F. Borrull. (2011). Overview of the novel sorbents available in solid-phase extraction to improve the capacity and selectivity of analytical determinations, *Contrib. Sci*. 6, 199–213.

Freixa Z and Van Leeuwen PW. (2003). Bite angle effects in diphosphine metal catalysts: Steric or electronic? *Dalton Transactions* (10):1890-901.

Fuleihan N.F. (2012). Phosphogypsum disposal-the pros & cons of wet versus dry stacking. *Procedia Eng*. 46, 195–205.

Fu F., Q. Wang. (2011). Removal of heavy metal ions from wastewaters: a review, *J. Environ. Manage*., 92, 407–418.

Gannaz, B., Antonio, M.R., Chiarizia, R., Hill, C., Cote, G. (2006). Structural study of trivalent lanthanide and actinide complexes formed upon solvent extraction. *Dalton Trans*.4553–4562.

Ganguli, R. and Cook, D.R., (2018). Rare earths: A review of the landscape. *MRS Energy & Sustainability*,5.

Galhoum AA, Mahfouz MG, Abdel-Rehem ST, Gomaa NA, Atia AA, Vincent T, Guibal E. (2015). Diethylenetriamine-functionalized chitosan magnetic nano-based particles for the sorption of rare earth metal ions [Nd (III), Dy (III) and Yb (III)]. *Cellulose* 22(4):2589-605.

Gasser, M.S.; Ismail, Z.H.; Abu Elgoud, A.; Abdel Hai, F.; Ali, O.I.; Aly, H.F. (2019). Process for Lanthanides-Y leaching from phosphogypsum fertilizers using weak acids. *J. Hazard. Mater*. 378, 12762.

Geist A, Nitsch W, Kim JI. (1999). On the kinetics of rare-earth extraction into D2EHPA. Chem Eng Sci. 54:1903.

Genkin, Mikhail Vladimirovich, Aleksey Vladimirovich Evtushenko, Aleksey Aleksandrovich Komkov, Alfiya Minerovna Safiulina, Vasiliy Sergeevich Spiridonov, and Sergey Vladimirovich Shvetsov. (2013) "A method for extracting rare-earth metals." U.S. Patent Application 14/773,725, filed November 8.

Genkin, M.V.; Evtushenko, A.V.; Komkov, A.A.; Safiulina, A.M.; Spiridonov, V.S.; Shvetsov, S.V.; Uralchem J.S.C. (2017). Methods for extracting rare-earth metals and preparing gypsum plaster from phosphogypsum hemihydrate. U.S. Patent 9,657,371.

Goodenough, K.M., Wall, F. and Merriman, D. (2018). The rare earth elements: demand, global resources, and challenges for resourcing future generations. *Natural Resources Research*, *27*(2), 201-216.

Golev, A.; Scott, M.; Erskine, P.D., Ali, S.H. and Ballantyne, G.R., (2014). Rare earths supply chains: Current status, constraints and opportunities. *Resources Policy*. 41, 52-59

Gupta, C.K. and Krishnamurthy, N. (1992). Extractive metallurgy of rare earths. *International Materials Reviews*, *37*(1), 197-248.

Grabas, K., Pawełczyk, A., Stręk, W., Szełęg, E. and Stręk, S. (2019). Study on the properties of waste apatite phosphogypsum as a raw material of prospective applications. *Waste and Biomass valorization*, *10*(10), 3143-3155.

Habashi, F., (1985). The recovery of the lanthanides from phosphate rock. J. *Chem. Technol. Biotechno*l. A 35, 5-14.

Hammas-Nasri, I.; Horchani-Naifer, K.; Férid, M.; Barca, D. (2016). Rare earths concentration from phosphogypsum waste by two-step leaching method. *Int. J. Miner. Process*. 149, 78–83.

Hammas-Nasri, I.; Horchani-Naifer, K.; Férid, M.; Barca, D. Production of a rare earths concentrate after phosphogypsum treatment with dietary NaCl and Na2CO3 solutions. *Minerals Engineering*. **2019**, 132, 169-174

Hammas, I., Horchani-Naifer, K. and Férid, M. (2013). Characterization and optical study of phosphogypsum industrial waste. *Studies in Chemical Process Technology*. *1*(2), 30-36.

Hakkarainen M. (2002). Aliphatic polyesters: Abiotic and biotic degradation and degradation products. In: Degradable aliphatic polyesters. *Advances in Polymer Science, Springer, Berlin, Heidelberg* (157) 113-138

He, H., Dong, F., He, P. and Xu, L., (2014). Effect of glycerol on the preparation of phosphogypsum-based $CaSO_4 \cdot 0.5 H_2O$ whiskers. *Journal of Materials Science*. *49*(5), 1957-1963.

Helfferich F. (1965). Ion-exchange kinetics. V. ion exchange accompanied by reactions. *The Journal of Physical Chemistry* 69(4):1178-1187.

Hibstie, A.; Chaubey, A.; Hailu, A. and Mamo, D. (2013): Thermal Neutron Activation Analysis Technique of Rock Samples from Choke Mountain Range, East Gojjam, Ethiopia. *Scope of Journal, 694*.

Hiremath N., G. Bhat. (2015). Melt blown polymeric nanofibers for medical applications-an overview, *Nanosci. Technol*. 2, 1–9.

Hidayah, N.N. and Abidin, S.Z., (2018). The evolution of mineral processing in extraction of rare earth elements using liquid-liquid extraction: A review. *Minerals Engineering*, *121*,146-157.

Hidayah, N.N. and Abidin, S.Z., (2017). The evolution of mineral processing in extraction of rare earth elements using solid-liquid extraction over liquid-liquid extraction: A review. *Minerals Engineering*, *112*, 103-113.

Horzum, N., Shahwan, T., Parlak, O. and Demir, M. (2012). Synthesis of amidoximated polyacrilonitrile fibers and its application for sorption of aqueous uranyl ions under continues flow, *Chemical Engineering Journal*. 213, 41-49.

Hong, G., Shen, L., Wang, M., Yang, Y., Wang, X., Zhu, M. and Hsiao, B.S. (2014). Nanofibrous polydopamine complex membranes for adsorption of Lanthanum (III) ions. *Chemical engineering journal*, *244*, 307-316.

Holloway, P.H., Vaidyanathan, P.N. (2009), "Characterization of metals and alloys", Momentum Press, New York.

Horwitz EP, McAlister D, Bond A, Barrans Jr RE. (2005). Novel extraction of chromatographic resins based on tetraalkyldiglycolamides: Characterization and potential applications. *Solvent Extraction and Ion Exchange*. 23(3):319-344.

Hopfe, S.; Konsulke, S.; Barthen, R.; Lehmann,F.; Kutschke, S.; Pollmann, K. (2018). Screening and selection of technologically applicable microorganisms for recovery of rare earth elements from fluorescent powder. *Waste Manage*. 79, 554–563.

Huang, L., McMillan, R.A., Apkarian, R.P., Pourdeyhimi, B., Conticello, V.P. and Chaikof, E.L. (2000). Generation of synthetic elastin-mimetic small diameter fibers and fiber networks, *Macromolecules*. 33(8): 2989-2997.

Huang, L., Apkarian, R.P. and Chaikof, E.L. (2001). High-Resolution analysis of engineered type I collagen nanofibers by electron microscopy, *Scanning*, 23, 372-375.

Huang, Z., Zhang, Y., Kotaki, M. and Ramakrishna, S. (2003). A review on polymer nanofibers by electrospinning and their applications in nanocomposites, *Composite Science and Technology*. 63, 2223-2253.

201

Huang M., H. Lu, X. Li. (2012). Synthesis and strong heavy-metal ion sorption of copolymer microparticles from phenylenediamine and its sulfonate, *J. Mater. Chem*. 22, 17685–17699.

Huan, S., Bai, L., Liu, G., Cheng, W. and Han, G., (2015). Electrospun nanofibrous composites of polystyrene and cellulose nanocrystals: manufacture and characterization. *RSC Advances*, *5*(63), 50756-50766.

https://pubs.usgs.gov/fs/2002/fs087-02/, Rare Earth Elements—Critical Resources for High Technology, access 14/07/21.

Iglesias M, Antic_o E, Salvad_o V, Masana A, Valiente M. (1999). Effect of Y(III) distribution between aqueous nitrate and organic D2EHPA solutions on the Y(III) precipitation stripping using oxalic acid. *Solvent Extr Ion Exch*. 17:277.

Innocenzi, V., De Michelis, I., Kopacek, B., Veglio, F., (2014). Yttrium recovery from primary and secondary sources: a review of main hydrometallurgical processes. *Waste Manag*. 34, 1237-1250.

Innocenzi, V., Ippolito, N.M., Pietrelli, L., Centofanti, M., Piga, L. and Vegliò, F., (2018). Application of solvent extraction operation to recover rare earths from fluorescent lamps. *Journal of Cleaner Production*, *172*, 2840-2852.

Ismail, Z.; Abu Elgoud, E.; Gasser, M.; Aly, H.; Abdel Hai, F.; Ali, I. (2015). Leaching of some lanthanides from phosphogypsum fertilizers by mineral acids. *Arab J. Nucl. Sci. Appl*. 48, 37–50.

Jeon C and Kwon T. (2012). Desorption and regeneration characteristics for previously adsorbed indium ions to phosphorylated sawdust. *Environmental Engineering Research* 17(2):65-67.

Jensen,M.P., Chiarizia, R., Urban, V., (2001). Investigation of the aggregation of the neodymium complexes of dialkylphosphoric, -oxothiophosphinic, and −dithiophosphinic acids in toluene. S*olvent Extr. Ion Exch*. 19 (5), 865–884.

Jepson, N., (2012). A 21st century scramble: South Africa, China and the rare earth metals industry.

Jha, M.K., Kumari, A., Panda, R., Kumar, J.R., Yoo, K. and Lee, J.Y., (2016). Review on hydrometallurgical recovery of rare earth metals. *Hydrometallurgy*, *165*,.2-26.

Jing, L., Shim, K., Toe, C.Y, Fang, T., Zhao, C., Amal, R., Sun, K., Kim, J.H. and Ng, Y.H. (2016). Electrospun Polyacrylonitrile−Ionic Liquid Nanofibers for Superior PM2.5 Capture Capacity, *ACS Applied Material Interfaces*, 8, 7030-7036.

Jin, H.X., Wu, F.Z., Mao, X.H., Wang, M.L. and Xie, H.Y., (2017). Leaching isomorphism rare earths from phosphorite ore by sulfuric acid and phosphoric acid. *Rare Metals*, *36*(10), 840-850.

Jin, L. and Bai, R. (2002). Mechanisms of lead adsorption on chitosan/PVA hydrogel beads, *Langmiur*,18, 9765-9770.

Jin, Y., Ma, Y., Weng, Y., Jia, X., Li, J., (2014). Solvent extraction of Fe3þ from the hydrochloric acid route phosphoric acid by D2EHPA in kerosene. *J. Ind. Eng. Chem*. 20, 3446-3452.

Jordens, A., Cheng, Y. P., & Waters, K. E. (2013). A review of the beneficiation of rare earth element bearing minerals. *Minerals Engineering*, *41*: 97-114.

Jyothi, R.K.; Thenepalli, T.; Ahn, J.W.; Parhi, P.K.; Chung, K.W.; Lee, J.Y. (2020). Review of rare earth elements recovery from secondary resources for clean energy technologies: Grand opportunities to create wealth from waste. *Journal of Cleaner Production*. 122048

Kandil, A.H.T., Cheira, M.F., Gado, H.S., Soliman, M.H. and Akl, H.M., (2017). Ammonium sulfate preparation from phosphogypsum waste. *Journal of Radiation Research and Applied Sciences*, *10*(1), 24-33.

Kanzel, A.V., Mazurkevich, P.A., Bortkov, I.A., Hares, N.K.:(2017). Method for complex processing of phosphogypsum. Patent RU 2639394 the Russian Federation.

Kajiya T., M. Aihara, S. Hirata. (2004). Determination of rare earth elements in seawater by inductively coupled plasma mass spectrometry with on-line column pre-concentration using 8-quinolinole-immobilized fluorinated metal alkoxide glass, Spectrochim. Acta Part B: *Atomic Spectroscopy*, 59, 543–550.

Karadaş C., D. Kara, A. Fisher. (2011). Determination of rare earth elements in seawater by inductively coupled plasma mass spectrometry with off-line column preconcentration using 2, 6-diacetylpyridine functionalized Amberlite XAD-4, Anal. Chim. Acta, 689, 184–189.

Kampalanonwat, P. and Supaphol, P. (2011). Preparation of Hydrolyzed Electrospun Polyacrylonitrile Fiber Mats as Chelating Substrates: A Case Study on Copper(II) Ions, *Industrial and Engineering Chemistry Research*, 50, 11912-11921.

Keller J.U., R. Staudt, (2005). Gas adsorption equilibria: experimental methods and adsorptive isotherms, *Springer Science & Business Media, New York, USA*, 1–421.

Khaironiel MT, Markom M, Meor Yusoff MS, Nazaratul Ashifa S (2014) Solvent extraction of light rare earth ions using D2EHPA from nitric acid and sulphuric acid solutions. *Adv Mater Res*. 970:209–213.

Khodakarami, M. and Alagha, L., (2020). Separation and recovery of rare earth elements using novel ammonium-based task-specific ionic liquids with bidentate and tridentate O-donor functional groups. *Separation and Purification Technology*, *232*, 115952.

Kidoaki, S., Kwon, I.K. and Matsuda, T. (2005). Mesoscopic spatial designs of nano and microfiber meshes for tissue-engineering matrix and scaffold based on newly devised multilayering and mixing electrospinning techniques, *Biomaterials*, 26, 37-46.

Kim, J.S. and Lee, D.S. (2000). Thermal properties of electrospun polyesters, *Polymer Journal*, 32 (7), 616-618.

Koh H, Yong T, Chan C, Ramakrishna S. (2008). Enhancement of neurite outgrowth using nano-structured scaffolds coupled with laminin. Biomaterials 29(26):3574- 82.

Koopman, C., & Witkamp, G. J. (2000). Extraction of lanthanides from the phosphoric acid production process to gain a purified gypsum and a valuable lanthanide by-product. *Hydrometallurgy*, *58* (1): 51-60.

Koski A, Yim K, Shivkumar S. (2004). Effect of molecular weight on fibrous PVA produced by electrospinning. *Materials Letters* 58(3):493-497.

Kolokolnikov, V.A., and Kovalev, M.I., (2009). "Processing rare-earth element concentrate obtained from phosphogypsum," *Chemistry for Sustainable Development*, 17, 261-266.

Kolokolnikov, V.A.; Kovalev, M.I. (2009). Technology for processing technical calcium carbonate obtained from phosphogypsum into pure calcium carbonate and rare-earth element concentrate. *Chem Sustain Dev*. 17, 387–393.

Kumar S.A., S.P. Pandey, N.S. Shenoy, S.D. Kumar. (2011). Matrix separation and preconcentration of rare earth elements from seawater by poly hydroxamic acid cartridge followed by determination using ICP-MS, *Desalination*, 281, 49–54.

Kulczycka, J.; Kowalski, Z.; Smol, M.; Wirth, H. (2016). Evaluation of the recovery of Rare Earth Elements (REE) from phosphogypsum waste–case study of the WIZÓW Chemical Plant (Poland). *J. Clean. Prod*. 113, 345–354.

Kybartiene, N.; Valancius, Z.; Leskeviciene, V.; Urbonas, L. (2015). Influence of the composition of phosphate rock on the amount of water-insoluble phosphate impurities in semi-hydrate phosphogypsum. *Ceramics-Silikáty*. 59, 29–36.

Ladizesky N and Ward I. (1995). A review of plasma treatment and the clinical application of polyethylene fibres to reinforcement of acrylic resins. *Journal of Materials Science: Materials in Medicine* 6(9):497-504.

Lambert, A.; Anawati, J.; Walawalkar, M.; Tam, J.; Azimi, G. (2018). Innovative application of microwave treatment for recovering of rare earth elements from phosphogypsum. *ACS Sustainable Chem. Eng*. 6 ,16471–16481.

Lakherwal D., (2014). Adsorption of heavy metals: a review, *Int. J. Environ. Res. Develop*. 4, 41–48.

Laurino, J.P.; Mustacato, J.; Huba, Z.J. (2019). Rare earth element recovery from acidic extracts of Florida phosphate mining materials using chelating polymer 1-octadecene, polymer with 2,5-furandione sodium salt. *Minerals*. 9, p 477.

Leonor I., H. Kim, F. Balas, M. Kawashita, R. Reis, T. Kokubo, T. Nakamura, (2007). Functionalization of different polymers with sulfonic groups as a way to

coat them with a biomimetic apatite layer, *J. Mater. Sci. Mater. Med.*, 18, 1923–1930.

Liu, W., Huang, C. and Jin, X., (2015). Electrospinning of grooved polystyrene fibers: effect of solvent systems. *Nanoscale research letters*, *10*(1), 1-10.

Liu, Y., Chen, J., Li, D., (2012). Application and perspective of ionic liquids on rare earths green separation. *Sep. Sci. Technol*. 47 (2), 223–232.

Liao, Y., Wang, R., Fane, A.G., (2014). Fabrication of bioinspired composite nanofiber membranes with robust superhydrophobicity for direct contact membrane distillation. *Environ. Sci. Technol*. 48, 6335-6341.

Li, W.J., Laurencin, C.T., Caterson, E.J., Tuan, R.S. and Ko, F.K. (2002). Electrospun nanofibrous structure: A novel scaffold for tissue engineering, *Journal of Biomedical Materials Research*, 60 (4), 613–621.

Liu, L., Luo, X.B., Ding, L. and Luo, S.L., (2019). Application of nanotechnology in the removal of heavy metal from water. In *Nanomaterials for the removal of pollutants and resource reutilization*. 83-147.

Liang, H.; Zhang, P.; Jin, Z.; DePaoli, D. (2017). Rare earths recovery and gypsum upgrade from Florida phosphogypsum. *Miner. Metall. Process*. *34,* 201-206.

Li X., X. Ma, J. Sun, M. Huang. (2009). Powerful reactive sorption of silver (I) and mercury (II) onto poly (o-phenylenediamine) microparticles, *Langmuir,* 25, 1675–1684.

Li X., Z. Zhou, G. Zhao, Z. Liu, (2008). Utilization of phosphogypsum for backfilling, way to relieve its environmental impact, Gospodarka Surowcami Mineralnymi 24, (18), 226–232.

Liao, Y., Wang, R., Fane, A.G., (2014). Fabrication of bioinspired composite nanofiber membranes with robust superhydrophobicity for direct contact membrane distillation. *Environ. Sci. Technol*. 48, 6335-6341.

Li, X.;Wu, P. (2017). Geochemical characteristics of dissolved rare earth elements in acid mine drainage from abandoned high-As coal mining area, southwestern China. *Environ. Sci. Pollut*. Res. 24, 20540–20555.

Long, K.R., Van Gosen, B.S., Foley, N.K. and Cordier, D., (2012). The principal rare earth elements deposits of the United States: A summary of domestic deposits and a global perspective. In *Non-renewable resource issues.* 131-155.

Lokshin, E.; Tareeva, O.; Elizarova, I. (2010). A study of the sulfuric acid leaching of rare-earth elements, phosphorus, and alkali metals from phosphodihydrate. *Russ. J. Appl. Chem.* 83, 958–964.

Lokshin E., Vershkova, Y.A.; Vershkov, A.; Tareeva, O. (2002). Leaching of lanthanides from phosphohemihydrate with nitric acid. *Russ. J. Appl. Chem.* 75, 1753–1759.

Lokshin, E.; Tareeva, O.; Elizarova, I. (2013). On integrated processing of phosphogypsum, *Russ. J. Appl. Chem.* 86, 463–468

Lü Q., M. Huang, X. Li, (2007). Synthesis and heavy-metal-ion sorption of pure sulfophenylenediamine copolymer nanoparticles with intrinsic conductivity and stability. *Chem. A Europ. J.*, 13, 6009–6018.

Lunderberg, J.M., Bartlett, R.J., Behm, A.M., Contreras, C., DeYoung, P.A., Hoogeveen, N.L., Huisman, A.J., Peaslee, G.F., Postma, J.K. (2008), "PIXE as a complement to trace metal analysis of sediments by ICP-OES", *Nuclear Instruments and Methods in Physics Research B;* 266, 4782 - 4787.

Luo, J., Luo, X., Crittenden, J., Qu, J., Bai, Y., Peng, Y., Li, J., (2015). Removal of antimonite (Sb(III)) and antimonate (Sb(V)) from aqueous solution using carbon nanofibers that are decorated with zirconium oxide (ZrO2). *Environ. Sci. Technol.* 49 (18), 11115-11124.

Lyons, J., Li, C. and Ko, F. (2004). Melt-electrospinning part I: processing parameters and geometric properties, *Polymer*, 45, 7597-7603.

Lyons, J. and Ko, F. (2005). Melt electrospinning of polymers: a review, *Polymer News*, 30,1 -9.

Ma, B., Xing, P., Wang, C., Chen, Y. and Shao, S., (2018). A novel way to synthesize calcium sulfate whiskers with high aspect ratios from concentrated calcium nitrate solution. *Materials Letters*, *219*, 1-3.

Mahalingam, S., Edirisinghe, M., (2013). Forming of polymer nanofibers by a pressurised gyration process. *Macromol. Rapid Commun*. 34, 1134-1139.

Mancheri, N.A., Sprecher, B., Bailey, G., Ge, J. and Tukker, A., (2019). Effect of Chinese policies on rare earth supply chain resilience. *Resources, Conservation and Recycling*, *142*, 101-112.

Mattila, H.P.; Zevenhoven, R. (2015). Mineral carbonation of phosphogypsum waste for production of useful carbonate and sulfate salts. *Front Energy Res*. 3 p 48.

Masmoudi-Soussi A.; Hammas-Nasri I.; Horchani-Naifer K.; Ferid, M. (2019). Study of rare earths leaching after hydrothermal conversion of phosphogypsum. *Chem. Africa*. 2, 415–422.

Masram, D.T., (2013). Polymer Based Ion Exchange Resin. In: A Book on Ion Exchange, Adsorption and Solvent Extraction. *Nova Science Publisher, USA*, 15–44.

Masmoudi-Soussi A., I. Hammas-Nasri, K. Horchani-Naifer, M. Ferid, (2019). Study of rare earths leaching after hydrothermal conversion of phosphogypsum, *Chem. Africa* 2, 415–422.

Massari, S., & Ruberti, M. (2013). Rare earth elements as critical raw materials: Focus on international markets and future strategies. *Resources Policy*, *38*(1): 36-43.

Maroufi, S.; Nekouei, R.K.; Hossain, R.; Assefi, M.; Sahajwalla, V. (2018). Recovery of rare earth (i.e., La, Ce, Nd, and Pr) oxides from end-of-life Ni-MH battery via thermal isolation. *ACS Sustain. Chem. Eng*. 6, 11811–11818.

McLemore, V.T., (2015). Rare earth elements (REE) deposits in New Mexico: Update. *New Mexico Geology*, *37*(3),.59-69.

McLellan, B.C., Corder, G.D. and Ali, S.H., (2013). Sustainability of rare earths— An overview of the state of knowledge. *Minerals*, 3(3), 304-317.

Mechi, N., Ammar, M., Loungou, M. and Elaloui, E., (2016). Thermal study of Tunisian phosphogypsum for use in reinforced plaster. *British Journal of Applied Science & Technology*, *16*(3),1-10.

Miao, M., Feng, X., Wang, G., Cao, S., Shi, W. and Shi, L., (2015). Direct transformation of FGD gypsum to calcium sulfate hemihydrate whiskers: Preparation, simulations, and process analysis. *Particuology*, *19*,.53-59.

Min M, Shen L, Hong G, Zhu M, Zhang Y, Wang X, Chen Y, Hsiao BS. (2012). Micro-nano structure poly (ether sulfones)/poly (ethyleneimine) nanofibrous affinity membranes for adsorption of anionic dyes and heavy metal ions in aqueous solution. *Chemical Engineering Journal* 197:88-100.

Middleton JC and Tipton AJ. (2000). Synthetic biodegradable polymers as orthopedic devices. *Biomaterials* 21(23):2335-2346.

Moalla, R., Gargouri, M., Khmiri, F., Kamoun, L. and Zairi, M., (2018). Phosphogypsum purification for plaster production: A process optimization using full factorial design. *Environmental Engineering Research*, *23*(1), 36-45.

Morillo Martín, D., Diaz Jalaff, L., García, M.A. and Faccini, M., (2019). Selective recovery of europium and yttrium ions with Cyanex 272-polyacrylonitrile nanofibers. *Nanomaterials*, *9*(12), p.1648.

Mohammadi, M., Forsberg, K., Kloo, L., De La Cruz, J.M. and Rasmuson, Å., (2015). Separation of Nd (III), Dy (III) and Y (III) by solvent extraction using D2EHPA and EHEHPA. *Hydrometallurgy*, *156*, 215-224.

Mohammad F. (2007). Specialty polymers: Materials and applications. (Eds) IK International Pvt Ltd - 588.

Mousa, S. and Hanna, A., (2013). Synthesis of nano-crystalline hydroxyapatite and ammonium sulfate from phosphogypsum waste. *Materials Research Bulletin*, *48*(2), 823-828.

Mukaba, J.L., Eze, C.P., Pereao, O. and Petrik, L.F., (2021). Rare Earths' Recovery from Phosphogypsum: An Overview on Direct and Indirect Leaching Techniques. *Minerals*, *11*(10), p 1051.

Mulopo, J.; Ikhu-Omoregbe, D. (2013). Phosphogypsum conversion to calcium carbonate and utilization for remediation of acid mine drainage. *J Chem. Eng Process Technol*. 3, 129.

Nataraj, S., Yang, K. and Aminabhavi, T. (2012). Polyacrylonitrile-based nanofibers—A state-of-the-art review, *Progress in polymer science*. 37, 487-513.

Neghlani, P., Rafizadeh, M. and Taroni, F. (2011). Preparation of aminated-polyacrilonitrile nanofiber membranes for the adsorption of metal ions: Comparison with microfibers, *Journal of Hazardous Materials*. 186,182-189.

Ndayambaje, G., Laatikainen, K., Laatikainen, M., Beukes, E., Fatoba, O., Van der Walt, N., Petrik, L. and Sainio, T. (2016). Adsorption of nickel(II) on polyacrylonitrile nanofiber modified with 2-(20-pyridyl) imidazole, *Chemical Engineering Journal*. 284,1106-1116

Ngah WW and Hanafiah, Megat Ahmad Kamal Megat. (2008). Removal of heavy metal ions from wastewater by chemically modified plant wastes as adsorbents: A review. *Bioresource technology*. 99(10):3935-3948.

Nguyen D, Hwang Y, Moon W. (2016). Electrospinning of well-aligned fiber bundles using an end-point control assembly method. *European Polymer Journal* 77:54- 64.

Nogami M., I. Ismail, M. Yamaguchi, K. Suzuki, (2003). Synthesis, characterization and some adsorption properties of TMMA chelating resin. *J. Solid State Chem.*, 171, 353–357.

O'Connell DW, Birkinshaw C, O'Dwyer TF. (2008). Heavy metal adsorbents prepared from the modification of cellulose: A review. Bioresource technology 99(15):6709-6724.

Ogata T, Narita H, Tanaka M. (2016). Adsorption mechanism of rare earth elements by adsorbents with diglycolamic acid ligands. *Hydrometallurgy* 163:156-60.

Ogata T, Narita H, Tanaka M. (2014). Immobilization of diglycol amic acid on silica gel for selective recovery of rare earth elements. *Chemistry Letters* 43(9):1414-1416.

Ogata T, Narita H, Tanaka M. (2015). Adsorption behavior of rare earth elements on silica gel modified with diglycol amic acid. Hydrometallurgy 152(0):178-182.

Olafadehan O., O. Jinadu, L. Salami, L. Popoola, (2012). Treatment of brewery wastewater effluent using activated carbon prepared from coconut shell. *Int. J. Appl. Sci. Technol.*, 2, 165–178.

Oliveira K., M. Menezes, E. Von Sperling, V. Jacomino, (2012). Transfer factor of rare earth elements from phosphogypsum amended Brazilian tropical soils to lettuce, corn and soybean, *J. Solid Waste Technol. Manage*. 38, 202–210.

Pan, J.; Zhou, C.; Liu, C.; Tang, M.; Cao, S.; Hu, T.; Ji, W.; Luo, Y.; Wen, M.; Zhang, N. (2018). Modes of occurrence of rare earth elements in coal fly ash: A case study. *Energy Fuels*. 32, 9738–9743.

Panteli, S., Savva, I., Efstathiou, M., Vekas, L., Marinica, O.M., Krasia-Christoforou, T. and Pashalidis, I., (2019). β-ketoester-functionalized magnetoactive electrospun polymer fibers as Eu (III) adsorbents. *SN Applied Sciences*, *1*(1) 1-12.

Papangelakis, V.G. and Moldoveanu, G., (2014), September. Recovery of rare earth elements from clay minerals. In *Proceedings of the 1st Rare Earth Resources Conference, Milos*. 191-202.

Pakade V, Cukrowska E, Darkwa J, Torto N, Chimuka L. (2011). Selective removal of chromium (VI) from sulphates and other metal anions using an ion-imprinted polymer. *Water SA* 37(4):529-38.

Parhi, P.K., Park, K.H., Nam, C.W. and Park, J.T., (2015). Liquid-liquid extraction and separation of total rare earth (RE) metals from polymetallic manganese nodule leaching solution. *Journal of Rare Earths*, *33*(2), 207-213.

Peelman, S.; Kooijman, D.; Sietsma, J.; Yang, Y. (2018). Hydrometallurgical recovery of rare earth elements from mine tailings and WEEE.
J. Sustain. Met.4, 367–377.

Peppard DF, Mason GW, Maier JL, Driscoll WJ. (1957). Fractional extraction of the lanthanides as their di-alkyl orthophosphates. *J Inorg Nucl Chem*. 4:334.

Peppard DF, Mason GW, Driscoll WJ, Sironen RJ. (1958). Acidic esters of orthophosphoric acid as selective extractants for metallic cations-tracer studies. *J Inorg Nucl Chem*. 7:276.

Pereao, O., Bode-Aluko, C., Fatoba, O., Laatikainen, K. and Petrik, L., (2018). Rare earth elements removal techniques from water/wastewater: a review. *Desalination Water Treat*, *130*, 71-86.

Pereao, O., Laatikainen, K., Bode-Aluko, C., Kochnev, I., Fatoba, O., Nechaev, A.N. and Petrik, L., (2020). Adsorption of Ce3+ and Nd3+ by diglycolic acid functionalised electrospun polystyrene nanofiber from aqueous solution. *Separation and Purification Technology*, *233*, 116059.

Pereao, O., Bode-Aluko, C., Laatikainen, K., Nechaev, A. and Petrik, L., (2019). Morphology, modification and characterisation of electrospun polymer nanofiber adsorbent material used in metal ion removal. *Journal of Polymers and the Environment*. 1-18.

Pereao, O.K., 2018. Functionalisation of electrospun nanofibre for lanthanide ion adsorption from aqueous solution. (PhD thesis, UWC).

Peiravi, M.; Dehghani, F.; Ackah, L.; Baharlouei, A.; Godbold, J.; Liu, J.; Mohanty, M.; Ghosh, T. (2020). A Review of Rare-Earth Elements Extraction with Emphasis on Non-Conventional Sources: Coal and Coal by products, Iron Ore Tailings, Apatite, and Phosphate by products. *Min. Metal. Explor*. 1-26.

Perämäki, S., (2014). Method development for determination and recovery of rare earth elements from industrial fly ash. *Research report/Department of Chemistry, University of Jyväskylä*, (178). (PhD thesis).

Pollmann, K.; Kutschke, S.; Matys, S.; Kostudis, S.; Hopfe, S.; Raff, J. (2016). Novel biotechnological approaches for the recovery of metals from primary and secondary resources. *Minerals*. 6, 54.

Pustam A.N., S.D. (2010). Alexandratos, Engineering selectivity into polymer-supported reagents for transition metal ion complex formation, *React. Funct. Polym*., 70, 545–554.

Pradhan, S., Swain, N., Prusty, S., Sahu, R.K. and Mishra, S., (2020). Role of extractants and diluents in recovery of rare earths from waste materials. *Materials Today: Proceedings*, *30*, 239-245.

Preston, J.S., Cole, P.M., Craig, W.M. and Feather, A.M., (1996). The recovery of rare earth oxides from a phosphoric acid by-product. Part 1: Leaching of rare earth values and recovery of a mixed rare earth oxide by solvent extraction. *Hydrometallurgy*, *41*(1), 1-19.

Prime, R.B., Bair, H.E., Vyazovkin, S., Gallagher, P.K. and Riga, A., (2009). Thermogravimetric analysis (TGA). *Thermal analysis of polymers: Fundamentals and applications*, 241-317.

Qi, Y.; Zeng, C.; Wang, C.; Ke, X.; Zhang, L. (2017). Continuous fabrication of calcium sulfate whiskers with adjustable aspect ratio in microdroplets. *Materials Letters*. *194*, 231-233.

Rahmani A., H.Z. Mousavi, M. Fazli, (2010). Effect of nanostructure alumina on adsorption of heavy metals, *Desalination*, 253, 94–100.

Rahal R., F. Annani, S. Pellet-Rostaing, G. Arrachart, S. Daniele, (2015). Surface modification of titanium oxide nanoparticles with chelating molecules: new recognition devices for controlling the selectivity towards lanthanides ionic separation, Sep. *Purif. Technol.*, 147, 220–226.

Ramakrishna S, Fujihara K, Teo W, Lim T, Ma Z. (2005). An introduction to electrospinning and nanofibers. *World Scientific*. 341.

Ramakrishna S, Fujihara K, Teo W, Yong T, Ma Z, Ramaseshan R. (2006). Electrospun nanofibers: Solving global issues. *Materials Today* 9(3):40-50.

Rathna, G.V.N., Birajdar, M.S., Bhagwani, M., Paul, V.L., (2013). Studies on fabrication, characterization, and metal extraction using metal chelating nonwoven nanofiber mats of poly (vinyl alcohol) and sodium alginate blends. *Polym. Eng. Sci*. 53, 321-333.

Rashad, A.M., (2017). Phosphogypsum as a construction material. *Journal of Cleaner Production*, *166*, 732-743.

Rasoulnia, P.; Barthen, R.; Lakaniemi, A.M. (2021). A critical review of bioleaching of rare earth elements: The mechanisms and effect of process parameters. *Critical Reviews in Environ. Science and Technol. 51*, 378-427.

Reid, S.; Walawalkari, M.; Azimi, G. (2017). Valorization of Rare Earth-Containing Landfilled Stocks of Industrial Process Residues: Phosphogypsum and Red Mud. *Proceedings of the Eres.* Santorini, Greece, 28-31 May 2017, 164-165.

Reed, D.W.; Fujita,Y.; Daubaras, D.L.; Jiao, Y.; Thompson V.S. (2016). Bioleaching of rare earth elements from waste phosphors and cracking catalysts. *Hydrometallurgy*. 166, 34–40.

Repo E, Warchol JK, Kurniawan TA, Sillanpää MET. (2010). Adsorption of Co(II) and Ni(II) by EDTA- and/or DTPA-modified chitosan: Kinetic and equilibrium modeling. *Chemical Engineering Journal* 161(1–2):73-82.

Romero-Hermida, M.I., Borrero-López, A.M., Alejandre, F.J., Flores-Alés, V., Santos, A., Franco, J.M. and Esquivias, L., (2019). Phosphogypsum waste lime as a promising substitute of commercial limes: A rheological approach. *Cement and Concrete Composites*, *95*, 205-216.

Roghani-Mamaqani H. (2015). Grafting polystyrene with various graft densities through epoxy groups of graphene nanolayers via atom transfer radical polymerization. Polymer Composites 38(11):2450-8.

Rutherford, P.M., Dudas, M.J., Arocena, J.M., (1995). Radioactivity and elemental composition of phosphogypsum produced from three phosphate rock sources. *Waste Manag. Res*. 13 (5), 407-423.

Rychkov, V.N.; Kirillov, E.V.; Kirillov, S.V.; Semenishchev, V.S.; Bunkov, G.M.; Botalov, M.S.; Smyshlyaev, D.V.; Malyshev, A.S. (2018). Recovery of rare earth elements from phosphogypsum. *J. Clean. Prod*. 196, 674-681.

Safiulina, A. M.; Matveeva, A. G.; Evtushenko, A. V.; Lizunov, A. V.; Goryunov, E. I.; Goryunova, I. B.; Brel, V. K. (2015). Recovery of lanthanides from digested phosphogypsum solutions using a new organophosphorus extractant, 5-(diphenylphosphoryl) hexan-3-one. *Russ. J. Gen Chem*. 85, 2128-2134.

Samonov, A. (2011). New data on mineral forms of rare metals in phosphogypsum wastes. *Doklady Earth Sciences, Springer*. 440, 1312–1315.

Santos, A.; Mazzilli, B.; Fávaro, D.; Silva, P. (2006). Partitioning of radionuclides and trace elements in phosphogypsum and its source materials based on sequential extraction methods. *J. Environ. Radioactiv*. 87, 52–61.

Satpathy, S. and Mishra, S., (2017). Extractive separation studies of La (III) and Ni (II) in the presence of lactic acid using DEHPA in petrofin. *Separation and Purification Technology*, *179*, 513-522.

Sato T. (1989). Liquid-liquid extraction of rare-earth elements from aqueous acid solutions by acid organophosphorus compounds. *Hydrometallurgy*. 22, p 121.

Salo, M.; Knauf, O.; Mäkinen, J.; Yang, X.; Koukkari, P. (2020). Integrated acid leaching and biological sulfate reduction of phosphogypsum for REE recovery. *Minerals Engineering*. *155*,106408.

Schreuder-Gibson, H.L, Gibson, P., Senecal, K., Sennett, M., Walker, J. and Yeomans, W. (2002). Protective textile materials based on electrospun nanofibres, *Journal of Advanced Materials*. 34(3): 44-55.

Schaefer, C.O., Cheriaf, M. and Rocha, J.C., (2017). Production of synthetic phosphoanhydrite and its use as a binder in Self-Leveling Underlayments (SLU). *Materials*, *10*(8), 958.

Selvan BR, Dasthaiah K, Suneesh A, Venkatesan K, Antony M, Gardas R. (2017). Diglycolic acid modified zirconium phosphate and studies on the extraction of Am (III) and Eu (III) from dilute nitric acid medium. *Radiochimica Acta* 105(4):275-83.

Seredin VV, Dai S, Sun Y, Chekryzhov IY (2013). Coal deposits as promising sources of rare metals for alternative power and energy-efficient technologies. *Applied Geochemistry*; 31:1–11

Shah BA, Shah AV, Bhatt RR. (2007). Studies of chelation ion-exchange properties of copolymer resin derived from salicylic acid and its analytical applications. *Iranian Polymer Journal* 16(3):173-84.

Sheng, Z.; Zhou, J.; Shu, Z.; Yakubu, Y.; Chen, Y.; Wang, W.; Wang, Y. (2018). Calcium sulfate whisker reinforced non-fired ceramic tiles prepared from phosphogypsum. *Boletín de la Sociedad Española de Cerámica y Vidrio*. *57*, 73-78.

Shields, K.J., Beckman, M.J. and Bowlin, G.L. (2004). Mechanical properties and cellular proliferation of electrospun collagen type II, *Tissue Engineering*. 10, 1510-1517.

Shimamura, K. Teramoto, T. Yoshioka, M. Tanaka, (1989). Polystyrene-based functional fibers, *Handbook M.Fiber Sci. Technol.*, 3, 209–252.

Shinozaki, T.; Ogata, T.; Kakinuma, R.; Narita, H.; Tokoro, C.; Tanaka, M. (2018). Preparation of Polymeric Adsorbents Bearing Diglycolamic Acid Ligands for Rare Earth Elements. *Ind. Eng. Chem. Res. 57*, 11424–11430.

Singh, M., Garg, M., Verma, C.L., Handa, S.K. and Kumar, R., (1996). An improved process for the purification of phosphogypsum. *Construction and Building Materials*, *10*(8), 597-600.

Smadi, M.M., Haddad, R.H. and Akour, A.M., (1999). Potential use of phosphogypsum in concrete. *Cement and concrete research*, *29*(9), 1419-1425.

Sohrin Y., S. Iwamoto, S. Akiyama, T. Fujita, T. Kugii, H. Obata, E. Nakayama, S. Goda, Y. Fujishima, H. Hasegawa, (1998). Determination of trace elements in seawater by fluorinated metal alkoxide glass-immobilized 8-hydroxyquinoline concentration and high-resolution inductively coupled plasma mass spectrometry detection. *Anal. Chim. Acta*, 363, 11–19.

Soltanzadeh, M., Kiani, G. and Khataee, A. (2013). Adsorptive Capacity of Polyacrylonitrile Modified with Triethylenetetramine for Removal of Copper and Cadmium Ions from Aqueous Solutions, *Environmental Progress and Sustainable Energy*, 00:1-9.

Sousa Neto V.O., G.S.C. Raulino, P.T.C. Freire, M.A. Araújo-Silva, R.F. (2013). do Nascimento, Equilibrium and kinetic studies in adsorption of toxic metal ions for wastewater treatment, Viewpoints, 7, 8.

Stankus, J.J., Guan, J., Fujimoto, K. and Wagner, W.R. (2006). Microintegrating smooth muscle cells into a biodegradable, elastomeric fiber matrix, *Biomaterials*, 27, 735-744.

Suneesh A, Jain R, Venkatesan K, Antony M, Bhanage B, Vasudeva Rao P. (2015). Novel diglycolamic acid functionalized iron oxide particles for the mutual

separation of Eu (III) and Am (III). *Solvent Extraction and Ion Exchange* 33(7):656-70.

Suneesh A, Venkatesan K, Syamala K, Antony M, Vasudeva Rao P. (2012). Mutual separation of americium (III) and europium (III) using glycolamic acid and thioglycolamic acid. *Radiochimica Acta International Journal for Chemical Aspects of Nuclear Science and Technology* 100(7):425-430.

Sun, H.; Tan, D.; Peng, T.; Liang, Y. (2016). Preparation of calcium sulfate whisker by atmospheric acidification method from flue gas desulfurization gypsum. *Procedia Environmental Sciences*. *31*,621-626.

Sun, P., Huang, K. and Liu, H., (2019). Separation of adjacent rare earth elements enhanced by "external push-pull" extraction system: An example for the separation of Pr and Nd. *Hydrometallurgy*, *189*, p 105136.

Shin D.H., Y.G. Ko, U.S. Choi, W.N. Kim, (2004). Design of high efficiency chelate fibers with an amine group to remove heavy metal ions and pH-related FT-IR analysis, *Ind. Eng. Chem. Res*. 43, 2060–2066.

Swain, N. and Mishra, S., (2019). A review on the recovery and separation of rare earths and transition metals from secondary resources. *Journal of cleaner production*. *220*, 884-898.

Szabadvary, F., (1988). The history of the discovery and separation of the rare earths. Handbook on the Physics and Chemistry of Rare Earths 11, 33–80.

Seeking Alpha, (2011). Rare Earth Metals Not So Rare but Valuable. /http://www. seekingalpha.com/article/103972-rare-earth-metals-not-so-rare-but-valuableS (accessed 08.12.21).

Tayibi, H., Choura, M., López, F.A., Alguacil, F.J. and López-Delgado, A., (2009). Environmental impact and management of phosphogypsum. *Journal of environmental management*, *90*(8), 2377-2386.

Tunsu, C., Petranikova, M., Gergori_c, M., Ekberg, C., Retegan, T., (2015). Reclaiming rare earth elements from end-of-life products: a review of the perspectives for urban mining using hydrometallurgical unit operations. *Hydrometallurgy* 156, 239-258.

Treacy M. J and J. B. Higgins (2001), "Collection of Simulated XRD Powder Patterns for Zeolites," 4th Edition. El- Sevier. Amsterdam, 379.

Uddin, T., Islam, A., Mahmud, S. and Rukanuzzaman, M. (2009). Adsorptive removal of methylene blue by tea waste, *Journal of Hazardous Materials*, 164, 53–60.

Uchida, S., Tagami, K., Tabei, K., Hirai, I., (2006). Concentrations of REEs, Th and U in river waters collected in Japan. *Journal of Alloys and Compounds* 408/412 (9), 525–528.

United States Geological Survey (USGS), 2018. Mineral Commodity Summaries 2018. https://www.usgs.gov/centers/nmic/rare-earthsstatistics-and-information.

Valkov, A. V.; Andreev, V. A.; Anufrieva, A. V.; Makaseev, Y. N.; Bezrukova, S. A.; Demyanenko, N. V. (2014). Phosphogypsum Technology with the Extraction of Valuable Components. *Procedia Chemistry*. 11, 176-181.

Van der Merwe, E.M. and Strydom, C.A., (2004). Purification of South African phosphogypsum for use as Portland cement retarder by a combined thermal and sulphuric acid treatment method: research in action. *South African journal of science*, *100*(9-10), 411-414.

Van der Hagen, M. and Järnberg, J., (2009). 140. Sulphuric, hydrochloric, nitric and phosphoric acids. Book, Sept 1.

Vander Hoogerstraete, T.; Blanpain, B.; Van Gerven, T.; Binnemans, K. (2014). From NdFeB magnets towards the rare-earth oxides: A recycling process consuming only oxalic acid. *RSC Adv*. 4, 64099–64111.

Velu S, Watanabe S, Ma X, Song C. (2003). Regenerable adsorbents for the adsorptive desulfurization of transportation fuels for fuel cell applications. American Chemical Society, Division of Fuel Chemistry Preprint Paper 48(2):526-528.

Walawalkar, M.; Nichol, C.K.; Gisele Azimi, G. (2016). Process Investigation of the Acid Leaching of Rare Earth Elements from Phosphogypsum Using HCl, HNO3 and H2SO4. *Hydrometallurgy*. 166, 195-204.

Wang, X.; Wang, L.; Wang, Y.; Tan, R.; Ke, X.; Zhou, X.; Geng, J.; Hou, H.; Zhou, M. (2017). Calcium sulfate hemihydrate whiskers obtained from flue gas desulfurization gypsum and used for the adsorption removal of lead. *Crystals*. *7*,270.

Wang, M., Li, X., Hua, W., Shen, L., Yu, X. and Wang, X., (2016). Electrospun poly (acrylic acid)/silica hydrogel nanofibers scaffold for highly efficient adsorption of lanthanide ions and its photoluminescence performance. *ACS applied materials & interfaces*, *8*(36),.23995-24007.

Wang, J., Luo, C., Qi, G., Pan, K. and Cao, B. (2014). Mechanism study of selective heavy metal ion removal with polypyrrole-functionalized polyacrylonitrile nanofiber mats, *Applied Surface Science*, 316, 245-250.

Wills, B.A. and Napier-Munn, T., (2006). An introduction to the practical aspects of ore treatment and mineral recovery. *Wills' Mineral Processing Technology*, 267-352.

Wilson, A.M., Bailey, P.J., Tasker, P.A., Turkington, J.R., Grant, R.A., Love, J.B., (2014). Solvent extraction: the coordination chemistry behind extractive metallurgy. *Roy. Soc. Chem*. 43, 123-134.

Wu D., Y. Sun, Q. Wang, (2013). Adsorption of lanthanum (III) from aqueous solution using 2-ethylhexyl phosphonic acid mono- 2-ethylhexyl ester-grafted magnetic silica nanocomposites, *J. Hazard. Mater*., 260, 409–419.

Wu, S., Wang, L., Zhao, L., Zhang, P., El-Shall, H., Moudgil, B., Huang, X. and Zhang, L., (2018). Recovery of rare earth elements from phosphate rock by hydrometallurgical processes–A critical review. *Chemical Engineering Journal*, *335*, 774-800.

Xie, F., Zhang, T. A., Dreisinger, D., & Doyle, F. (2014). A critical review on solvent extraction of rare earths from aqueous solutions. *Minerals Engineering*, *56*: 10-28.

Xu, F., Weng, B., Gilkerson, R., Materon, L.A., Lozano, K., (2015). Development of tannicacid/chitosan/pullulan composite nanofibers from aqueous solution for poten-tial applications as wound dressing. *Carbohydr. Polym*. 115, 16–24.

Yahorava, V.; Bazhko, V.; Freeman, M. (2016). Viability of phosphogypsum as a secondary resource of rare earth elements. *In XXVIII International Mineral Processing Congress Proceedings.*

Yadav, K.K., Singh, D.K., Anitha, M., Varshney, L., Singh, H., (2013). Studies on separation of rare earths from aqueous media by polyethersulfone beads containing D2EHPA as extractant. *Separ. Purif. Technol*. 118, 350-358.

Yang Y., S.D. Alexandratos, (2010). Mechanism of ionic recognition by polymer-supported reagents: immobilized tetramethylmalonamide and the complexation of lanthanide ions, *Inorg. Chem*., 49, 1008–1016.

Yang, S., Chen, S., Chang, Y., Cao, A., Liu, Y. and Wang, H. (2011). Removal of methylene blue from aqueous solution by graphene oxide, *Journal of Colloid and Interface Science*. 359, 24–29.

Yang, J. (2017). Reprocessing of Phosphogypsum for Recovery of REE. *Prometia Scientific Seminar, Barcelona., Spain*, 28-29 November 2017.

Yang, X.; Makkonen, H.T.; Pakkanen, L. (2019a). Rare Earth Occurrences in Streams of Processing a Phosphate Ore. *Minerals*. 9, p 262.

Yang, X.; Salvador, D.; Makkonen, H.T.; Pakkanen, L. (2019). Phosphogypsum processing for rare earths recovery—a review. *Nat. Resources*. 10, p 325.

Yee, W.A, Nguyen, A.G., Lee, P.S., Kotaki, M., Liu, Y. and Tan, B.T. (2008). Stress-induced structural changes in electrospun polyvinylidene difluoride nanofibers collected using a modified rotating disk. *Polymer*, 49, 4196-4203.

Yu, J., Fridrikh, S. and Rutledge, G. (2006). The role of elasticity in the formation of electrospun fibers, *Polymer*, 47, 4789-4797.

Zawisza, B., Pytlakowska, K., Feist, B., Polowniak, M., Kita, A. and Sitko, R., (2011). Determination of rare earth elements by spectroscopic techniques: a review. *Journal of Analytical Atomic Spectrometry*, *26* (12), 2373-2390.

Zawierucha, I., Kolodziejska, M., Kozlowska, J., Kozlowski, C., (2016). Removal of gold (III) from hydrochloric acid solutions using N-(diethylthiophosphoryl)-aza [18] crown-6 immobilized into membranes and Amberlite XAD-4 resin. *Separ.Sci. Technol*. 51, 2657-2666.

Zhanheng, C.H.E.N., (2011). Global rare earth resources and scenarios of future rare earth industry. *Journal of rare earths*, *29*(1), 1-6.

Zhou, B., (2017). Global potential of rare earth resources and rare earth demand from clean technologies. *Minerals* 7, 203–217.

Zhou, D.; Wei, R.; Zhu, Y.; Long, H.; Huang, B.; Wang, Y.; Wu, S. (2021). Calcium sulfate whisker one-step preparation using semi-dry flue gas desulfurization ash and directional growth control. *J. Clean. Prod. 290*, 125754.

Zhu, L., Guo, L., Zhang, Z.J., Chen, J., Zhang, S.M., 2012. The preparation of supported ionic liquids (SILs) and their application in rare metals separation. Sci. *China Chem*. 55 (8), 1479–1487.

Zielinski, S., Szczepanik, A., Buca, M., & Kunecki, M. (1993). Recovery of lanthanides from Kola apatite in phosphoric acid manufacture. *Journal of Chemical Technology and Biotechnology*, *56* (4): 355-360.

https://www.steenkampskraal.com/

https://pubs.usgs.gov/fs/2002/fs087-02/, Rare Earth Elements—Critical Resources for High Technology, access 14/07/21
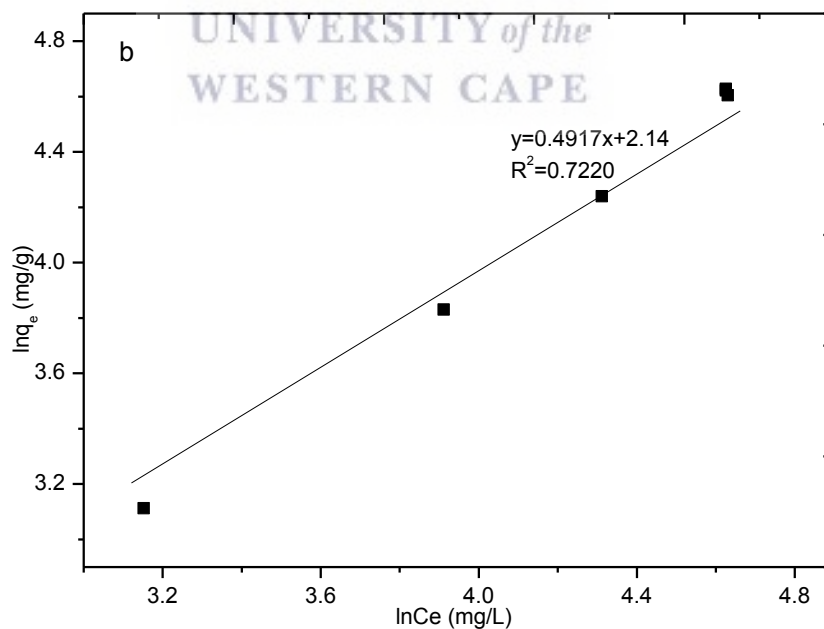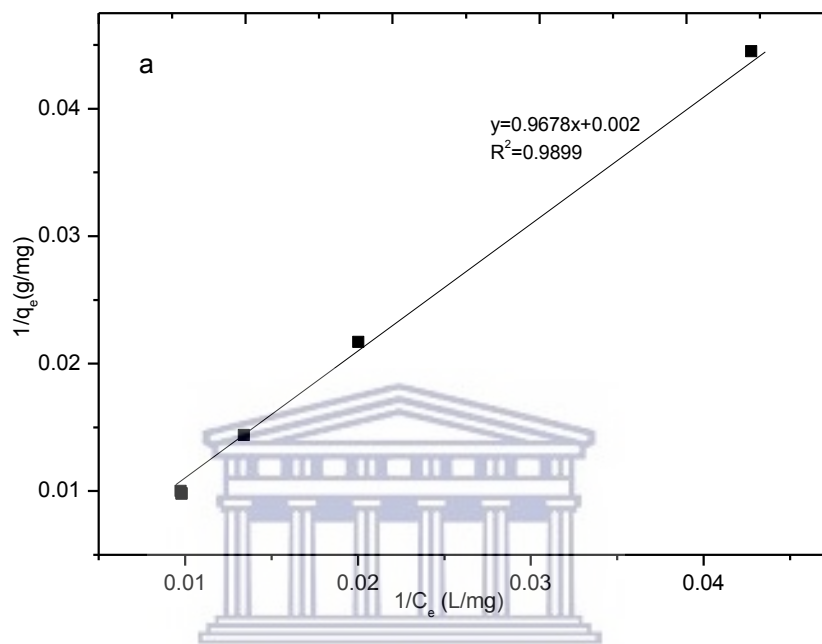
221

APPENDIX

APPENDIX A: Linearized graphs of Langmuir (a) and Freundlich (b) isotherms for adsorption of Ce^{3+} onto DH-PS20 nanofiber.
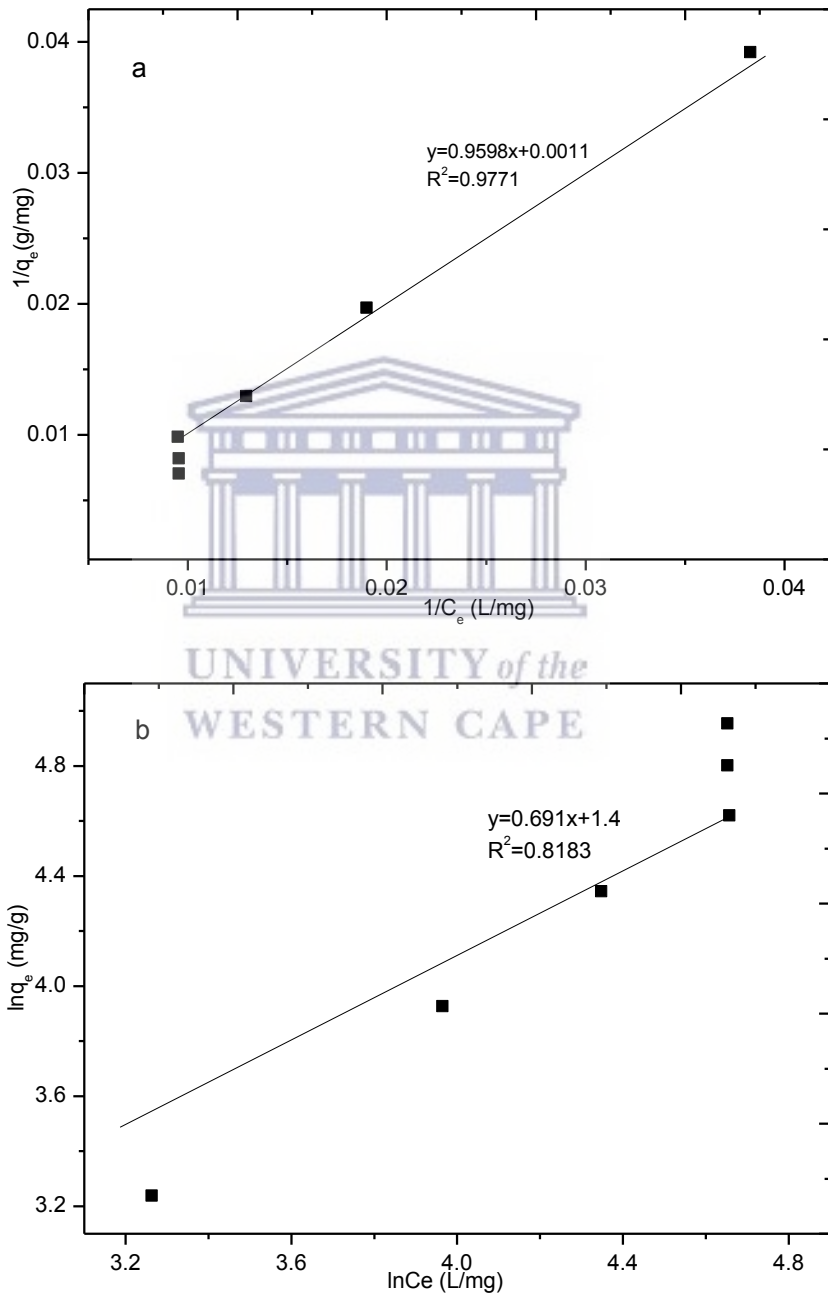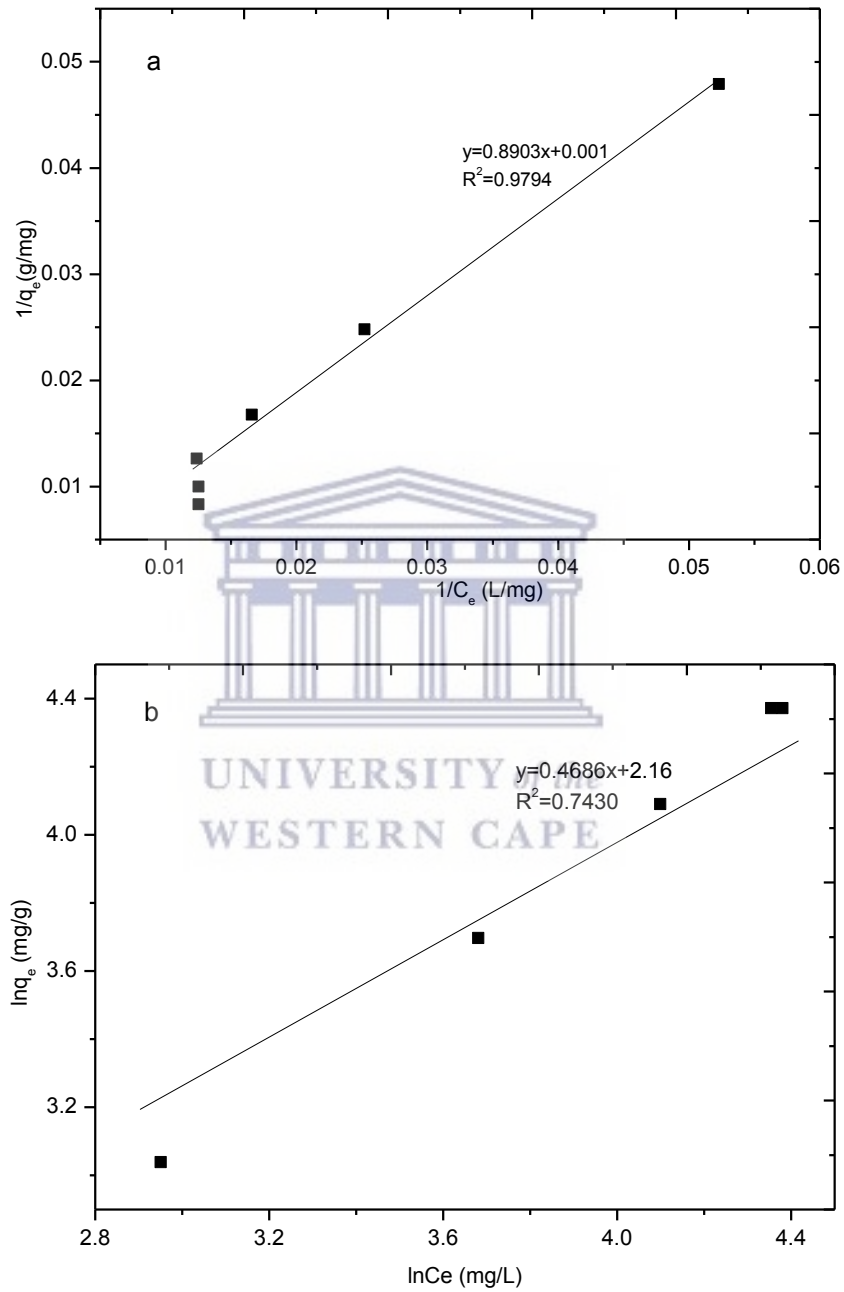
APPENDIX B: Linearized graphs of Langmuir (a) and Freundlich (b) isotherms for adsorption of Nd^{3+} onto DH-PS20 nanofiber.

223
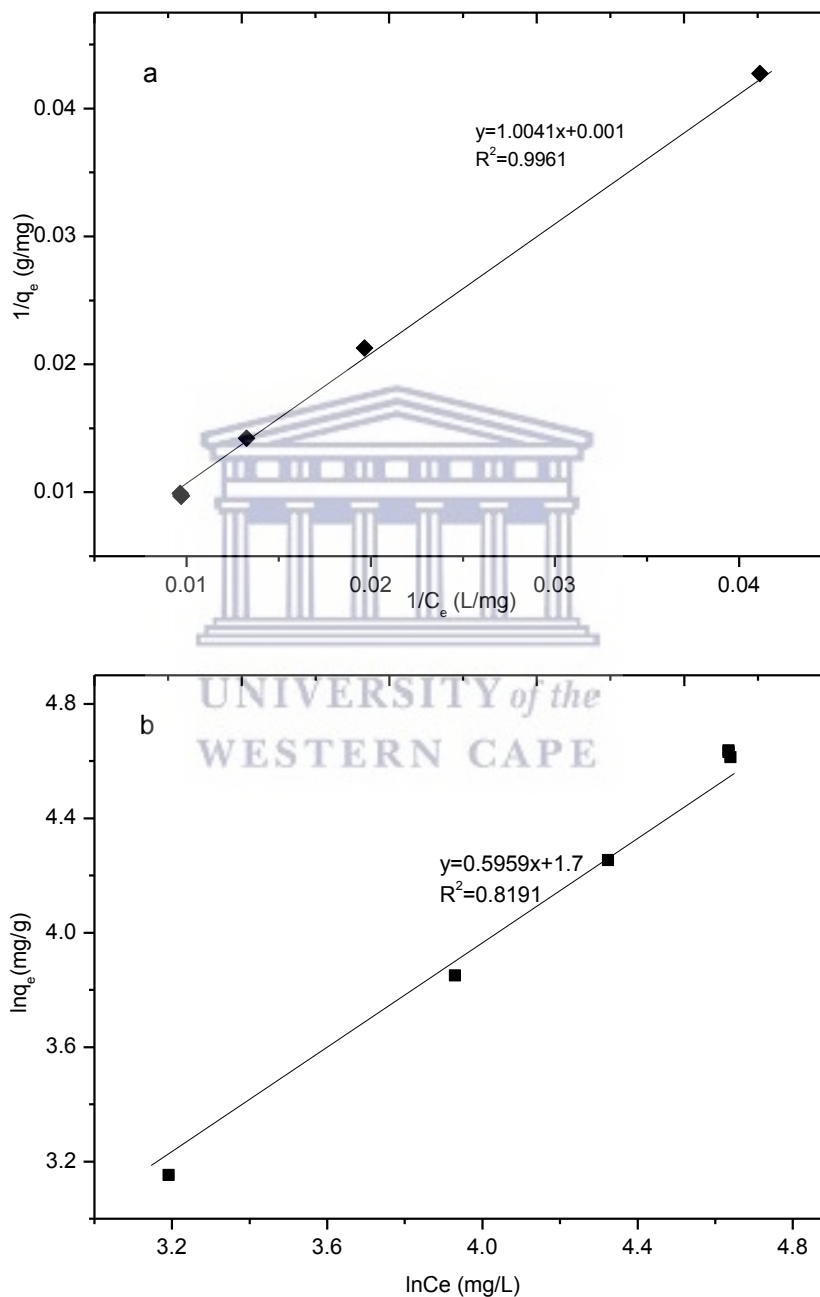
APPENDIX C: Linearized graphs of Langmuir (a) and Freundlich (b) isotherms for adsorption of Ca^{2+} onto DH-PS20 nanofiber.
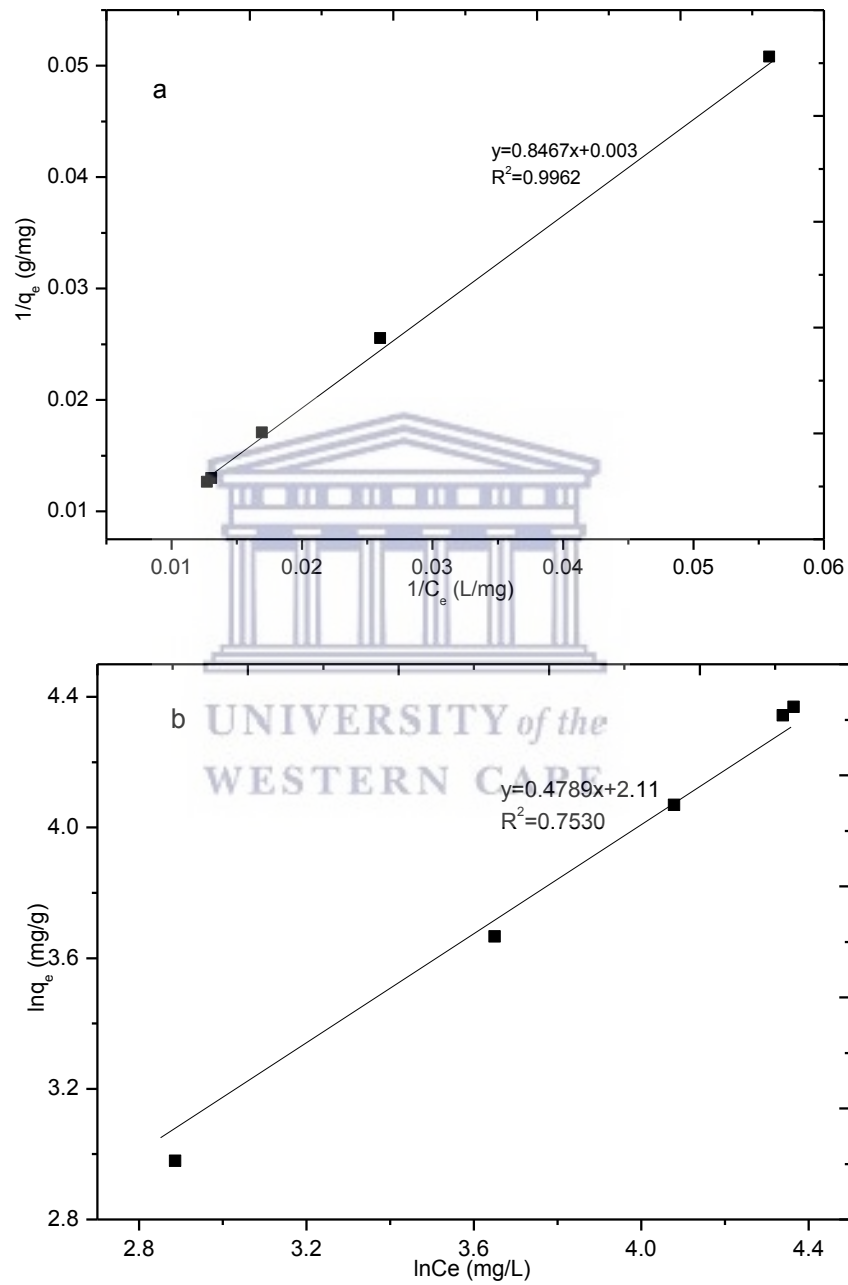
APPENDIX D: Linearized graphs of Langmuir (a) and Freundlich (b) isotherms for adsorption of Ce^{3+} onto DG-PS2 nanofiber.

APPENDIX E: Linearized graphs of Langmuir (a) and Freundlich (b) isotherms for adsorption of Nd^{3+} onto DG-PS2 nanofiber.

APPENDIX F: Linearized graphs of Langmuir (a) and Freundlich (b) isotherms for adsorption of Ca^{2+} onto DG-PS2 nanofiber.